UNIVERSITÀ DEGLI STUDI
DI MODENA E REGGIO EMILIA

International Doctorate School in Clinical and Experimental Medicine (CEM)

Cycle XXXII

Targeting folate-pathway enzymes with unconventional approaches: switching of the active/inactive conformational equilibrium of human thymidylate synthase and photoactivation of a methotrexate-like cytotoxic molecular device

Candidate: *Simone Vitiello*

Tutor: *Prof. Glauco Ponterini*

PhD Program Coordinator: *Prof. Giuseppe Biagini*

Timendi causa est nescire.

Acknowledgements

As this thesis work gets to completion, I believe it is important to acknowledge those who supported me during this journey.

In no particular order, I would like to thank my family for encouraging me to give more each and every time. I felt the importance of this in the face of new and greater challenges. Too much to be thankful for, too little space to do so.

I would like to acknowledge Prof. Glauco Ponterini, for his help, although at times misunderstandings have come between us, I've appreciated the importance of working through the hardships and the do's and don'ts in the laboratory life.

I would like to thank Matteo Santucci and acknowledge him for being the special person that he is. From making me feel welcome, his mentoring and help allowed me to realize what it means to have something at heart and to work on it.

I would like to thank Antonio Quotadamo and acknowledge him for his knowledge and for being discreet in discussing and resolving work and life issues, always with the biggest smile. "Pacciaria" never dies. Best sous chef ever.

I would like to thank Pasquale "Cicirinella" Linciano and acknowledge him for demonstrating how passions may fuel and improve the work done, to never let your guard down and always try and find ways to do better.

I would like to thank and acknowledge Davide Farina for having found yet another person to call a friend in Modena.

I would like to thank and acknowledge Angela Lauriola for her patience and the energy in making everything simple and accessible, as I learned a lot in the little time shared in the laboratory.

I would like to thank Luca "dank" Pinzi, (soon to be :P) Dr. Eleonora Truzzi and Dr. Natalia Oddone, Eleonora Maretti, Virginia Brighenti, Enrico Paradisi, Lucia Marchetti, Annachiara Tinivella, Gina Paola Hoyos Ceballos for sharing a large part of the journey, for their friendship and the laughs we had together. Tito calls you.

I would like to thank Giulia Parisella and Edoardo Cavani, because mentoring them helped me understand what I missed and improve in ways.

I would like to thank Alexandre Gomila and Ricardo Zamora, for far too many reasons to be listed here, picking one would be unjust.

I would like to thank Carlo Matera and Fabio Riefolo for their assistance and friendship.

I would like to thank Rosalba, Rossella, Aida, Marta, Alba, Nerea, Davia, Galyna, and Clara for the fun times we had together.

I would like to thank the laboratory crew, Claude, Filippo and Lorenzo, for their assistance and help in the day by day laboratory practice. A special thanks to Paola for her support, especially in the laboratory work, with the hopes of improving skills day in and day out.

I would like to thank and acknowledge Prof. Giuseppe Cannazza and Prof. Luca Costantino for mentoring by the example, for their ability to always find five minutes to hear us and support us through the best and the not so best.

I would give my sincere thanks to Dr. Giorgia Pavesi and Dr. Donatella Tondi for her counseling and help.

I would like to thank Dr. Nuria Camarero for her patience and understanding, allowing me to work productively, encouraging me to solve issues and problems, and for her outgoing and cheering nature.

I would like to thank Prof. Dr. Pau Gorostiza for giving me yet another chance to prove myself in his laboratory.

I would like to thank Prof. Monica Caselli for her support and mentoring in the process of dealing with certain aspects of the work done.

I would like to thank Prof. Barbara Ruozi, Prof. Giovanni Tosi and Prof. Flavio Forni for their time and their support.

I would like to thank Prof. Maria Paola Costi for allowing me to work in her laboratory.

I would like to thank Prof. Giuseppe Biagini for his help and patience in these three years.

Abstract

Human Thymidylate Synthase (hTS) is a fairly conserved homodimeric enzyme whose function is to convert dUMP to dTMP by means of a methylation reaction catalyzed by a cofactor: N_5-N_{10} mTHF. This enzyme is overexpressed in tumor cells, hence the reason for being one of the most pharmacological renowned targets. The catalytic activity is exclusive of the homodimer, although the monomer seems involved in a negative feedback mechanism where it bounds its own mRNA and those of biologically relevant molecules like c-myc and p53. hTS is the only orthologue that shows a catalytically active and an inactive conformation, identified via X-ray crystallography.

Current pharmacological treatments tend to mimic either the substrate or the cofactor. stabilizing the homodimeric structure, inhibiting the monomeric fraction's feedback mechanism, leading to pharmacoresistance. These strategies sometimes lack specificity and are prone to the development of important side effects. Lack of information regarding certain aspects of the molecular mechanisms of the enzyme may prevent further and more efficient target portions to be found and exploited in such a sense. Within this vast context, the aims of the thesis, whose work is in part contribution of an AIRC Project "Protein-protein interaction inhibitors of thymidylate synthase against colorectal cancer" (AIRC2015-IG16977) can be summed up in three key elements:

- introducing changes to existing protocols, leading to improvements in the quality of the data obtained from the experiments described

- describe how different inhibition strategies led to the development of different molecules and how the information gathered from testing them may impact the pharmacoresistance issue.
- The role and contribution of thermodynamic and spectrophotometric techniques in building models that may represent a step forward to explain currently unknown molecular mechanisms of the human Thymidylate Synthase.

Improved pharmacological strategies either stabilize the inactive conformer, disassemble the dimeric structure, or are based upon molecules that can selectively be activated through light induced conformational changes. Spectrophotometrical and thermocalorimetric techniques improve the current model as they allow to follow changes in specific molecular parameters in real time, which can be associated to changes in the molecular structure, used to "fingerprint" a conformer, and define variables of a model of the target molecule. Experimental conditions have been improved in quality through the purification in a phosphate free buffer retaining the same catalytic characteristics, and in quantity with improvements in the purification process yield.

Abstract italiano

La timidilato sintasi umana (hTS) è un enzima cataliticamente omodimerico abbastanza conservato. Questo svolge una funzione piuttosto rilevante, quella di convertire dUMP a dTMP per mezzo di una reazione di metilazione, coadiuvata da un cofattore, N5-N10 mTHF. In quanto particolarmente espresso in alcune linee cellulari tumorali, questo enzima è da tempo un target farmacologico, dato il ruolo critico svolto all'interno di queste. Sebbene l'attività catalitica sia esclusiva dell'omodimero, anche il monomero sembra essere funzionale a meccanismi di controllo dell'espressione dell'enzima stesso come anche di molecole biologicamente rilevanti come c-myc e p53. Questa viene svolta legando sia il proprio mRNA, sia quello delle altre molecole. hTS è l'unico ortologo che presenta due conformeri a diversa attività catalitica, identificati per mezzo di cristallografia a raggi X.

Come target farmacologico, diversi riscontri di molecole in grado di mimare substrato o cofattore sono presenti in letteratura. Tuttavia, queste tendono a stabilizzare il conformero omodimerico attivo, impedendo l'attività di repressore dell'espressione, causando farmacoresistenza. Tali strategie mancano talvolta di specificità, ponendo le basi per lo sviluppo di importanti effetti indesiderati. In questo contesto, uno degli elementi carenti più critici è la mancanza di informazioni su taluni meccanismi molecolari della molecola target. Comprendere questi potrebbe portare sia allo sviluppo di nuovi approcci farmacologici al fine di inibire questa molecola, sia all'identificazione di nuove porzioni dell'enzima da usare come bersaglio.

All'interno di tale vasto contesto, gli obiettivi della tesi, il cui lavoro è in parte contributo di un progetto AIRC "*Protein-protein interaction inhibitors of thymidylate synthase against colorectal cancer" (AIRC2015-IG16977)* può essere riassunto in tre elementi chiave:

- Introdurre cambiamenti ai protocolli esistenti, al fine di migliorare la qualità dei dati ottenuti e migliorare le rese delle procedure qui descritte
- Descrivere diverse strategie di inibizione e le molecole da esse derivate, e come approfondire la loro conoscenza possa impattare la problematica crescente della farmacoresistenza
- Il ruolo ed il contributo di tecniche termodinamiche e spettrofotometriche nel fornire variabili ai modelli correntemente esistenti, definendo meccanismi molecolari ad oggi ignoti della Timidilato Sintasi umana.

All'interno di questa tesi di dottorato si mostreranno strategie farmacologiche in grado di stabilizzare il conformero cataliticamente inattivo della TS, disassemblare la sua struttura dimerica e molecole "*proof of concept*" in grado di poter permettere un controllo spaziotemporale definito sull'attività inibitoriale. Le tecniche spettrofotometriche e termocalorimetriche migliorano il modello corrente permettendo di seguire anche nel tempo variabili che possono tradursi anche in cambiamenti di struttura molecolare. Queste tecniche sono inoltre state adoperate nel contesto di individuare dei set di variabili in grado di definire "l'impronta digitale" di un conformero della TS. Le condizioni sperimentali sono migliorate qualitativamente, con la purificazione di TS in un buffer privo di fosfato e miglioramenti nella resa enzimatica.

Page intentionally left blank

Table of contents

Table of Abbreviations

2-[[1,3-dihydroxy-2-(hydroxymethyl) propan-2-yl] amino] ethanesulfonic acid TES

3-(4,5-dimethylthiazol-2-yl)-5-(3-carboxymethoxyphenyl)-2-(4-sulfophenyl)-2H-tetrazolium MTS

2′ – deoxythymidine – 5′ – monophosphate dTMP

2′ – deoxyuridine – 5′ – monophosphate dUMP

5′-FluoroUracil5′-FU

Absorbance A

Anisotropy Decay r(t)

Arbitrary Units AU

Attenuance D

Calcium Chloride $CaCl_2$

Catalytic constant k_c

Circular Dichroism CD

Difference of Potential DP

Dihydrofolate DHF

Dihydrofolate reductase DHFR

Dimethyl Sulfoxide DMSO

Dithiothreitol DTT

Donor decay-time when the acceptor molecule is absent τ_d

Double strand DNA dsDNA

Dulbecco's Modified Eagle Medium DMEM

Ethylenediaminetetraacetic acid EDTA

Excited state lifetime T

Fluorescence quantic yield ϕ

Folylpolyglutamate synthetase FPGS

Förster distance R_0

Förster Resonance Energy Transfer FRET

Free energy of binding: ΔG_{bind}

Free energy ΔG

FRET efficiency ΦFRET

Intensity of incident light, I_o

Intensity of transmitted light, I

International Unit U

Intrinsically disordered protein(s) IDP(s)

Isopropyl β-d-1-thiogalactopyranoside or IPTG

Isothermal Titration Calorimetry ITC

Katal kat

Kinetic constants of binding K_{on}

Kinetic constants of disassociation K_{off}

Length of the optical path within the cuvette used l

Lipopolysaccharides LPS

M Molar

Maximum velocity V_{max}

Mega Pascal MPa

Methotrexate MTX

Michaelis – Menten constant K_m

Microcalorie µcal

Micrometer μm

Micro molar μM

Milliliter mL

Milli Molar mM

Molar absorption coefficient ϵ

N_5N_{10}methylentetrahydrofolate mTHF

Natural lifetime τ_n

Overnight ON

Optical Density OD

Overlap between donor emission spectra and acceptor absorption spectra J(λ)

Phototrexate PHX

Polytetrafluoroethylene PTFE

Quantum rate of the donor in the absence of the acceptor probe ϕ

Rate of energy transfer k_τ

Refraction index of the medium between donor and acceptor η

Revolutions per minute rpm

RFC – Reduced Folate Carrier

Rotational correlation of the sphere θ

Serine hydroxymethyltransferase SHMT

Single strand DNA ssDNA

Site receptor density B_{max}

Sodium Dodecyl Sulphate – Polyacrylamide Gel Electrophoresis SDS-PAGE

Sodium phosphate monobasic NaH_2PO_4

Thermodynamic constant of disassociation or K_d

Thickness of the sample d

Titration calorimetry TC

Transition dipoles of the donor and acceptor molecules κ^2

Transmittance T

Tryptophan Trp

Ultraviolet – Visible spectrum UV-Vis

Variation in difference of potential ΔDP

Variation in free energy ΔΔG

Variation in FRET efficiency ΔΦFRET

Wavelength of excitation λ_{exc}

Wild type wt

Page intentionally left blank

List of Figures

List of Graphs

List of Tables

List of Equations.

Page intentionally left blank

Chapter 1 – Introduction

1.1. Overview on enzymes and their activity

Current targeted pharmacological treatments, as the word "targeted" suggests, are mostly aimed to interact and inhibit a target molecule whose biological activity is critical for cancer cell survival and/or growth. It comes to no one's surprise that the inhibition of a molecular target well depends upon the kind of target itself. Target inhibition comes in different shapes and forms: for instance, human Thymidylate Synthase (TS) is an enzyme. Enzymes catalyze reactions which would take longer times to happen spontaneously. The characteristics and the specifics of enzymes' catalytic activity is widely discussed by many sources; for all needs and purposes of this thesis, some information will be delved in for clarity purposes.

Enzymes are complex molecules, capable of lowering the amount of free energy of activation needed for a reaction to happen. This phenomenon usually happens without any consumption of enzyme molecules: this means that a small concentration of enzymes can convert important amounts of substrate molecules into product. Specificity is one of the most important features: they tend to catalyze a specific reaction with specific molecules. This gets to a point where stereospecificity is an important factor that can make or break the catalysis of a reaction. Alpha amylase, for instance, catalyzes the hydrolysis of glucose from starch but not from cellulose. This is due to the different nature of glycosidic links between the sugar constituents; in the former these are α (1 -> 4); in the latter,β(1 -> 6). It is accustomed that for a reaction to be catalyzed, the substrate(s) need to be closer to

the enzyme, to the point where a bind may be formed between the two. The enzymatic region where the bind happen Is called “active site”. The term indicates any cleft or pocket in which the substrate is capable of binding, hence allowing the enzyme to exert its catalytic activity. This is due mostly to multiple chemical groups acting in a very limited space, whose function may range from easing up the binding process, to transferal of molecules. As any other molecule exerting any kind of function, the tridimensional structure is critical to ensure proper activity. The interaction mechanism between substrate(s) and enzyme comes a long way. Initially the mechanism was identified as a “lock and key” one, where the enzyme (lock) has a site that specifically fits only one molecule (key). There are cases however, where this is not necessarily correct; the enzyme, subsequent to substrate binding, may undergo a series of conformational changes which may help stabilize the substrate in place (induced fit), a mechanism refined in what is a current “selection” of the active site conformation.

1.1.1. Factors in substrate – product rate conversion

The general form in which any substrate – product conversion reaction is catalyzed by an enzyme, can be written as

$$E+S \rightleftarrows ES \rightleftarrows E+P$$

E: Enzyme, S: Substrate, P: Product.

As such, there are four different rate constants which explain the speed at which a certain reaction occurs. It is custom to indicate rate constants as positive when describing forward reactions, whilst negative ones describe reverse reactions.

It is important to stress how enzymes only affect the rate at which certain reaction happen, and usually do not interfere with the equilibrium between substrate and product. This is because usually enzymes are capable of catalyzing reactions in both senses.

As many other biomolecules, enzyme activity can be modified through different parameters.

- One of such is temperature: it is generally agreed upon that higher temperatures correlate directly with an enhance in the substrate – product rate conversion. This is because an increase in temperature can be directly correlated to an increase of kinetic energy of the molecules within a known system, thus increasing chances for substrate(s) and enzyme to connect. This is not indefinitely true: as all molecules, enzymes can undergo denaturation. As previously stated, tridimensional structures are fundamental for their ability to exert an effect – in such a case, increasing the rate of a reaction. Hence, optimal temperatures exist for each enzyme, which characterize the best condition in which said enzyme functions.
- pH is another important factor in this sense. The effect of pH in the conversion rate from substrate to product is threefold. It is understandable how, for instance, the ionized side chains of amino acids at the active site may be influenced by changes

in pH. These changes, however, do not affect exclusively the enzyme, but the substrate and the enzyme-substrate complex as well. This means that as much as with temperature, an optimal pH condition can be identified. The main difference with temperature would be that, in this case, if a graph would have to be made comparing the pH and the consequent activity of the enzyme, said graph would most likely be a bell curve. pH activity dependence may be exploited to gain information regarding the composition of the active site side chains.

- Concentration of substrate and enzyme: just like any other reaction, enzyme – substrate interactions obey the mass-action law. Usual conditions for enzyme catalyzed reactions are one in which the concentration of enzyme is far lower than the substrate concentration. Thus, it is possible to imagine how in these conditions, the concentration of enzyme may be the greatest influencer in the substrate-product synthesis. This is especially true if concentrations between enzyme ([E]) and substrate ([S]) are relevant. The reaction reaches a velocity (v) that cannot be increased any further by any amount of substrate. If a reaction velocity vs [S] would be made, this would most definitely have a specific shape, a rectangular hyperbola, which is typical of most non-allosteric enzyme catalyzed reaction.

1.1.2. Michaelis – Menten equation

Reaction catalyzed by most enzymes can be written out in a very simple form, where the step from enzyme – substrate complex to enzyme plus product is considered one way only. In other words:

$$E+S \rightleftarrows ES \rightarrow E+P$$

Equation 1: Enzyme - substrate - product reaction

The idea was to simplify enzyme catalysis from a kinetic standpoint. Michaelis and Menten in 1913 proposed a kinetic mechanism that was later modified by Briggs and Haldane in such a way to include more relationships between the constant rates in the previous reaction.

$$v = \frac{V_{max}[S]}{K_m + [S]} = \frac{k_c[E]_t[S]}{K_m + [S]}$$

Equation 2: Michealis - Menten Equation.

This equation is known as the "Michaelis – Menten equation". In short:

- It relates the initial rate of an enzyme catalyzed reaction to the substrate concentration ([S]) and two constants, K_m (Michaelis constant) and k_c (catalytic constant). These constants may be considered as a way to express how well the enzymatic active site binds the substrate, thus how well it catalyzes the reaction.
- Michaelis – Menten equation considers that [S] >> [E]. Thus, it can be derived that the first steps of the reaction are much faster than the last step.
- If [S] >> K_m, the reaction reaches a maximum velocity (V_{max}) which is limited by enzyme concentration. This condition, thus, proves optimal in studying enzyme activity. V_{max} is related to the reaction velocity by the formula

$$v = k_c[E] = V_{max}$$

Equation 3: v and V_{max} relation.

k_c is to be considered the enzyme turnover number for the substrate i.e. a proportionality constant that relates the enzyme ability to convert substrate in product, within optimal conditions.

- If v = ½ V_{max}, K_m corresponds to [S] at such a velocity. In this condition, Km can be considered a rough estimate of the enzymatic affinity for the specific substrate considered.
- In the condition [S] << K_m, the previous equation linking v to k_c and K_m can be simplified to

$$v = k_c[E_t] * \frac{[S]}{K_m}$$

Equation 4: Simplification of Michaelis - Menten equation for [S] << Km

In this condition, the reaction depends linearly from both [E_t] and [S]; k_c/K_m can be considered a measure of the total catalytic efficiency of the enzyme for the substrate and can be compared between enzymes that act upon the same substrate molecule.

Michaelis – Menten equation allows one to obtain a more general overview in what is happening in an enzyme catalyzed reaction. There are some interesting elements to be discussed which pertain to this realm:

- K_m can be considered a specific constant that characterizes an enzyme – substrate couple, whilst being completely independent from the concentration of both. If the rate from ES to E+P is considerably smaller vs the rate of ES to E+S, the value of Km resembles the one from the equilibrium constant for the bind of substrate to the enzyme. This has important effects,
    - as K_m becomes K_s, and it's equal to the ratio between the rates from E+S to ES and the rate between ES to E+S.
    - V_{max} depends strictly upon the enzyme concentration; with [S] saturating, it also becomes independent of substrate concentration.
- As stated before, catalytic activity is dependent of pH and temperature, hence K_m and k_c are also dependent on these factors.
- Should an enzyme bind more than one substrate, each K_m can be interpreted as a general understanding of the enzyme – substrate affinity (smaller K_m indicate higher affinities)
- Most reactions catalyzed by an enzyme are characterized by an important free energy (-ΔG) gap; this can be intended as the reaction being irreversible. This is how the system can justify losing one rate – the one going from E+P to ES – considering only the forward reaction.

- k_c/K_m ratio can be used in a metabolic pathway to identify a limiting step. This would correspond to the lowest ratio found, related to the supposed slower step.
- Turnover numbers usually range from 1 to 10^4. Rare exceptions are 10^5.
- Enzymatic efficiency is usually expressed as units of activity. One unit is often defined as the concentration of enzyme that catalyzes the conversion of 1 µmol of substrate to product each minute, under optimal conditions. Units are either expressed as International Unit (U), U/mL or U/L; similarly, another option is to express such a unit as katal. One katal (kat) is considered the amount of enzyme that converts one mole of substrate to product in one second. It is understandable how both units are specific for a set of condition (pH, temperature and so on…) in which the reaction occurs.

1.1.3. Plotting the equation

Dealing with enzymes most often than not means dealing with constant rates. Thus, the main interest should lie in understanding the values of k_c and K_m of an enzyme – substrate couple. Graphical representations of the Michaelis – Menten equation can help in such a sense, as they linearize information, or in some situation in which not all data is readily available to describe the rectangular hyperbola. There are many different instances in this sense: the most known however are two: Lineweaver-Burk and Eadie-Hofstee plots

- Lineweaver-Burk plot: also known as double reciprocal plot (1/v vs 1/[S]) presents relevant limitations with regards to how k_c and K_m are obtained. This graph is heavily

dependent on the first data obtained from low concentrations of [S]. Such data may offer less precision than one obtained from higher concentrations of [S]. Formula to obtain v:

$$\frac{1}{v} = \frac{K_m}{V_{max}} \frac{1}{[S]} + \frac{1}{V_{max}}$$

Equation 5: Equation from Lineweaver - Burk plot correlating v to V_{max}.

Name derives from being obtained by taking the reciprocal of both parts of the MM equation across the equal sign.

- Eadie-Hofstee plot: an improvement to some critical issues of the L-B plot.

1.2. Outline of function and structure of Thymidylate Synthase

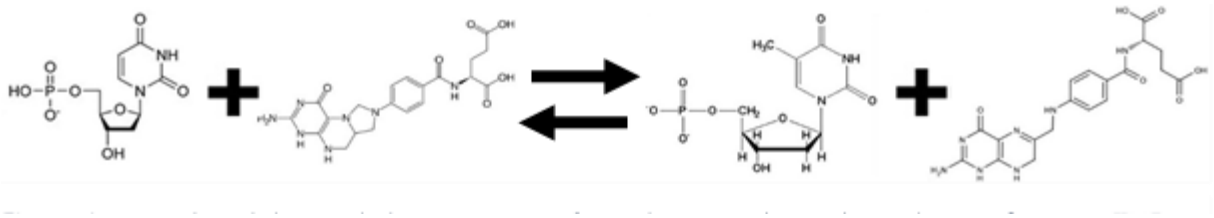

Thymidylate synthase is a homodimeric enzyme of 70 KDa. It is expressed in different species, from viruses to humans.

It methylates 2′ – deoxyuridine – 5′ – monophosphate (dUMP) to 2′ – deoxythymidine – 5′ – monophosphate (dTMP). The methylation of dUMP to dTMP is aided by a co-factor, N_5N_{10}methylentetrahydrofolate (mTHF), donating the required CH_3. As such, it represents one of the most egregious cellular pathways to ensure DNA synthesis.

TS's catalytic function is paramount in cancer cells. Its expression is mostly high during the synthesis of new DNA strands, particularly so during the S phase of the cell cycle [1–4]

A distinctive feature, these cells replicate at a very high rate. This can be achieved only by ample synthesis of much-needed nucleotides. Given the characteristics of the enzyme and its critical role in the synthesis of new deoxynucleotides, it does not surprise this enzyme being one of the most relevant targets in pharmacology. The main idea behind the concept is well illustrated. Targeting this process would unable tumor cells - or any alike - to replicate its DNA, due to the lack of one of the components. This translates to a halt to DNA synthesis, hence to cell proliferation. As such, this would represent a viable option in engaging diseases where cell proliferation is a known issue[5].

Methylation as a molecular mechanism involving TS is a profusely described process.

- TS binds dUMP, which then interacts with mTHF, forming a non-covalent ternary complex (TS - dUMP - mTHF).
- mTHF's N10 is then protonated, activating the co-factor, as an imino ion. This complex is an unstable intermediate.
- A key element to the process: TS' CYS195 residue. The thiol of this cysteine binds to dUMP's C_6. The methylenic unit of the imino ion then binds dUMP's C_5 in a "trans" position to the cysteine.

This process ends with mTHF reduced to dihydrofolate (DHF). DHF re-enters in the process as mTHF via a two-step process. DHF is reduced to Tetrahydrofolate (THF) from NADPH in

a reaction catalyzed by the enzyme dihydrofolate reductase (DHFR). Serine hydroxymethyltransferase (SHMT) catalyzes the hydroxymethyl transfer from its serine to THF, producing mTHF and glycine.

TS's catalytic activity may very well be considered one of a kind. Among the known processes who use THF as a co-factor, this is one of the few knowns that alter its oxidation state[6]

1.2.1. hTS vs TS

As it has become accustomed to the scientific world, knowing the structure of a molecule allows one to infer on its perks and characteristics. Within this spirit, a great deal of information has come from X-ray crystallography studies.

X-ray crystallography allows for a molecule to be crystallized under precise conditions. After preparing the crystal - a process that comes with a plethora of issues by itself - the sample is then analyzed via X-rays. The rays hit the crystal, diffracting. X-rays diffraction is analyzed and interpreted to obtain tridimensional information about the atomic and molecular structure. Published structures are collected in a protein data bank. Structures are readily available from the PDB website (www.rcsb.org), and can be downloaded, free of charge.

Such a process doesn't come without a fair share of issues. For once, there is no assurance that a molecule can be crystallized. This may be due to different factors, one of them being

the abundant use of salts in the process. Even obtaining one is an error and trial process that requires a long time.

Although with its quirks and perks, there is no denying that X-ray crystallography studies have helped the scientific progress. The case of TS is no exception.

Given its importance as a cancer target, TS's structure is vastly reported upon. A query in the Protein Data Bank website shows a plethora of structures, more than a hundred to this day. As previously stated, TS is a fairly conserved enzyme, synthesized by different species, from viruses to humans. Structurally speaking, however, there are differences worth stressing. Human TS is composed of 313 amino acidic residues for each monomer. Known secondary structures are eight alpha helices, ten beta-sheets, and six 3/10 helices. Another renowned TS structure is from bacteria. By superimposing the two structures, three main differences become evident.

- N-term of hTS has an extension of 28 to 29 residues
- an insertion of twelve residues in position 117
- another one of eight residues in position 146

Another structural feature of the human orthologue: two different conformers of the same enzyme were discovered. By superimposing their structures, three main differences arise:

- The main one: the orientation of the catalytic (181-197) loop. They are at a 180 degrees' rotation reach. Thus, the Cys-195 is outside the active site: hence, this conformer is catalytically inactive. In such a conformer, Cys-195 is found at the

monomers interface. The distance between C_α of the Cys-195 in the two conformers is around 10Å. This can be better appreciated in Fig.1.

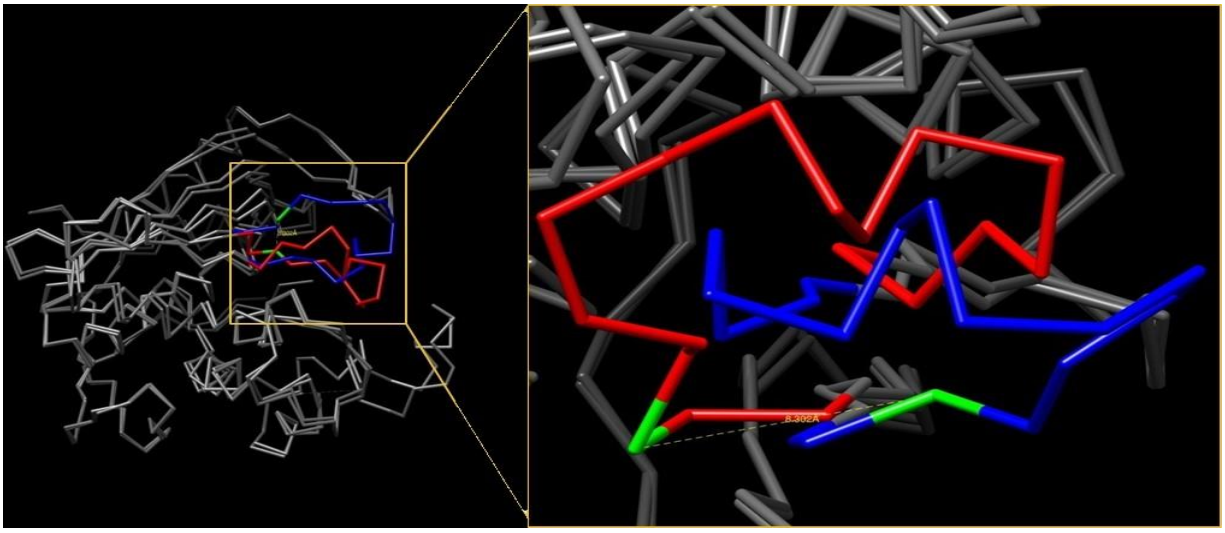

Figure 1 Alpha carbon structure of the active and inactive monomers of hTS. In red, the active loop, in blue, the inactive one. In green, the position of Cys195.

- 107-128 loop is disordered in the catalytically inactive conformer, while ordered in the catalytically active one.
- An N-term extension - specific to the human orthologue - contributing to the enzyme's intracellular stability.[7,8]

1.2.2. Outline of the active and inactive conformer structures

The TS sequence is known to be well conserved, a fifth of the human one is found in other living species.[9,10]As previously stated, the active-inactive structural differences start at the orientation of the 181-197 turn.

hTS-wt structure was first determined through ammonium sulfate crystals. Structures showed a different conformation of the active loop than the one observed in bacteria, where Cys-195 is outside the active site, found at the monomer-monomer interface. An arginine residue in position 163 may be involved in the stabilization. Arginines are basic amino acids. The guanidine group in the side chain can form hydrogen bonds with the carbonyl groups from the main chains of alanine 191 and leucine 193). Arg-163 is not evolutionally conserved: murine TS, for instance, has a lysine residue in that position. Its side chain, however, is too small to interact as the arginine. R163K hTS mutant, for instance, seems unable to convert to its inactive conformer.

Ammonium sulfate salts allowed high-quality wild type hTS (hTSwt) crystals to be obtained. As previously reported, sulfates and phosphates ions act as effectors towards the active-inactive equilibrium, bringing it closer to the inactive conformer. Consequently, hTSwt crystals obtained with this procedure would describe the inactive conformer. This is not an issue per se; it depicts, however, the challenges in obtaining crystals of the active conformer. As the inactive conformer can't bind any substrate - inhibitors included - crystallizing the active conformer became a necessity. A concept further sustained by failed experiments in which "inactive" hTS crystals soaked with effectors known to induce the switch towards the active conformer. It seemed obvious, at that point, that something in the process favored the crystallization of the inactive conformer. This evidence supports the idea of an equilibrium between the active and inactive conformer in solution, as much

as showing the existence of molecules capable of bringing said equilibrium closer to one of the two conformers[11].

Bioinformatic simulations allowed the evaluation of the active loop dihedral angles. This data seems to support a model in which the transition process is asymmetrical and sequential. The two active loops rotate one after the other, to assume the final conformation. Cys-195 can usually move in two ways: a flip through the active loop or a torsion outside the loop[7].

Within the catalytic loop there is another amino acidic residue worth analyzing: a tryptophan residue in position 182.

This amino acid is one of the three fluorescent ones - the others that naturally occurs in proteins being tyrosine and phenylalanine. The tryptophan emission spectrum is sensitive to the surrounding environment. This may be expressed as changes in the fluorescent emission spectrum. Such changes may be monitored to hint at differences in the protein structure. These studies, which rely only on the analysis of the fluorescence of these two amino acids, are called intrinsic fluorescence studies.

In this case, Trp-182's relevance for such studies is punctually summarized:

- Among the 5 Trp residues, 182 is the closest one to the catalytic cysteine 195
- One of the main structural differences between the active and inactive conformer is the orientation of the catalytic (181-197) loop.

- Differences in the whereabouts of Trp-182 and Trp-182' in the two conformers are sufficient to significantly impact the emission properties of this residue. Hence, two different emission profiles may be assigned to two different conformers.[11]
- 182 and 182' residues are positioned close to each other at the monomer-monomer interface

Indeed, in preliminary experiments, adding phosphate or sulphate ions to a TS solution indeed increased the tryptophans' emission spectra, as much as adding dUMP to the same solution decreased the signal even lower than its intrinsic value, as shown on Fig.2.

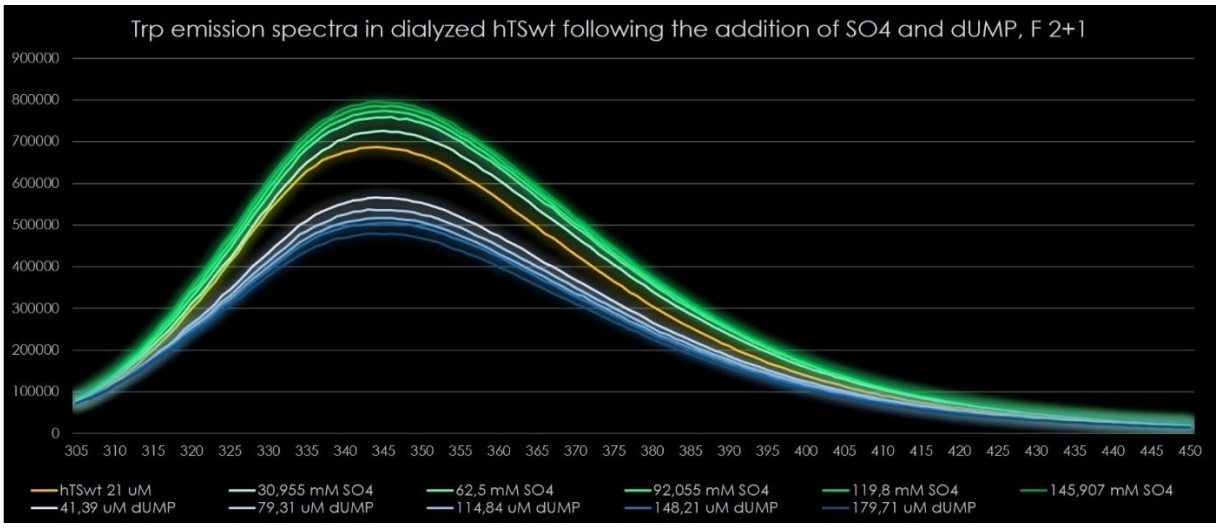

Figure 2;Tryptophan emission spectra of hTS wildtype - in gold - following the addition of SO_4 ions - in green - and of dUMP - in blue. F 2+1.

Such preliminary experiments suggest the following:

- Indeed, fluorescent amino acidic residues may be used to hint at structural changes in a molecule

- by analyzing the intrinsic fluorescence spectrum of hTS and the same one after dUMP addition, there seems to be a clear hint of an inactive population of TS being present. Such evidence sustains the existence of the inactive conformer as evidenced in X-ray crystallography studies.
- such changes in the emission spectrum were not evidenced in bacterial TS; such phenomenon suggests that indeed this conformer is unique to the human orthologue.
- Intrinsic fluorescence studies support the existence of two different conformers, hints at the existence of an equilibrium between the two conformers in solution, and hints at the role of some molecules as effectors, capable of bringing the equilibrium close to one conformer.[12]

1.3. Homodimer – monomer features, equilibrium and function.

As stated in the previous units, TS presents itself as a homodimer. About one-fifth of its sequence is well conserved in different living species, from viruses to humans. X-ray crystallography studies helped in the identification of said conserved residues, located in the contiguity of the active site. Enzyme kinetics data seem to suggest that at a minimum energy state, the homodimer exists in an asymmetric form. In other words, only one monomer is in the active conformation. Such consideration, however, is not hTS exclusive. Different studies, such as ones from Danenberg and co. point out that the same conclusion

can be reached with *L.casei* TS. This can be inferred by analyzing the titration of TS with molecules capable of interacting with tiolic groups of cysteines. As a result, only one of the catalytic cysteines seems to be oxidized.

The catalytic site of each monomer presents an important cysteine residue in position 195. These are labeled CYS195 and CYS195'. As previously discussed, these residues are at the core of the catalytic activity. The active site is, however, incomplete in the monomers. It requires two amino acidic residues (two arginines), each given by one monomer to the other. Consequently, the catalytic activity is dimer exclusive. TS may be considered, hence, an obligated dimer.

Monomers and homodimers are at equilibrium in solution. TS is synthesized starting from its monomers, which then assemble as required. Monomers play as much as a mattering role in this process. TS is one of few enzymes capable of self-regulating their transcription process. The molecular mechanisms around this role are still under scrutiny. It seems, however, that an accepted model is one where the monomer binds its mRNA via specific sequences. The nature of the interaction is not covalent, most likely ionic interactions between positively charged residues and negatively charged PO_4^{3-} groups. Such a mechanism may fall under the negative feedback regulation group. In other words, the higher the monomeric concentration, the higher the repression of the transcription process. Early scientific literature seems to indicate how this phenomenon does not occur

only with its own mRNA, but it is actually extended even to those of other relevant intracellular proteins such as c-myc or p53[13].

An additional consideration for such a process comes from the observation of pharmacologically treated cancer cells. Literature in this regard is prolifering: treated cancer cells tend to express more TS than untreated ones. A reasonable interpretation of such a phenomenon may find an explanation in the characteristics of current pharmacological treatments. The main idea behind such drug design is to mimic the natural substrates of the enzyme, competing at the active site, thus acting as competitive inhibitors. As with the natural substrates, however, their binding may stabilize the di-active conformer, tilting the monomer-dimer equilibrium in favor of the dimer. Treated cancer cells answer to this by producing TS monomers, nullifying the negative feedback regulation previously discussed[14].

1.4. Targeted therapies

Before delving into the issue of pharmacoresistance, it is important to understand the context underlying this thesis work, introducing the concept of targeted therapies.

As reported, human TS is overexpressed in cancer cell lines. This concurs in the increased growth rate, a characteristic aspect of these cells. Scientific literature is well endowed in articles aiming at reducing the efficacy of this enzyme. Given its important role in the DNA synthesis, it really doesn't come as a surprise how this enzyme was chosen as a target for different pharmacological approaches.

Any therapy aimed at inhibiting molecules whose activity affects directly – or indirectly for all that matters – the growth, progression and/or spread of cancer falls under the category of "Targeted cancer therapy" (cancer.gov)

The main aspect of targeted therapy vs chemotherapy can be resumed in three points:

- Chemotherapeutics act on a more general level, mostly preventing the cancer cells from spreading, without differentiation on physiological and cancer cells. Targeted therapy, in its idea, hits one or few molecular targets known in the scientific literature to be involved in one such processes described before.
- Usually chemotherapics are chosen because of their cytotoxic activity; targeted therapy outputs molecules known to inhibit specifically some molecules within cancer cells.
- This brings to the third consideration: chemotherapics are cytotoxic; targeted therapy molecules aim to be cytostatic – that is, aim at halting cancer growth.

Targeted therapies, however, do not come issue-free. The main challenges regard mostly the phenomenon known as pharmacoresistance. Such term identifies a resistance to a pharmacological treatment, which mostly comes due to mutations and selectivity towards a certain molecule. This resistance may be expressed in either the target being overexpressed to the point that the pharmacological treatment becomes useless, or the cancer cell employs a new pathway to achieve the same result. Other relevant issues in targeted therapies come from difficulties related to the pathway in which the target

molecule resides or act within – signal molecules are one such example. Further issues represented by side effects of these treatments cannot be ignored.

Targeted therapies exemplify the importance of new pharmacological approaches to optimize the effect whilst reducing side effects. The Food and Drug Administration has approved more than thirty new drugs coming from such efforts.

1.5. Enzymatic inhibition

Interactions between a target molecule and an inhibitor candidate can be defined under different terms. Without overcomplicating the matter at hand, a starting point can surely be the required conditions for an interaction to be formed. These conditions can be summed up in two elements: structural complementarity, as previously stated, is paramount for any molecule wishing to interact with another one. Another key element is, however, the formation of matrices of low-energy bonds[15]. These are not quite as strong as other types of bonds – covalent bonds for instance – hence they are easier to break if taken alone. Small amount of energy, however, means also that these interactions can happen quite more often than the aforementioned high energy bonds. However weak alone, small energy interactions become critical when considered in numbers, requiring, more often than not, less constraints to develop with regards to high energy interactions.

Low energy bonds are electrostatic, van der Waals and hydrophobic interactions, but also hydrogen bonds. A relative low number of these may characterize a first step in the

interaction between two molecules. Interactions characterized by these premises are defined surmountable interactions, as their relative stability, given their relative strength, still allow room for other, stronger interactions to form.

Other interactions, however, either rely on relative high numbers of small interactions or an important amount of stronger ones, to the point that the interaction is timely considerable, relatively stable and thus can be defined as an unsurmountable interaction. [16]If numbers and quality of the interaction between two molecules are important, the molecular mechanisms underlying the association are as important. This concept evolved in time, thanks to the developments in the scientific technology at disposal. To sum it up, three different mechanisms can be considered[16]:

- The lock-and-key model, which assumes a structural rigidity of the two molecules interacting; only the molecule with the correct structure and length is capable to interact at the binding site of the second one.
- The induced fit model diverges from the first one by taking into account some flexibility of the binding site. The initial interactions with its ligand start a series of structural changes with the aim of finding a conformation fitting the ligand.
- A recently proposed model regards "fuzzy" proteins. First described by Monika Fuxreiter[17], the model comprehends an interesting concept regarding intrinsically disordered proteins (IDPs). Well represented in eukaryotic proteomes, these structures seem to evade the aforementioned structure-function association,

between its folded 3-D structure and its function. IDPs tend to function by molecular recognition: binding of a molecule may be followed by either "induced folding" or "disorder-to-order transition" advocating for IDPs to become ordered in a "functional context". This however is not always the case, as function seems to preserve under relevant structural disorder whilst complexed with their binding partner(s). This event was defined "fuzziness" – from fuzzy logic in mathematics – which describes one such phenomenon where either structural disorder or polymorphism is functionally quintessential for an IDP complex.

- A rather recent model proposed by Straub, on the other hand, considers a "fluctuating molecule" capable of changing its conformation to one such structure capable of binding its ligand. In other words, it differs from the previous ones by taking into account that a complex molecule, capable of binding, may very well exist in different conformations. Choosing the most appropriate one to bind a ligand is not a phenomenon due to the ligand itself. As many different conformations may be available in solution, these may very well be in equilibrium with each other. The ligand is not hindered in any way, shape, or form in its binding process with the enzyme, as it is only a matter of finding the closest conformation capable of binding.

Taking back the concepts of surmountable and insurmountable interactions. The former case can be very well described through the mass action law[18]., which is characterized by three parameters. These parameters are:

- The thermodynamic constant of disassociation or K_d;
- Kinetic constants of binding and disassociation k_{on} and k_{off},
- Site receptor sites, B_{off} and RT.

The reaction between a molecule capable of binding, for instance an enzyme (E), and its ligand (L) can be described as the following

$$E + L \underset{k_{off}}{\overset{k_{on}}{\leftrightarrow}} EL$$

Equation 6: Enzyme - Ligand reaction scheme.

Taking this concept to a drug – enzyme interaction,

- k_{on} would represent the kinetic constant of the complex formation, expressed in M^{-1} s^{-1}; it is a measurement of the amount of time required for the complex to reach its equilibrium state, during the process of the drug binding to the enzyme. This is affected mostly on the concentration of the drug vs the enzyme, and especially so by how accessible the enzyme's binding site for the drug is.
- k_{off} would represent the reverse constant of disruption of the drug-enzyme complex, expressed in s^{-1}; as it represents for how long the complex exists (its lifetime) this is greatly influenced on the low energy bonds matrix that exists between the drug and the enzyme. K_{off} thus describes the affinity of a ligand for its bound molecule – in this case an enzyme.

It is also true, however, that the disassociation process also depends on other factors, such as, for instance, chemical properties of the two bound molecules. When these are similar, a higher affinity can be determined, which translates to a sort of equilibrium between the rate of association and disassociation of the complex. In other words

$$k_{on}[E][L]=k_{off}[EL]$$

Equation 7: Correlation between k_{on} and k_{off}.

which allows for the determination of K_b, a binding constant, to be defined as the ratio between the two aforementioned constants, k_{on} and k_{off}

$$K_b=\frac{k_{on}}{k_{off}}$$

Equation 8: Kinetic binding constant.

It is also true, however that:

$$\frac{k_{on}}{k_{off}}=\frac{[EL]}{[E][L]}$$

Equation 9: Binding constant expressed in terms of enzyme - ligand and EL complex concentrations.

and, if the binding constant is the ratio between k_{on} and k_{off}, its inverse is determined as the disassociation constant, K_d, which is expressed in M.

$$K_b = \frac{k_{on}}{k_{off}} = \frac{[E][L]}{[EL]} = \frac{1}{K_d}$$

Equation 10: Binding and disassociation constants correlation.

These constants are all consequential and co-related with each other. This means that whenever a particular enzyme-ligand couple has a high kinetic association constant paired to a low kinetic disassociation constant, the binding and disassociation constant will also have the same high/low value. In this case, this directly translates to a high affinity index.

Experimentally, K_d can be determined through a set of two experiments:

- binding studies in saturating conditions: the target is incubated with increasing concentrations of ligand, until equilibrium is reached. It is then possible to determine the amount of bound ligand with the formula

$$\frac{B_{max}[L]}{[L]+K_d}$$

Equation 11: Kinetic constant of disassociation from binding studies in ligand saturating conditions.

It seems clear that in this equation there has to be a term that underlies the number of binding sites available for the ligand on the receptor molecule. Such a term is B_{max}. To be precise, B_{max} actually represents the so-called site receptor density, which

corresponds to the maximum number of ligand molecules capable of binding the target molecule. The assumption that this number reflects the total amount of receptor sites on the target molecule for the ligand can only be made in such a case where there is only one binding molecule and only one binding site.

Saturation is achieved by the time no more binding is observed, irrelevant of the increasing concentration of ligand in solution with the target molecule.

- Competitive binding studies, in which the ligand is not labelled: this has to compete with a known labeled ligand for the binding at the target molecule. As this competition is concentration dependent, by deriving the concentration of the bound labeled ligand one can infer the concentration of the bound unlabeled one.

1.6. Current pharmacological treatments and pharmacoresistance.

The role of hTS in tumors has been described in the previous chapter. The main idea is that by blocking this synthetic pathway, the tumor cell is not able to produce more thymidine, bringing its own cell cycle to a halt during the DNA replication step. This should allow molecules like p53 to induce an apoptotic path.

Such a reason sparked the interest in design and synthesis of hTS inhibitors, which initially were structurally derived from either its substrate (dUMP) or its co-factor (N_5,N_{10}-metylenetetrahydrofolate).

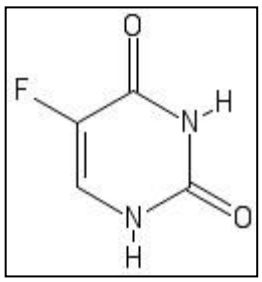

In such a sense, 5'-FluoroUracil or 5'-FU, a dUMP analogue, is known to be one of the first and most potent antitumoral molecules directed versus hTS. As soon as it enters the tumor cell, it is converted in its active form Floxuridine.

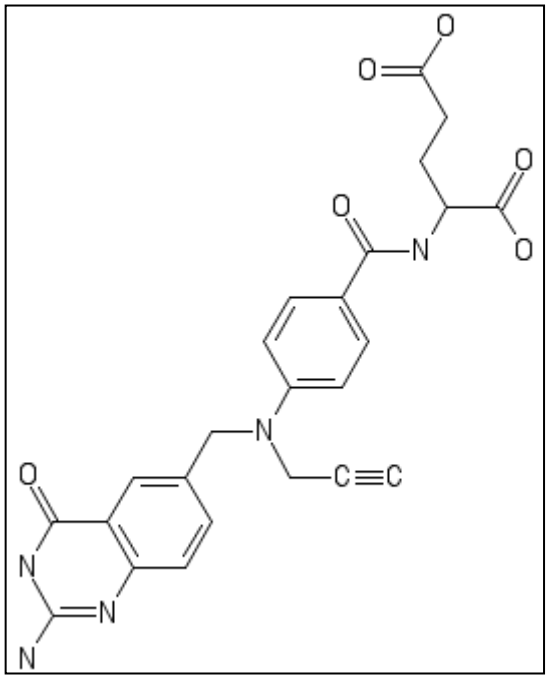

CB3717 on the other hand was the first selective folate analogue for TS, unable to interact with DHFR[19]. These compounds do, however, show some mild to severe side effects. For instance, F-dUMP, after being transformed in a nucleoside triphosphate, is not selective for hTS, and can interact with other molecules, like RNA for example, where it could be inserted, causing severe side effects[202122]. Such side effects may however be due to the fact that they mostly follow the same pathway as their substrate counterpart. The two most important steps regard getting through the membrane, which is accomplished first step, getting over the cell membrane by means of a carrier called RFC – Reduced Folate Carrier. The second step, once in they can be reworked by an enzyme called Folylpolyglutamate synthase (FPGS). This causes an increase of the molecule's concentration within the cell, accumulating there and showing increasing affinity for both hTS and DHFR.[2324]

1.6.1. Resistance mechanisms

It comes to no surprise how the enzymes included in this pathway represent a critical step in the process of looking for a plausible cellular resistance at the genic level[25]Resistance could very well be due to[26]

- a reduced intracellular carrying effect by RCF,
- to a reduced FPGS activity or
- an increment in the intracellular concentration of hTS due to genic amplification.

Another source of resistance can be due to an increase of intracellular γ-Glutamyl Hydrolase concentration. This enzyme can be considered part of a family of mitochondrial enzymes capable of hydrolyzing the γ bond of the polyglutamic chain, reducing the inhibitor affinity for the enzyme.[25]

Another relevant issue regarding the resistance mechanisms regards the role of some aforementioned molecules. These tend to compete at the binding site with hTS natural substrates. Once they bind, they are not converted into product, as their structure only mimic the substrate one. The binding process between the enzyme and the antimetabolites shows increased affinity, to the point where the dimeric form is overly stabilized by the binding. This, however, is an issue in its own right: as previously described, hTS has its own regulatory mechanism, which strongly relies on the monomer. Stabilizing the dimer does not help the situation: the tumor cells respond to this by synthesizing more hTS molecules, 2-4 times more than untreated ones[27]. It is not difficult to imagine how the

ability for hTS to bind mRNA is at its peak when no ligands are bound to it; alike, this is at its lowest when hTS forms the tertiary complex.

There is another level of complexity, one where the transcription process of hTS is regulated by molecular factors like E2F. It does not come as a surprise that the overexpression of said factors, in particular E2F1, seemed to increase TS-mRNA levels, suggesting a potential role of this molecule as an *in vivo* regulator of TS levels[28].

1.7. LR and Hotspot project

Protein-protein interactions are interesting elements in the pharmacological and biochemical world. Effects of protein interaction affect single molecules as well as tissues and organs. In this context, a particular element of interest is given, when such interaction become of medical interest. Attempts at interfering with these are not always linear, as interfaces between interacting proteins may be much more extended than the ones between a molecule and a target site. In this context, the energetic contribution of each residue (ΔG_{bind}) at the interface, may prove informatively rich.

hTS monomers present hydrophobic residues capable of forming an ordered structure defined "clathrate ordered structure". This structural element is not so common in nature, as in, not all biomolecules are capable of such a behavior; even so, requirements for this to happen are quite stringent. It requires that a hydrophobic environment is enclosed by water molecules, and hydrogen bonds to happen. Clathrate hydrates are usually characterized by multiple repeated pentagonal ring structures.

As the monomers assemble into a dimer, water molecules in the structure break, causing a positive change in the variation of entropy, and a consequent binding, with a negative contribution to the free energy, ΔG, Free energy of binding or ΔG_{bind} from the resulting PPIs can be calculated from the disassociation constant of the protein-protein interface of the target protein. This can be done by taking into account the general free energy of binding:

$$\Delta G_{bind} = RTIn(K_d)$$

Equation 12: Free energy of binding.

This value is experimentally obtainable through a molecular approach called "alanine scanning". In this process, a single mutation is induced in the target protein, one that substitutes one amino acidic residue with an Alanine.

This process is completed by measuring the variation in free energy ΔΔG caused by replacing said residue. This value can be calculated from the formula in Eq.13[29]

$$\Delta \Delta G_{bind_{Mut-WT}} = RTIn\left(\frac{K_{d_{Mut}}}{K_{d_{WT}}}\right).$$

Equation 13; Variation in free energy of binding.

Through this process, it was possible to demonstrate that the free energy binding contribution did not equally distribute itself along the whole interface, but some amino acidic residues and regions – "hotspots" – contribute more than others in the binding

energy as a whole. In general, these contributions seem to pertain more to 3 residues in particular, Trp, Tyr and Arg. This may be due to the fact that these particular residues are particularly fit to interact with other molecules through van der Waals interactions or hydrogen bonds. Mutating these in Ala means that connections may be lost, hence the variation of free energy will be higher. On the other hand, Leu, Val, Ser residues do not have such binding characteristics, hence their mutation into Alanine yields smaller variations of free energy.[30] In hTS this process led to the identification of highly conserved residues which most contribute to the amount of free binding energy, at the monomer – monomer interface. As hTS catalytic activity is strictly homodimeric, binding molecules at such interface could possibly lead to inhibition due to structure disassociation. This would be an innovative inhibition mechanism, one that would override the current issues in pharmacological approaches to hTS.

The analysis of these residues was first studied through a computational approach, which calculated the free binding energy contribution in each residue of the monomer – monomer interface. The same was also done to assess the dimer stability.[31] Hotspots were defined whenever a residue was capable of providing about 4,2 kJ/mol as a contribution to the binding free energy. As every residue was mutated in Alanine, each contribution was measured and classified quantitatively, to identify the most relevant residues. With these results, mutants were designed with the aim to evaluate the effects of such modification in the context of both monomer – dimer equilibrium and dimer stability. In this sense, the most relevant residues in hTS were K47 - F59 - I178 - W182 - L198 - Y202. Resonance

energy transfer (RET)-based assays were employed to investigate dimer stability, expressed in K_d terms. Results allowed to determine the stability of all mutants and compare them with the wild – type enzyme.

Results of this determined the following sequence, from the most to the least stable conformation:

hTSwt > K47A ~ Y202A > W182A ~ L198A ~ I178A > F59A

Of each mutant, K_m and k_{cat} were measured and compared to the wild – type. Circular dichroism was employed to ensure that the secondary structures of TS were not affected by the mutation. This was also required to attribute differences, if any, in structure integrity and substrate binding directly to the single point mutation at the interface. K47, F59, L198, Y202 were all characterized as having less stability than the wild – type enzyme, whilst holding a comparable kinetic activity, which could have been used to compare the activity of some compounds.

The data from the computational approach was then combined with that coming from previous works, whose aim was to study the monomeric interface by means of peptides, designing and synthesizing a peptide-based allosteric inhibitor capable of acting at said interface. From this data, a 20-mer fragment (C20 peptide) was designed, with the aim to mimic the whole hTS interface. This fragment was later divided in smaller, seven to eight peptides, which demonstrated to be effective in halting the growth of ovarian cancer cell lines. By different chemical approaches, libraries of octapeptides from the C20 were

created and tested on their ability to inhibit hTS.[32] This screening allowed the LR (LSCQLYQR) peptide to be chosen as the most promising peptidic inhibitor acting at the monomer – monomer interface. This was also confirmed through X-ray crystallography, which also suggested that the binding happened when the enzyme was in its di-inactive conformation.[33]

LR's IC_{50} on hTS was 50 μM, at 37°C, following 1 hour of incubation. In the quest to improve the inhibiting features of this peptide, one such increase was obtained when the D-Gln4 analogue was obtained (LSCqLYQR). The only difference in the two structures is that the residue in position 4 is in its D-conformation. Such a single mutation boosted the efficacy in IC_{50} to 30 μM. The added feature, also proven in cell lines, was that the LR inhibitors were capable of inhibiting hTS without the side effect of enhancing either mRNA or enzyme expression, unlike modern pharmacological approaches, like those employing 5'-FU.

Gap of knowledge and thesis aim

As previously shown, one of the most important elements in the research environment is the understanding of how a certain target molecule works. Knowledge about its molecular mechanisms is at the base of the identification of sensible targets, exclusive of the molecule at hand. This does not apply only to human thymidylate synthase, but to any other pharmaceutical target. Current pharmacological choices are riddled with an alarming increase of the pharmacoresistance phenomenon. This issue is the constant reminder that

tumor cells may and can still develop resistance strategies to ensure their own survivability. Many pharmacological treatments currently available do still cause an important amount of side effects, meaning that there is more work to be done in both molecule design and delivery process.

Human thymidylate synthase is, in this regard, an example of how different pharmacologic strategies can be developed with the aim to fight pharmacoresistance, one of the most troubling elements known in pharmacology, especially in the oncologic field. Its features allow for different approaches to be developed. Whether a dissociative inhibitor, a stabilizer of the inactive conformer, or rather a derivative molecule of drugs known for their past efficacies, new strategies need to be developed not only to surmount this issue, but to ameliorate the conditions of patients tout-court.

Whilst some important information has surfaced thanks to structural studies on hTS, much more needs to be uncovered in this sense. Little to no information is currently known about the molecular mechanisms at the base of the active – inactive transition process, and vice-versa. Such information could translate into the identification of more potent and influential target residues or loops, resulting in an increased efficacy of new pharmacological approaches.

Given the potential role of these mechanisms in the pharmacology, it is paramount that the information gathered reflect different properties of the target element. This may be achieved by improving the current experimental background with the aim of including

such information to build a model which progressively resembles the real molecular behavior in the human body. Within this context, information coming from thermodynamic and spectrophotometric techniques can contribute to the definition of a better behavior model. The advantage of said techniques is one where, with the right setup and analysis model, parameters and information, like the fluorescence emission of tryptophans and tyrosines or the thermogram associated to the titration with a specific molecule, can be translated into structural information to be added towards building a better molecular model.

Another rather important advantage of these techniques is that once a parameter has been chosen – may it be an endothermic contribution in a thermogram or the emission spectrum of tryptophans – with the right instrumental setup, any change to said parameter can be followed and recorded in real time.

In such a vast context, the aims of the thesis, whose work is in part contribution of an AIRC Project "Protein-protein interaction inhibitors of thymidylate synthase against colorectal cancer" (AIRC2015-IG16977) can be summed up in three key elements:

- introducing changes to existing protocols, leading to improvements in the quality of the data obtained from the experiments described
- describe how different inhibition strategies led to the development of different molecules and how the information gathered from testing them may impact the pharmacoresistance issue.

- explore the role and contribution of thermodynamic and spectrophotometric techniques in building models that may represent a step forward to explain currently unknown molecular mechanisms of human thymidylate synthase.

Page intentionally left blank

Chapter 2 – Results and conclusions

2.1 Methodological advances

2.1.1. Protocol improvements allowed for increases in the experimental quality

In the three years of this Ph.D. project, many different challenges have been overcome. Some coming from the experimental setups, some other from the understanding of the processes underlying the experimental data. In the discovery process that is the work of research, evolving methods and integrating new and improved ways to achieve a better result should always be the main objective.

Within this spirit, protocols presented in this thesis are the effort of tweaks and improvements. Some of these are the fruit of the collaboration with Dr. Matteo Santucci.

2.1.2. Improvements in the purification process translated into higher purified protein yields

One of the most critical steps in the making of this project was the purification process of hTS and its mutants. During the last year of the project there were some issues that prevented the purification from being successful. These issues were identified in the induction step: this process was unsuccessful, hence little protein was synthesized from the cells, with the obvious outcome of little to no enzyme purified. As the occasion arose, the protocol was subjected to some improvements.

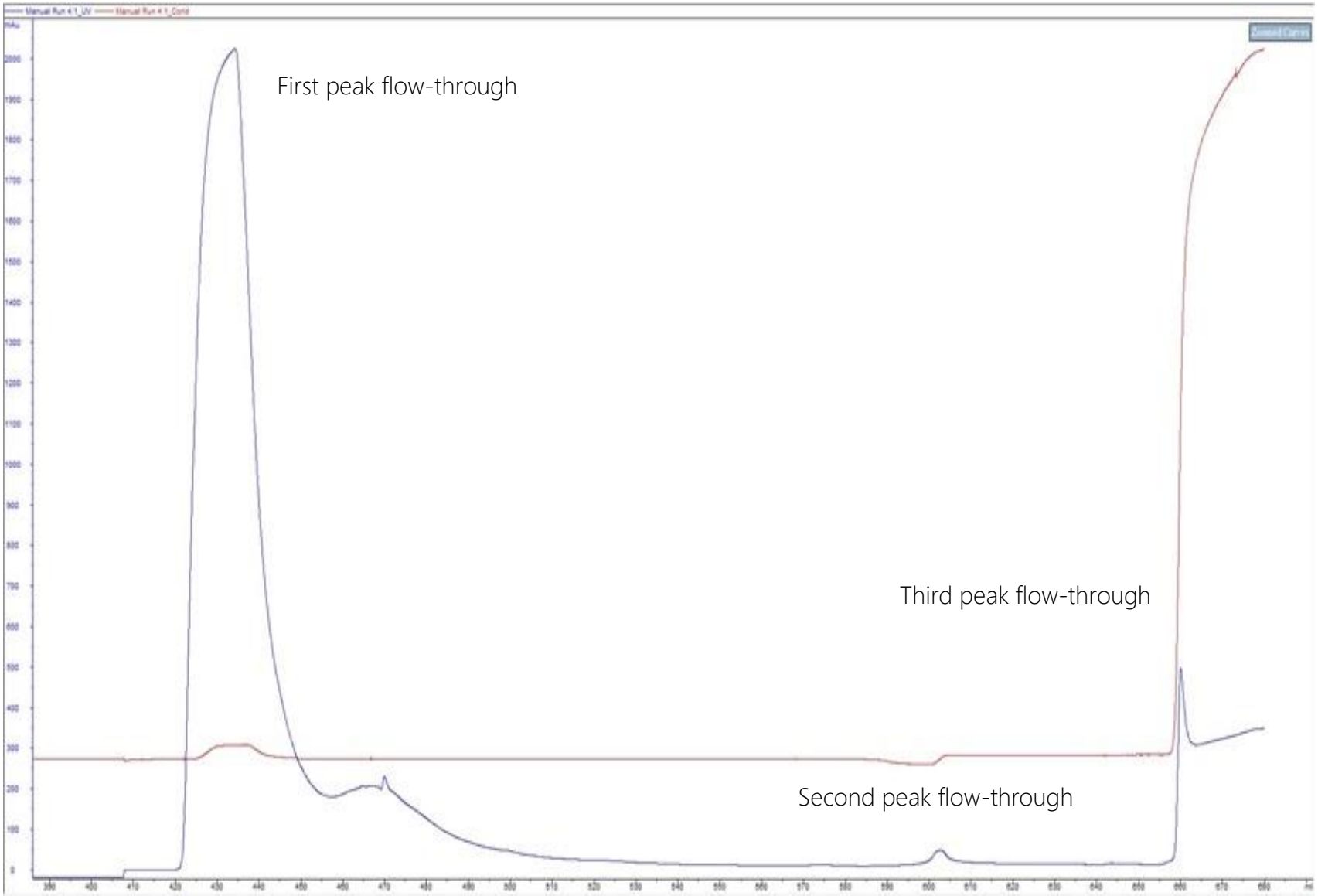

Figure 3: This chromatogram (mAu vs mL)represents a failed purification attempt. UV signal in blue, conductance in red. Third peak flow-through corresponds to enzyme elution. Its intensity is lower than usual. Spectrophotometry readings of the fractions confirmed initial impressions.

This issue was strongly tackled during the second year of the project, which lead to the decision of completely renewing all reagents and introducing more controls and improvements in the protocol.

Almost all elements of the purification process were changed. Among these, great care was put in obtaining new batches of cells and plasmids: preparations were made as explained in the protocol described in the previous chapter. One main issue was later identified as an incorrect induction process, due to a batch change in the cells lead to new cells being employed. These showed higher grow rates than the previous batch: as a result, the induction process was carried on with a very dense concentration of cells. This was tackled and resolved through checking the cell growth, making sure that the cells were induced with an optical density that allowed proper protein expression. Some attempts have been done in trying to induce to an Optical Density (OD) at 600 nanometers slightly lower (0.5) than the recommended range (0.6 – 0.8) but this process yielded little to no benefit – data not shown – hence it was discarded. In Figure 4 a brief example of the issue during the chromatography step.

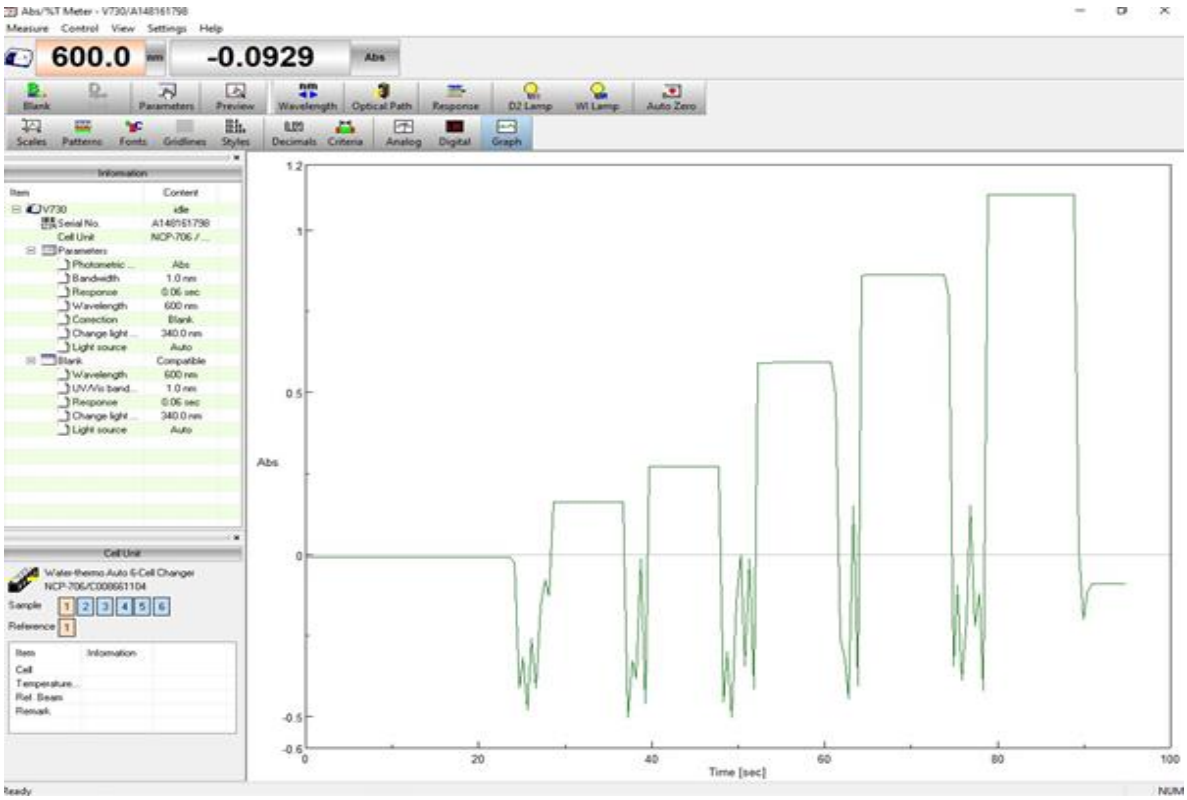

Figure 4: Example of cell culture OD measurement @ 600 nm, with the Jasco V-730 Split Beam Spectrophotometer.

Cells + fresh LB Broth volumes	ΔOD/min, 600nm
30µL + 970µL	0.16
50µL + 950µL	0.27
100µL + 900µL	0.58
150µL + 850µL	0.85
200µL + 800µL	1.12

Table 1 OD readings @ 600 nm of cell culture dilutions

Using the Jasco V-730 It was possible to obtain control over the optical density of the cell culture, as represented in both Fig. 6 and Table 1. This translated to an improved process of induction of expression.

Another major element improved was the sonication process. Due to a change of the instrument used to carry over this portion of the protocol, a new probe was used, one that better handled volumes over 10 milliliters. Moreover, the process was completely carried within the Falcon tube containing the resuspended cell culture. The new probe sonicator was also equipped with a timed program, which greatly helped in standardizing the procedure and cycles.

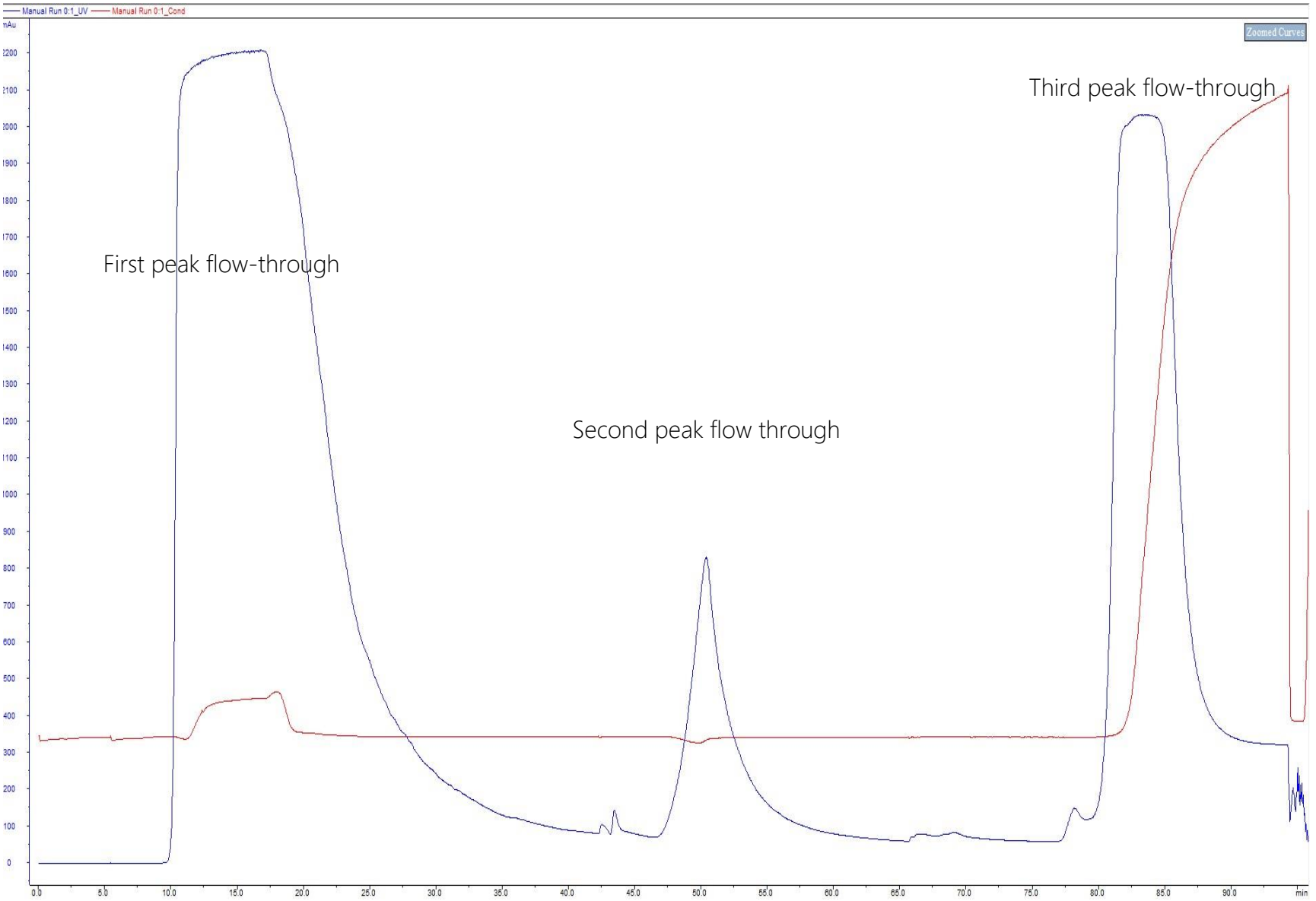

Figure 5: Chromatogram representing a purification process through the classic protocol for hTS expression and purification

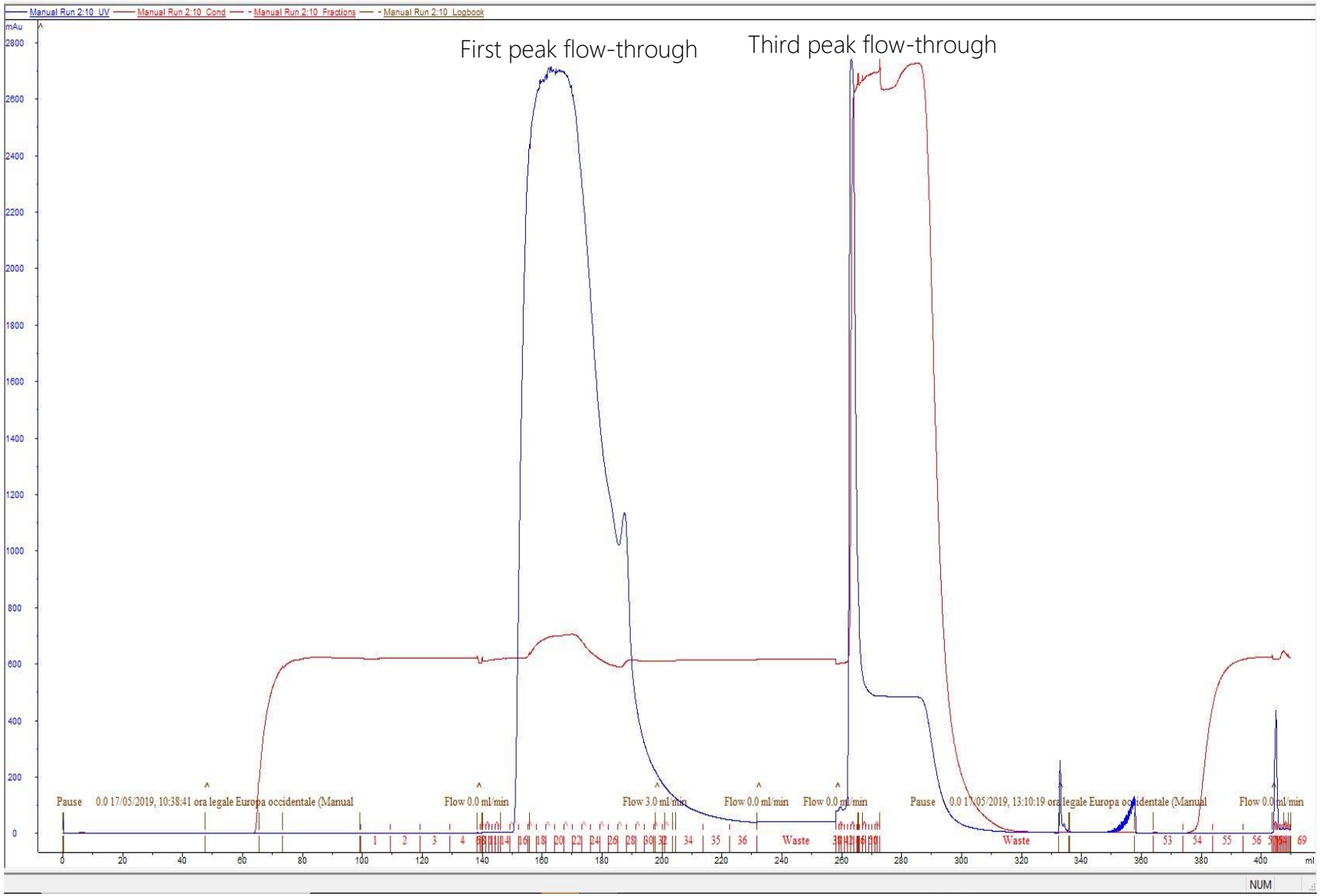

Figure 6: Chromatogram representing a purification process through the improved protocol for hTS expression and purification.

The chromatogram in Fig. 5. represents one purification process done with the old protocol, whilst the one on Fig. 6 represents one purification process completed with the new protocol. Both protocols were prepared with the same amount of cell pellet, about 12 grams.

One main difference that can be appreciated is the difference of intensity of the third peak, the one regarding the enzymatic elution. The UV detector reached quota 2800 milliAU in the latter and about 2100 in the former. In general, the minimum absorbance delta of the third peak, measured through the instrument, was around 15%, with maxima slightly over 30% increases. Spectrophotometrically, the most concentrated fractions still kept the same difference in concentration.

After the desalting passage, a great deal of effort was done over avoiding the precipitation of the protein. This phenomenon may happen for different reasons: pH not suitable for the protein to maintain its structure, insufficient ionic force of the buffer, or high molecule concentration. In particular, the latter has proven to be one of the most important points of failure of a purification process. This process can be seen whenever, on a single fraction, taking aliquots to be measured spectrophotometrically, two different results are given. A clear evidence of this happening, the deeper the aliquot is taken from the fraction containing enzyme, the higher its concentration.

The issue was easily resolved adopting two different enzyme concentration pools. This measure was already integrated in the old purification protocol. However, given the

increase in concentration obtained through the tweaking, this passage was deemed even more critical. In practice, it is a very simple measure that consists in first choosing two different concentrations, known to be devoid of precipitation issues. These concentrations were chosen on the premises of the experiments to be conducted in a later phase. Experiments with the ITC for example, required somewhat a higher concentrated aliquot than experiments regarding inhibitor testing. With this element in mind, the higher concentrated fractions were united with the lower concentrated ones, in order to reach said target concentrations. Aliquots volumes have also been prepared as a function of the experiments that would have been conducted after the purification, avoiding waste of purified protein.

2.1.3. Purified enzyme in a phosphate free buffer retains its catalytic activity

As previously reported in the "Materials and Methods" chapter of this thesis, human Thymidylate Synthase was also purified in a phosphate free buffer.

The original purification protocol allowed the enzyme to be purified in a buffer containing sodium phosphate monobasic (NaH_2PO_4). Once in water, sodium phosphate is still able to disassociate and free phosphate ions (PO_4^{3-}). The disassociation of the molecule regards first the sodium ion:

$$NaH_2PO_4 \rightleftarrows Na^+ + H_2PO_4^-$$

The disassociation process continues with the hydrogen ions,

$$H_2PO_4^- \rightleftarrows H^+ + HPO_4^{2-}$$

$$H_2PO_4^- \rightleftarrows H^+ + HPO_4^{2-}$$

a process that leads to the liberation in water of phosphate ions. As described in the introduction, these ions are capable of switching the active – inactive equilibrium towards the inactive conformer. As this may be considered a bias in the experiments delving into the structural investigation, the situation required the enzyme to be purified in a phosphate free environment.

The buffer of choice came from previous attempts in the laboratory. The evolution of the protocol, however, was not so direct. The first attempts done in this sense were to dialyze the protein in a phosphate free buffer. An example can be seen in Fig.7.

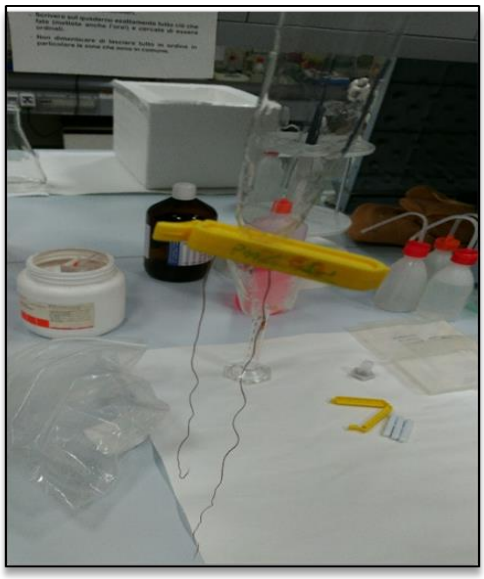

Figure 7: Representation of a dialyzation attempt of hTS in a phosphate free buffer

The dialysis was considered to be a safer alternative to a head-on approach to purification with the new buffer, as there was no assurance that the new buffer would have led the enzyme to remain in solution. An aliquot of enzyme was taken, the concentration spectrophotometrically assessed before the dialysis process – data not shown – and then let to be dialyzed overnight. This process was done overnight, at +4°C, in agitation.

The results of this first attempt were poor at best. After a couple of trials, the general understanding was that the process was not completely satisfying; issues and drawbacks mostly concerned the safety of the purified protein. Suspicions were confirmed the next day, as the spectrophotometric assay of the dialyzed protein led to believe there has been a decrease in concentration.

Whilst disappointing, dialysis results did not highlight, however, precipitation of the protein once the buffer changed, nor the decrease in protein concentration could have been associated with such a process. This led to at least entertain the idea of approaching this new buffer change with an entire purification process. Buffers were prepared following the same idea of the previous ones: three buffers, at different imidazole concentrations (0, 20 mM and 1 M). Buffers were prepared and filtered following exactly the same protocol reported in the previous chapter.

Protein expression was conducted following the same protocol reported in the Materials and Methods section. The only noteworthy difference was that at each passage where the

cell pellet resuspension was required, this was done using the phosphate free buffer, in place of the usual one. The purification protocol was also conducted directly using the phosphate free buffers. Towards the end of the purification process, after the desalting process, the fractions with the lowest concentrations were kept away to check their concentration and confront their value with the ones obtained with the canonical buffer.

Hence one aliquot of said purification was employed to test for concentration, activity, K_m and K_{cat} measurements. The first two were conducted on the Cary 100 UV-Vis spectrophotometer: the former with Suprasil Quartz Hellma Cuvettes, reduced light path, the latter two with Kartell™ Spectrophotometry Polystyrene Cuvettes, reduced light path and the Jasco V-730 UV-Vis split beam spectrophotometer.

Fig.8 represents one such attempt in concentration

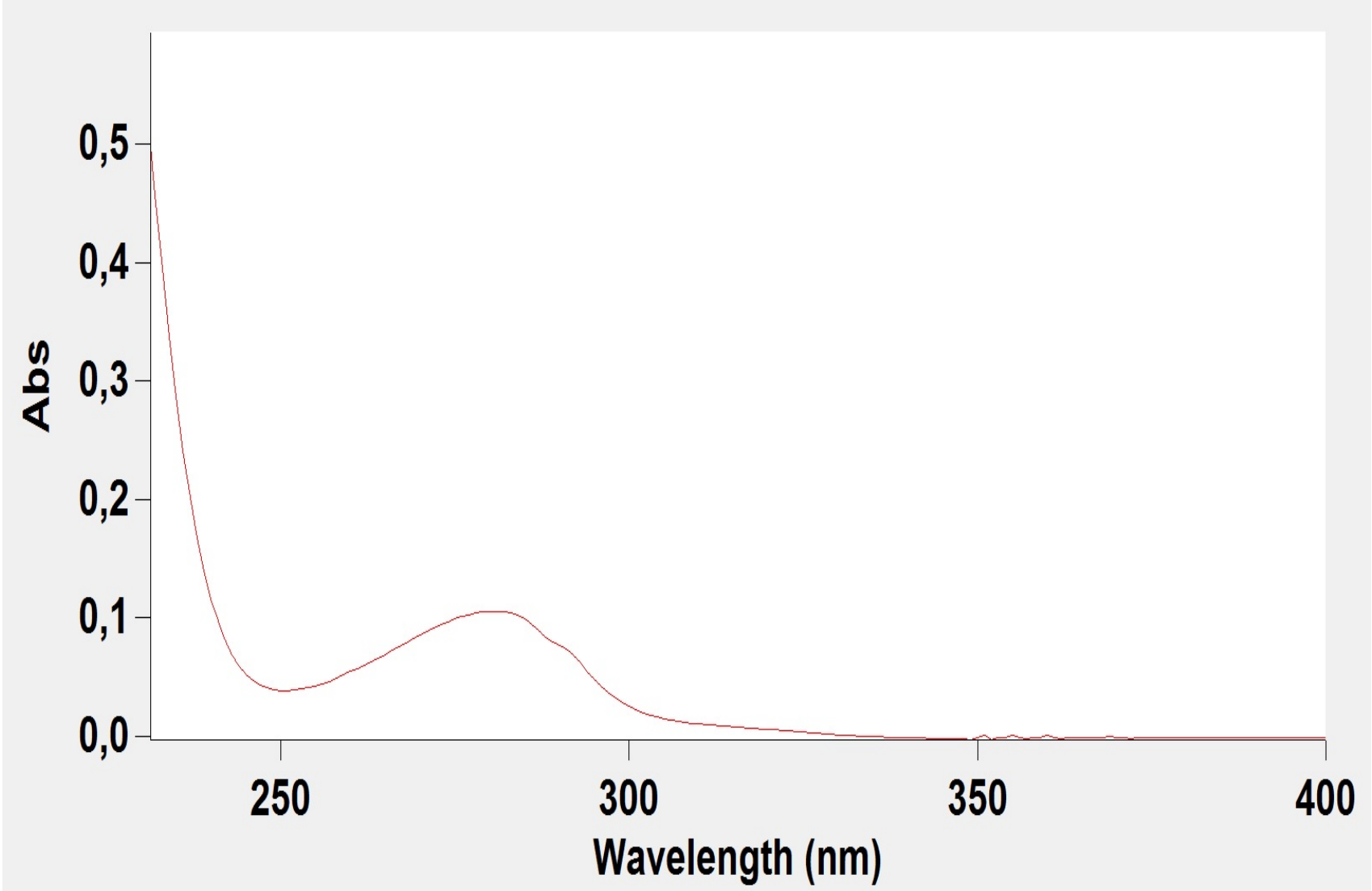

Figure 8:Absorption spectrum of one purified fraction of hTSwt enzyme in phosphate free buffer. The spectrum was obtained by diluting an aliquot of the fraction, In the case being, 50 microliters of the original fraction were taken and diluted in 800 microliters of the same phosphate free Buffer 1. The reading at 280 nanometers was around 0,11.

To obtain the concentration, this value is divided for the molar extinction coefficient of the dimeric enzyme, 87780 L/mol x cm.

$$\frac{0{,}11}{87780\ \frac{L}{mol \times \cancel{cm}} \times 1\ \cancel{cm}} = 1{,}25 \times 10^{-6}\ M$$

This value needs to be multiplied by the dilution factor:

$$\frac{800}{50} = 16\ ;$$

$$1{,}25 \times 10^{-6}\ M \times 16 = 2 \times 10^{-5}\ M = 20\ \mu M$$

Hence, the concentration of the fraction was 20 micromolar. Once the concentration was obtained, the next step was to assess the enzyme activity in the new buffer. This step is required every time a new enzyme batch is purified. This is done in addition to all other tests, to ensure that every purified batch contains an enzyme that is actually working as intended. The test was conducted as reported in the Materials and Methods section: the enzyme (final concentration 300 nM) is added in an excess of substrate (10 times the K_m) and co-factor (10 times the K_m). TES buffer as half of the volume, milliQ to bring up to volume. The kinetic assay is observed over a 180 seconds time interval. The V_{max} was calculated from the Michealis – Menten plot as the slope of the tangent to the initial portion of the curve.

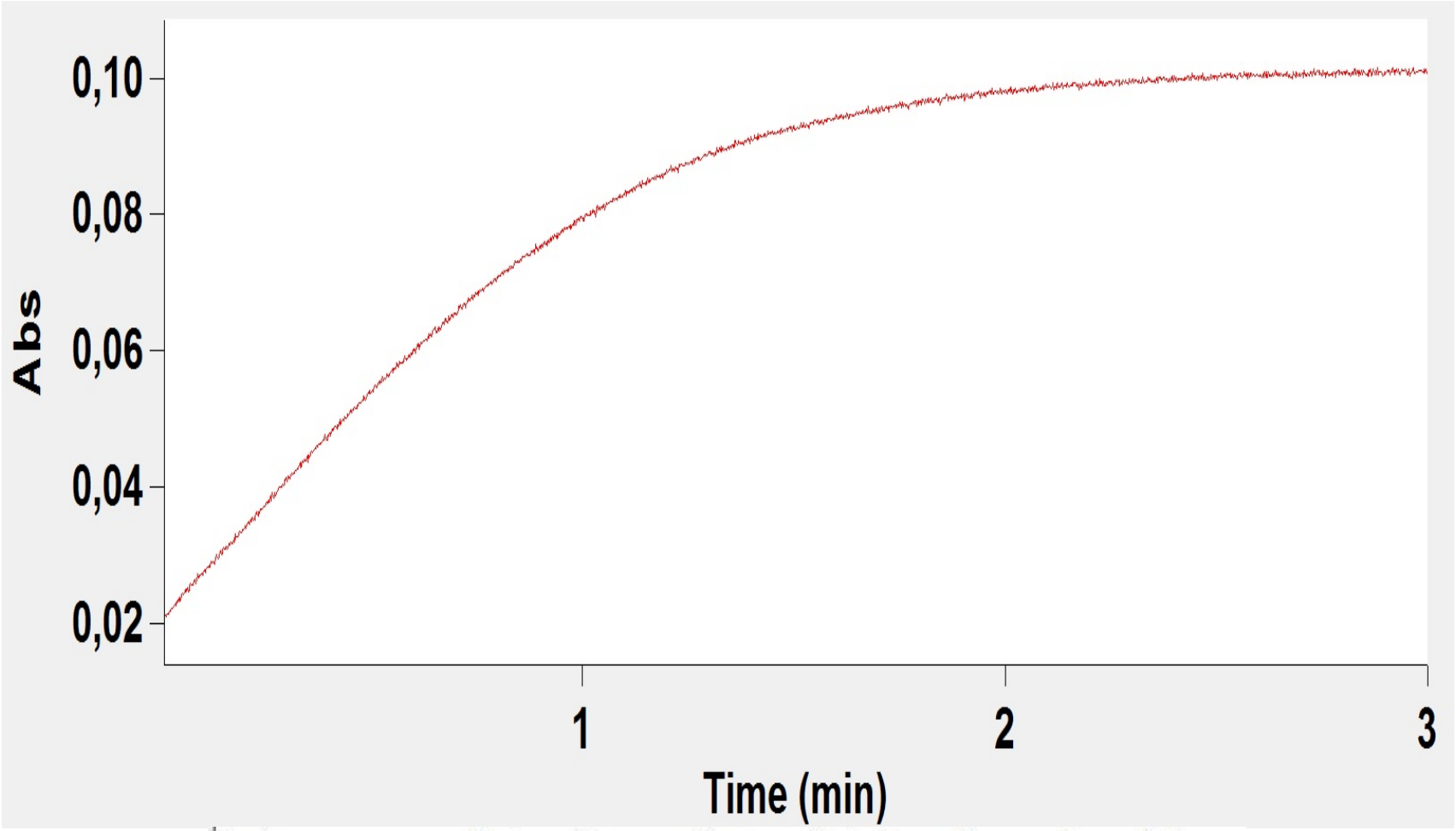

Sample	Start (min)	Stop (min)	Slope (Abs/min)	Factor* Slope	A Start	A Stop	S.D.
Sample 1	0.000	0,500	0,0680	0,0680	0,0203	0,0538	0,0003

Figure 9: The image shows the result of the enzymatic assay. The Cary 100 Win UV software automatically calculates the value of the slope given the time interval.

In the case being, the time interval was set for the first 30 seconds of the reaction. This time interval was chosen as it represents the linear phase of the enzyme activity. Enzyme activity in the phosphate free buffer, was comparable with the activity in the canonical buffer.

The enzyme purified in the phosphate free buffer has comparable activity to the same purified in the canonical one.

As per protocol, the following step was to assess the Michaelis – Menten constants for mTHF and dUMP. Tests were conducted with the Jasco V-730 UV-Vis Spectrophotometer, as it had the optional 6 cuvette holder, which would have allowed a single multirun to be executed.

Sample preparations were conducted as per protocol, explained in the Materials and Methods section. Six cuvettes plus a control were prepared, with different concentrations of either dUMP or mTHF, depending on the Km measured, whilst keeping fixed the other concentrations. The reaction is then started by adding up the final reagent, depending again on the constant that is being measured. In this case, polystyrene cuvettes were employed, as the measurements were conducted at 340 nm.

As in the general enzyme activity test, kinetics was observed for a period of time of 180 seconds. From each curve, the maximum velocity was taken and then graphed vs the concentration of either the substrate or the co-factor, as usual depending on the constant

being measured. Figure 10 represents one such reading attempt; Figure 11 the determination of the V_{max} value

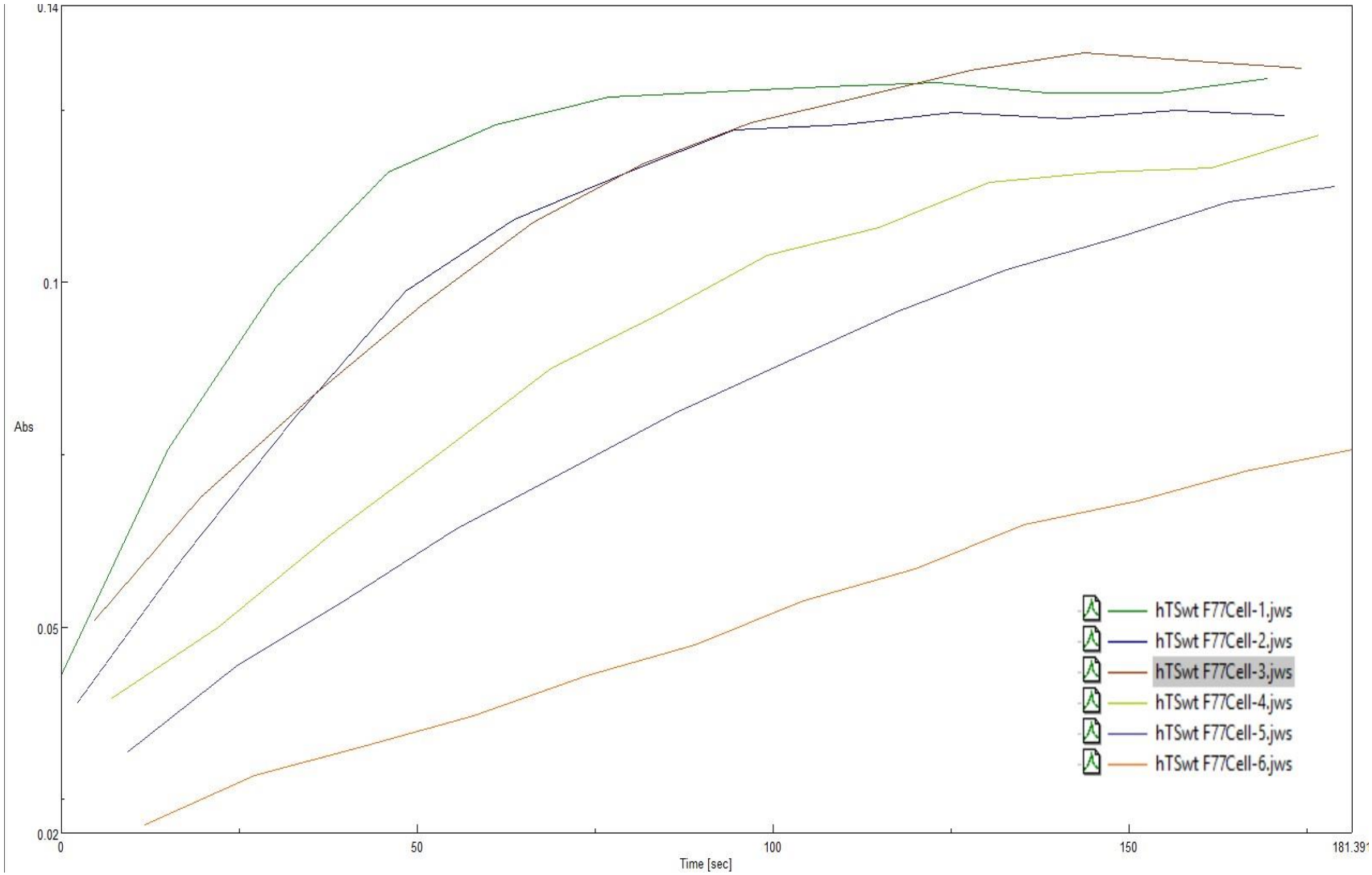

Figure 10: This image represents the final result given by the instrument as the run is terminated. Each curve represents the product synthesis, with different concentrations of the limiting reagent. The Spectra Analysis companion software allows for the single speed values to be had, by tracking directly the tangent to the curve, through the "Enzymatic" function button, as shown in the next image.

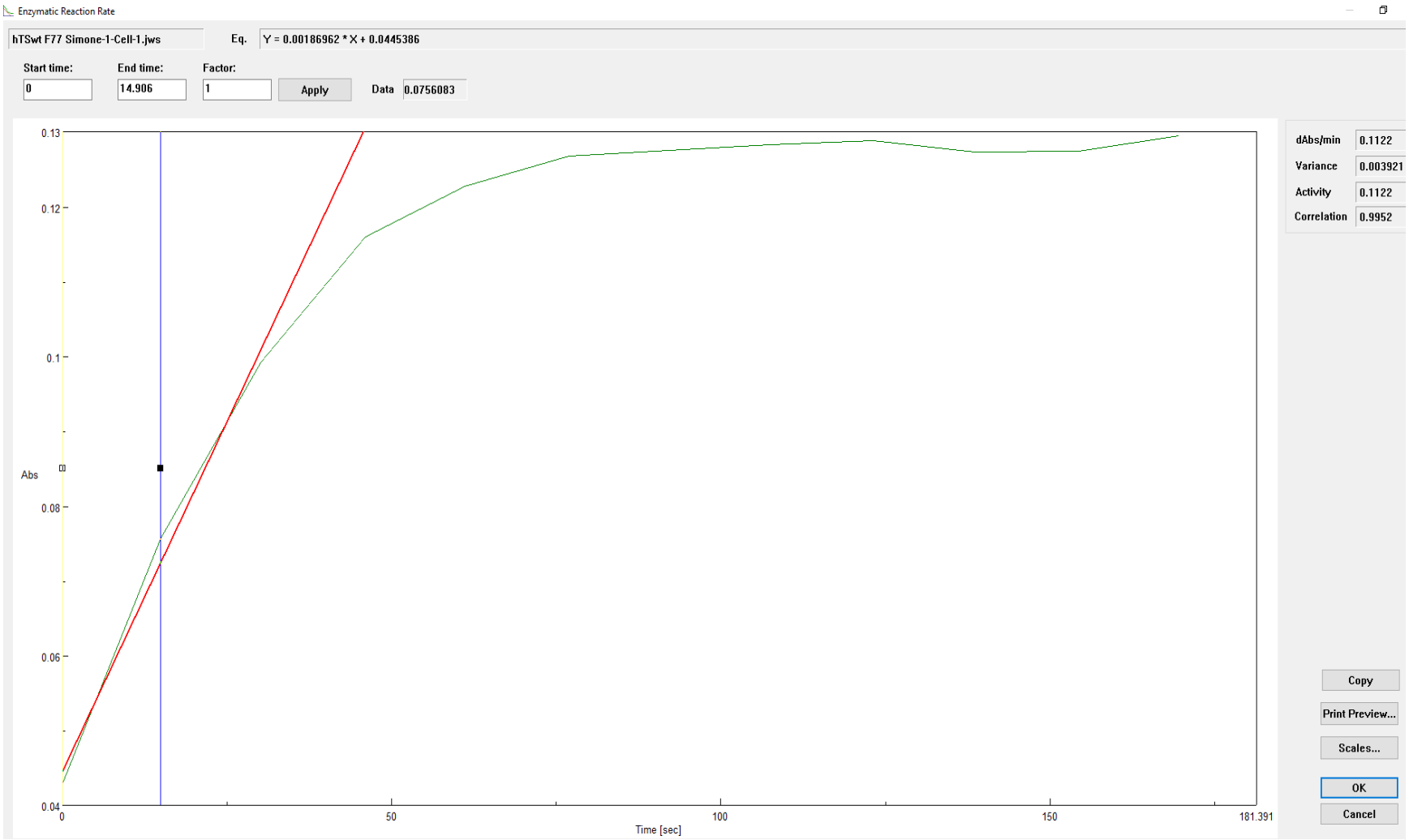

Figure 11: The two blue lines represent the starting and ending point for the software to draw the tangent to the curve. Due to hardware drawbacks, runs containing multiple samples will have a limited amount of points. This is due to the fact that the system has to cycle through each cuvette sample: one cycle usually takes about a dozen seconds. This is the time interval from one point to the other on the graph, corresponding to the time interval that the system needs to read two different points on the same cuvette sample.

This time interval has a minimum value that depends on the amount of cuvette samples that compose the run. The higher the cuvette amount, the higher this minimum time becomes.

The blue lines in the "Kinetics" software, hence, move "time-wise" allowing one to choose the start and finishing time of the linear portion of the reaction. With this, the software also calculates in real time, based on the given interval, both the dOD/min ratio and the correlation factor between the tangent (the red line) and the selected portion of the kinetic assay.

The dOD/min ratio is the parameter collected for each curve. This data is the reported in a dOD/min vs concentration of limiting substrate. The K_m is the concentration of limiting substrate corresponding to half the maximum speed of conversion. The same protocol was applied to the Km vs dUMP. Results obtained were comparable with the data obtained in the canonical buffer.

K_{cat} was also assessed as per protocol, as presented in the Materials and Methods chapter. In this case, the limiting element for the reaction is the enzyme concentration. Samples were prepared as described in the previous K_m section. As this test would require a multirun to be had, the instrument used was the Jasco V-730 UV-Vis split beam spectrophotometer. Samples were prepared with a concentration of substrate and co-factor equaling 10 times their respective Km, to reflect the situation where the only limiting factor in this case is the enzyme concentration. The data was acquired with the same

method reported in the previous section. In this case, the graph plotted will be Vmax vs enzyme concentration. The slope of the fitted linear trendline will be equal to the turnover number. The turnover number of the enzyme purified in the phosphate free buffer was comparable with the one obtained with the purification of the same in the canonical buffer.

As the results obtained with this buffer were satisfactory, the same process was applied to the mutant used in structural experiments of the thesis, the hTS W182A. As reported in the Materials and Methods section, the adopted protocol for expression and purification was identical to the wild-type enzyme.

Mutant yields, however, are sometimes quantifiable as fractions of the wild-type molecule. This may be due to different issues that have their own weight in the final concentration. Among these issues, a critical one is the mutant structural deviation from the wild-type molecule. Mutations are usually introduced within a relevant target to assess the presence of amino acidic residues that are most critical for either maintaining the tridimensional structure, and/or for the function of the molecule. Such an in vitro process does not come, however, without its share of issues. The mutant, for example, may have different expression conditions than the wild-type, or the deviation from the wild-type structure may render it a target for protease enzymes. Another rather important element is that the structural deviation may render either impossible its purification, especially if said mutation heavily disturbs the tridimensional structure; this is especially true for multidomain molecules. Another element of disturb may be the fact that the structural deviation due to

the mutant presence may lead this to a stronger bind to the non-soluble fraction of the cell pellet, once sonicated.

Hence multiple aspects need to be accounted for, whenever a mutant is purified. In the case being, the W182A mutant is within one such case. The concentration of the purified molecule was less than one fifteenth of the usual wild-type yield.

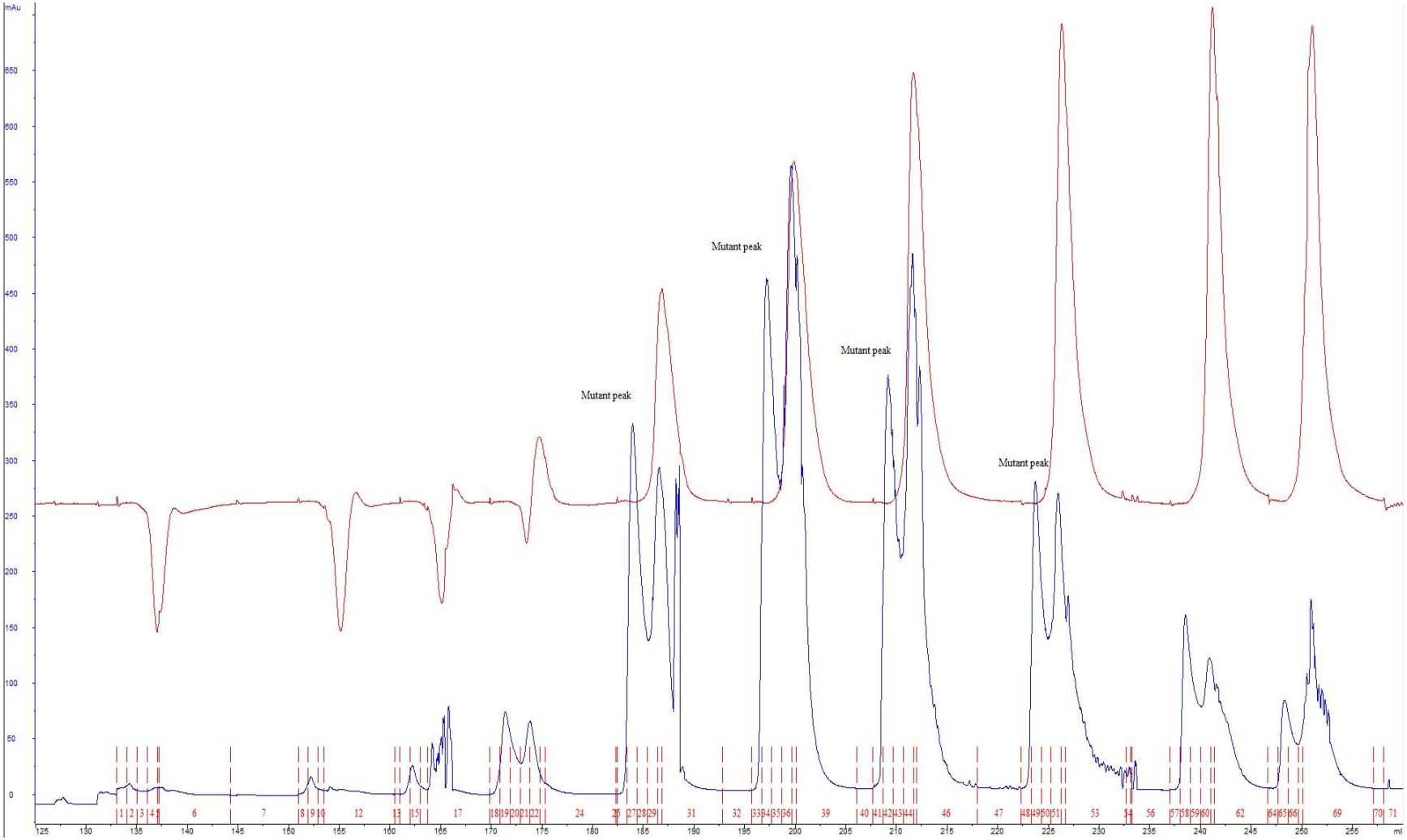

Figure 12: This chromatogram represents the desalting phase of the W182A mutant purification. Mutant peaks have been highlighted: each desalted fraction is composed of at least two peaks: the protein is eluted first, and then right after, the imidazole salt is eluted. The desalted process was carried out as described in the Materials and Methods section of this thesis. As the chromatogram shows, the general UV measurement for the peaks containing the mutant are nowhere near the values obtained from the wild-type purification.

The spectrophotometric assay – data not shown – confirmed the chromatogram data. The highest value obtained was still less than 10 micromolar, about 1/20th of the wild-type yield. K_m and K_{cat} assays. Prof. Glauco Ponterini confirmed that the constants of the mutant in the phosphate free buffer were comparable with previous results obtained in the canonical buffer. Data from spectrophotometry and the kinetic assay seem to support the idea that the mutant was successfully purified in a phosphate free environment, whilst retaining its enzymatic features.

2.1.4. Conclusions

The first aim of the project was to improve the current protocols, in order to enhance the quality of the experiments and to ease up all involved processes.

The importance of this step was due to the fact that progress and research do not shy away from the eventual improvements of established protocols. This process aims to streamline the procedure, decrease points of failure and time needed to complete tasks, improve safety. In addition, as the need for better buffer solutions were required, attempts have been made to retrieve previous protocols to improve them in order to fit the current needs and necessities.

The effort to improve protocols has brought increases in yields of the purified protein. These increases however, have highlighted a point of failure given by precipitation due to high concentration. Hence, measures have been employed in this sense to safeguard the purified molecules, by improving in the process of pool concentration to avoid

precipitation. The new protocol was easily adopted by laboratory students, with satisfactory results. The chromatogram on page 112 is one such example, working independently on said protocol.

Thus far, the improvements have allowed to a better overall process of purification and aliquot stocking.

This process cannot be considered over. Improving should be something to aim at in the daily laboratory practice, whether it be on new algorithms for data analysis, better handling of reagents or any other situation aimed at relieving stress on the operator. Future improvements on this process may come from adopting a different purification protocol that may allow a single-step purification process. These are currently available, improving both the time and the general quality of the purified product.

Another rather delicate point of view is the amount of time required from the beginning to the end to carry over the purification protocol. This was another element that was tackled during the optimization process. The whole process, devoid of any errors, takes about 4 to 5 working days. About half of this amount of time is required to obtain transformed BL21(DE3) cells with the pQE-80L plasmid – about two days – Hence, one of the points that was subjected to improvements was to start the purification process directly from cells that were already transformed with the required plasmid. This would decouple the transformation element from the expression induction and the purification. The amounts of benefits to be had from this were multiple.

- For once, decoupling the two elements would allow to sensibly shorten up the purification process to a 2-3 days' work. This translates to less work pressure during the week.
- If the concentration of the transformed cells were to be standardized to the final broth volume, this would ease the process to get to the OD target at 600 nm. In this way, aliquots would be thawed based on the liters of broth to be had in the final scale-up step. As the later steps in the purification process remain the same, this would also lead to less fluctuations in the final enzyme concentration between purification instances.
- Ready to use, transformed cell aliquots would also limit the amount of manipulation of cells and plasmid, decreasing chances of contamination, especially from first time users.

This process was still in the making of the last quarter of the third year of the project.

As this may be seen as a long-time process, one that would not require much time would be centrifuging the samples to eliminate the imidazole salts. This would pose another point of failure however, as centrifugation is known to aggregate molecules, improving chances of precipitation. Particular care in setting up a protocol like this could mean a decrease in the time required to complete purification, improving nonetheless the working conditions.

2.2 Innovative inhibition strategies may help fight pharmacoresistance

The second aim of the thesis was to present different pharmacological approaches that have been delved into during this project.

As reported in the Introduction chapter of this thesis, human thymidylate synthase is a renewed anti-tumoral target, due to its unique function in the DNA synthesis.

As this target is overexpressed in tumor cells, efforts have concentrated over the inhibition at the active site. This was initially achieved through molecules that mimic either the substrate or the co-factor. Their binding, however, has higher affinity for the enzyme than their original substrate. Such a binding stabilizes the dimer conformation, which is an issue in itself. This is due to the double role of the molecule: while the catalytic activity is exclusive to the dimer, the monomer has been reported to bind its own mRNA as well as those of c-Myc and p53. This process is known as negative feedback mechanism, and it's one where the binding avoids the synthesis of new protein molecules.

Hence, stabilizing the dimer conformation leads to an imbalance between the two, a situation that, for different causes, brings the tumor cell to synthesize new TS molecules, about 4 times more than non-treated cells. This is one reason that brings more and more articles in literature to conclude that the pharmacoresistance phenomenon is just at its beginning.

This calls for different and innovative inhibition strategies, that may help introduce new models of inhibition not only for TS, but also for many more molecular targets of pharmacological interest.

In particular, three different inhibition mechanisms have been presented.

- The first mechanism is represented by molecules which aim to bind at the monomer-monomer interface, creating a steric clash impeding the correct closure of the active sites, which in return, would disassociate the dimer into its monomeric elements.
- The second mechanism is represented by octapeptides which aim at inhibiting hTS by stabilizing its inactive conformer. This would allow for the dimeric conformer to "naturally" disassociate into its monomeric components.
- The third mechanism is represented by a derivative of methotrexate, modified with a photochromatic moiety that allows its thermodynamically stable conformation to be inactive. Light is capable of activating the molecule, giving it a spatiotemporal control over its activity. A "proof-of-concept" mechanism to allow a safer delivery process. This may represent a way to limit one of the most important drawbacks of current pharmacological treatments, side effects.

2.2.1 hTS dissociative inhibitor data encourage the exploration of a novel inhibition pathway

One of the mechanisms presented in the Materials and Methods section regarded a class of molecules whose ability to bind at the monomer-monomer interface constitutes an innovative inhibiting strategy for hTS.

The aim of these molecules is one where they tend to weaken intermonomer interactions thus favoring dissociation of the active dimer into inactive monomers. These molecules were synthesized in Prof. Maria Paola Costi's group based on previous works on inhibitors mimicking the monomer-monomer interaction interface of hTS. From this work, a promising scaffold was found.

To sustain the idea of binding at the dimeric interface, a computational model was prepared, which seemed to highlight a pocket interface delimited by three different residues, R175, R64 and Y202, the latter being the most important residue for the binding event. This residue is tridimensionally close to another one, F59, of the opposite monomer. In short, this residue with the Y202, created a stacking interaction between the two phenyl rings. The scaffold was capable of mimic the Y202 ring, hence interact with F59, perturbating the dimeric structure.

As attempts at obtaining the X-ray structure of an hTS-inhibitor complex proved unsuccessful, a panel of hTS mutants were created to assess the efficacy of these dissociative inhibitors in perturbing the dimeric structure of these single-amino acid

mutants and explore the role of specific residues at the interface in the protein/inhibitor binding interactions. K47A, F59A, L198A, Y202A, Q62R and T251E were all tested to understand if these inhibitors effectively decreased also their catalytic activity.

Within this context, this thesis work supported experiments conducted by Dr. Matteo Santucci and Prof. Glauco Ponterini, collaborating in expressing and purifying K47A and F59A mutants, as well as conjugating with probes the two aforementioned mutants and the wt hTS enzyme.

2.2.2. Enzyme purification and FRET experiments

The process of expressing and purifying the mutants was conducted as a collaboration with Dr. Matteo Santucci. As explained in the "Materials and Methods" section, this was done according to the same protocol adopted to express and purify the wild type enzyme. This was possible thanks to multiple elements: mutants were expressed with the same His-tag as the wild type, for once. This allowed to make sure that the expression conditions and the purification process was maintained from the wild type enzyme to the mutants.

K47A yield, as documented in the following chromatogram (Fig.13), was comparable to the wild-type enzyme, in according to previous purification instances. The chromatogram only shows the desalting process, whose yield was over 70 micromolar of protein on the most concentrated peaks. Following the purification attempt, constants K_m and K_{cat} were measured and resulted comparable with previous instances (16.7 μM and 19 μM for mTHF and dUMP respectively, and 0,65 s^{-1}). F59A was also successfully purified in the same

buffer, albeit with a lesser yield when compared to F59A and the wt enzyme – data not shown – and its K_m and K_{cat} measured (13.86 μM and 11.22μM for mTHF and dUMP respectively, and 0.4569 s^{-1}, roughly half of the hTSwt enzyme).

Following the purification, the wild type hTS and its mutants were conjugated with fluorescein and tetramethylrhodamine maleimide. As reported in the Materials and Methods, once completed, to purify the functionalized protein, the mixture was chromatographically separated via size exclusion. The chromatogram of Fig.13. represents the result of this process for the hTSwt enzyme. This process outputs 3 peaks, the first containing hTS functionalized with probes, whilst the second and the third represent the co-elution of excess dUMP + MTX and probes, respectively, that did not interact with the protein.

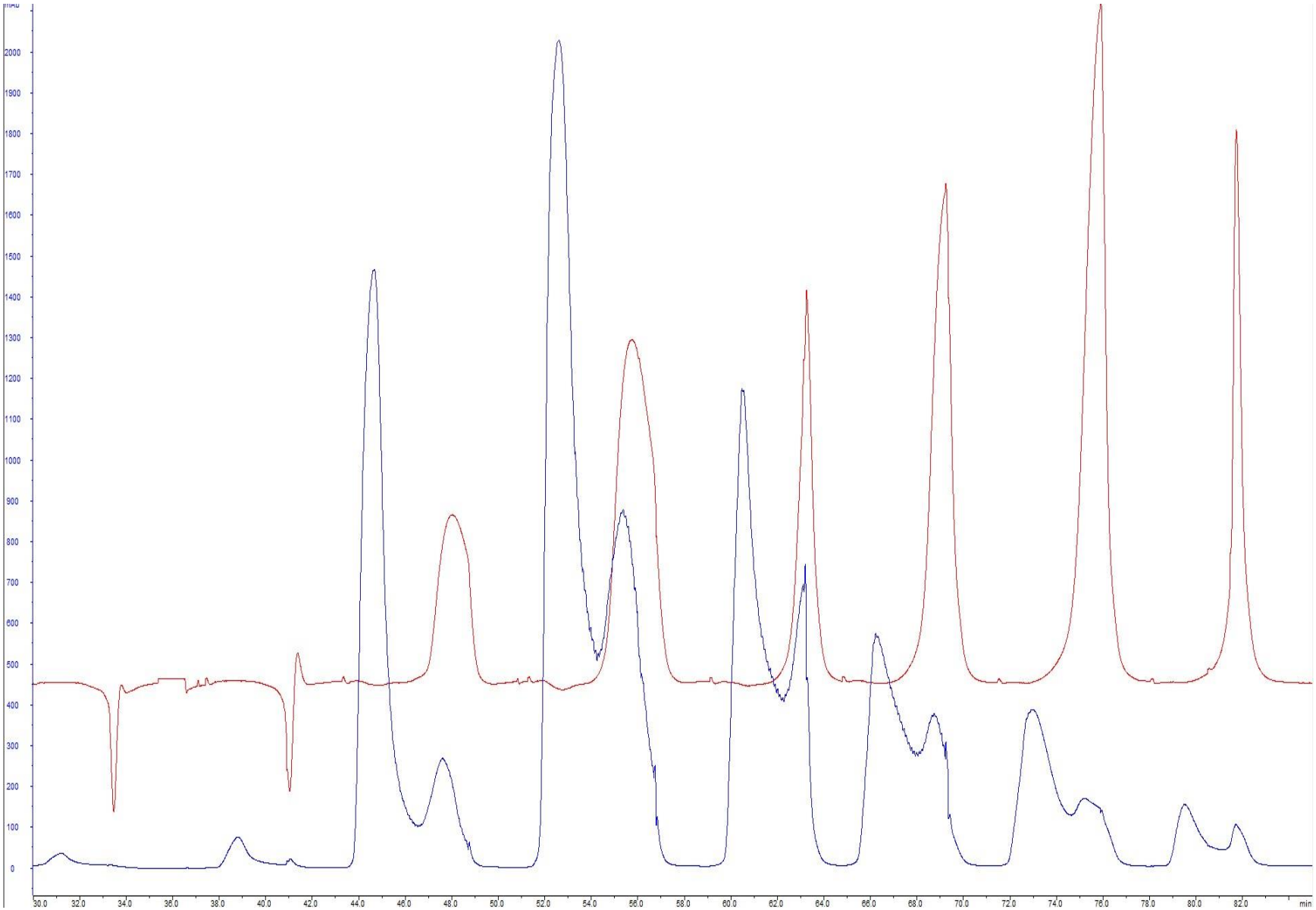

Figure 13: K47A desalting chromatogram. Yield was comparable with the wt enzyme.

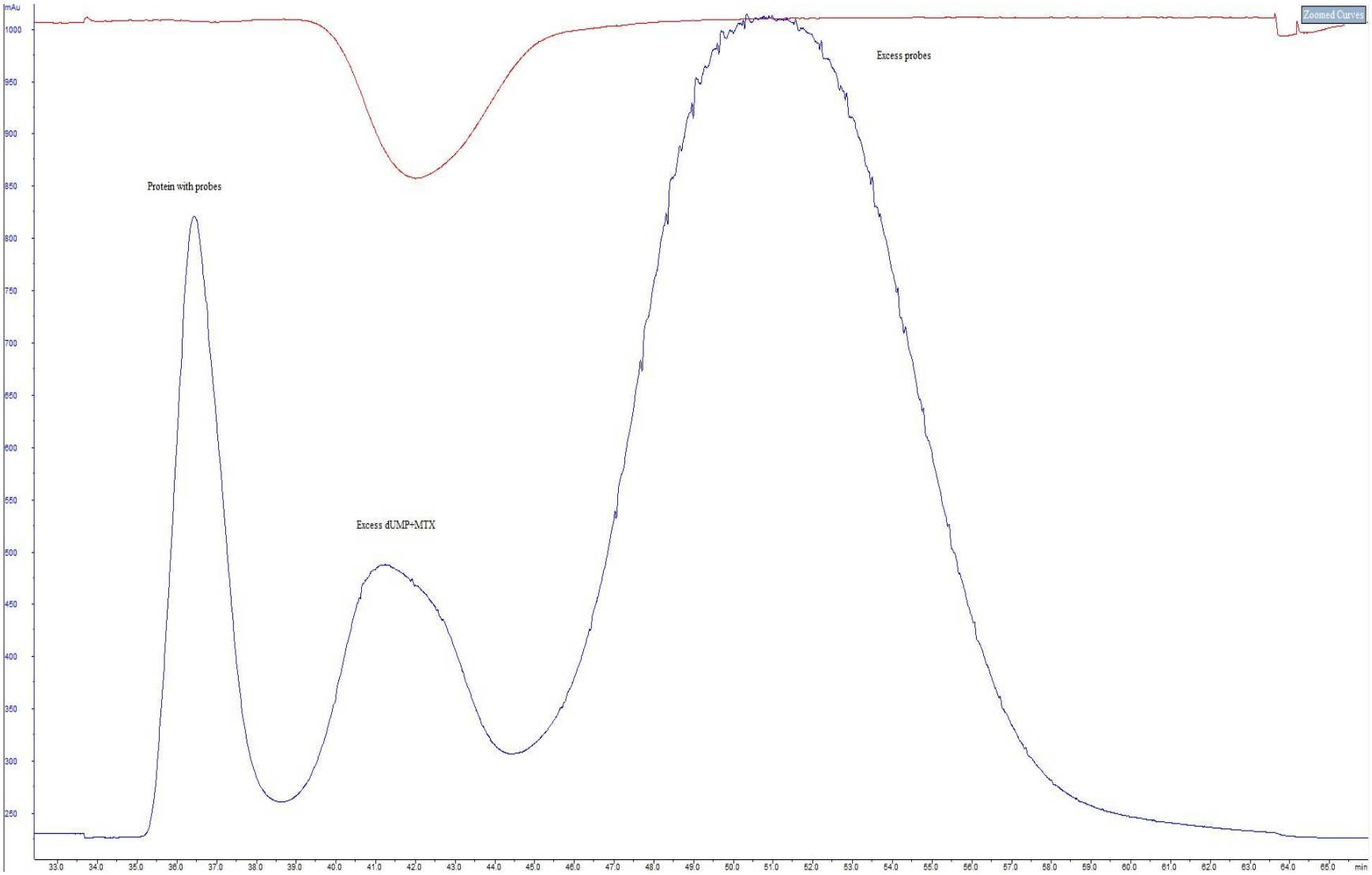

Figure 14: Desalting chromatogram of a functionalized enzyme with Fluorescein maleimide and Tetramethylrhodamine maleimide. Three distinctive peaks can be seen, the first representing the elution of the enzyme with the probes, the second representing the co-elution of excess dUMP and MTX, the third representing the elution of excess probes.

As it can be seen on Fig.14 by the blue line representing the UV signal, and as reported in the Materials and methods section of this thesis, this process requires important initial concentrations of enzyme to obtain workable concentration yields as a final result. Following this process, the absorption spectrum of the purified fraction was analyzed on the Cary-100 UV-Vis Spectrophotometer. This step has different reasons to be made. First of all, through this analysis, it was possible to obtain the concentration of enzyme and probes. This is important to check, for instance, if one of the probes has bound more protein than the other, which is important in the general context of the following FRET experiments. Another key element that has to be analyzed is the presence of dUMP in the conjugated fractions. The presence of excess substrate may lead to stabilization of hTS dimers, and for this reason, it is important that the conjugated protein fractions do not contain dUMP.

This can be checked by means of spectroscopy, as dUMP tends to form a shoulder at 260 nanometers – typical of nucleic acids. All dUMP-free fractions were subsequently taken to evaluate the potential F-T probe FRET signal, exciting the sample at 450 nm. FRET efficiency (ΦFRET) was obtained calculating the ratio between the emission intensities at the respective maximum emission wavelengths of the probes, corrected by the spectral sensibility curve of the spectrofluorometer instrument. The dissociative ability of the compounds tested was measured immediately and after incubating the molecule for one hour as a relative decrease in FRET efficiency from the value in the absence of the inhibitor.

This assay was executed via a 96 well plate TECAN GENios Fluorescence Multiplate reader, at room temperature, in duplicates, at the inhibitor concentration of 20 micromolar.

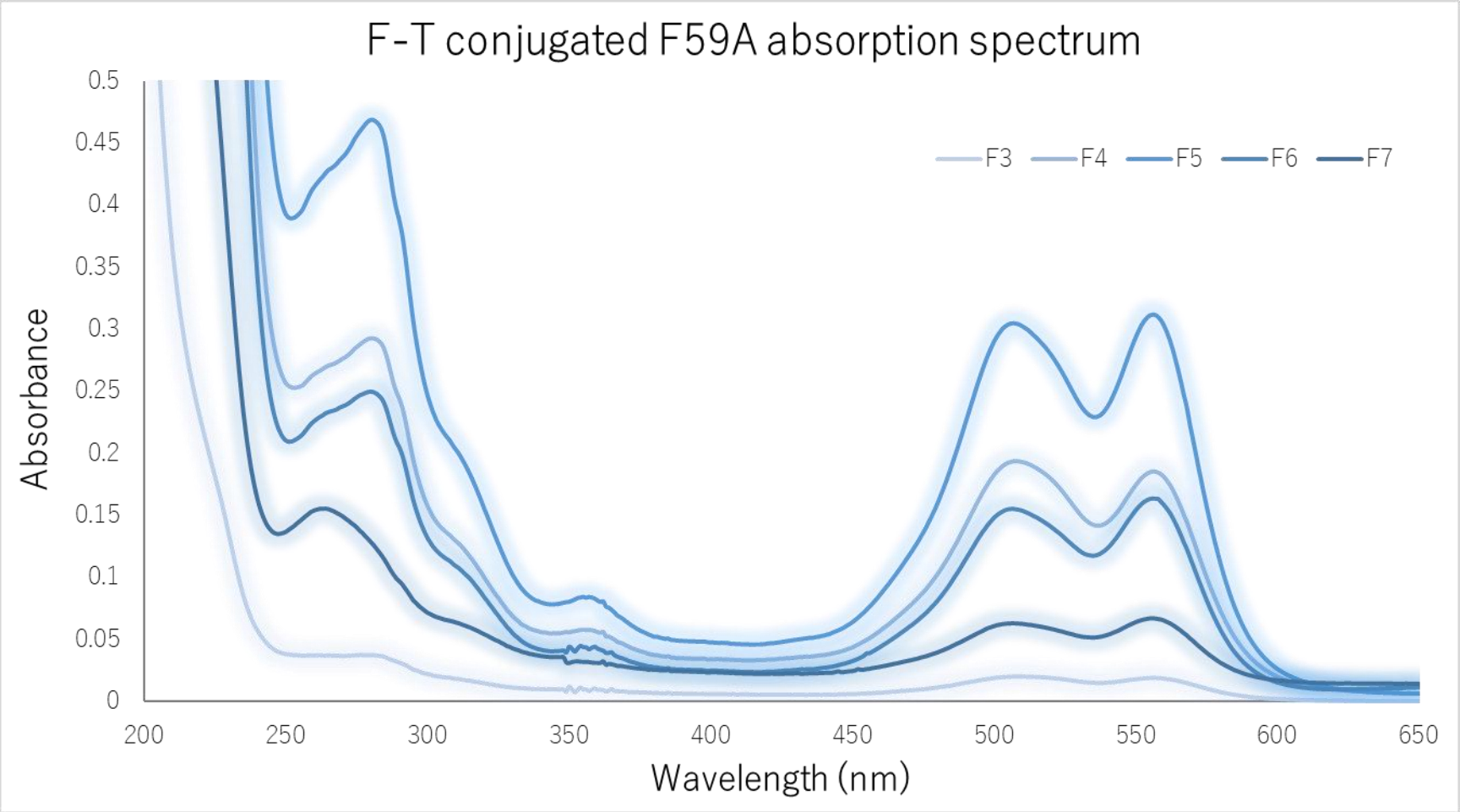

Graph 1: In the graph above, the representation of the absorption spectrum of F-T conjugated F59A fractions. For each fraction, the concentration of probes and enzyme was calculated with the following formulas: $[T] = A_{(550nm)} / 109000\ M^{-1}cm^{-1}$;$[F] = [A_{490nm} - (0.215 * A_{550nm})] / 79000\ M^{-1}cm^{-1}$;$[hTS] = [A_{280nm} - (0.75 * A550nm)] / 87780\ M^{-1}cm^{-1}$. The different contributions of the probes to the general absorption spectrum are due to the fact that Tetramethylrhodamine, for instance has a partial absorption contribution in the absorption spectrum region of Fluorescein, quantifiable to around 20%. The same consideration is to be done on the hTS concentration, where the partial absorption contribution of the Tetramethylrhodamine corresponds to about 75% of its absorption at 550 nm.

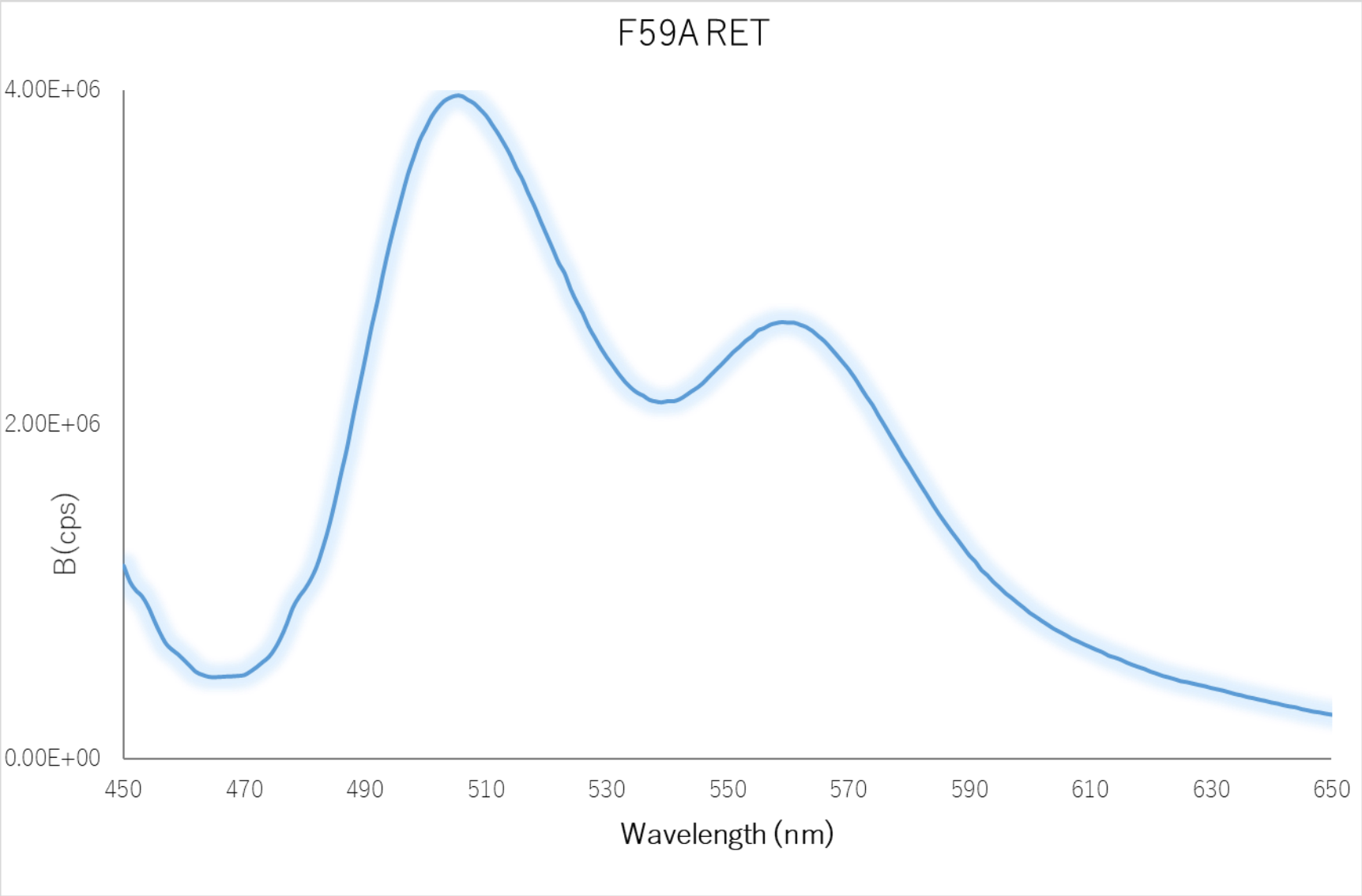

Graph 2 In the graph above, an example of a F-T conjugated fraction emission spectrum. This process was done for hTSwt, F59A and K47A – data not shown -. At this point, an enzymatic FRET value was obtained.

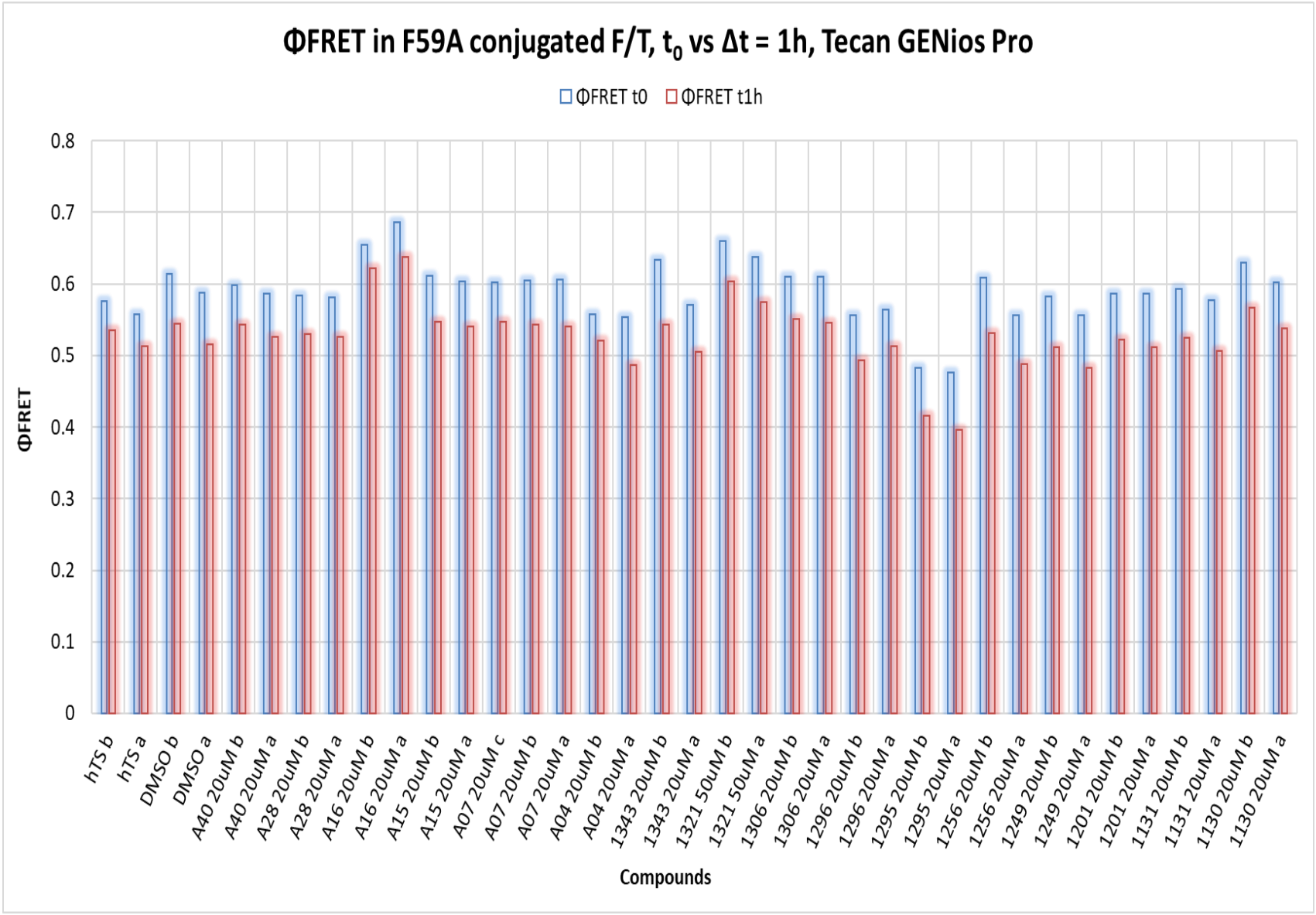

Graph 3: ΦFRET evaluation in F59A conjugated with Fluorescein maleimide and Tetramethylrhodamine maleimide of tested compounds.

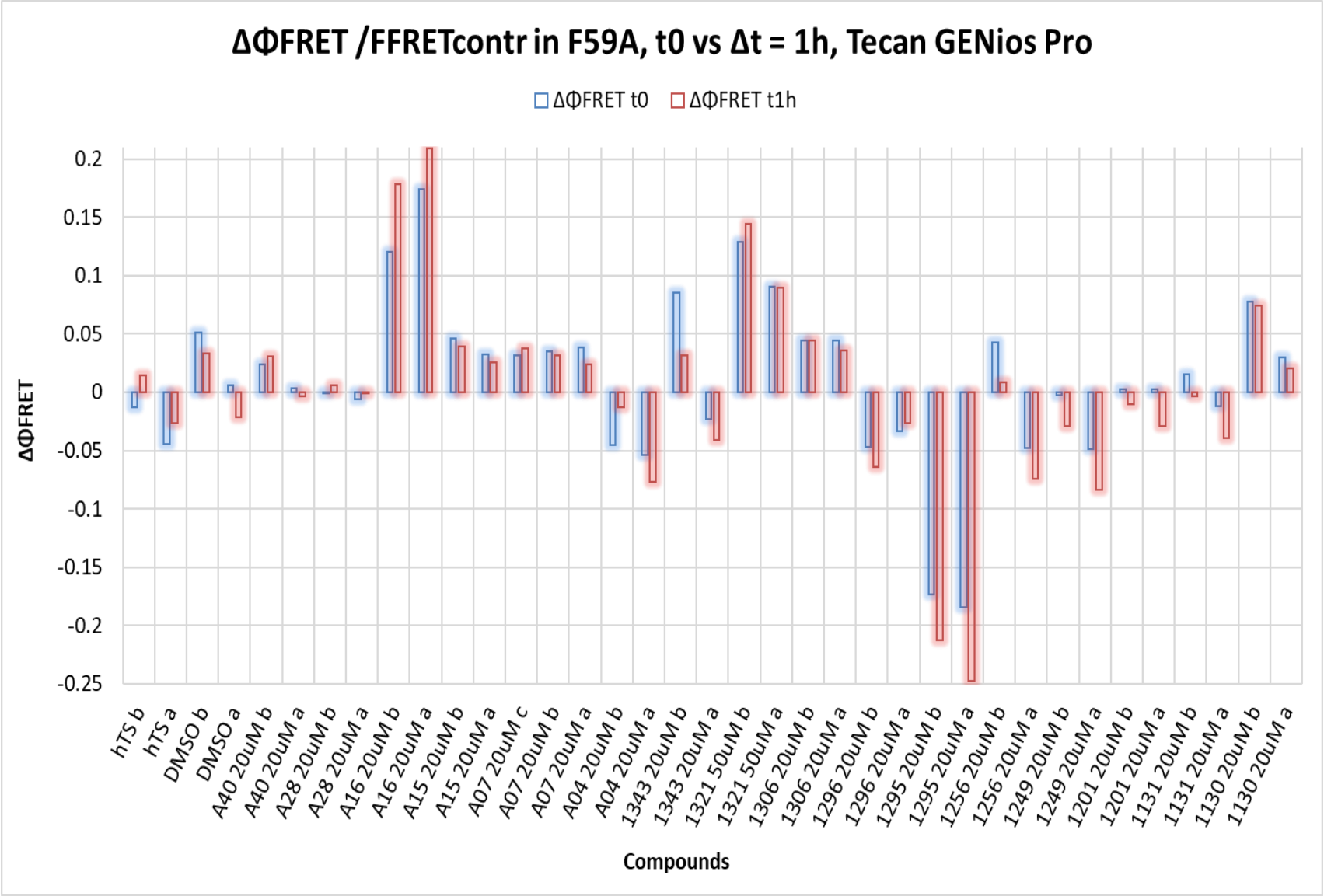

Graph 4: ΔΦFRET evaluation in F59A conjugated with Fluorescein maleimide and Tetramethylrhodamine maleimide of tested compounds.

Hence, for each compound a ΦFRET value was obtained, at time= 0s and after one hour of incubation; data shown on F59A in Graph 3. This can assume values from 0 (complete disassociation) to 1 (complete association). The graph here describes values obtained for the compound library. The ΔΦFRET value ($\Phi FRET_{with\ inhibitor}$ - $\Phi FRET_{without\ inhibitor}$) was then obtained. This can assume all values between 0 (the compound causes no change in the dimeric assembly) and -1 (the compound causes the dimer to dissociate completely), as shown in Graph 4. Positive values, i.e., apparent increases in FRET efficiency due to the inhibitor, are usually found with very poorly water-soluble compounds. These favor a co-aggregation of the protein, with intermolecular FRET, i.e., involving energy transfer from fluorescein bound to an hTS monomer to tetramethylrhodamine bound to any of the monomers in the protein aggregate. In this page, the graph indicates the ΔΦFRET value obtained for the compound library tested. Data suggests that a time – dependent response may exist. This type of experiment was later conducted on both K47A and hTS wild type – data not shown.

Conclusions

This portion of the project was conducted to study a novel class of inhibitors whose main point of action is to dissociate the dimer unity. At its core, this mechanism may allow for a different point of view when dealing with the hTS enzyme. FRET in itself has been long used to "measure" distances at the angstrom level, and this application may help in developing even more efficient inhibitors.

Further experiments have been conducted on this matter by Dr. Matteo Santucci on different mutants (Y202A and Q62R). Compounds were also retested at multiple concentrations (5 to 40 micromolars) to investigate a plausible dose-dependence effect. Preliminary data in this sense seem to assess that the ΔΦFRET data obtained from these mutants show significant and specific differences with respect to the data obtained with the wild-type one. This may suggest relevant mechanistic hypotheses that involve the molecular features of inhibitor binding and its structural consequences.

Within this context, interesting results have been obtained with LC-1130, LC-1295, LC-1296, AIC-A04, AIC-A016, AIC-A028 and AIC-A040.

Improvements in the operative context should mostly regard the purification process of the conjugated enzyme. This is quite expensive in terms of reagent to product yield (around 40%). In this sense, as the purification process is one where a size-exclusion element is used, centrifugation has been attempted with interesting results. By centrifuging samples with VivaSpin units, at a relatively high rotational speed, the general yield of the process increased to about 70%.

From the compound point of view, on the other hand, identified molecules will be further tested in tumor cell lines. This would allow to understand if the dissociative activity presented with the enzyme may also be studied in such a complex environment.

2.2.2 Proline-mutated peptide inhibitors exhibit higher efficacy than the original octapeptides

Pharmacoresistance and side effects are limiting the current pharmacological treatment choice in tumors. These phenomena call for innovative inhibiting strategies which aim at identifying molecular targets of interest, inhibiting their action. Human Thymidylate Synthase is one such target, which converts deoxyuridine monophosphate into deoxythymine monophosphate. This methylation process is possible thanks to a cofactor, N5-N10 methylenetetrahydrofolate. In this context, the design of peptides that mimic portions of interfacial regions in the assemblies of multimeric proteins has led to the identification of inhibitors binding at protein – protein interfaces. Following this concept, a series of peptides were synthesized, deriving from the parent C20, a sequence coming from the monomer – monomer interface region of hTS. Our approach has resulted in the discovery of the lead LR peptide, acting with an allosteric inhibition profile against homodimeric hTS, engaging the protein in the cellular environment and leading to cancer cell growth inhibition without increasing hTS levels.

With the aim to move toward more rigid peptides that maintain this mechanism of inhibition at the biochemical and cellular levels, a proline scanning of the LR peptide was performed and the conformational preferences of the mutants investigated by a combined experimental and computational approach based on CD spectroscopy and MD.

Journal of Medicinal Chemistry

Brief Article

Cite This: J. Med. Chem. 2018, 61, 7374−7380

pubs.acs.org/jmc

Conformational Propensity and Biological Studies of Proline Mutated LR Peptides Inhibiting Human Thymidylate Synthase and Ovarian Cancer Cell Growth

Puneet Saxena,[†,▽] Leda Severi,[†] Matteo Santucci,[†] Laura Taddia,[†] Stefania Ferrari,[†] Rosaria Luciani,[†] Gaetano Marverti,[‡] Chiara Marraccini,[†,○] Donatella Tondi,[†] Marco Mor,[§] Laura Scalvini,[§] Simone Vitiello,[†] Lorena Losi,[†,∥] Sergio Fonda,[†] Salvatore Pacifico,[⊥] Remo Guerrini,[⊥,#] Domenico D'Arca,[‡] Glauco Ponterini,*[,†] and Maria Paola Costi*[,†]

[†]Department of Life Sciences, University of Modena and Reggio Emilia, Via Campi 103, 41125 Modena, Italy

[‡]Department of Biomedical Sciences, Metabolic and Neural Sciences, University of Modena and Reggio Emilia, Via Campi 287, 41125 Modena, Italy

[§]Dipartimento di Scienze degli Alimenti e del Farmaco, Università di Parma, Parco Area delle Scienze 27/A, I-43124 Parma, Italy

[∥]Pathological Anatomy, Via del Pozzo 71, 41124 Modena, Italy

[⊥]Department of Chemical and Pharmaceutical Sciences, University of Ferrara, Via Luigi Borsari 46, 44121 Ferrara, Italy

[#]LTTA (Laboratorio per le Tecnologie delle Terapie Avanzate), Via Fossato di Mortara 17-19, 44100 Ferrara, Italy

Supporting Information

ABSTRACT: **LR** and [D-**Gln**^{4}]**LR** peptides bind the monomer−monomer interface of human thymidylate synthase and inhibit cancer cell growth. Here, proline-mutated LR peptides were synthesized. Molecular dynamics calculations and circular dichroism spectra have provided a consistent picture of the conformational propensities of the [Pro^n]-peptides. [**Pro**^{3}]**LR** and [**Pro**^{4}]**LR** show improved cell growth inhibition and similar intracellular protein modulation compared with **LR**. These represent a step forward to the identification of more rigid and metabolically stable peptides.

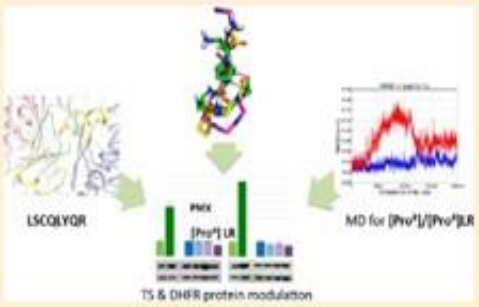

INTRODUCTION

Human thymidylate synthase (hTS) is a homodimeric protein involved in the folate metabolic pathway. In its active form, hTS converts 2′-deoxyuridine 5′-monophosphate (dUMP) to 2′-deoxythymidine 5′-monophosphate (dTMP) in the presence of the cofactor *N*5,*N*10-methylenetetrahydrofolate (mTHF). hTS also regulates protein synthesis by interacting with its own and the mRNAs of other proteins involved in the cell cycle.[1−4] This observation has made hTS an important drug target for fighting cancer.[5−7] However, prolonged dosage of clinically approved drugs such as 5-fluorouracil (**5FU**) the prodrug of 5-fluoro-2′-deoxyuridine 5′-monophosphate, raltitrexed,[8] and pemetrexed (**PMX**),[9] i.e., folate-cofactor analogs, leads to hTS overexpression, resulting in drug resistance.[10] To prevent and combat such resistance mechanism, drugs with new modes of action are needed. The design of peptides that mimic portions of interfacial regions in the assemblies of multimeric proteins has led to the identification of inhibitors binding at protein−protein interfaces.[11−14] Following this concept, we have previously synthesized a series of peptides derived from the parent **C20** peptide, a sequence coming from the monomer−monomer interface region of hTS (Figure 1).

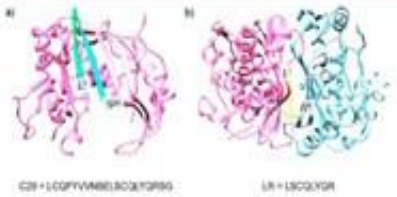

Figure 1. (a) Monomer of hTS taken from PDB code 3N5E. The region corresponding to the **C20** peptide is colored in green. (b) Crystal structure of the complexes of **LR** peptide (in yellow) with hTS (with the two monomers colored in pink and blue, respectively) (PDB code 3N5E). The protein in the two images has been rotated by 90° around the vertical axis of the image.

Received: November 22, 2017
Published: July 23, 2018

DOI: 10.1021/acs.jmedchem.7b01699
J. Med. Chem. 2018, 61, 7374−7380

Our approach has resulted in the discovery of the lead **LR** peptide and its diastereomer [D-**Gln4**]**LR** acting with an allosteric inhibition profile against homodimeric hTS, engaging the protein in the cellular environment and leading to cancer cell growth inhibition without increasing hTS levels.[15,16] Mass spectrometric proteomic studies on cancer cells with the mentioned peptides have led to the identification of a panel of proteins, namely, TS, dihydrofolate reductase (DHFR), heat shock protein HSP 90α (HSP90), heat shock protein 75 kDa, mitochondrial (TRAP1), bifunctional purine biosynthesis protein PURH (ATIC), and trifunctional purine biosynthetic protein adenosine-3 (GART), whose modulation is associated with the peptidic inhibitors activity.[17] Clinically approved drugs and peptidic inhibitors share a common target, hTS, but they show different effects on the proteomic profiles of cancer cells. The modulation of the protein panel so far identified can be considered a marker of the intracellular effects these peptides exert.[17] The crystal structures of the complexes of hTS with two peptides, **LR** (PDB code 3N5E) and **CQLYQRSG** (PDB code 4FGT), confirm their binding at the monomer−monomer interface of hTS interacting with the Ala181-Ala197 loop (sequence residue numbers are taken from 4FGT) in the inactive form.[18] In these complexes, the peptides adopt folded, helical-type conformations, a finding further confirmed by circular dichroism (CD) and molecular dynamics (MD) experiments.[19] With respect to the parent peptide, **LR**, [D-**Gln4**]**LR** presents enhanced rigidity, a tendency to assume an α-helical conformation, and a stronger cellular growth inhibition. With the aim to move toward more rigid peptides that maintain this mechanism of inhibition at the biochemical and cellular levels, we have performed a proline scanning of the **LR** peptide and have investigated the conformational preferences of the mutants by a combined experimental and computational approach based on CD spectroscopy and MD. It is well-known that tumors express higher TS levels than normal tissues and that ovarian tissue is among those with the highest levels of TS expression.[20] An enhanced expression of the TS cycle is a frequent consequence of cell treatment with **5-FU**[21,22] and has been associated with cross-resistance to **5-FU** and methotrexate (MTX) of cisplatin-resistant human ovarian carcinoma cell lines.[23−26] Therefore, the inhibition profile of these LR peptide derivatives against recombinant hTS and their activity at the cellular level against ovarian cancer cells have been evaluated. These peptides represent a step forward toward the development of more rigid, biochemically stable and active peptides.

RESULTS AND DISCUSSION

Inhibitory Activities and Conformational Propensities. The eight proline derivatives ([**Pro**^{1}]**LR** to [**Pro**^{8}]**LR**) have been tested against recombinant hTS (Table S1, Figure S1). They showed, at 100 μM, percentages of inhibition between 24% and 56%, similar to their parent peptide LR.[15] [**Pro**^{2}]**LR** is the most active mutant. The propensity of a peptide to assume a secondary structure in the proximity of a target protein molecule reduces the entropic penalty associated with the loss of translational degrees of freedom due to complexation with the protein and usually increases its affinity for the target and its activity.[19] To investigate the conformational propensities behind the biological activities of these peptides, we performed MD simulations and CD experiments. 20 ns MD simulations were run on peptides [**Pro**^{2}]**LR** and [**Pro**^{6}]**LR**, taken as cases representative of Pro-mutated octapeptides carrying in their sequence a proline residue near the N and the C termini, respectively. The two mutated peptides in the MD equilibrated complexes with hTS showed structural similarities with the **LR** reference peptide in the crystal structure of the complex with hTS (Figure 2).[19] For all

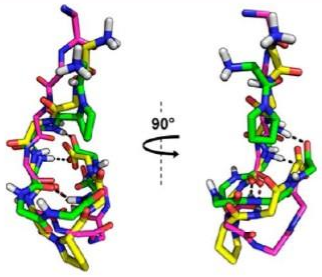

Figure 2. Superimposition of peptides **LR**, [**Pro**^{2}]**LR**, and [**Pro**^{6}]**LR**. The figure combines the X-ray diffraction structure of peptide **LR** (PDB code 3N5E; C atoms of the backbone in magenta) and the 20 ns MD structures of the [**Pro**^{2}]**LR** (C atoms of the backbone in green) and [**Pro**^{6}]**LR** (C atoms of the backbone in yellow) peptides in their complexes with hTS (PDB code 3N5E). N atoms are shown in blue, O in red, H in white. For clarity purposes, only the backbones and the proline residues side chains of the peptides are shown. The black and dark-red dotted lines represent hydrogen bonds in [**Pro**^{2}]**LR** and [**Pro**^{6}]**LR**, respectively.

of them, the conformation of the N-terminus region was extended. Given the absence of intrapeptide hydrogen bonding interactions, this portion is disordered in all peptides, though less likely so for [**Pro**^{2}]**LR** because of the decrease in the inner degrees of freedom of this peptide due to the presence of the proline cycle at position 2. On the other hand, **LR**, [**Pro**^{2}]**LR**, and [**Pro**^{6}]**LR** exhibited turns that involved the residues near the C terminus, and at least two of them showed intramolecular hydrogen bonds. Within peptide [**Pro**^{6}]**LR**, only CO(Gln^4) and NH(Gln^7) were hydrogen bonded to each other. This likely stabilizes a distorted β-turn that includes the Pro^6 residue. On the contrary, intramolecular hydrogen bonds between CO(Gln^4) and NH(Gln^7) and between CO(Arg^8) and the two NH(Cys^3) and NH(Gln^4) in the [**Pro**^{2}]**LR** derivative promote formation of a compact helical turn. Finally, in the crystallographic structure of its complex with hTS, the **LR** peptide exhibits a longer extended portion that involves residues from Leu^1 to Leu^5, while a turn involves only the last three residues at the C terminus. Consistently, no intramolecular hydrogen bond could be identified; only CO(Leu^5) and NH(Gln^7) were within hydrogen bond distance but at an unfavorable orientation (N−H−O angle = 115°).

These findings provide clues for interpreting the CD spectra of peptides [**Pro**^{1}]**LR** to [**Pro**^{7}]**LR** in distilled deionized water (DDW) in a 1:4 v/v mixture of DDW and trifluoroethanol (TFE) and in TFE, a solvent known to induce ordered secondary structures (Figures 3 and S2). We simulated the measured spectra as linear combinations of the CD signatures of several secondary structural motifs (Figure S3, Table S2). Contributions from unordered regions, characterized by negative bands with minima around 198 nm, dominate the spectra of all peptides in water. The spectra of all of them except [**Pro**^{6}]**LR** feature a positive band between 220 and 235 nm attributable to an electric-dipole allowed tyrosine transition that couples with chiral backbone transitions.[27] Consistent

DOI: 10.1021/acs.jmedchem.7b01699
J. Med. Chem. 2018, 61, 7374−7380

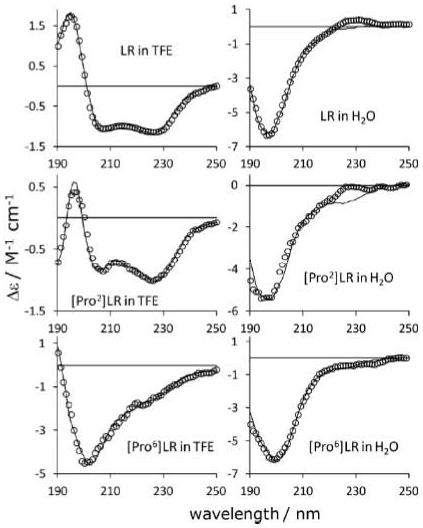

Figure 3. CD spectra of peptides **LR**, [**Pro**^{2}]**LR**, and [**Pro**^{6}]**LR** in water and TFE (circles) and their simulation as combinations of secondary structural motif CD signatures (solid lines).

with the MD structural information on [**Pro**^{6}]**LR**, contributions from a type IB-β-turn and an unordered region account for the spectra observed for the peptides [**Pro**^{6}]**LR** and [**Pro**^{7}]**LR** in TFE, where the effect of TFE as a structure-inducing medium is rather weak. The spectra of peptides **LR**, [**Pro**^{1}]**LR**, [**Pro**^{2}]**LR**, and [**Pro**^{3}]**LR** in TFE show similar shapes, with a positive band with maximum near 196 nm and two negative bands with minima near 206 and 227 nm. Our attempts to simulate them in terms of standard spectra for secondary structural motifs met with poor results. However, consistent with MD structural findings, the above features are reminiscent of the CD spectrum of a 3(10)-helix.[28] We therefore simulated the spectra of these peptides as combinations of the spectrum of [**Pro**^{3}]**LR** in TFE, assumed to correspond to a 3(10)-helix spectrum, and those of the other structural motifs in Figure S2. The results in Table S2 suggest a strong similarity among the structural propensities of the four above-mentioned peptides, with a pronounced structure-inducing effect of TFE and only a minor tendency to increased disorder as the mutated position shifts toward the N terminus. Finally, the spectra of the peptides that have proline at central positions, [**Pro**^{4}]**LR** and [**Pro**^{5}]**LR**, show similarities with the spectra of the peptides mutated near the N and the C terminus, i.e., a positive band with maximum at 199 nm, about 3 nm to the red of the 3(10)-helix bands of peptides [**Pro**^{1}]**LR** to [**Pro**^{3}]**LR**, and a broad negative band that extends toward 240 nm. To simulate them, we had to combine contributions from three different β-turn structural motifs, a necessity suggesting for these peptides a β-turn-like structure, consistent with the presence of a rigidifying residue such as proline at positions 4 and 5.

Overall, mutation to proline at positions 5 and especially 6 and 7 generates peptides with lower propensities for assuming ordered secondary structures in TFE. The spectra in TFE and the solvent mixture suggest that the peptides that bear proline near the N terminus are more ordered and, taking a 3(10)-type helical conformation rather than a β-turn-like conformation, are likely more compact than the peptides mutated near the C terminus. This suggestion is supported by calculations addressing the rigidness of the two peptides representative of the insertion of proline near the N and C terminus, [**Pro**^{2}]**LR** and [**Pro**^{6}]**LR**, and their compactness (Figure 4). The root-

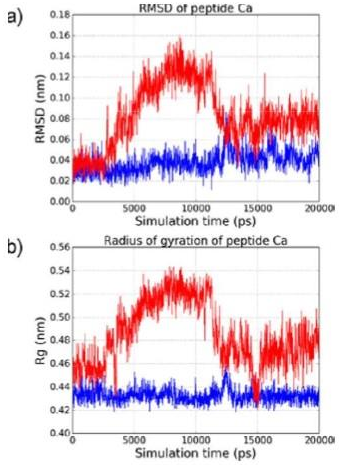

Figure 4. (a) RMSD calculated for the Cα carbon atom positions of the peptides [**Pro**^{6}]**LR** (in red) and [**Pro**^{2}]**LR** (in blue). (b) Radius of gyration (R_g) calculated for the peptides, [**Pro**^{6}]**LR** (in red) and [**Pro**^{2}]**LR** (in blue). MD simulation were performed on peptides engaged in their complexes with hTS (PDBid 3NSE).

mean-square deviation (rmsd) of the backbone Cα atoms of the two Pro-peptides during the first 3 ns of the MD simulations was 0.03 ± 0.01 nm (see Figure 4a). In [**Pro**^{2}]**LR**, the value of the rmsd remained stable in the first 12 ns of simulation and increased to 0.04 ± 0.01 nm in the last 8 ns of simulation. Analysis of the trajectories revealed that the hydrogen bonding network observed for [**Pro**^{2}]**LR**, which involves CO(Gln^4) and NH(Gln^7), and CO(Arg^8), NH(Cys^3), and NH(Gln^4), was maintained throughout the entire simulation time, which accounts for the high stability of the peptide conformation. On the other hand, the rmsd value of [**Pro**^{6}]**LR** showed a wider fluctuation, raising up to 0.12 ± 0.02 nm between 5 and 12 ns of simulation and stabilizing to a value of 0.075 ± 0.01 nm in the last 8 ns. The transitory increase of the rmsd values coincided with loss of the polar interaction between CO(Gln^4) and NH(Gln^7) and with an augmented movement of the C terminus residues. Notably, the intramolecular hydrogen bond was reinstated after 15 ns of MD simulation, allowing the [**Pro**^{6}]**LR** peptide to assume a conformation similar to the initial one. This result confirms that [**Pro**^{2}]**LR** is more rigid than [**Pro**^{6}]**LR**. [D-**Gln**^{4}]**LR**, a peptide more active and ordered than the parent **LR**, had exhibited an rmsd of 0.075 ± 0.02 nm, a value similar to that of [**Pro**^{6}]**LR**.[15] The calculated radii of gyration in Figure 4b suggest that [**Pro**^{6}]**LR** is characterized by a larger surface area than [**Pro**^{2}]**LR**. More specifically, while the radius of gyration of [**Pro**^{2}]**LR** was stably around 0.43 nm, the radius of gyration calculated for [**Pro**^{6}]**LR** increased from 0.45 nm at 3 ns to 0.53 nm at 12 ns, and then it remained 0.47 ± 0.02 nm in the last 8 ns. Once again, this is quite similar to the 0.48−0.49 nm gyration radius found for [D-**Gln**^{4}]**LR**.[15]

The peptides carrying the proline mutation near the N terminus are slightly more ordered than the peptides with

DOI: 10.1021/acs.jmedchem.7b01699

proline near the C terminus. This difference likely stems from the rigidifying effect of the mutation in the extended and conformationally looser region at the N terminus. However, this decrease in disorder is intrinsic and is expected to occur in the free and in the bound peptide; thus, it is not expected to generate any entropy-related gain in affinity toward hTS. In conclusion, the propensity of the peptides [**Pro**^{1}]**LR** to [**Pro**^{7}]**LR** to arrange residues from 3 to 7 in a compact turn, of β or of 3(10)-helical types, likely correlates with their similar activities versus hTS, as the inverted cone geometry of the hTS monomer−monomer interface binding region provides optimum space for such compact turns (Figure S4).

Biological Activity. For cancer cell growth inhibition studies we selected three human ovarian carcinoma cell lines, 2008 (cisplatin-sensitive), C13* (cisplatin-resistant phenotype showing high expression levels of the folate-cycle enzymes, TS and DHFR[26]), and IGROV-1 (cisplatin-sensitive) because ovarian cancer tissue is among those with the highest levels of TS expression linked to drug sensitivity.[20] Peptides [**Pro**^{1}]**LR** to [**Pro**^{7}]**LR** were tested against the above cancer cell models using the SAINT-PhD delivery system. [**Pro**^{3}]**LR**, [**Pro**^{4}]**LR**, and [**Pro**^{7}]**LR** were the most active ones (Figure 5a and Table S3). The percentages of cell viability were calculated by comparing cell cultures exposed to the peptides for 72 h versus untreated control cultures. Their effectiveness were compared with those of the lead peptides, **LR** and [D-**Gln**^{4}]**LR**, and that of **5FU**, taken as a reference drug. The cisplatin-sensitive cell line 2008 showed the greatest sensitivity to all tested peptides, its survival being about 20−25% lower than that of the cisplatin-resistant counterpart, the C13* cells, and of the IGROV-1 cells (Figure 5a). The IC_{50} values of the [Pro^{n}]-peptides are in the range 0.96−1.57 μM toward 2008 cells (orange histograms in Figure 5b) and in the ranges 3.55−8.1 μM and 4.32−12.1 μM toward C13* (gray histograms) and IGROV-1 (yellow histograms) cells, respectively. With respect to **LR** and **5FU**, the [Pro^{n}]-peptides showed improved growth inhibition on 2008 cells (IC_{50} = 0.96−1.57 μM vs 4.6 and 6 μM) and a slightly but consistently better growth inhibition on C13*cells (IC_{50} = 3.55−8.1 μM vs 9.5 and 12.1 μM growth inhibition compared to **LR** and **5FU** (IC_{50} values are in the range 3.55−8.1 μM for proline mutated peptides and 9.5 and 12.1). Finally [**Pro**^{3}]**LR** and [**Pro**^{7}]**LR** showed better growth inhibition than **5FU** and **LR** on IGROV-1 cells (IC_{50} = 6.2, 4.32, 10.6, and 8.2 μM, respectively, for [**Pro**^{3}]**LR**, [**Pro**^{7}]**LR**, **LR**, and **5FU**). We reason that the overall improved cytotoxicity of the [Pro^{n}]-peptides relative to the parent **LR** peptide could be ascribed to the proline pyrrolidine ring limiting the conformational freedom of the LR analogues and generating a secondary amide bond in the peptide backbone able to reduce their susceptibility to peptidase action.[29−31] Thus, the general higher cytotoxic effect of the [Pro^{n}]-peptides with respect to **LR** and in particular the effect on 2008 cells could be in part explained by an increase in the half-life of the peptides in the cell assay conditions. To verify a possible correlation between cytotoxicity and intracellular TS inhibition, we evaluated the effects of [**Pro**^{3}]**LR**, [**Pro**^{4}]**LR**, and [**Pro**^{7}]**LR** on the TS activity of IGROV-1 cells.[32] Following incubation with [**Pro**^{3}]**LR** and [**Pro**^{4}]**LR** at 5 μM, the intracellular TS activity decreased by 25%, a result similar to that of 5FU at the same concentration. On the other hand, at the same concentration, [**Pro**^{7}]**LR** inhibited the enzyme activity by more than 30% (Figure 5b, Table S3, Figure S5). **LR** showed a similar effect against 2008 and C13* cell lines

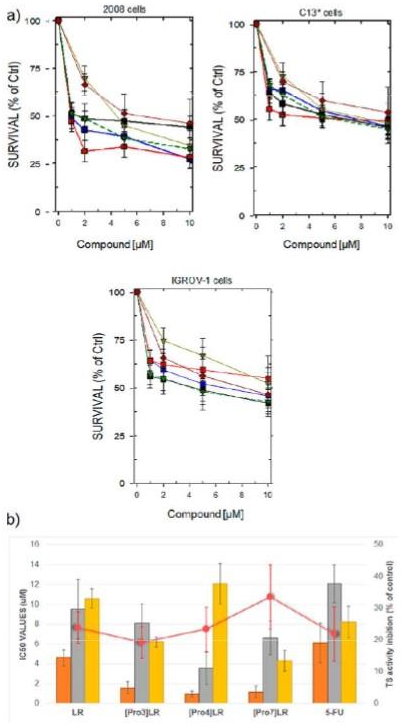

Figure 5. (a) Dose−response curve of 2008, C13*, and IGROV-1 cell growth after 72 h exposure to [**Pro**^{3}]**LR** (blue squares), [**Pro**^{4}]**LR** (red squares), [**Pro**^{7}]**LR** (black squares), **5FU** (dark red diamonds), **LR** (golden triangles down), [D-**Gln**^{4}]**LR** (green triangles down). Cell survival percentages are the mean ± SEM of three separate experiments performed in duplicate. (b) Combination graph of the percentage of TS activity inhibition in IGROV-1 cells treated for 72 h (red scatter graph) and IC_{50} against 2008 (orange histograms), C13* (gray histograms), and IGROV-1 (yellow histograms) human ovarian cancer cell lines. For the percentage of TS activity inhibition IGROV-1 cells were treated with 5 μM 5FU or peptides (transfected by SAINT-PhD system). Percentages are calculated by comparison with the TS activity in IGROV-1 cells untreated, used as control. For **LR**, the value against 2008 cells at 10 μM is reported.[19] TS activity inhibition percentages and IC_{50} values are the means ± SEM of three independent experiments.

(TS activity decreased in the range 20−40% at 10 or 20 μM).[19] Thus, the observed inhibition of intracellular TS activity by the three peptides confirms that TS is one of the target of the peptides.

Evaluation of Protein Expression Associated with Peptides Inhibition Activity. For a deeper exploration of the cellular mechanism of these peptides, the evaluation of the protein set modulation associated with their activity was analyzed. A quantitative analysis of the expression of proteins TS, DHFR, TRAP, and HSP90 has been carried out on IGROV-1 cancer cells following treatment with peptides [**Pro**^{3}]**LR** and [**Pro**^{4}]**LR**. **PMX** was considered as drug of reference because it binds to hTS active site and it shows a well-known inhibition mechanism.[9,15] The analysis was performed via Western blot, and results were compared with the results previously obtained with the lead **LR** and [D-**Gln**^{4}]**LR**.[15] The changes in the expression levels of the four proteins after treatment with **PMX** and with peptides [D-

DOI: 10.1021/acs.jmedchem.7b01699

Gln[4]LR, [**Pro[3]**]**LR** and [**Pro[4]**]**LR** are shown in Figures 6 and S6. The quantitative data were represented through heat-map (Figure 6a) and histograms, respectively, to give a comprehensive visualization of the changes.

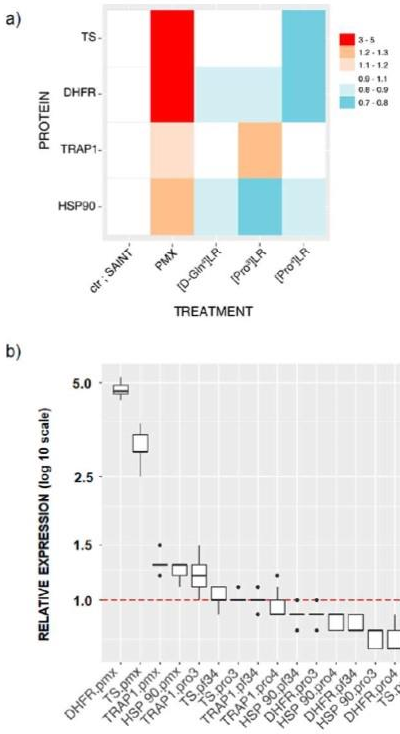

Figure 6. (a) Heat map of the protein expression modulation profile of the tested compounds in IGROV-1 human cisplatin-sensitive ovarian cancer cell line. Each expression value is standardized by subtracting the corresponding value in the control sample (ctr or SAINT). The scale in the legend illustrates the extent of up (red)- and down (green)-regulation. (b) Box plot representation of the expression level modulation of each protein (HSP90, TRAP1, TS, DHFR) due to each treatment ([**Pro[3]**]**LR**, [**Pro[4]**]**LR**, [**D-Gln[4]**]**LR**, and **PMX**). The labels along the *x*-axis are composed in the format "protein.treatment", and the boxplots are ordered according to decreasing median values. The horizontal dashed red line at $y = 1.0$ represents the control samples (ctr or SAINT).

The results obtained in the treatments with the peptides showed that proteins TS, DHFR, and HSP90 were similarly modulated in IGROV-1 cells. TS is the known target of **LR** and its derivatives. DHFR is the second enzyme in the thymidylate cycle. **PMX** caused a modulation of the expressions of these three proteins different from those of the three peptides. Similar results have been observed in comparison with **LR** and also in other cell lines.[15] [**Pro[4]**]**LR** showed the typical protein profile defined for **LR** and [**D-Gln[4]**]**LR**.[15] [**Pro[3]**]**LR** exhibits the same trend as [**Pro[4]**]**LR**, except for TRAP1, a mitochondrial chaperone associated with chemoresistant and antiapoptotic phenotypes,[33] that shows an unexpected up-regulation with respect to the control. TRAP1 was down-regulated by [**Pro[4]**]**LR** and [**D-Gln[4]**]**LR** in IGROV-1 cells and the same behavior was detected also with **LR** in IGROV-1 and other cell lines.[15] We performed a statistical analysis of the results to assess the significance of the observed changes. The modulation of each protein expressions by each cell treatment is represented in the box plots of Figure 6b. The highest modulation of expression levels is observed for TS and DHFR after treatment with **PMX** (TS.PMX and DHFR.PMX couples median = 3.0 and 4,7, mean = 3.1 and 4.8, respectively). All the other pairs have median and mean expression values lower than 1.5. Thus, treatment with **PMX** produces the strongest data difference effect. The analysis points out that **PMX** and the peptides have different proteins set expression. We interpret this difference as a consequence of different mechanisms of hTS inhibition that is then translated in a different behavior at the cellular level, as previously highlighted by a comparison between **LR**, [**D-Gln[4]**]**LR**, and **PMX**[15] and the similarity between the proline mutated peptides and the leads.

ANOVA test using the multiple comparisons method of Tukey-HSD (honest significant differences) (Figure S7) definitely confirmed the results obtained with the statistical analysis.

CONCLUSION

We have discovered two derivatives, [**Pro[3]**]**LR** and [**Pro[4]**]**LR**, that show stronger inhibition on ovarian cancer cell growth with respect to the lead peptide **LR** and better than or comparable with **5FU**. CD spectroscopic evidence on the investigated [Pro[n]]-peptides, supported by the MD simulations performed on [**Pro[6]**]**LR** and [**Pro[2]**]**LR**, has shown conformational propensities similar to those of **LR** and its more rigid and active derivative, [**D-Gln[4]**]**LR** but more compact shapes. A similarity between the inhibition of the catalytic activity of the recombinant protein and of the intracellular TS activity is observed supporting the concept that at least part of the effect in the cancer cell may be due to hTS inhibition. Like **LR** and [**D-Gln[4]**]**LR**, these peptides do not induce intracellular hTS overexpression and cause modulation of a protein set that is similar to that observed for the two reference octapeptides,[15] and statistically significantly different from that obtained with **PMX**. This provides further support to the claim that the cellular mechanism of action is similar for all the studied peptides but different from that of **PMX**. Moreover the introduction of proline likely stabilizes the peptides vs the peptidase degradation, thus increasing their intracellular concentration and activity. For all these reasons, the LR proline analogs represent a step forward toward the identification of more active and metabolically stable anticancer peptides. These peptides may show a broader cancer cell inhibition activity, as it extends to cancer cells expressing high hTS levels such as those obtained from patients treated with cisplatin- and 5FU-based chemotherapy.

EXPERIMENTAL SECTION

General. Amino acid derivatives, reagents, and solvents were purchased from Sigma-Aldrich (Steinheim, Germany) or Bachem (Bubendorf, Switzerland). The purity of the tested compounds has been assessed by reverse-phase high-performance liquid chromatography (RP-HPLC). All compounds showed >95% purity. Exact mass was recorded with an Agilent ESI-Q-TOF 6520 instrument.

Peptide Synthesis. All peptides were synthesized with an automatic solid phase peptide synthesizer Syro II (Biotage, Uppsala Sweden) using Fmoc/tBu chemistry.[34] A preloaded 4-benzyloxybenzyl alcohol resin (Wang resin) was used as a solid support for the synthesis of LR derivatives replaced with Pro in positions 1−7 while [**Pro[8]**]**LR** was obtained starting from H-Pro-2-chlorotrityl resin, a

DOI: 10.1021/acs.jmedchem.7b01699

solid support useful to minimize diketopiperazine formation.[35] The Fmoc protecting group was removed by treatment with 40% v/v piperidine/dimethylformamide (DMF). All the Fmoc amino acids (4 equiv) were coupled to the growing peptide chain by using HATU (4 equiv) in DMF in the presence of an equimolar concentration of 4-methylmorpholine (NMM), and the coupling reaction time was 1 h. To improve the analytical profile of the crude peptide, capping with 3:1 v/v acetic anhydride (0.5 M in DMF) and NMM (0.25 M in DMF), 2 mL/0.2 g of resin, was performed at each step. The protected peptide−resin was treated with reagent B[36] (trifluoroacetic acid (TFA)/H_2O/phenol/triisopropylsilane 88:5:5:2; v/v; 10 mL/0.2 g of resin) for 2 h at room temperature. After filtration of the resin, the solvent was evaporated in vacuo and the residue triturated with ether. Crude peptides were purified by preparative reverse phase HPLC to yield a white powder after lyophilization. Details about peptides purification are included in Supporting Information. p 19.

hTS Purification and Enzymatic Assay. hTS purification and protein inhibition assays were performed as previously reported.[18] Details are reported in the Supporting Information.

CD Studies. All CD spectra were measured with a Jasco spectropolarimeter. Each spectrum is the average of 2−6 acquisitions. Experiments were performed as already reported.[11] Details are reported in Supporting Information.

MD Simulations. MD simulation were conducted with the software GROMACS[37] applying parameters and protocols as already reported for previously studied similar systems.[15] Details are reported in the Supporting Information.

Cell Line Growth and Cytotoxicity Evaluation. 2008, C13*, and IGROV-1 human ovarian carcinoma cell lines were grown and treated as reported.[15] Details are reported in Supporting Information.

Cellular TS Activity Evaluation. The catalytic activity of TS after cell incubation with peptides was determined by measuring the amounts of ^3H released during the TS catalyzed conversion of [5-^{3}H]dUMP to dTMP.[32] Details are reported in the Supporting Information.

Protein Extraction and Western Blot Analysis for Protein Semiquantification. Identification and semiquantification of TS, DHFR, TRAP1, and HSP90 has been performed as already reported.[17] Details are reported in the Supporting Information.

Statistical Analysis. Details are reported in Supporting Information.

■ ASSOCIATED CONTENT

Supporting Information

The Supporting Information is available free of charge on the ACS Publications website at DOI: 10.1021/acs.jmedchem.7b01699.

Peptide percentage of inhibition of recombinant hTS, CD spectra of [Pro1]LR−[Pro7]LR, CD spectra of secondary structure motifs, contributions of CD signatures of secondary structural motifs in the simulation of the CD spectra of peptides [Pro1]LR−[Pro7]LR, the peptide binding site, proline mutated LR peptides IC_{50} values against 2008, C13*, and IGROV-1 cell lines, inhibition of cellular TS activity in IGROV-1 cells, comparison of expression levels modulation by pair of treatments, protein expression modulation profile of the tested compounds in IGROV-1 human cisplatin-sensitive ovarian cancer cell line, HPLC profiles of peptide characterization, and experimental details (PDF)

Coordinates information for hTS in complex with [Pro^2]LR (PDB)

Coordinates information for hTS in complex with-[Pro^6]LR (PDB)

Coordinates information for complex (PDB)

Coordinates information for complex (PDB)

■ AUTHOR INFORMATION

Corresponding Authors

*G.P.: phone, 0039-059-2058593; e-mail, glauco.ponterini@unimore.it.

*M.P.C.: phone, 0039-059-2058579; e-mail, mariapaola.costi@unimore.it.

ORCID

Stefania Ferrari: 0000-0003-1149-5953

Donatella Tondi: 0000-0002-5195-5531

Marco Mor: 0000-0003-0199-1849

Laura Scalvini: 0000-0003-3610-527X

Maria Paola Costi: 0000-0002-0443-5402

Present Addresses

[V]P.E.: Excelra Knowledge Solutions Pvt. Ltd., 6th floor, Wing B, NSL SEZ Arena, Plot No. 679, Survey No. 1, IDA UppalMallapur, Nacharam, Hyderabad 50003976, India.

[O]C.M.: Transfusion Medicine Unit, ASMN-IRCCS, Reggio Emilia, Italy.

Notes

The authors declare no competing financial interest.

■ ACKNOWLEDGMENTS

The authors acknowledge Prof. Els Berns of the Erasmus Institute, Rotterdam, for making the IGROV-1 cell line available. This research benefits from the HPC (High Performance Computing) facility of the University of Parma, Italy (http://www.hpc.unipr.it). This work was financially supported by the Italian Association for Cancer Research (Grants IG 10474 and IG 16977 to M.P.C.).

■ ABBREVIATIONS USED

5FU, 5-fluorouracil; CD, circular dichroism; DDW, distilled deionized water; DHFR, dihydrofolate reductase; DMF, dimethylformamide; DMSO, dimethyl sulfoxide; dUMP, 2′-deoxyuridine 5′-monophosphate; HSP90, heat shock protein HSP 90α; hTS, human thymidylate synthase; IC_{50}, inhibitor concentration reducing enzyme activity of 50% or inhibitor concentration able to reduce cell line growth of 50%; K_m, Michaelis−Menten constant; MD, molecular dynamics; mTHF, *N*5,*N*10-methylentetrahydrofolate; PMX, pemetrexed; rmsd, root-mean-square deviation; TFA, trifluoroacetic acid; TFE, trifluoroethanol; TRAP1, heat shock protein 75 kDa, mitochondrial; TS, thymidylate synthase.

■ REFERENCES

(1) Chu, E.; Allegra, C. J. The role of thymidylate synthase as an RNA binding protein. *BioEssays* **1996**, *18*, 191−198.

(2) Chu, E.; Koeller, D. M.; Casey, J. L.; Drake, J. C.; Chabner, B. A.; Elwood, P. C.; Zinn, S.; Allegra, C. J. Autoregulation of human thymidylate synthase messenger RNA translation by thymidylate synthase. *Proc. Natl. Acad. Sci. U. S. A.* **1991**, *88*, 8977−8981.

(3) Chu, E.; Voeller, D.; Koeller, D. M.; Drake, J. C.; Takimoto, C. H.; Maley, G. F.; Maley, F.; Allegra, C. J. Identification of an RNA binding site for human thymidylate synthase. *Proc. Natl. Acad. Sci. U. S. A.* **1993**, *90*, 517−521.

(4) Liu, J.; Schmitz, J. C.; Lin, X.; Tai, N.; Yan, W.; Farrell, M.; Bailly, M.; Chen, T.-m.; Chu, E. Thymidylate synthase as a translational regulator of cellular gene expression. *Biochim. Biophys. Acta, Mol. Basis Dis.* **2002**, *1587*, 174−182.

(5) Carreras, C. W.; Santi, D. V. The catalytic mechanism and structure of thymidylate synthase. *Annu. Rev. Biochem.* **1995**, *64*, 721−762.

(6) Stroud, R. M.; Finer-Moore, J. S. Conformational dynamics along an enzymatic reaction pathway: thymidylate synthase, "the movie.". *Biochemistry* **2003**, *42*, 239−247.
(7) Finer-Moore, J. S.; Santi, D. V.; Stroud, R. M. Lessons and conclusions from dissecting the mechanism of a bisubstrate enzyme: thymidylate synthase mutagenesis, function, and structure. *Biochemistry* **2003**, *42*, 248−256.
(8) Jackman, A. L.; Taylor, G. A.; Gibson, W.; Kimbell, R.; Brown, M.; Calvert, A. H.; Judson, I. R.; Hughes, L. R. ICI D1694, a quinazoline antifolate thymidylate synthase inhibitor that is a potent inhibitor of L1210 tumor cell growth in vitro and in vivo: a new agent for clinical study. *Cancer Res.* **1991**, *51*, 5579−5586.
(9) Shih, C.; Chen, V. J.; Gossett, L. S.; Gates, S. B.; MacKellar, W. C.; Habeck, L. L.; Shackelford, K. A.; Mendelsohn, L. G.; Soose, D. J.; Patel, V. F.; Andis, S. L.; Bewley, J. R.; Rayl, E. A.; Moroson, B. A.; Beardsley, G. P.; Kohler, W.; Ratnam, M.; Schultz, R. M. LY231514, a pyrrolo[2,3-d]pyrimidine-based antifolate that inhibits multiple folate-requiring enzymes. *Cancer Res.* **1997**, *57* (6), 1116−1123.
(10) Sayre, P. H.; Finer-Moore, J. S.; Fritz, T. A.; Bier-mann, D.; Gates, S. B.; MacKellar, W. C.; Patel, V. F.; Stroud, R. M. Multi-targeted antifolates aimed at avoiding drug resistance form covalent closed inhibitory complexes with human and Escherichia coli thymidylate synthases. *J. Mol. Biol.* **2001**, *313*, 813−829.
(11) Cardinale, D.; Salo-Ahen, O. M. H.; Ferrari, S.; Ponterini, G.; Cruciani, G.; Carosati, E.; Tochowicz, A. M.; Mangani, S.; Wade, R. C.; Costi, M. P. Homodimeric enzymes as drug targets. *Curr. Med. Chem.* **2010**, *17*, 826−846.
(12) de Vega, M. J. P.; Martín-Martínez, M.; González-Muñiz, R. Modulation of protein-protein interactions by stabilizing/mimicking protein secondary structure elements. *Curr. Top. Med. Chem.* **2007**, *7*, 33−62.
(13) Fletcher, S.; Hamilton, A. D. Targeting protein-protein interactions by rational design: mimicry of protein surfaces. *J. R. Soc., Interface* **2006**, *3*, 215−233.
(14) Loregian, A.; Palù, G. Disruption of protein-protein interactions: towards new targets for chemotherapy. *J. Cell. Physiol.* **2005**, *204*, 750−762.
(15) Pelà, M.; Saxena, P.; Luciani, R.; Santucci, M.; Ferrari, S.; Marverti, G.; Marraccini, C.; Martello, A.; Pirondi, S.; Genovese, F.; Salvadori, S.; D'Arca, D.; Ponterini, G.; Costi, M. P.; Guerrini, R. Optimization of peptides that target human thymidylate synthase to inhibit ovarian cancer cell growth. *J. Med. Chem.* **2014**, *57*, 1355−1367.
(16) Ponterini, G.; Martello, A.; Pavesi, G.; Lauriola, A.; Luciani, R.; Santucci, M.; Pelà, M.; Gozzi, G.; Pacifico, S.; Guerrini, R.; Marverti, G.; Costi, M. P.; D'Arca, D. Intracellular quantitative detection of human thymidylate synthase engagement with an unconventional inhibitor using tetracysteine-diarsenical-probe technology. *Sci. Rep.* **2016**, *6*, 27198.
(17) Genovese, F.; Gualandi, A.; Taddia, L.; Marverti, G.; Pirondi, S.; Marraccini, C.; Perco, P.; Pelà, M.; Guerrini, R.; Amoroso, M. R.; Esposito, F.; Martel-lo, A.; Ponterini, G.; D'Arca, D.; Costi, M. P. Mass spectrometric/bioinformatic identification of a protein subset that characterizes the cellular activity of anticancer peptides. *J. Proteome Res.* **2014**, *13*, 5250−5261.
(18) Tochowicz, A.; Santucci, M.; Saxena, P.; Guaitoli, G.; Trande, M.; Finer-Moore, J.; Stroud, R. M.; Costi, M. P. Alanine mutants of the interface residues of human thymidylate synthase decode key features of the binding mode of allosteric anticancer peptides. *J. Med. Chem.* **2015**, *58*, 1012−1018.
(19) Cardinale, D.; Guaitoli, G.; Tondi, D.; Luciani, R.; Henrich, S.; Salo-Ahen, O. M. H.; Ferrari, S.; Mar-verti, G.; Guerrieri, D.; Ligabue, A.; Frassineti, C.; Pozzi, C.; Mangani, S.; Fessas, D.; Guerrini, R.; Ponterini, G.; Wade, R. C.; Costi, M. P. Protein-protein interface-binding peptides inhibit the cancer therapy target human thymidylate synthase. *Proc. Natl. Acad. Sci. U. S. A.* **2011**, *108*, E542−E549.
(20) Li, Q.; Boyer, C.; Lee, J. Y.; Shepard, H. M. A novel approach to thymidylate synthase as a target for cancer chemotherapy. *Mol. Pharmacol.* **2001**, *59*, 446−452.
(21) Wilson, P. M.; Danenberg, P. V.; Johnston, P. G.; Lenz, H.-J.; Ladner, R. D. Standing the test of time: targeting thymidylate biosynthesis in cancer therapy. *Nat. Rev. Clin. Oncol.* **2014**, *11*, 282−298.
(22) Taddia, L.; D'Arca, D.; Ferrari, S.; Marraccini, C.; Severi, L.; Ponterini, G.; Assaraf, Y. G.; Marverti, G.; Costi, M. P. Inside the biochemical pathways of thymidylate synthase perturbedby anticancer drugs: Novel strategies to overcome cancer chemoresistance. *Drug Resist. Updates* **2015**, *23*, 20−54.
(23) Scanlon, K. J.; Kashani-Sabet, M. Elevated expression of thymidylate synthase cycle genes in cisplatin-resistant human ovarian carcinoma A2780 cells. *Proc. Natl. Acad. Sci. U. S. A.* **1988**, *85*, 650−653.
(24) Lu, Y.; Han, J.; Scanlon, K. J. Biochemical and molecular properties of cisplatin-resistant A2780 cells grown in folinic acid. *J. Biol. Chem.* **1988**, *263*, 4891−4894.
(25) Newman, E. M.; Lu, Y.; Kashani-Sabet, M.; Kesavan, V.; Scanlon, K. J. Mechanisms of cross-resistance to methotrexate and 5-fluorouracil in an A2780 human ovarian carcinoma cell subline resistant to cisplatin. *Biochem. Pharmacol.* **1988**, *37*, 443−447.
(26) Marverti, G.; Ligabue, A.; Paglietti, G.; Corona, P.; Piras, S.; Vitale, G.; Guerrieri, D.; Luciani, R.; Costi, M. P.; Frassineti, C.; Moruzzi, M. S. Collateral sensitivity to novel thymidylate synthase inhibitors correlates with folate cycle enzymes impairment in cisplatin-resistant human ovarian cancer cells. *Eur. J. Pharmacol.* **2009**, *615*, 17−26.
(27) Sreerama, N.; Manning, M. C.; Powers, M. E.; Zhang, J. X.; Goldenberg, D. P.; Woody, R. W. Tyrosine, phenylalanine, and disulfide contributions to the circular dichroism of proteins: circular dichroism spectra of wild-type and mutant bovine pancreatic trypsin inhibitor. *Biochemistry* **1999**, *38*, 10814−10822.
(28) Andersen, N. H.; Liu, Z.; Prickett, K. S. Efforts toward deriving the CD spectrum of a 3(10) helix in aqueous medium. *FEBS Lett.* **1996**, *399*, 47−52.
(29) Mentlein, R. Proline residues in the maturation and degradation of peptide hormones and neuropeptides. *FEBS Lett.* **1988**, *234*, 251−256.
(30) Cunningham, D. F.; O'Connor, B. Proline specific peptidases. *Biochim. Biophys. Acta, Protein Struct. Mol. Enzymol.* **1997**, *1343*, 160−186.
(31) Vanhoof, G.; Goossens, F.; De Meester, I.; Hendriks, D.; Scharpé, S. Proline motifs in peptides and their biological processing. *FASEB J.* **1995**, *9*, 736−744.
(32) van Triest, B.; Pinedo, H. M.; van Hensbergen, Y.; Smid, K.; Telleman, F.; Schoenmakers, P. S.; van del Wilt, C. L.; van Laar, J. A.; Noordhuis, P.; Jansen, G.; Peters, G. J. Thymidylate synthase level as the main predictive parameter for sensitivity to 5-fluorouracil, but not for folate-based thymidilate synthase inhibitors, in 13 nonselected colon cancer cell lines. *Clin. Cancer Res.* **1999**, *5*, 643−654.
(33) Loizeau, K.; De Brouwer, V.; Gambonnet, B.; Yu, A.; Renou, J.-P.; Van Der Straeten, D.; Lambert, W. E.; Rébeillé, F.; Ravanel, S. A genome-wide and metabolic analysis determined the adaptive response of arabidopsis cells to folate depletion induced by methotrexate. *Plant Physiol.* **2008**, *148*, 2083−2095.
(34) Benoiton, N. L. *Chemistry of Peptide Synthesis*; Taylor & Francis: New York, 2006; pp 65−90.
(35) Barlos, K.; Gatos, D.; Papaphotiou, G.; Schäfer, W. Synthese von calcitonin-derivaten durch fragmentkondensation in Lösung und am 2-Chlortrityl-Harz. *Liebigs Ann. Chem.* **1993**, *1993*, 215−220.
(36) Sole, N. A.; Barany, G. Optimization of solid-phase synthesis of [Ala^8]-Dynorphin A. *J. Org. Chem.* **1992**, *57*, 5399−5403.
(37) Hess, B.; Kutzner, C.; van der Spoel, D.; Lindahl, E. GROMACS 4:Algorithms for highly efficient, load-balanced, and scalable molecular simulation. *J. Chem. Theory Comput.* **2008**, *4*, 435−447.

DOI: 10.1021/acs.jmedchem.7b01699

2.2.3 A proof-of-concept: a light-based allosteric system allows for controlled activity of inhibitors

Improving a molecule in targeted therapies is no easy task. A relevant issue at hand in the context of tumor cells, pharmacoresistance is one hot topic in today's pharmacology.

As the current pharmacological lines of treatments appear to be progressively failing, improvements are required not only in the search of newer and more efficient targets to be hit, but also to rethink delivery strategies.

This process is not one to be underestimated. The average human cell has multiple in and out ways, but many of these can cause modifications to the drug molecule which may result in less efficacy. Hence, one of the most important elements in this process is to ensure the structural integrity of the inhibitor as it comes into contact with its target. Another rather important issue is one where the inhibitor needs to be active only when it is close to its target. This would dramatically improve the efficacy of an inhibitor, by decreasing the cross-activity, hence the potential side effects.

In this context, a derivative of methotrexate (MTX) has been developed in prof. Pau Gorostiza's group, Phototrexate™(PHX), by incorporation of a photochromic unit into the structure of MTX. The main element of this molecule was its design to be inactive when in its thermodynamically stable configuration. Light induces the activation of the molecule,

allowing to exert its action. As reported in[34] the molecule has been successfully tested in vitro and with zebrafish larvae, where its activity was comparable to its parental drug.

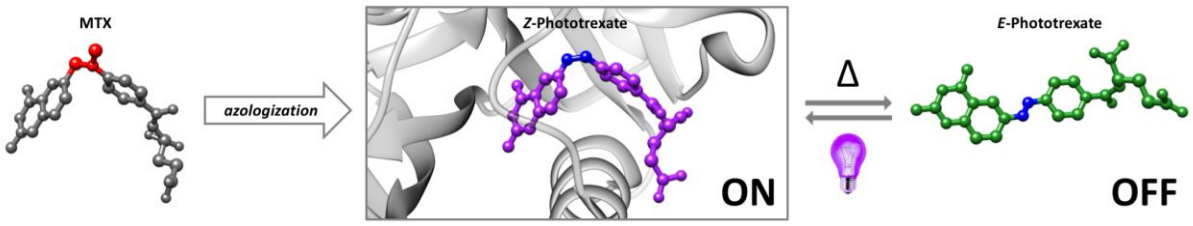

Figure 15: MTX vs PHX structure. Thanks to Carlo Matera for allowing the insertion of the image.

A project was thus developed to test this molecule in different cell lines of bladder cancer, as it represents a rather "accessible" tissue, as it is fairly on surface, thus more easily irradiated, when compared with other cancer types. Within this context, six different cell types have been tested for this compound. The experiment aimed at comparing PHX in its conformations, and MTX in these cells. This work was achieved under the supervision of Dr. Nuria Camarero Palao.

Among tested cells, RT112, 5637, J82, and 97-1 are all bladder cancer cell lines. Each cell line does, however, have its own characteristic, as described in the Materials and Methods section.

As there was not a defined protocol for the experiment, this was built along the way. This was mainly due to the fact that these cell types exhibited different behaviors in culture. The main concerns regarded reflecting the average growth pattern of the tumor cells and to

maintain a spectrophotometric signal that was still in the linear response portion of the instrument.

The first element of the process was to assert a baseline of sorts which would have helped in pointing out the basic elements:

- How many cells per well
- Duration of treatment
- Issues and points of failure

One main element of concern was the MTS assay. This assay would give out best results only when diluted in PBS, rather than in DMSO medium. This issue was one to account for as the main reason that influenced the switch from MTT to MTS was that it would require less cell manipulation after the treatment. Although the MTS protocol required a 490nm filter to be used for reading purposes,

				450 nm				
Dmem + R	Dmem - R	PBS	Dmem + R + NaOH		Dmem + R	Dmem - R	PBS	Dmem + R + NaOH
0.431	0.501	0.291	0.427		0.401	0.273	0.249	0.936
0.400	0.319	0.254	0.437		1.295	0.327	0.289	0.411
0.415	0.337	0.270	0.434		0.457	0.297	0.285	0.394
0.446	0.314	0.262	0.458		0.622	0.328	0.276	0.411
				540 nm				
Dmem + R	Dmem - R	PBS	Dmem + R + NaOH		Dmem + R	Dmem - R	PBS	Dmem + R + NaOH
0.291	0.220	0.066	0.280		0.289	0.087	0.042	0.379
0.262	0.083	0.039	0.270		1.192	0.088	0.041	0.299
0.271	0.100	0.043	0.275		0.315	0.091	0.043	0.315
0.286	0.098	0.040	0.299		0.464	0.087	0.043	0.305

Table 2: Table representing MTS readings in different solutions. The idea was to obtain a baseline of sorts that would allow a better understanding of the best assay conditions.

Promega representatives confirmed that the assay could be done at both 450 and 540nm, suggesting that, for better results, a measurement at 620 nm was to be done as a baseline to be subtracted from the readings.

In short, the baselines were exceptionally high when DMEM (Dulbecco's Modified Eagle Medium) medium was used. Best case scenario was the usage of PBS (Phosphate Buffer Solution) to dilute MTS (3-(4,5-dimethylthiazol-2-yl)-5-(3-carboxymethoxyphenyl)-2-(4-sulfophenyl)-2H-tetrazolium), which require an ulterior step in taking away the medium from the cells and feed the MTS+PBS solution to obtain low baselines.

Setting up the protocol was mostly done with HeLa cells (data not shown) and 5637 and RT112 cell lines, by testing them with MTX.

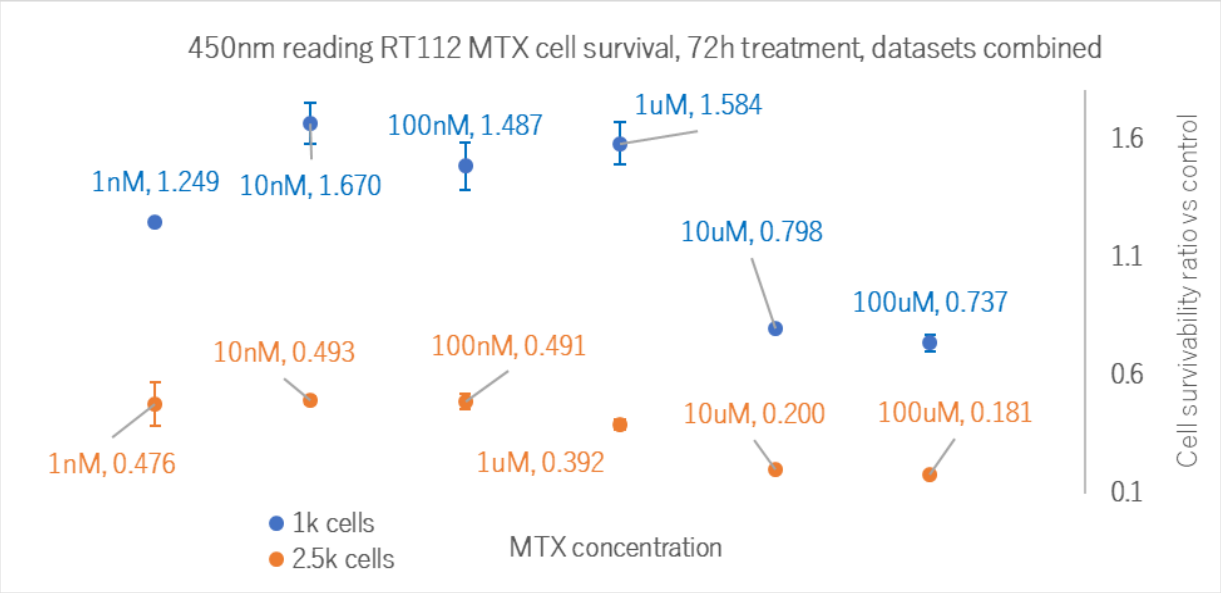

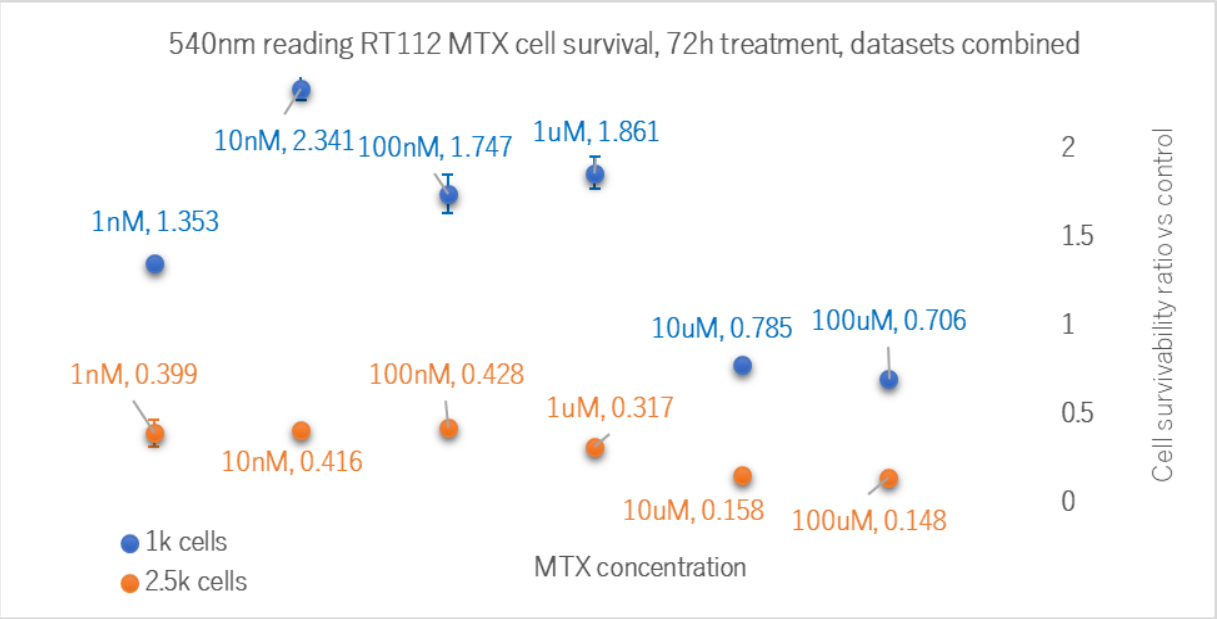

As reported in the Materials and Methods section, six different concentrations were tested, at different amounts of cells per well, as reported here on Graph 5.

Graph 5: Graphs representing datasets of RT112 cells treated with 6 different concentrations of MTX at two different cell counts per well. Combined datasets from two different experiments in two different weeks. Dataset from 1k cells proved unreliable hence it was discarded from further experiments. Graphs show readings at 450 nm (upper graph) and 540 nm (lower graph).

The next step regarded the treatment time for these cells. There are multiple instances where suggested times were between 48 and 72 hours. As this protocol was built to be considered an "internal standard" of sorts, the previous tests were also done with these two different treatment periods – 1k data @ 48 hours not shown -

Combining the data at 2,5k cells at 48 and 72 hours of those experiments the following graph – Graph 6 – is obtained.

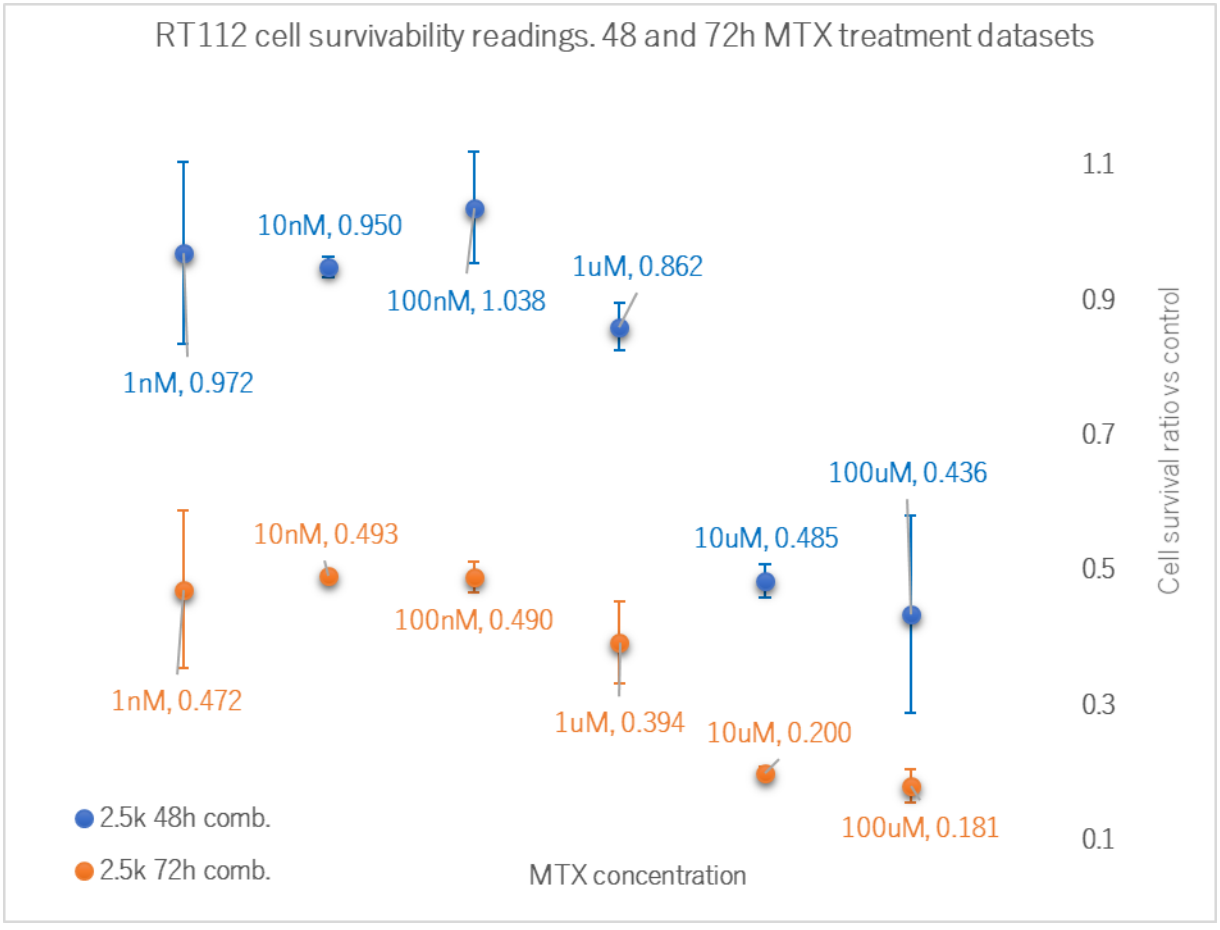

Graph 6: Experiments conducted on RT112 cells, with MTX at 6 different concentrations. Datasets combined for tests at 48 and 72 hours of treatment. Readings at 450 nm.

This experiment was very useful in giving out interesting insights on the protocol. First and foremost, as anticipated, 2500 cells per well seem to work better than 1000 cells per well. Another interesting point is the effect of the treatment time interval. The two options seem to dish out some interesting elements. A clear difference between timings in the two treatments is the cell survivability, about the half at 72 vs 48 hours. Another interesting element was the standard deviation, which in the graphs (and in all the following ones) is expressed by the error bars. 48 hours seemed to offer a some more standard deviation than 72 hours.

Data presented in the previous graphs seemed to support the idea that the sweet spot would be 2500 cells per well, 72 hours of treatment. Another element caught the attention, however. If an IC50 were to be considered from this graph, one could argue that this value is lower than 1 nanomolar for MTX. This may be however, a bias result given by favorable conditions for MTX.

Hence this data was corroborated with further experiments at 5000 and 10000 cells per well, at 48 and 72 hours. Data from these experiments seemed to sustain the idea that with this number of cells, the dose-response curve was a little more realistic. As the 5637 cells became available to be used for experiments, it became clear that this process needed to be tailored for each cell type, to find the best spot to test all cell lines. This was due to the fact that the different cell lines exhibited different growth rate, although the growth protocol itself was confirmed to be used in literature, as shown from Graph 7

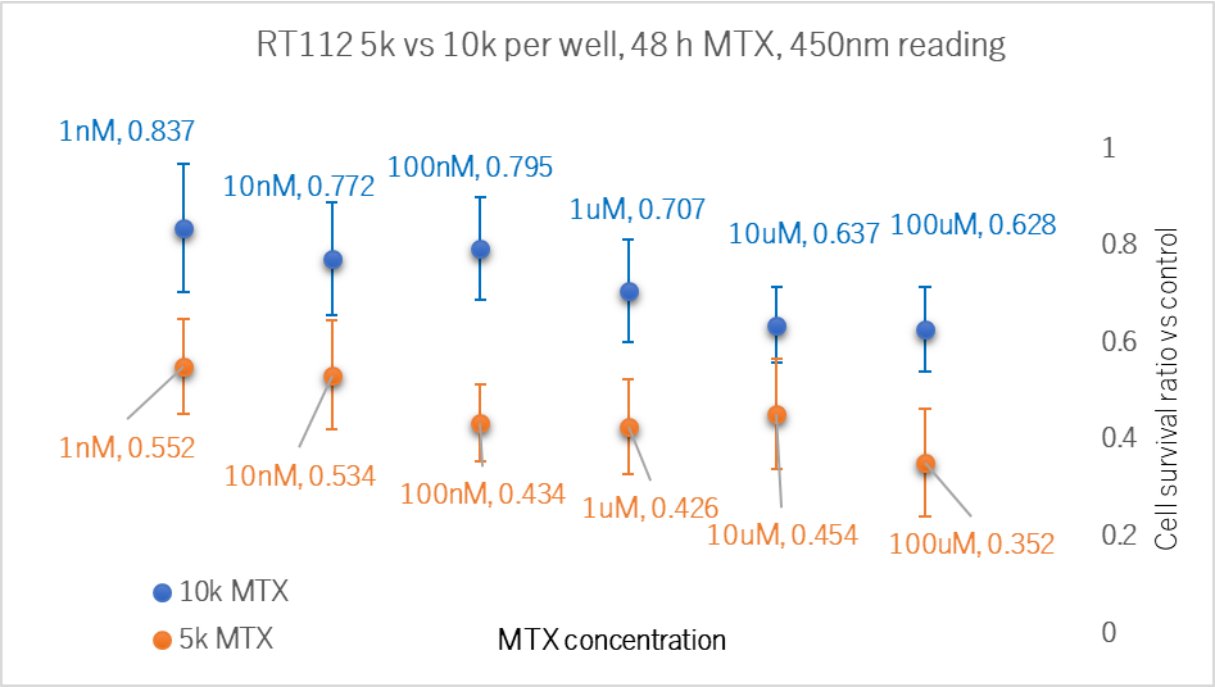

Graph 7 RT112 survivability test with 5k and 10k cells per well.

In the end, RT112 data seemed to support the idea that increasing the number of cells and shortening the treatment's time interval may give much more realistic responses. This preliminary data helped in the first experiment with PHX. Isomerization of PHX, as reported in the Materials and methods section, was achieved with a transilluminator and an LED plaque capable of emitting UVA light. This process was done on the stock solution, which was then diluted in DMSO (Dimethyl Sulfoxide) +100 nM NaOH for all dilutions. PHX trans conversion was obtained by heating up the stock solution at 65°C and then proceed with the dilutions. For RT112 – Graph 8 – the optimal testing conditions were found at 5k cells, 48 hours of treatment.

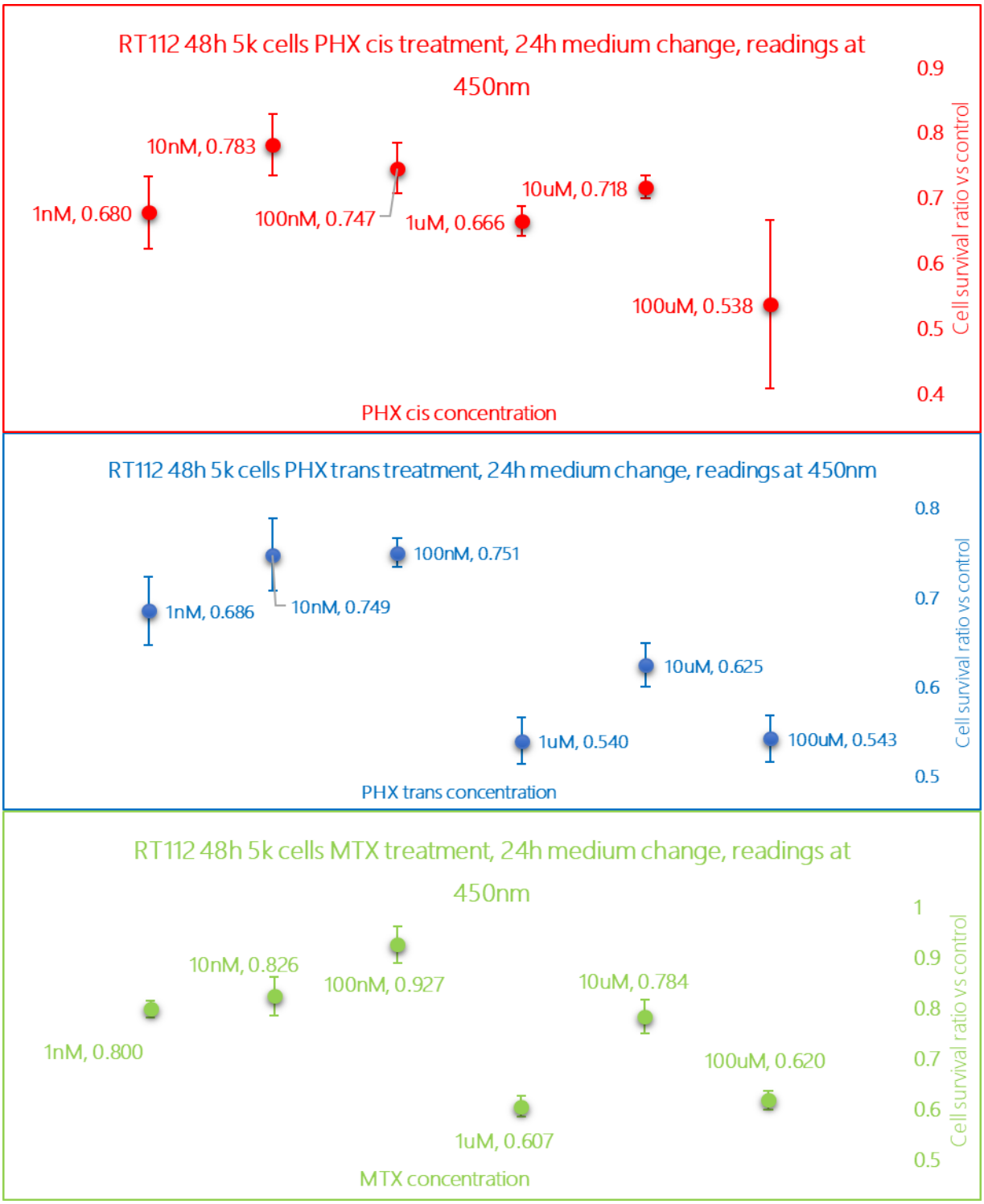

Graph 8 RT112 treatment with MTX, PHX cis and trans, at 5k cells per well, 48 hours treatment, and 24 hours medium change.

As Graph 8 shows, cells received a medium change every 24 hours. This was done to ensure the maximum effectiveness of PHX and MTX.

Within the testing conditions, data seemed to suggest that MTX is more efficient than PHX. Another tested cell line in this sense was 5637. Aliquots and dilutions of PHX and MTX were prepared as described before and in the Materials and Methods section of this thesis. The main difference was that the optimal conditions for this cell line was found at 10 thousand cells per well, 72 hours treatment. As with RT112, medium was changed every 24 hours. Data obtained from the experiments – Graph 9 – supported the idea that 5637 cells did not exhibit different sensibility to either isomers of PHX or MTX.

The results obtained with PHX cis could be due to the fact that it may interconvert back to the trans isomer whilst in solution

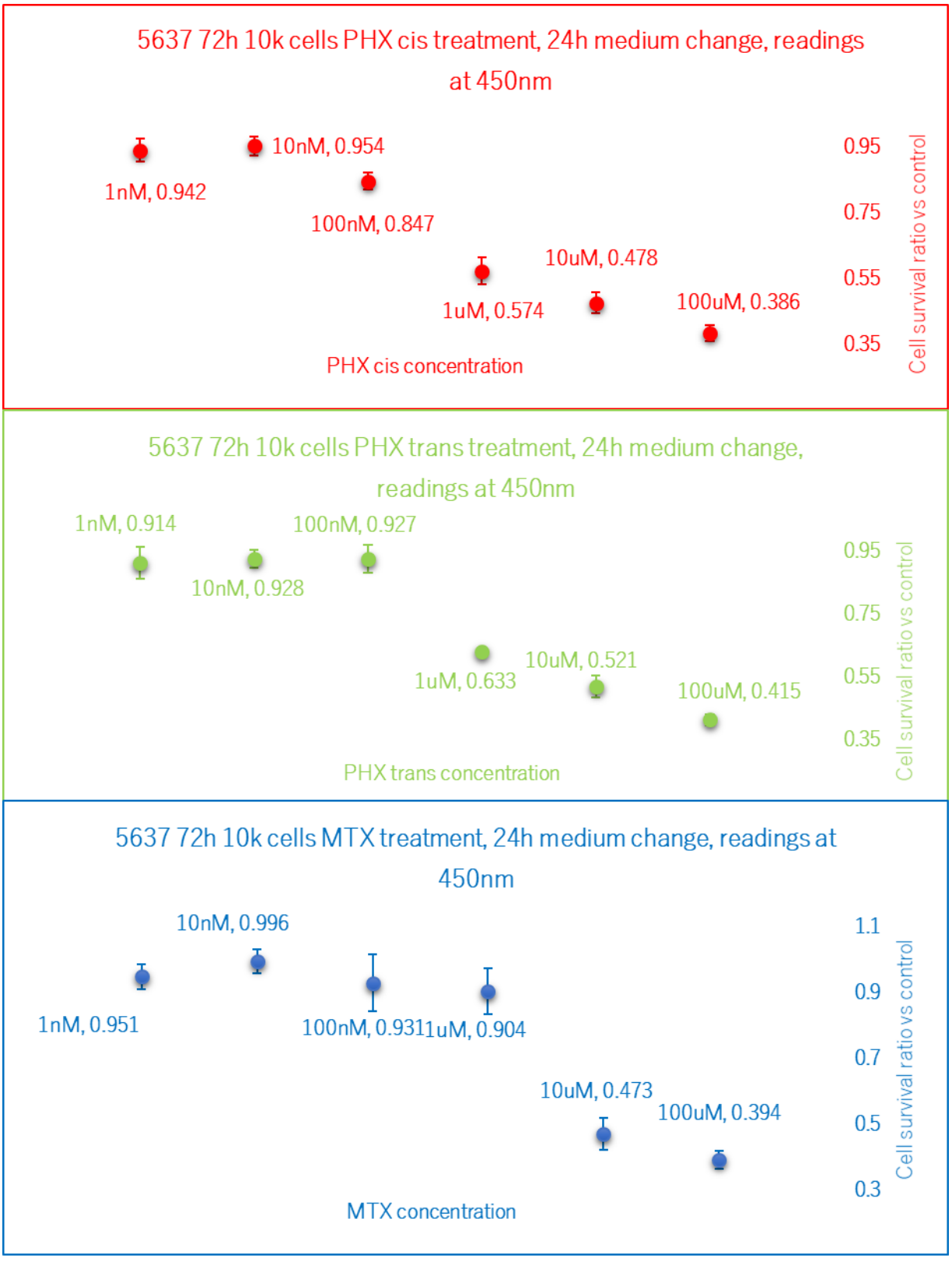

Graph 9: 5637 tests with both MTX and PHX. Conditions reported as graph title.

This idea was supported by parallel experiments ran in another group, which seem to support the idea that PHX cis concentration decreases within a matter of hours chosen as they tended to represent three different bladder cancer stages: MGH-U3, J82 and 97-1. Of these three, however, experiments were conducted only on the last two, as the former did happen to have issues growing in flasks.

As the following graph – Graph 10 – shows, 97-1 cell line did not exhibit differences at 5k cells per well, 72h of treatment, 2x day media change, with PHX cis and trans, and MTX.

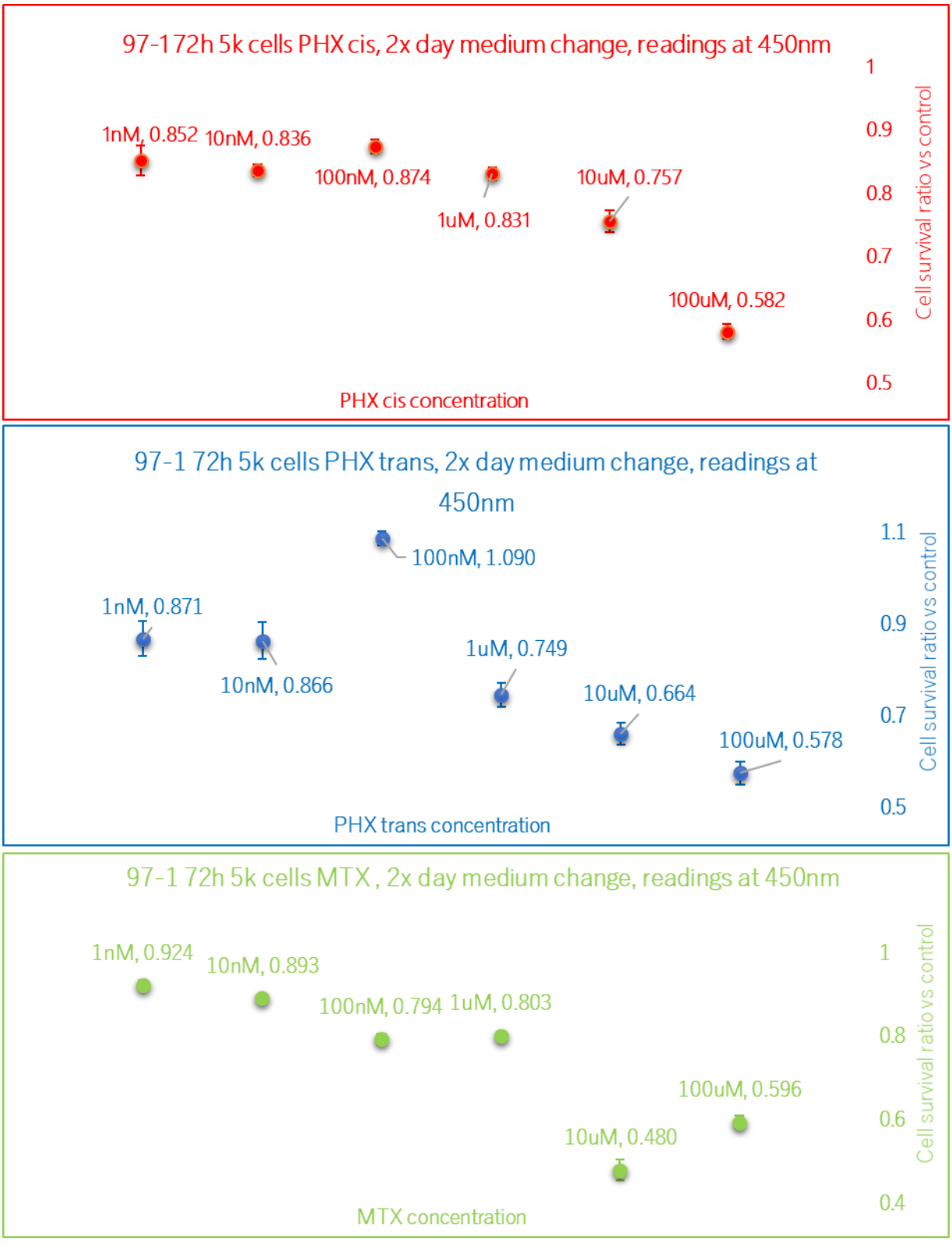

Graph 10: 97-1 cell line tests with PHX and MTX. Conditions in the graph title.

A little more interesting were the results of J82 cells, as resumed in Graph 11.

Graph 11: J82 cell line tested with PHX and MTX. Conditions listed as graph title.

Within the same conditions, J82 cell line exhibited different survivability when treated with PHX and MTX. Even more interesting in this case, data from this experiment suggests a higher effect of PHX cis vs trans and MTX.

Conclusions

Systemically administered anticancer treatments are one of the first lines of treatment when it comes to pharmacologically approach tumors. These molecules do come from a background where the idea is to design molecules which can interact with highly sensible targets which either halt the tumor cell growth and/or induce apoptosis to said cells.

These molecules, however, appear to be issued with some drawbacks. Increase of pharmacoresistance and side effects can sometimes limit the approaches in this sense. In particular, the latter may be somewhat limited by means of controlling the interaction between the molecules and the target to a point and time where they are actually close one to the other. In this sense, Phototrexate, synthesized by Prof. Dr. Pau Gorostiza group, is a molecule that mimic the structure of methotrexate, but it is structured so that its trans conformer, more thermodynamically stable, is also inactive. Activity of the molecule may be induced by shining UVA light.

This portion of the thesis was conducted in the Bellvitge Hospital, Barcelona, as part of the period abroad for the Ph.D. course. The experiments were conducted under the supervision of Dr. Nuria Camarero Palao and Prof. Dr. Pau Gorostiza.

As this process was tailored over different cell lines, multiple attempts have been done to find the "sweet spot" for each cell line. The process was enriching, and it helped discover a potential cell line, J82, whose data shows to be promising.

Multiple improvements may be added to the in vitro testing. For once, as the interconversion trans – cis of PHX seem to happen in hours, one plausible element to be improved is to rationalize even further the treatment timings, to explore the full potential of this molecule.

Another interesting point of view is the media change. This was originally done as samples' illumination in DMSO may have led to the formation of free radicals, hence to a bias. This issue may be alleviated by using culture media that may allow such a modification to be had. Culture media like this are commercially available (MEMO for instance) although in these, cell growth is not granted as some photosensible molecules are missing. This also means that these culture media may be used for a limited amount of time, hence long periods of exposure (over 72h) may lead to issues.

As for the molecule itself, it inserts in a mechanism consisting of clinically approved light-therapies (PDT and PUVA for instance) enhancing the chances of medical and regulatory acceptance. As the wavelength at which PHX isomerizes to cis may scatter and absorbed by human skin – albeit at very low skin penetrations, as reported by Prof. Gorostiza group [35]. Improvements in this sense may come from a different isomerization approach, one

that would require red to NIR (Near Infra-Red) wavelengths, as such wavelengths are capable of orders of magnitude of tissue penetration.

2.3 Spectrofluorometry and thermocalorimetry may define a working model for the hTS enzyme

As defined in the aims of the thesis, spectrophotometry and thermocalorimetry techniques have been employed in the context of this thesis: the aim was to determine variation in properties that may be somehow linked to variations in structural elements of the enzyme.

The main idea behind this portion of the thesis was to compliment known information about the structural element of hTS with data coming from sources which may be used to support a model of hTS closer to reality.

Spectrofluorometry data has been long used to correlate and follow emissions and absorptions of molecules with structural changes. Within this project, observables like steady spectra, quantum yields and lifetimes have been monitored in different conditions to determine their properties in both the active and inactive conformer. Hence, information gathered may help in defining fluorometric "fingerprints" of the two conformers, which can be used for both identification purposes, and to have a better grasp at hinting structural changes.

Thermocalorimetry data deals into the world of energies and the quantifications in energetic terms of molecular interactions. Stoichiometry and thermocalorimetric information from interactions of molecules may be used to infer on eventual

quantifications of the thermodynamic features of both intramolecular, e.g., a structural rearrangement, and intermolecular phenomena (binding).

2.3.1 Intrinsic fluorescence identifies the active and the inactive conformations of human thymidylate synthase

Intrinsic fluorescence may offer a suitable set of observables to sketch the conformational landscape of a protein and monitor changes within it.

Thymidylate synthase, a 70 KDa homodimeric protein, is a folate-dependent enzyme that catalyzes the methylation reaction of 2′-desossiuridine-5′-monophosphate to 2′-desossithymidine-5′-monophosphate using methylene-tetrahydrofolate as the methylene donor and the reducing agent[9]. This reaction is the only de-novo source of dTMP in humans and its inhibition halts the nucleic acid synthesis and the cell replication. For this reason, human TS (hTS) has been known for more than 50 years as a target in anti-cancer therapy

The protein sequence is highly conserved. The main differences between the sequences of human and bacterial TSs are at the N-terminus and for two insertions at positions 117 (12 residues) and 146 (8 residues) of the human protein[11]. More than 100 TS crystal structures are presently stored in the Protein Data Bank. A peculiarity of the TS structure that has relevant functional consequences concerns the 181-197 residue loop. In the crystal structure of hTS, this can be found in two main conformations connected with each other by a twist of 180°. The 'active' conformation is similar to the conformation found with all non-human

TSs and features the side chain of C195 (the 'catalytic' cysteine) lying in the protein active site. In the 'inactive' conformation, instead, C195 lies at the interface between the two monomers of the protein[11]. This structural peculiarity of the human protein has been associated with residue R163 that is specific of hTS. R163 can stabilize the inactive form by establishing hydrogen bonds between its guanidinic H atoms and the main-chain carbonyl O atoms of A191 and L192 in the other monomer. In murine TS, this arginine is replaced by lysine and, because of its shorter side chain, K163 cannot establish such hydrogen bonds. Indeed, the R163K mutant of hTS is found in the active conformation[8,36]

While sulfate or phosphate anions favor crystallization of the inactive form of hTS, when the crystals are produced in the presence of dUMP, or some of its analogues, the active conformation is obtained[8,11] Attempts to produce a transition between the two conformations in crystals by soaking the inactive protein crystals with ligands that stabilize the active conformation have failed. However, such a transition has been computationally simulated, with the 181-197 loops of the two monomers that twist one after the other, and the catalytic C195 that can either flip across the loop or undergo a torsion outside it[7]. Experimental evidence of the population of interchanging active and inactive conformations of hTS in solution has been obtained indirectly from enzyme activity and inhibition measurements and, more directly, from intrinsic fluorescence experiments. The R163K mutant was found to be 1.33 times more active than wt hTS, a finding that suggests that, in the conditions of the kinetic experiments, about 1/3 of the native protein is in the

inactive conformation[8]. Additionally, the observation of positive cooperativity between two inhibitors, one binding the inactive form and the other the folate binding site, led to the suggestion that, in those experimental conditions, hTS may exist as an asymmetric dimer, with a monomeric subunit in the inactive and the other in the active forms[8].

The tryptophan emission intensity of hTS was observed to increase following addition of phosphate ions, that favor the inactive form, and to markedly decrease when dUMP, that favors the active form, was subsequently added. Consistently with the interpretation of the observed intensity changes as associated with the active↔inactive interconversion, E. coli TS, that has always been found in a single, active form in crystals, did not exhibit any emission modulation by phosphate ions or dUMP [12]. In spite of the presence of five tryptophans per monomeric unit, the pronounced change in the overall hTS emission intensity when the protein switches between the inactive and the active conformations is believed to result mainly from W182 whose indole fluorophore undergoes a large displacement (about 5 Å) and change in local environment when the twist of the 181-197 loop takes place [11,37]

The aim of the work accounted herein is to provide an as much as possible rational fluorometric picture of the active and inactive conformations of hTS. We have investigated several fluorometric observables – steady-state spectra, quantum yields, decay profiles, anisotropies, both steady-state and time-resolved, quenching by the iodide ion – and have tried to provide a structural interpretation of the differences observed between

fluorescence properties measured in conditions in which either the inactive or the active forms of hTS prevail. The analysis was boosted by the availability of the W182A hTS mutant; this enabled us to identify, within the overall wt hTS fluorescence response, the often relevant, hence easily identifiable contributions from W182, thus highlighting the consequences of the above mentioned change of environment of the indole fluorophore of this residue when an active↔inactive interchange takes place. The fluorometric features here described will serve as well characterized sets of observables in a forthcoming investigation of the dynamics and of the thermodynamic features of this functionally crucial interconversion.

Results

Because the position of the equilibrium between the active and the inactive conformations of hTS is expected to depend on the concentration of phosphate ions (Pi) and dUMP, we will show and discuss in parallel the fluorescence observables of this protein in solutions where, based on the reported literature, we expect it to be mainly in the inactive conformation ([Pi]=150 mM, [dUMP]=0), in the active conformation ([Pi]=150 mM, [dUMP]=220 μM) and in a mixture of the two ([Pi]=20 mM, [dUMP]=0).

To begin, we will try to identify the contributions to the protein intrinsic fluorescence of W182, a residue that being included in the 181-197 loop most directly involved in the conformational active↔inactive interconversion may act as a fluorometric reporter of any

such conformational change. We thus expressed the W182A hTS mutant and will now compare its fluorescence properties with those of the WT protein.

Contributions of W182 to the WT hTS steady-state emission

The W182A mutation causes an overall blue shift of the protein emission. The maximum moves from 338 to 333 nm when both tyrosines and tryptophans are excited at 280 nm (1st graph in the picture below, a) and from 340 to 336 nm upon selective tryptophan (Trp) excitation at 295 nm. The emission spectrum of the W182A mutant could be well fitted by one gaussian band with maximum at 334 nm and breadth 4800 cm-1; the WT emission spectrum by two gaussian bands with maxima at 335.5 and 362 nm and breadths 4100 and 5000 cm-1 (2nd and 3rd graph respectively, from Fig. 16 below, b and c).

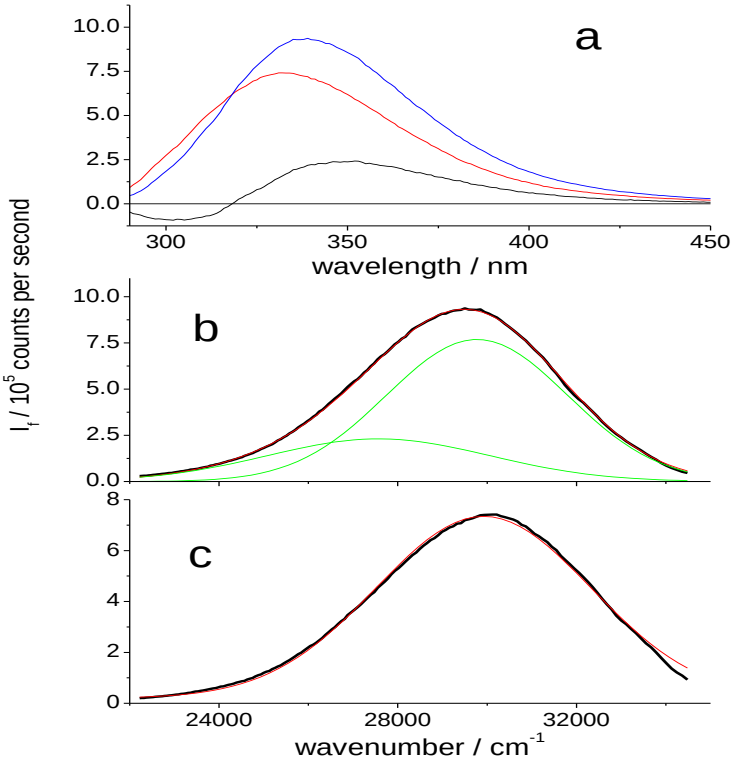

Figure 16: a) Emission spectra of WT (blue) and W182A hTS (red) in phosphate buffer ([Pi]=20 mM) at pH 7.5. in black, difference between the two spectra (WT-W182A). b) and c): fitting of the emission spectra of, respectively, WT and W182A hTS in terms of two and one Gaussian bands (green). Solvent: PBS ([Pi] = 20 mM, pH 7.0). Excitation at 280 nm.

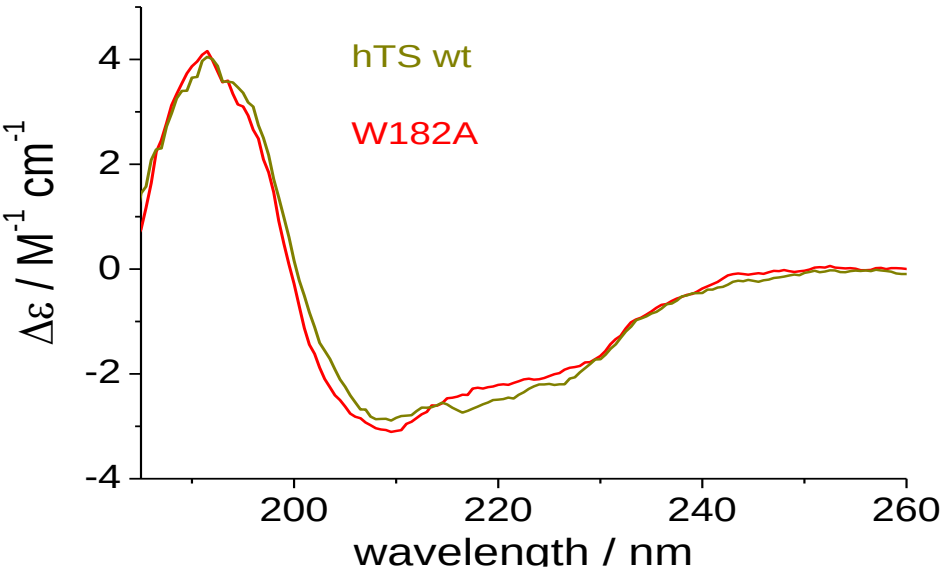

Figure 17: Far UV circular dichroism spectra of hTSwt (in dark green) and W182A (in red).

The single W182A mutation does not cause relevant changes in the far-UV CD spectrum of hTS, as shown on Fig. 17, hence in the secondary structure of the protein.

This lends support to the assumption that the local environments of the other Trps are similar in the WT and mutant proteins. As a consequence, the observed spectral shift suggests that the W182 contribution lies in the bathochromic region of the protein emission, i.e., that this residue is on average more exposed to the polar solvent than the other Trps. Indeed, the difference spectrum in Fig.16, section a (black line) has its maximum at 350 nm, i.e., 10-12 nm on the red of the WT hTS emission maximum.

.

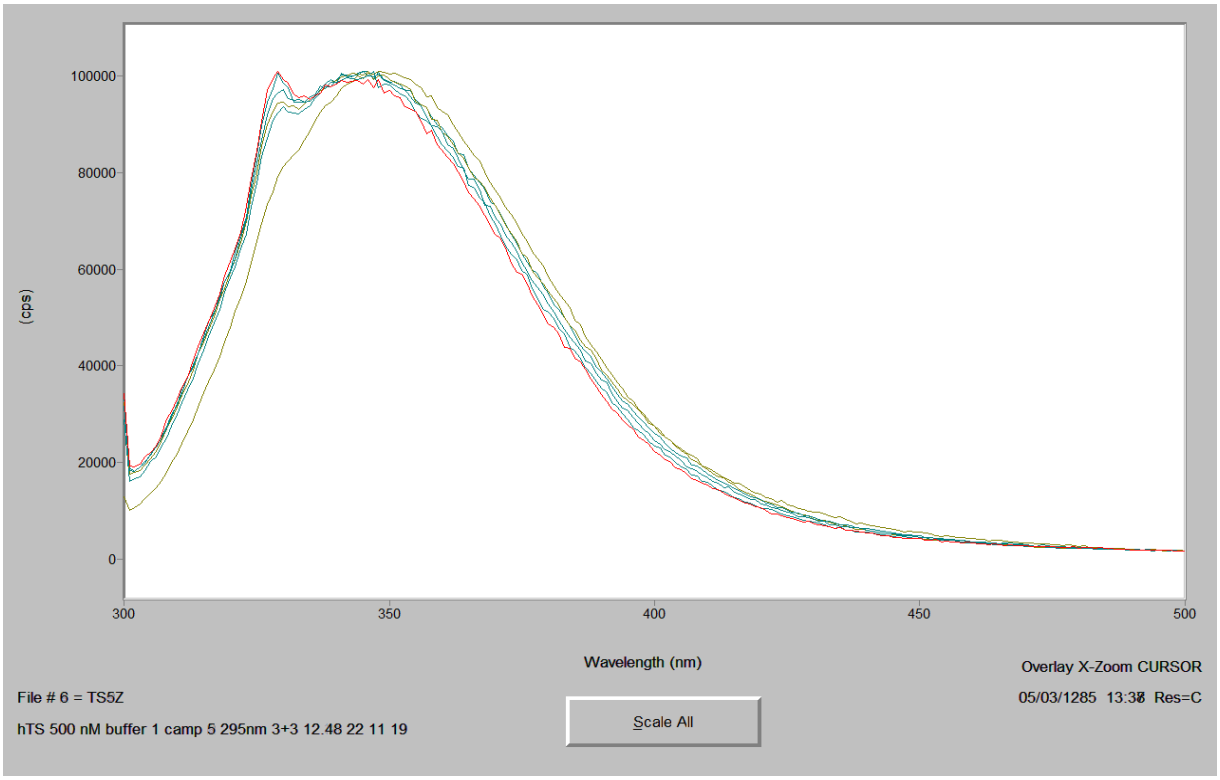

Figure 18:Normalized emission spectra of hTS at, from right to left, KI concentrations 0, 0.025, 0.05, 0.1, 0.2 and 0.3 M. λ_{exc} = 295 nm.

To confirm the larger average solvent exposure, hence the larger accessibility to water-soluble quenchers of the WT hTS Trps relative to the mutant protein Trps, we found that, at equilibrium, 0.3 M iodide quenched the steady-state Trp emission of 500 nM WT and W182A hTS by, respectively, 80% and 50%.

The preferential quenching of more exposed Trps was shown, in both cases, by a blue shift of the emission surviving iodide quenching relative to the unquenched emission – as shown in picture 18.

The emission spectra on Fig.18 were obtained from samples with the same absorbance at the excitation wavelength and show that the WT protein has a stronger emission than the W182A mutant. This is quantitatively established by the relative quantum yields in the table below (Table 3). The W182A/WT relative emission quantum yield, as reported in the table below, decreases when the excitation wavelength is moved towards the red edge of the absorption spectrum, where Trps are selectively excited. We thus conclude that W182 contributes to the overall hTS emission with a larger quantum yield than the average of the other four Trps.

λ_{ecc}	270 nm	280 nm	290 nm	295 nm
$\Phi_f^{W182A} / \Phi_f^{WT}$	0.75	0.8	0.65	0.6

Table 3: W182A/WT hTS relative emission quantum yields at different excitation wavelengths. Solvent: phosphate buffer saline ([Pi] = 20 mM, pH 7.0).

Time-resolved emissions of W182 and WT hTS

The decays of the Trp emission (the excitation wavelength was 296 nm) of the WT and W182A proteins in the PBS buffer ([Pi] = 20 mM, pH 7.0) were well deconvoluted from the measured emission and excitation time-profiles as a four-exponential function (an example is shown in Fig. 20).

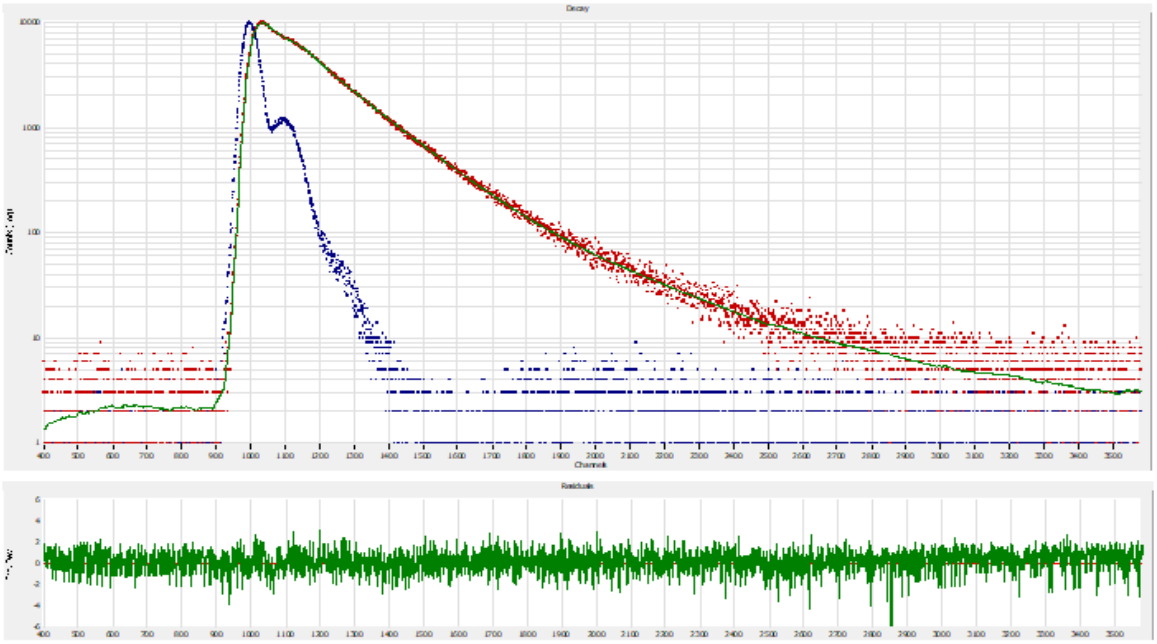

Figure 19: Representative example of time-resolved emission analysis for WT or W182A hTS in PBS buffer. Shown are the time-profiles of the protein emission (red dots) and of the excitation pulse (296 nm, blue dots), the five-exponential fitting curve and the associated residual plot (green). See text for additional details.

A fifth exponential component, with a lifetime in the tens of ns/microsecond range, was usually employed to fit the tail of the time profiles but had abundances of the order of 1% or less. In order to obtain a homogeneous description at all tested experimental conditions, we found useful to reduce the number of degrees of freedom in the deconvolution analysis with least-square residue minimization by keeping fixed the 8 ns lifetime value. This was checked not to force a biased set of fitting parameters by first performing a few fully free 5-exponential fitting analyses. In all these cases, an 8.0±0.3 ns component came out.

The four significant component lifetimes and relative abundances are plotted in Fig. 20 for WT and W182A hTS at three emission wavelengths, from 320 to 380 nm, to allow for a direct comparison between the lifetime profiles of the WT and the mutant protein in spectral regions where emissions from Trps lying in environments with increasing polarities occur. In all cases, short (0.1-0.5 ns) components appear with abundances that are always low and decrease from 320 nm to the higher wavelengths.

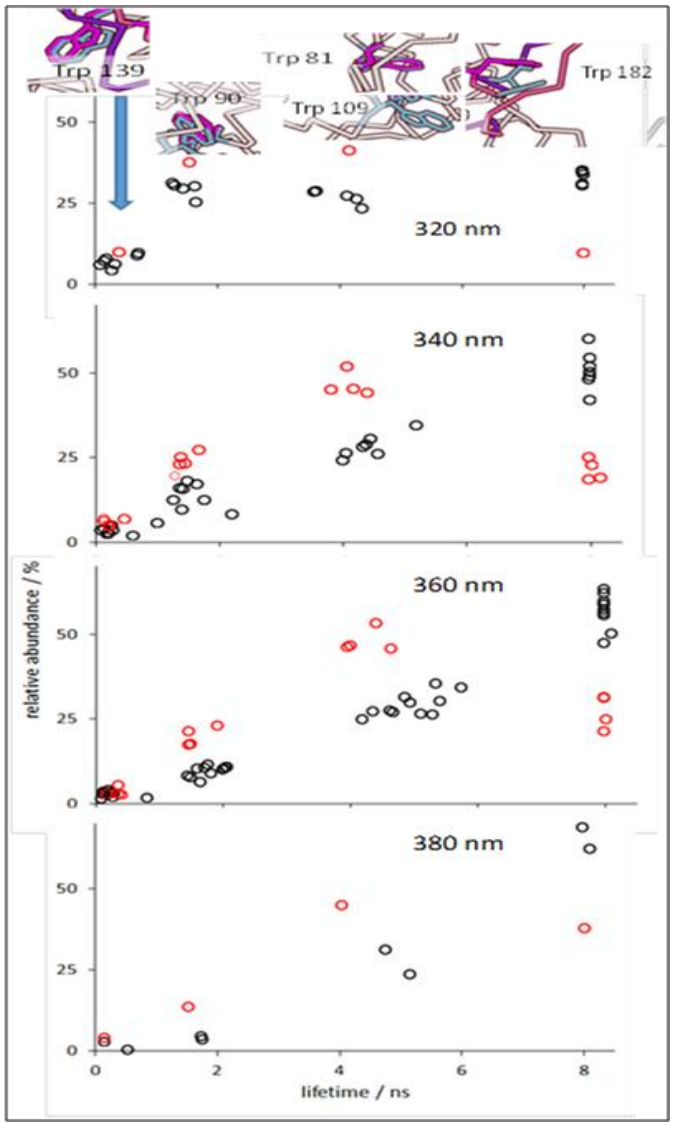

Figure 20: Fluorescence lifetimes and corresponding relative abundances obtained by analyzing the emission time-decays of WT (black circles) and W182A (red circles) hTS at the reported emission wavelengths with a 5-exponential fitting, keeping the 8 ns component lifetime fixed. Solvent: PBS buffer with [Pi] = 20 mM and pH 7.0. Excitation at 296 nm. T = 19 °C. Each line represents a result of a different experiment or, in few cases, of a different fitting of the same decay performed using different initial estimates of the fitting parameters. The sketches on the top represent possible prevailing assignments of the components to individual Trps.

This indicates that in both proteins the most quenched components are attributable to Trps lying in low-polarity, likely hydrophobic domains. Based on the XRD structure of the active and inactive forms of WT hTS (a sketch is shown in Fig.21) we tentatively assign this component to Trp 139.

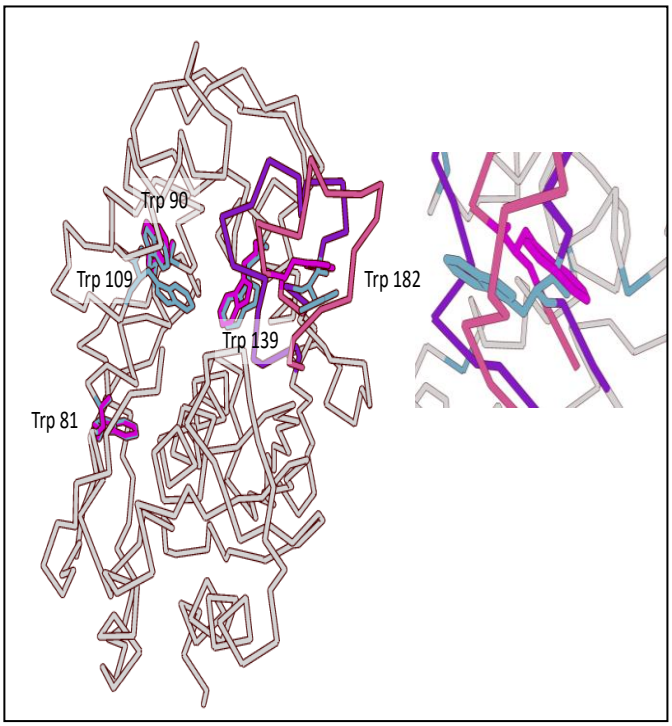

Figure 21: XRD structure (pdb 1HVY) of one of WT hTS monomers. In white, the backbone of the active form; in red and purple the catalytic loop in the inactive (protruding out towards the other monomer) and active forms; the Trps are shown in fuchsia (inactive form) and cyan (active form). Trp 109 is not resolved in the active form XRD structure.

On the other extreme, the abundance of the longest component, 8 ns, is large at all emission wavelengths for WT hTS, and increases from 30% at 320 nm to almost 70% at 380 nm. Thus, the least quenched Trps are the most water-exposed ones. For the mutant protein, the abundances of the 8 ns component are from 1/3 to half the abundances in the WT protein. This indicates that in the WT hTS conformations that are encountered in the PBS buffer the Trp 182 residue strongly contributes to this component and is less quenched and more exposed to water than the other Trps. This is consistent with the steady-state spectra and quantum yields of the mutant in Fig. 16 and Table 3. Of the two additional lifetimes, 1.6 ± 0.3 and between 4 and 5 ns, the shorter one has an abundance that decreases when the emission wavelength is moved to larger values and is thus attributable to Trps lying in low-polarity environments. A possible assignment is to Trp 90. On the other hand, the abundance of the 4-5 ns component is around 25% at all emission wavelengths, but the lifetime distribution moves to larger average lifetime values as the emission moves to the red, from 4 ns at 320 nm to 5 ns at 380 ns. This suggests such a component to correspond to a variety of conformations that are characterized by a broad range of polarities of the Trp microenvironment. A plausible assignment is to the two remaining Trps, 81 and 109. The drastic decrease, relative to WT hTS, in the abundance of the 8 ns component of the W182A mutant makes the 4-5 ns component the prominent one in the decays of this protein at all emission wavelengths. Apart from this, the mutation does not seem to have a strong impact on the lifetime profile, both concerning the lifetime

values and their relative abundances. This finding combines with the similar far-UV CD spectra showed before and suggests that the macroscopic decrease in activity of the mutant relative to the WT proteins ($k_{catW182A}/ k_{catWT}$ = 2/100[31]) likely results from structural changes near the mutated Trp, i.e., in the catalytic loop directly involved in the active/inactive interchange.

Effects of the phosphate ion and dUMP on the conformational variability of WT hTS

As previously reported, addition to an hTS solution in PBS buffer (Pi = 20 mM) of phosphate ions to a final concentration 150 mM causes a small increase (+15%) in the overall intensity; the subsequent addition of dUMP to a final concentration of 220 μM causes a marked intensity decrease (-45%) as shown in the figure on top, as well as a 2.7 nm blue shift of the emission: the band centroid moves from 353.5 to 354.5 and back to 352.8 nm. However, as shown in Fig.23, much lower dUMP concentrations are sufficient to produce the fluorometric changes. Because inner filter effects due to dUMP can be ruled out (Fig. 23), the observed fluorometric changes do reflect a conformational change of WT hTS and, as already said, correspond to a full conversion to the inactive form at high Pi concentrations and to the active one at high dUMP concentrations. We could never revert the inactive-to-active conversion, even at low dUMP concentrations, by adding Pi. Again, as previously reported, we did not observe relevant changes in the emission spectrum of W182A hTS in parallel experiments with added Pi and dUMP. This suggests that if Trp 182

is replaced by alanine either no conformational change is caused by dUMP (in keeping with the mentioned much lower activity of this mutant) or, should any conformational change occur, it would not significantly affect the remaining four Trps.

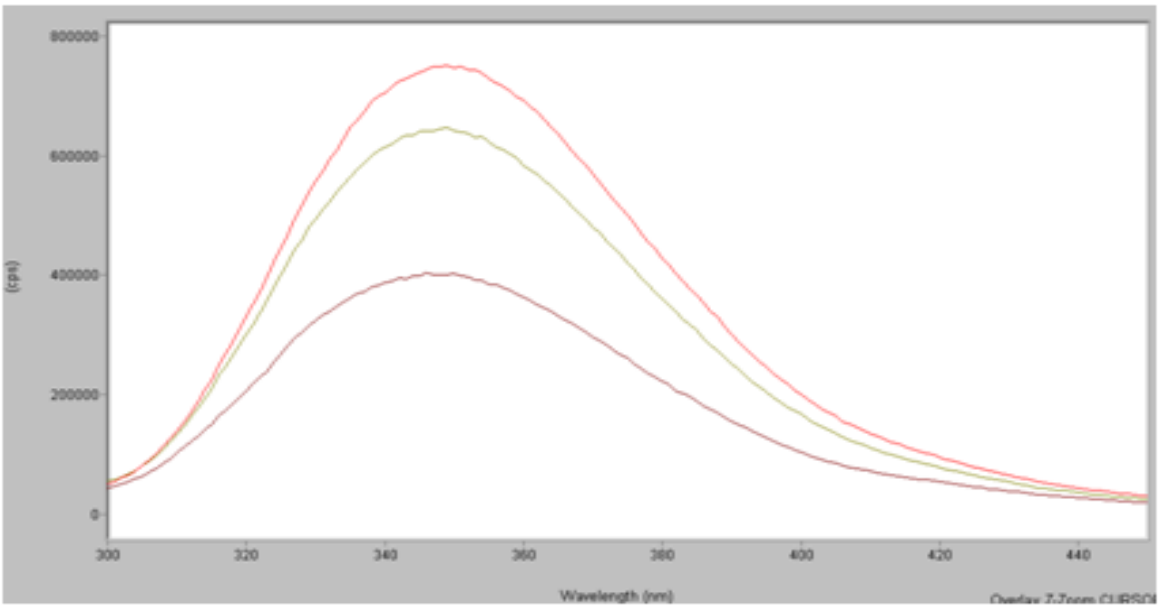

Figure 22: Emission spectra of WT hTS in PBS ([Pi]=20 mM, grey curve), [Pi]=150 mM (red curve), [Pi]=150 mM and [dUMP]=220 µM (purple curve). Uncorrected spectra, Excitation at 295 nm.

So, we have confirmed the already reported steady-state observations. However, our aim is now i) to provide additional fluorometric observables to characterize the different hTS conformations, thus making a fluorescence-based portrait of each form and, as far as possible, ii) to deduce information on the structural changes involving the Trp regions when the active/inactive interconversion takes place.

Concerning the latter point, a spectroscopic tool classically employed to highlight fine changes in the conformation of a protein is CD in the near UV (the 250-310 nm region, where absorption by the chromophoric amino acids occurs). In the CD spectra of WT hTS

shown in Fig. 24, we find that in the Trp absorption region, above 290 nm, the spectra are similar in the three conditions, perhaps only slightly more intense with high [Pi] and no dUMP. We have thus no solid evidence of a marked change in Trp mobility as the conformational changes induced by Pi and dUMP addition take place.

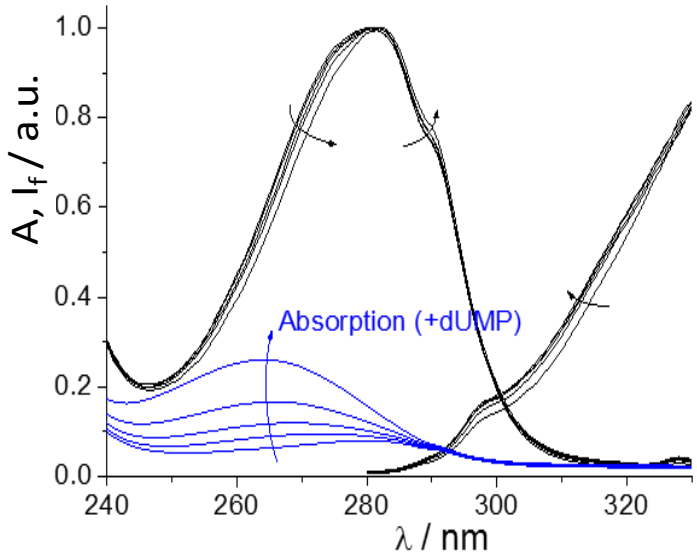

Figure 23: Excitation spectrum and detail of the emission spectrum of hTS in PBS and 150 mM Pi with increasing concentrations of dUMP (0, 1.9, 3.7, 7.2, 13.6 μM). In blue, the absorption of dUMP, showing the absence of inner-filter effects.

On the other hand, a marked negative band in the tyrosine and phenylalanine absorption regions (250-285 nm) becomes visible after dUMP addition. Its minimum lies around 272 nm, 6-7 nm to the red of the dUMP absorption maximum, described in Fig.23. It is thus unlikely that it be completely due to a CD induced in the uridine chromophore of the substrate by coupling with a chiral portion of the protein in the hTS-dUMP complex.

Therefore, a reasonable interpretation is that conversion of the hTS conformation from the inactive to the active forms induced by dUMP binding may cause immobilization of some tyrosines/phenylalanines.

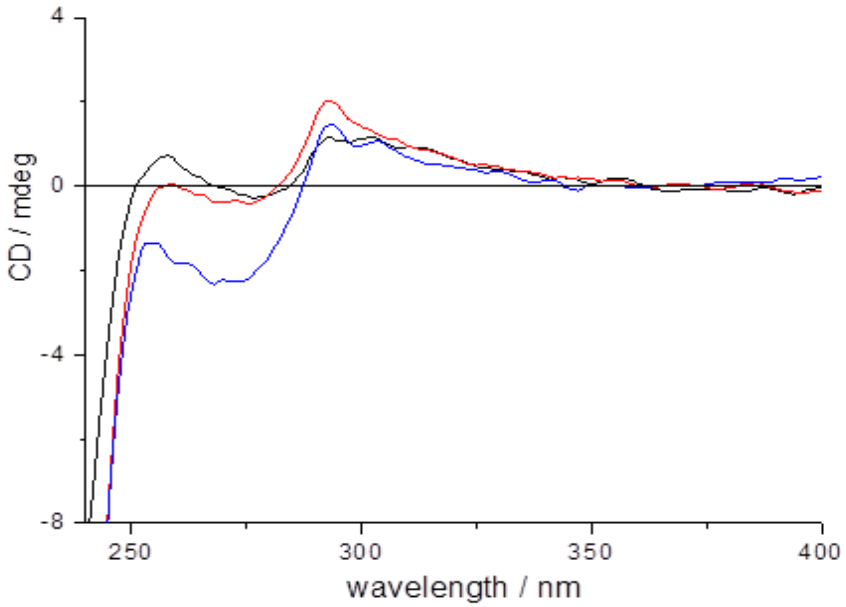

Figure 24: Near-UV CD spectra of WT hTS in Tris buffer ([Pi]=0, black curve), with added Pi (100 mM, red curve) and dUMP (100 μM, blue curve). [hTS] ~ 5.5 μM.

Useful conformation information may be obtained from fluorescence anisotropy. In the table below we show that in the inactive conformation that prevails at high P_i concentration, the most water-exposed Trps, i.e., those with the most red-shifted emission (370 nm, thus Trp 182 above all), have lower excitation anisotropies than the 'average' Trp value (345 nm), 0.035 vs 0.055 at [Pi]=200 mM, in keeping with the larger contribution of the longest lifetime (8 ns) at longer emission wavelengths. Because of the complex

emission decays at the different wavelengths, we do not want to force the analysis to the point of extracting single local rotational diffusion times. For the moment, we limit ourselves to noticing that the increase in Pi concentration, i.e., with full conversion to the inactive form, the anisotropy of the most exposed Trps decreases significantly

	[Pi]=200 mM	10 mM	0.8 mM	0.1 mM
r_{exc} (em. 370, exposed Trps)	0.035	0.050	0.07	0.075
r_{exc} (em. 310, Tyrs + buried Trps)	0.135	0.145	0.145	0.120
r_{exc} (345 nm, average for Trps)	0.055	0.077	0.095	0.095

Table 4: WT hTS fluorescence excitation anisotropies as functions of the emission wavelengths and of the Pi concentration, in the absence of dUMP. Excitation measured between 250 and 295 nm.

Overall, these observations indicate that the most exposed and less quenched Trps are subject to the largest changes in conformation/mobility/environment driven by P_i/dUMP addition.

The lifetime profiles in Fig. 25 fully confirms this suggestion. Again, while small changes are found following addition of Pi to a final concentration of 140 mM starting from a 20 mM solution, more marked changes follow dUMP addition up to a 210 μM concentration.

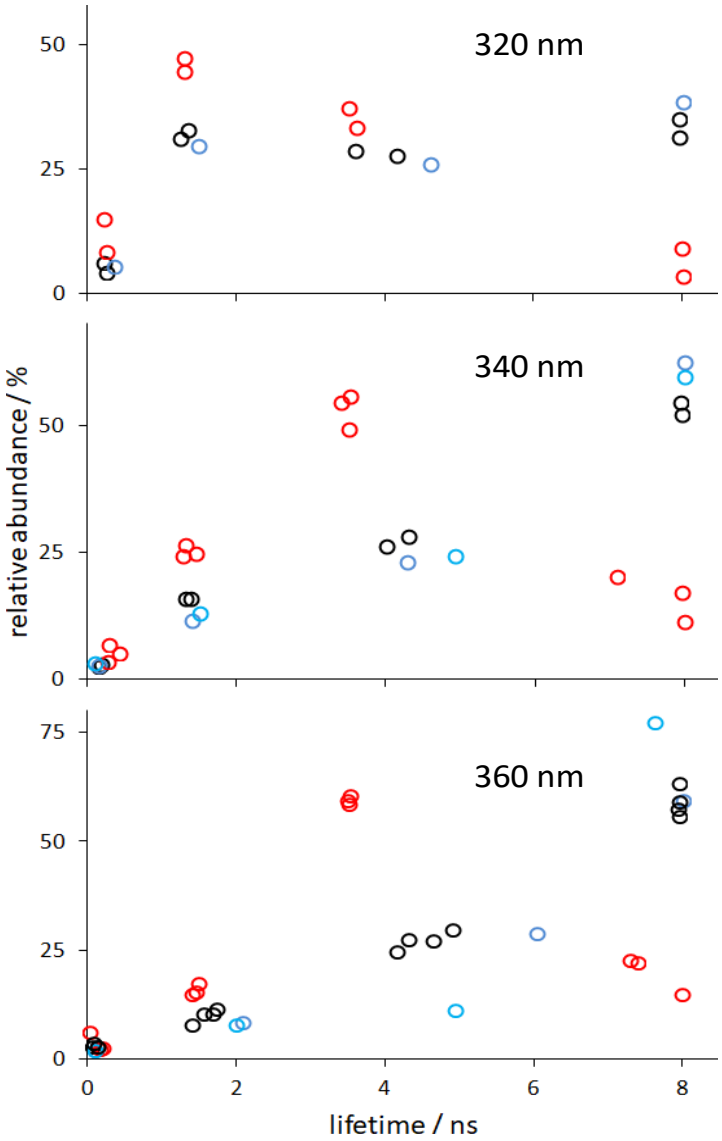

Figure 25: Fluorescence lifetimes and corresponding relative abundances of WT hTS at the reported emission wavelengths with a 5-exponential fitting. Solvent: PBS buffer. [Pi] = 20 mM (black circles), 140 mM (blue circles); [Pi] = 140 mM and [dUMP]=210 μM (red circles). Excitation at 296 nm. T = 19 °C. Each line represents a result of a different experiment or, in few cases, of a different fitting of the same decay performed using different initial estimates of the fitting parameters.

As for the best fitting lifetime values, while the other lifetimes are almost unmodified, a significant decrease is observed for the second longest lifetime, from 4.5 to 3.5 ns at 340 nm and 360 nm. Together with the already mentioned distribution breadth, this finding supports the idea that such a component represents a broader, thus more modifiable collection of conformations around a Trp residue than the other three lifetimes.

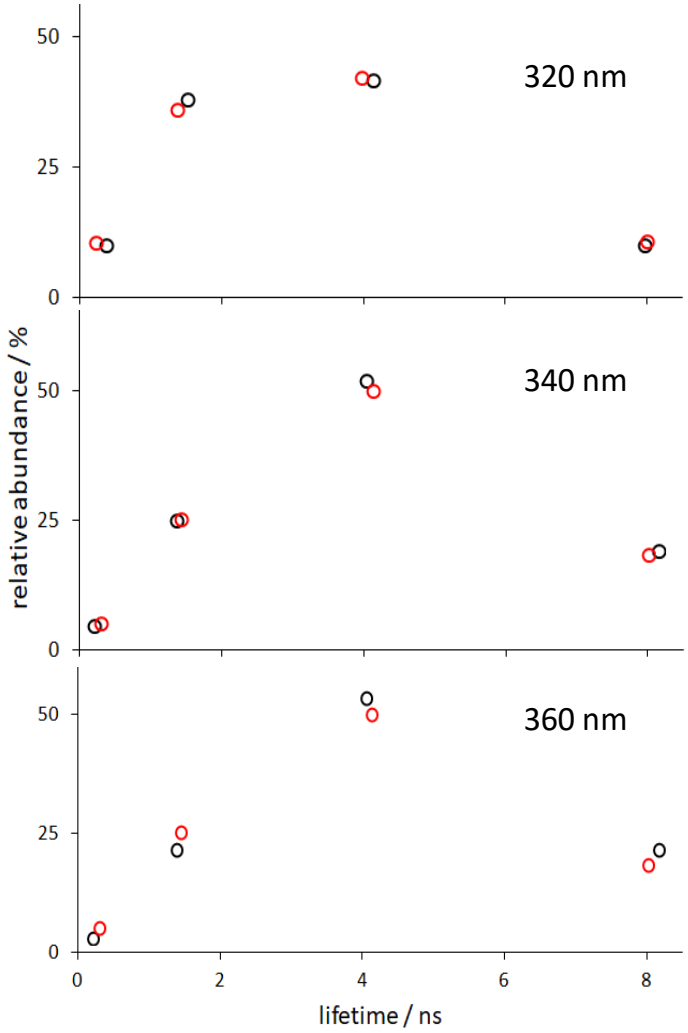

Figure 26: Fluorescence lifetimes and corresponding relative abundances of W182A hTS at the reported emission wavelengths with a 5-exponential fitting. [Pi] = 20 mM (black circles); [Pi] = 140 mM and [dUMP]=210 μM (red circles). For other details, see the legend to Fig.25.

The main change brought about by dUMP addition, hence by conversion to the active protein conformation, and seen at all emission wavelengths is the marked decrease in the 8 ns component relative abundance. This drops from 35 to 6% at 320 nm, from 55 to 15% at 340 nm, from 65 to 20% at 360 nm. As an obvious consequence, the relative abundances (A%) of the other components increase. Their relative proportions are roughly reproduced, but the abundance of the 3.5-4.5 ns component is significantly increased, particularly on the red portion of the emission spectrum: A%(3.5-4.5 ns)/A%(1.5 ns) holds 2 and 2.2 at 340 nm, and 2.5 and 3.5 at 360 nm without and with dUMP, respectively. Quite interestingly, the lifetime profile of WT hTS at high dUMP concentrations, thus in the active form, bears a close resemblance with the lifetime profile of the very little active W182A mutant. The latter exhibits no sensitivity to dUMP addition (Fig.23), in keeping with the previously mentioned indifference of the mutant steady-state emission to P_i or dUMP addition.

As shown in the Fig.21, Trps 81, 90 and 139 are almost superimposable with themselves in the active and the inactive XRD conformations of WT hTS. While we cannot say anything about Trp 109, unresolved in the active conformation, the indole fluorophore of Trp 182 must undergo a ~180° flip and a ~ 5 Å displacement of the centre of mass as a result of the large displacement of the catalytic loop occurring along with the active/inactive transition. Such a relatively large displacement might create the conditions for quenching of this fluorophore, possibly by a nearby backbone peptide group. We may therefore

suggest that the macroscopic decrease in the abundance of the 8 ns component, the decrease in the second longest lifetime, from 4.5 to 3.5 ns, and the increase in its abundance relative to the abundances of the shorter lifetime components result mainly from quenching of the emission from the Trp 182 indole in the active conformation of the protein produced by dUMP binding.

Additional experimental evidence is presently being collected in our laboratory for giving sounder bases to the lifetime assignments and to gain information on the protein dynamics. They consist in: i) collisional, Stern-Volmer quenching experiments to assess the accessibilities of the Trps to quenchers carried by solvent; ii) steady-state and, more informative, time-resolved emission anisotropy, to obtain information on the local protein dynamics in the Trp environments; iii) unfolding by chaotropic agents, to explore the conformational stabilities of the Trp-containing protein domains.

Conclusions

Although yet to be completed, the experimental work reported in this chapter of the thesis clearly shows how intrinsic fluorescence of hTS may provide us a set of observables useful to build fluorometric portraits of the conformational landscapes of hTS in the presence of Pi (so-called inactive conformation) and dUMP (active conformation).

In particular, we have shown that out of the five Trps per monomeric unit, it is Trp 182 that offers the most interesting changes in observables associated with the active/inactive

conformational transition. It mainly exhibits an unquenched (8 ns) and red-shifted emission, likely associated with its exposure to an aqueous (or otherwise polar) environment when the catalytic loop to which it belongs is twisted out of its monomer, facing the other monomer, in the inactive form of the protein. It is instead quite markedly quenched in the active form leaving a much less abundant 8 ns component and producing a 45% decrease in the steady-state emission intensity. The findings, possibly enriched by rotational mobility, quencher accessibility and conformational stability information to be obtained by additional experiments that are underway, can define fluorometric portraits of the two main functionally relevant conformational collections of hTS, the 'active' and the 'inactive' ones. One or more of them can be employed to gain structural and dynamic information on crucial features of the active/inactive interconversion of this protein.

2.3.1.1 Preliminary exploration of some dynamical features of the active/inactive interconversion of hTS

Fluorometric monitoring of the time courses of the hTS conformational changes induced by phosphate-ion and dUMP

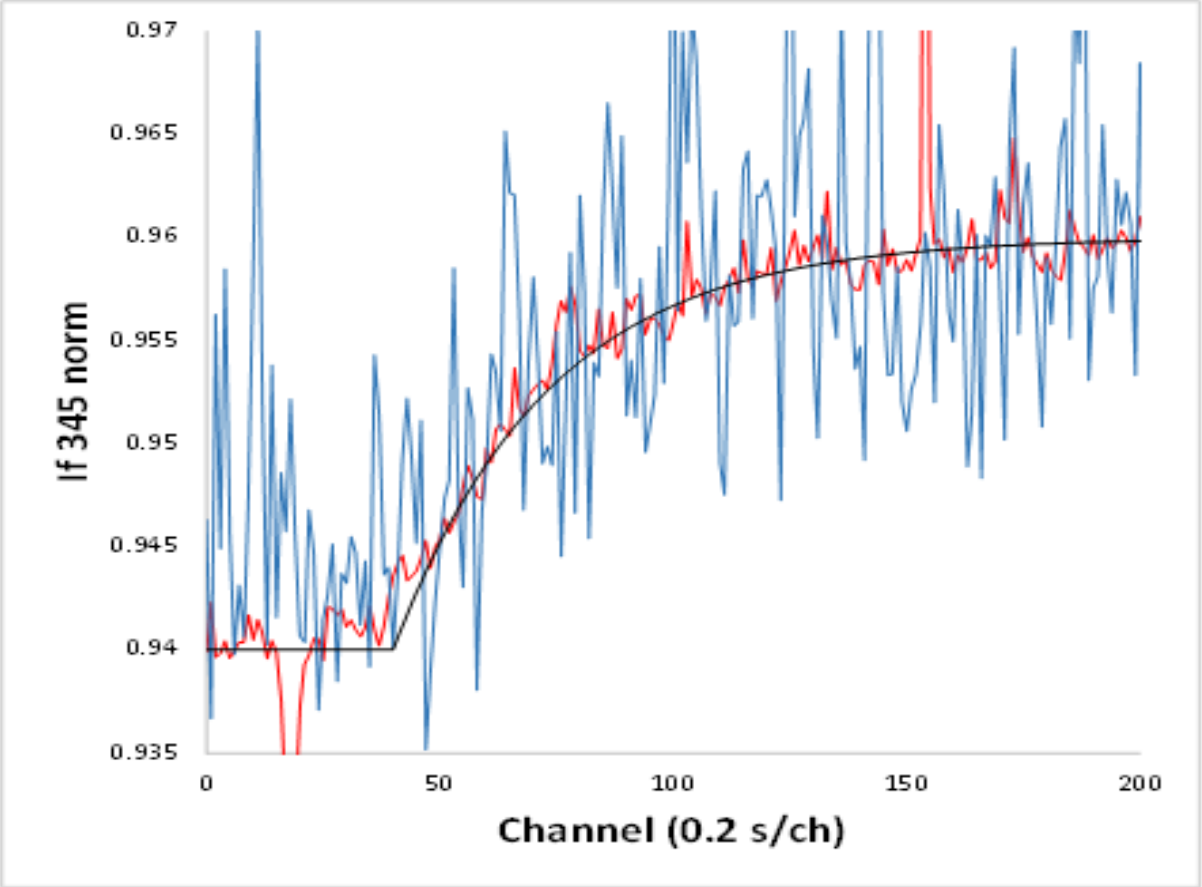

Figure 27: Time course of the WT hTS emission intensity at 345 nm following addition of 10 (blue curve) e 100 µl (red curve) of 2 M Pi. [hTS] = 2 µM in 1 mL. Excitation at 295 nm. T = 13 °C.

Fast addition of Pi to final concentrations 20 and 200 mM to WT hTS in Tris buffer caused the intrinsic emission increase shown in Fig.27. The emission increase, that we have

associated with full conversion to the inactive conformation, follows a first-order kinetics with a rate constant 0.15 s^{-1}, corresponding to a time of 7 s.

As the observed kinetics does not depend on the volume of 2M Pi added, hence, on the final Pi concentration. This likely rules out the possibilities that the observed kinetics be controlled either by a pseudo-first order, Pi-concentration-dependent binding of phosphate ions to hTS or by the process of mixing of the two solutions, i.e., of Pi concentration homogenization (this would hardly show as a single-exponential process independent of the added volume and Pi final concentration). It should thus represent the

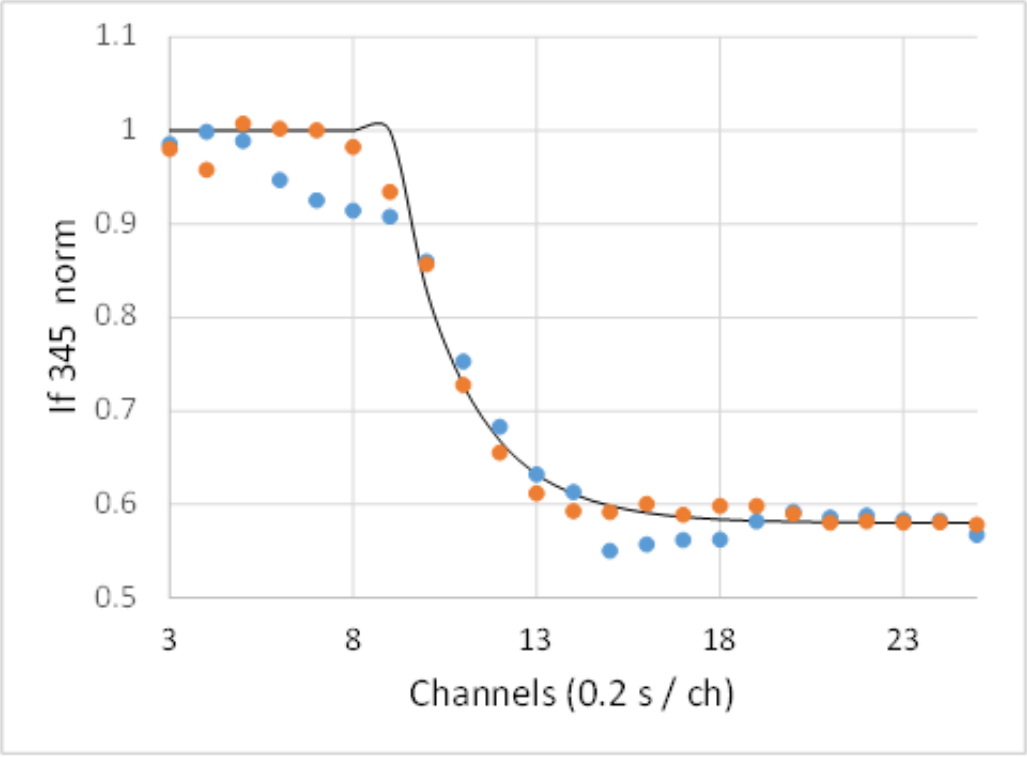

Figure 28:Time course of the WT hTS emission intensity at 345 nm following addition of 10 µl of 8.7 mM dUMP to 1 mL of 2 mM protein. The results of two repetitions of the experiment are shown. Excitation at 295 nm. T = 13 °C.

kinetics of the active-to-inactive conversion of the protein, likely the rate-limiting step in the overall process.

In keeping with the steady-state results previously shown, the final value is 42% lower than the initial one, thus consistent with conversion from the inactive to the active forms of the protein. This process is more than one order of magnitude faster than the opposite conversion shown above. Fitting of the data with a single exponential function yields a rate constant of 2.5 s^{-1}, corresponding to a time of 0.4 s. Such times may be close to the time resolution of our spectrofluorometer and stirring system. So, we will not dwell into a far-reaching analysis of these kinetic data. Stopped-flow experiments with fluorescence detection are needed to check the reliability of these results and have been scheduled in the near future.

In any case, these experiments clearly prove that the conformational hTS interconversions triggered by the phosphate ions and dUMP take place in time scales that are not longer than few seconds. This, in turn, proves that in the steady-state and time-resolved experiments illustrated in the previous paragraphs the measurements, performed a few minutes after Pi or dUMP addition, probed fully equilibrated systems.

2.3.2 Preliminary Isothermal-Titration-Calorimetry (ITC) experiments explore the thermodynamics of the processes following dUMP addition to the inactive form of hTS

As presented already in the introduction chapter of this thesis, hTS presents two different conformers, a quite unique quality among all other orthologues. Differences between the two stems from structural changes that the enzyme undergoes in certain conditions. As explained, some molecules in this regard may act as "effectors" in the active-inactive equilibrium, bringing this closer to either one of the structures. It still remains unknown, at this point and time, how this process works, and if any amino acidic residues may be most engaged in this.

As such a process is one where structural changes are involved, attempting at the quantification of such energies may allow a general working model of the enzyme to be had, which can be used as a basis for further analysis.

Within this context, the Isothermal Titration Calorimetry (ITC) was employed to study the inactive-active transition process. This, as reported in the introduction, happens whenever dUMP is added to a purified hTS solution: its binding switches the conformer from the inactive state to the active one. The idea was to replicate one such situation where the inactive conformer was mostly represented, and slowly titrating dUMP to this solution to study the inactive-active change.

As reported In the Materials and Methods section of this thesis, the ITC was performed with the MicroCal VP-ITC instrument. Two identical solutions were prepared, with 180 mM of Sodium Phosphate, 20 micromolars of hTSwt in Phosphate free Buffer 1, about 4 mL. In this case, the solution was degassed before adding the protein, to avoid precipitation. The titration process was conducted over a total of 125 injection, with a stock concentration of dUMP equal to 1.21 mM. The final concentration in the sample cell solution was 180 μM. To subtract the contribution of sodium phosphate presence in the process, a second run was done, with the same characteristics as the first, minus the protein.

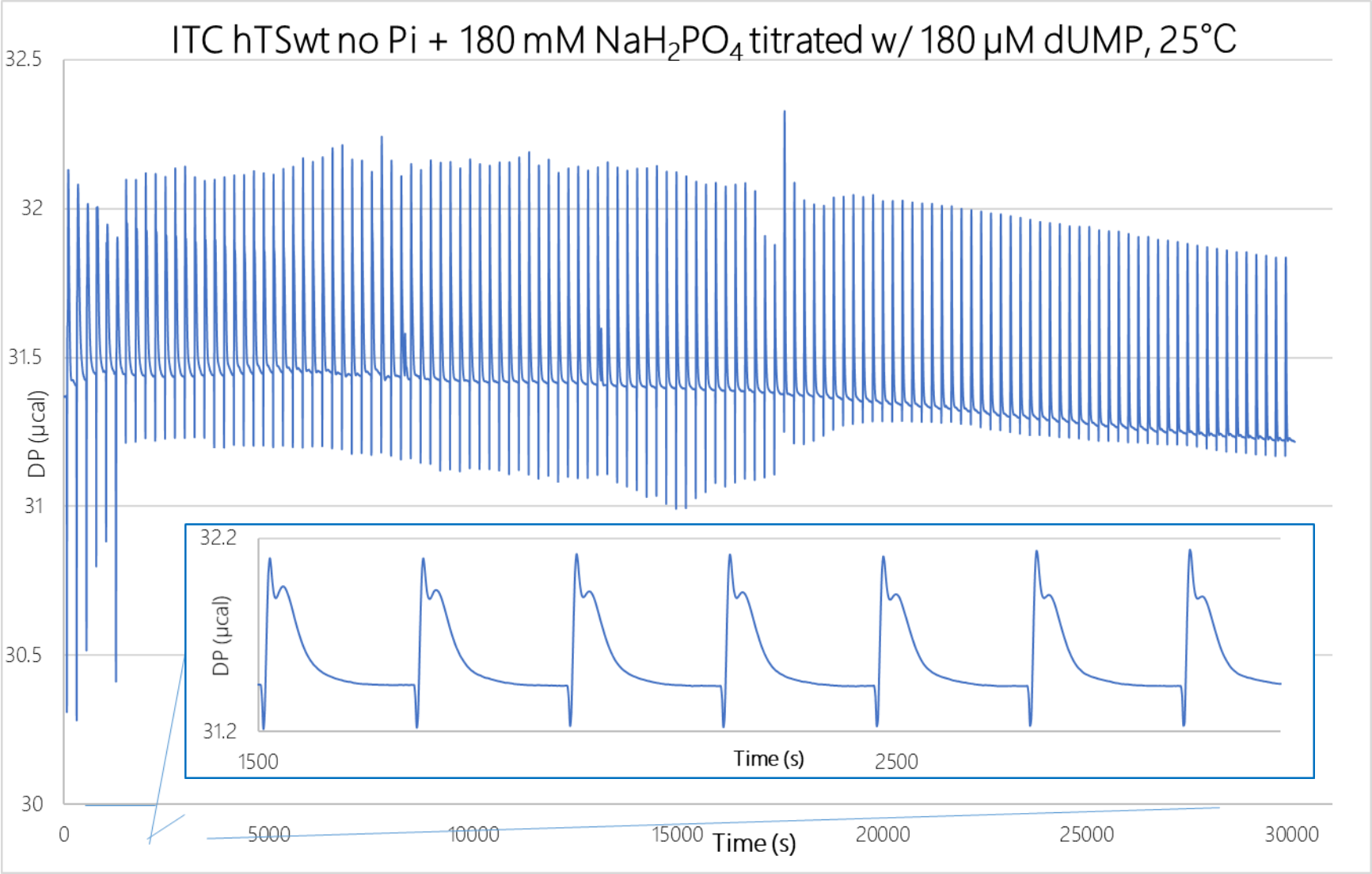

Graph 12: ITC data of dUMP titration of hTSwt in Phosphate free buffer, after adding NaH_2PO_4. Experiment conducted at 25°C.

The previous page reports the result of the dUMP titration of the solution containing the enzyme – graph 12. Given the huge data amount, a portion of the data was selected to show a particular behavior observed at the beginning of the process. This small picture of the graph represents 7 injections and the correspondent instrument response. Each injection of the group, better appreciated in the picture here below – Fig.29, is characterized by 3 – 4 events that happen in chronological order.

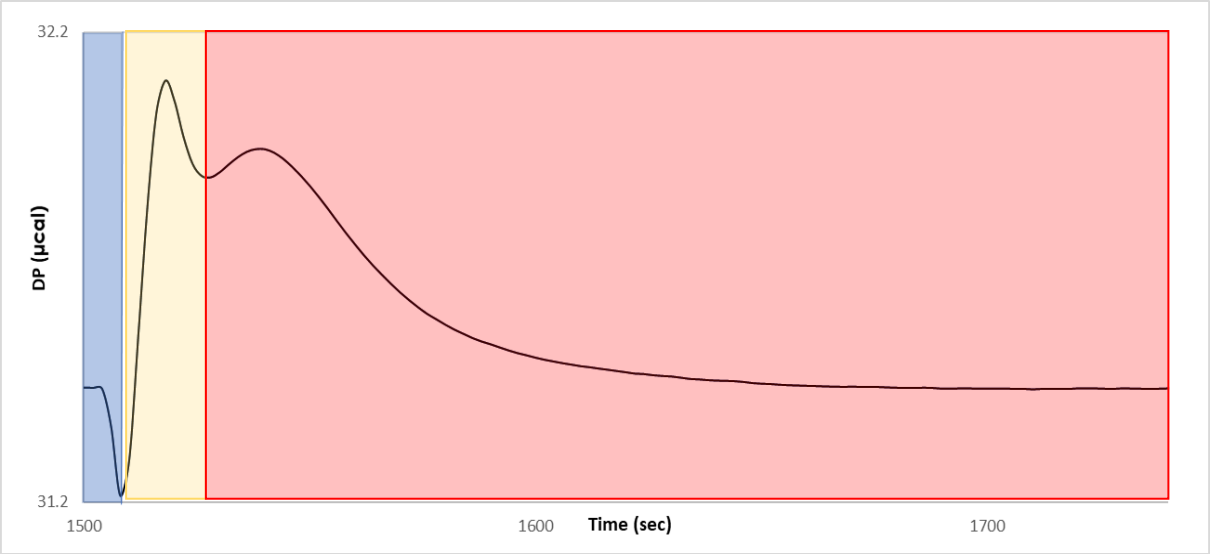

Figure 29: Single ITC injection of Graph 12.

In time order, the first event is a fast exothermic (in blue), then a second fast endothermic one, characterized by a 1 microcal amplitude (yellow). As this one ends, another endothermic event seems to happen, albeit a much slower one (red). In later injections a 4th endothermic element is present – not shown in the picture above. However, with the sole enzymatic titration analysis, it is impossible to define if any of these contributions pertain to more or less specific events. Hence, as explained before, another experiment

was devised, without the protein (Graph 13 next page). In this case, whatever the contribution be, if anything different can be observed, it has to be due to the protein's presence.

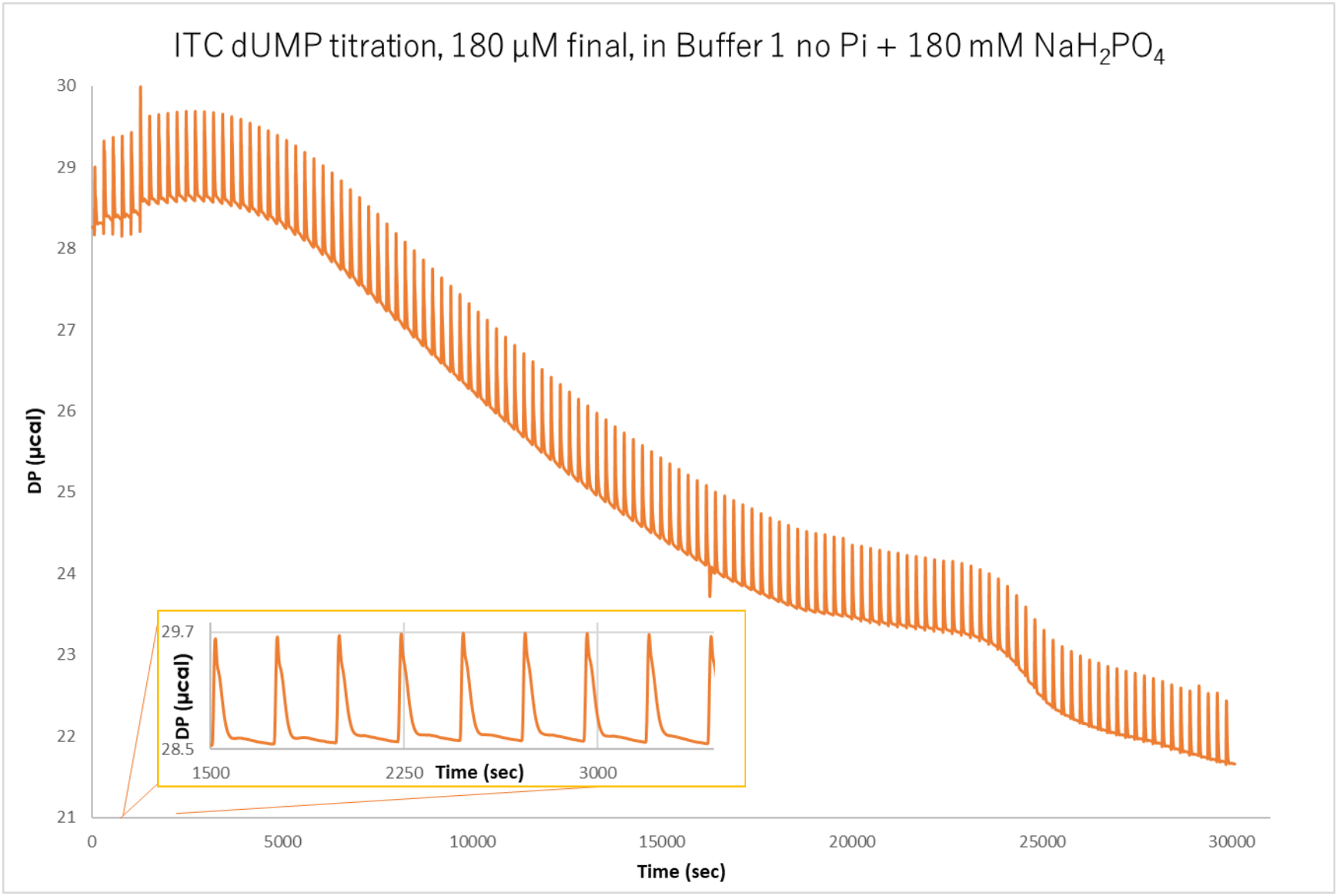

Graph 13: ITC data of dUMP titration of Phosphate free buffer, after adding NaH_2PO_4. Experiment conducted at 25°C.

The analysis was conducted thanks to Prof. Glauco Ponterini.

The descendent tendency of the graph was due to a baseline issue, which can be resolved mathematically, by first averaging the DP value of the control measurement, to 240 points of the measured values. Hence, the first value of the averaged control data would be 240 seconds delayed (more or less one injection) and its DP value would be the average of the first 240 DP values measured, corresponding to 1-239 seconds (240 values).

This is done via a simple formula in Excel:

$$DP_{avg}=AVERAGE\ (A1:A239)$$

done on the column A (in this example) containing said values. Hence the second averaged value would contain the average of (A2:A240) values and so on for all values. These averaged values are then used in a simple point to point subtraction process, adding 25.

$$DP_{new}=(DP_{old}-DP_{avg}) + 25$$

This allows to obtain a nicer baseline, whenever this is not possible to be obtained due to environmental conditions. The results can be seen in the next graph – Graph 14 –

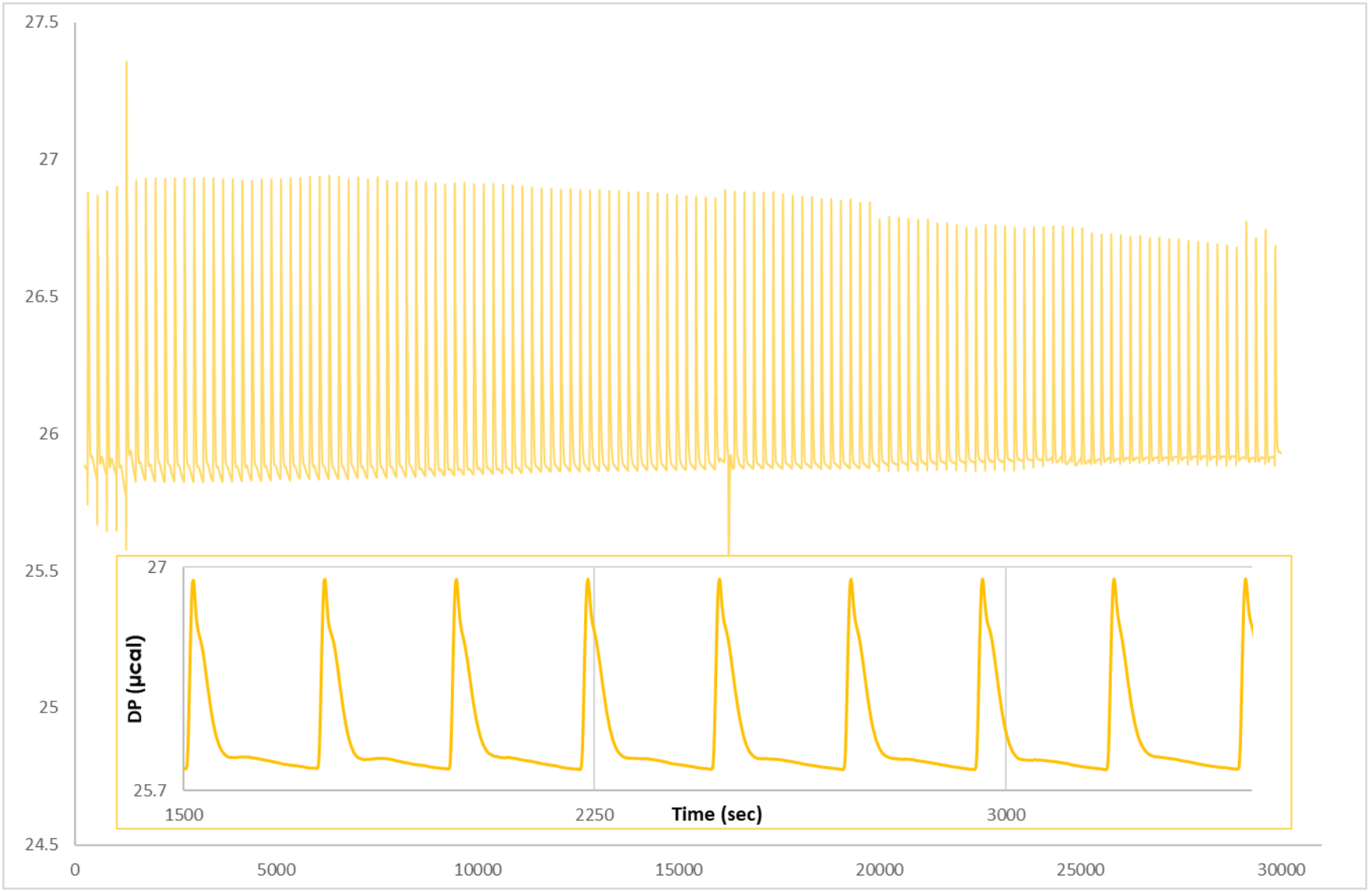

Graph 14: Graph 13 corrected for baseline.

In order to understand if this process was completed correctly, one could simply compare data from the two sets to see if the two are identical – Fig.30. In orange, the original data, in yellow the averaged data with the corrected base line.

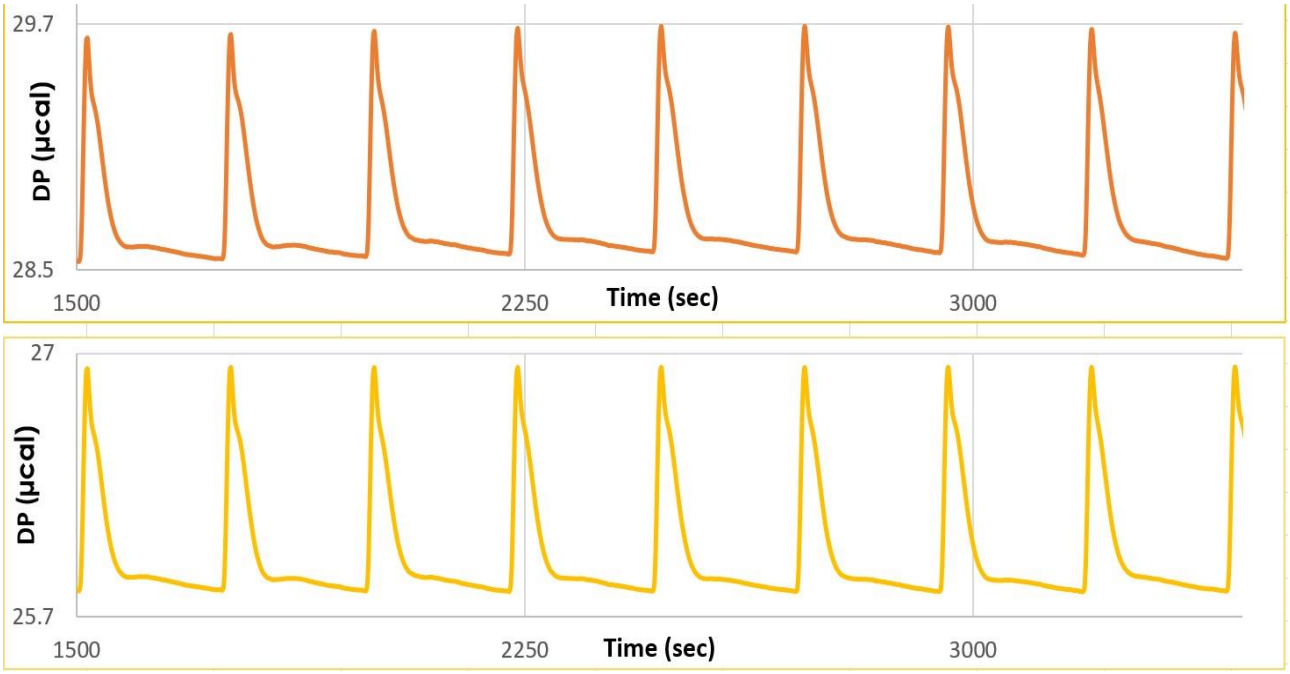

Figure 30: Injections confront between "raw" ITC data from Graph 13 and "corrected" ITC data from Graph 14.

Moving on to the analysis of a single injection (Fig.31): in this case, three different contributes may be in place: the first, a rather fast endothermic process, (green) followed by a mostly subtle second, slower process (in red) and finally to a very low intensity endothermic process (blue).

To have a better understanding now of what's going on in the making of the titration, one such idea would be to subtract the value of the control to the value of the signal.

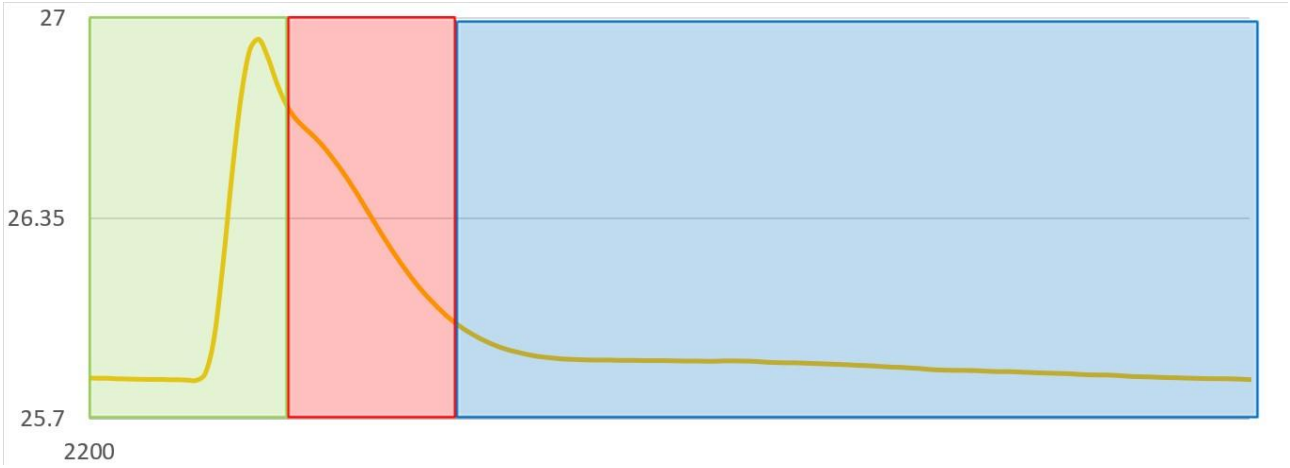

Figure 31: Single Injection analysis of an injection from Graph 14.

This was attempted, as shown in the next graph. The general idea was to take the signal data from the enzymatic titration and then point to point subtract the value of the control. Going step by step, the data from the enzyme-dUMP titration was subtracted point to point with the data obtained from the control titration in absence of enzyme.

The latter however, had a baseline issue, which required one to be prepared so that the data could at least be compared. There is another issue given by the fact that the "weight" of the subtraction process is unknown, and a process of error and trial may allow to understand the situation. The latter, especially, is an important feature, as it measures the "weight" of the control titration.

Following this concept, a point to point subtraction was done through this formula:

$$DP_{res} = DP_{enz}-(DPavg_{enz}-25.84)-\varepsilon*DP_{cont+1}+25$$

where DP_{res} is the value of DP resulting from the calculation, DP_{enz} is the DP value in the enzymatic titration, avg_{enz} is the average of DP value in the enzymatic titration, ε is a correction factor that may range from 0 to +1, Dp_{cont+1} is the DP value of the control titration on the next

step with respect to the one considered. The result of this calculation, for ε=1, can be seen in the next graph.

Graph 15: ITC data result from the subtraction of control titration - no protein - from the hTSwt titration with dUMP.

The result of this calculation brings us to a first, visible conclusion. The exothermic processes, which are represented by depressions in the graph – Graph 15 – that come at the initial moments of the injection, exclusively pertain to the enzymatic titration and were not in fact present in the control titration.

Figure 32: Single Injection data from Graph 15.

Analyzing a single injection gives allows also the following remarks:

- First and foremost, from a calorimetric point of view, the processes analyzed in this fashion tend to take quite more time than one could initially suspect. The whole process, calorimetrically, is completed in a matter of hundreds of seconds.
- Within this time, there are many different contributions at hand, two rather fast exothermic processes, with a rather high signal (yellow and blue squares) when compared with the only endothermic process (green) which seems to be rather slow in comparison, and particularly less intense if compared with the two previous ones.
- The whole process has a ΔDP just shy of 800 nanocalories, which is interesting in itself, as most of the contribution in this are due to exothermic processes, most often assigned to molecules interacting and binding. Endothermic processes, on

the other hand, are usually associated with dilution heats and, more interestingly, structural reassortments.

Conclusions

Given how literature tends to correlate peaks and contributions, and based on the data obtained thus far, one could try and assign the contributions to dUMP binding exothermically, and to whatever molecular mechanism may follow (included the inactive-active transition).

The titration process presented in this thesis is one where the enzyme is titrated with more or less 1,44 micromoles/liter of dUMP for each addition. With an initial hTS concentration of about 20 micromoles/liter, and two binding sites. To fill out all binding sites, 40 micromolars would be required. This amount would be reached between the 27^{th} and the 28^{th} injection. At 240 seconds between injections, this would mean 6667.67 seconds from the beginning of the process. It is interesting to notice how powerful a technique ITC is, allowing one to follow a certain process time wise. In this case, comparing the processes at 1400 seconds and those at 6000 seconds, some differences start to arise. As a matter of fact, the endothermic feature that is interestingly present in the first injections disappears; this is also partially true for one of the exothermic contributions, the slower one (in blue, in the colored injection analysis). From the analysis presented thus far, it seems that these two contributions seem to be intertwined; differences in this sense need to be looked from the calorimetric point of view first, then from the kinetic one. The progressive diminishing of the intensity of the second exothermic peak may be due to an endothermic one that is occurring at the

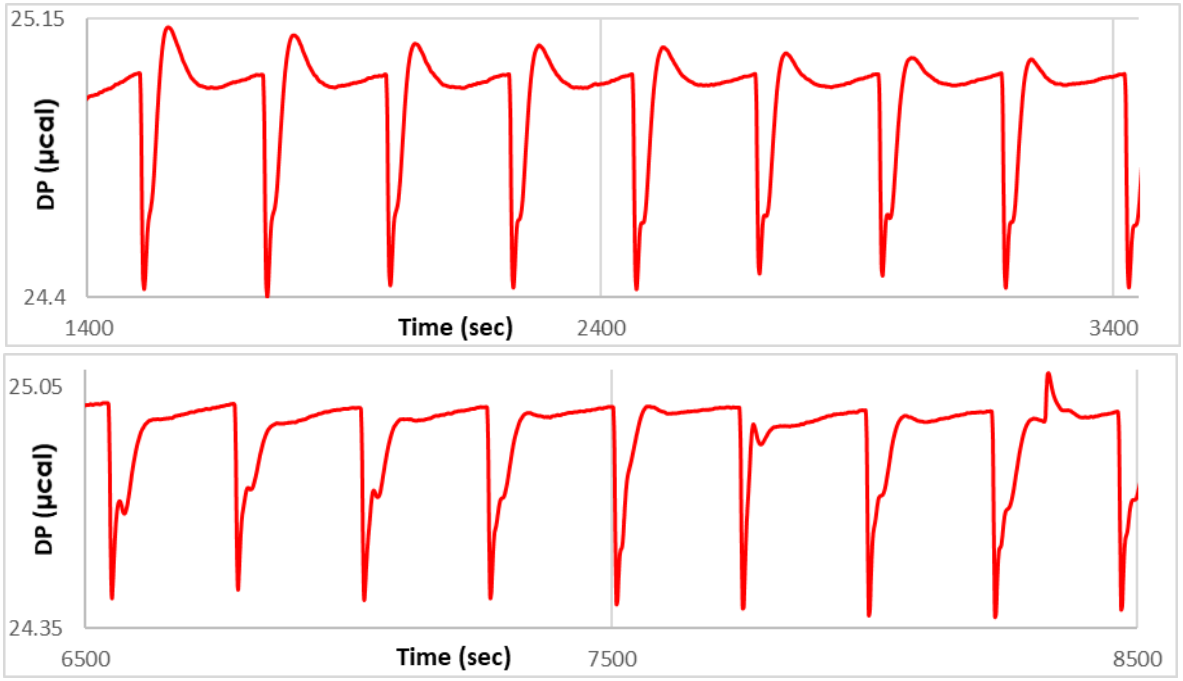

Figure 33: Different elements from Graph 15. On top, 2000 seconds of data; the endothermic contribution is appreciable but disappears later in the titration – bottom picture.

same time, which could explain why the first exothermic contribution mostly remains the same and only the second-third ones do happen to change. Following this line of reasoning, one could say that the first contribution is indeed due to the binding process of dUMP to the enzyme.

Regarding how to assign the second and third contributions, it is not such an easy task. If a consecutive event happens after the dUMP binding, it is reasonably expected to do so as a direct consequence of it, immediately after. If any contribution in the inactive-

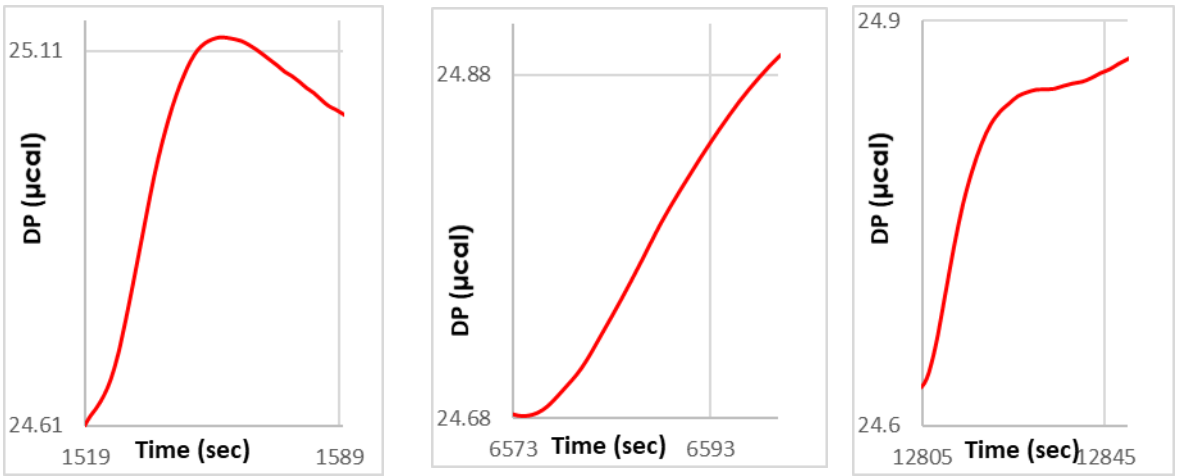

Figure 34: Differences in ITC data – variation of 2nd and 3rd portion of Fig. 32 at different times.

active transition were to be looked for, it would be reasonable enough to further investigate this 200 to 300 nanocalories event and how much time it takes to complete itself. This subtle analysis requires a complex, combined thermodynamic and kinetic model and is left for work to be done in the near future with the collaboration of an ITC expert (Prof. D.Fessas, University of Milan).

-

Page Intentionally left blank

Chapter 3 – Materials and Methods

Experiments conducted on the human TS required its expression and purification. Such a process allows one to obtain a mostly purified protein by inducing its expression in an appropriate vector, usually *E. coli* cells, using plasmids which are usually characterized by at least two elements: an induction and an antibiotic resistance gene. The former allows to control the protein expression during a phase where the vector culture is mostly active. The latter confers resistance to an antibiotic, selecting only those cells that effectively obtained the plasmid.

The purification process allows for the target protein to be effectively isolated from any other molecule synthesized by the vectors. This is usually achieved by means of liquid chromatography, an incredibly sensible and accurate technique allowing for an effective separation of molecules given their chemical and/or physical properties.

All experiments have been conducted at an environmental temperature of 22 ± 2°C, unless diversely specified.

3.1 General information on expression and purification of hTS molecules.

Human TS wild type and mutant molecules were enclosed in pQE80L plasmids and expressed in *E. coli* BL21(DE3) cells.

3.1.1 pQE-80L plasmid

pQE-80L is a synthetic DNA construct of 4751bp, high copy number plasmid. It is one of the most used plasmids paired to *E. coli* expression.

Its key features are:

- T5 promoter for the *E. coli* RNA polymerase, contained between bp 10 and 54
- lac repressor moiety (bp 30 and 46; 62 and 78) which binds to the lac operator in order to inhibit the transcription whilst in *E. coli*. This is encoded by lacI
- Ribosome binding site at bp 101 to 106
- Start codon at bp 115
- 6xHis affinity tag at bp 127 to 144
- lacI repressor between bp 1249 to 2331. It binds to the lac operator to inhibit the transcription whilst in *E. coli*.
- laclq mutant promoter between bp 2332 and 2409. The mutation increases 10-fold the expression of the lacI gene.
- High Copy Number origin, bp 2927 and 3515

- A Beta-Lactamase gene (bla), bp 3686 to 4546, that confers resistance to ampicillin, carbenicillin and other related antibiotics.
- bla promoter, bp 4547 to 4561.

3.1.2 BL21(DE3) *E. coli* colonies

E. coli is a Gram-negative bacterium, either nonmobile or using flagella for mobility. It is facultative anaerobic, capable thus of both respiratory and fermentative metabolisms, commonly found in the gut of animals.

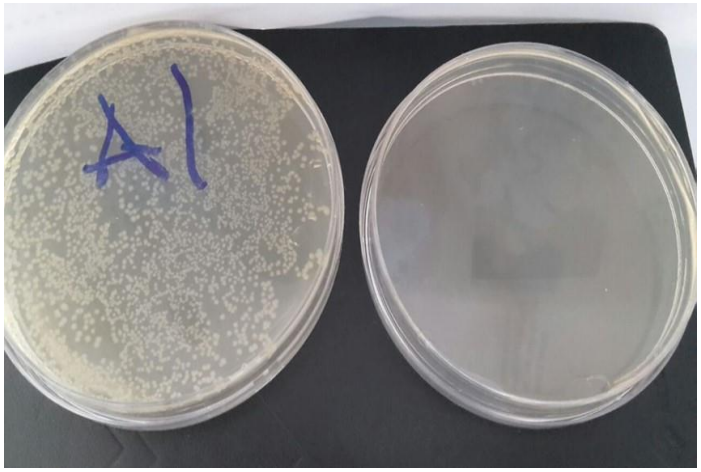

Figure 35: *E. coli* in a Petri's dish vs a control one.

E. coli B strain is a known research model in science whose applications range from studies on phage sensitivity, to restriction-modification system, to expression and synthesis of proteins in life science laboratories. Among the B strain, BL21(DE3) is the most used.

BL21(DE3) cells are a B strain *E. coli* cells whose main characteristics are:

- Lack of two proteases: Lon (cytoplasm) and OmpT (outer membrane) which is typical of E. coli cells pertaining to B-strain.
- Presence of λDE3 lysogen, carrying the gene for the T7 RNA, under control of the lacUV5. BL21(DE3) is also suitable for the T5 promoter system.

3.2 Spectrophotometry

Spectrophotometry is one such technique that allows the analysis of the interaction between matter and electromagnetic radiations, in order to quantitatively determine either reflective or transmissive properties of the former, expressed as a wavelength function. As a world of its own, spectroscopy has multiple applications which are not limited to the biological or biochemistry. On the matter of this thesis, however, only the near UV-vis electronic absorbance spectroscopy will be further delved and discussed. Such is the term that identifies absorption phenomena of light radiations in the visible (700 nm – 350 nm) and near ultraviolet or UV region (350 nm – 250 nm) of the electromagnetic spectrum. Absorbance of said radiations cause the most external electrons of a molecule to transition.

Any spectrophotometric assay, irrespective of its ultimate goal, is based two principles which combined give the Beer – Lambert Law.

- Lambert's law: "*the fraction of light absorbed by a transparent medium is independent of the incident light intensity, and each successive layer of the medium absorbs an equal fraction of the light passing through it*". In other words, light intensity decays in an exponential fashion, best described with the following equation:

$$\log_{10}\left(\frac{I_0}{I}\right) = kl$$

Equation 14: Lambert's Law.

where I_o the intensity of incident light, I is the intensity of transmitted light, l is the length of the optical path within the cuvette used and k is a constant described in Beer's law

- Beer's law: "*the amount of light absorbed is proportional to the number of molecules of the chromophore through which the light passes*" explains how the constant k and the concentration of the chromophore are proportional:

$$k = \epsilon c$$

Equation 15: Beer's Law.

ϵ is defined as the molar absorption coefficient, which is an intrinsic property of chromophores, and corresponds to the absorption of a molar solution (1 mol litre^{-1}) in a cm unit wavelength light path. Hence molar absorption coefficient can be either expressed in liter cm^{-1} mol^{-1} or M^{-1} cm^{-1}.

Combining the two equations into one give Eq.16:

$$\log_{10}\left(\frac{I_o}{I}\right) = \epsilon c l$$

Equation 16: Beer - Lambert Law.

The logarithm is defined Absorbance (A) or sometimes referred as Attenuance (D). Whilst the pathlength is expressed in cm, wavelength is expressed in nm, both are usually found as subscripts of the absorbance (e.g. $A_{1cm\ 380}$). To be noted that whilst pathlength measure

unit is used as it may differ depending from the cuvette used, wavelength measure unit is never specified as it is intended to be expressed in nanometers. Another way to quantify the amount of light passing through a sample within a cuvette is Transmittance (T), which is equal to the argument of the base 10 logarithm in the previous equation:

$$T = \frac{I}{I_0}; \qquad A = \log_{10}\left(\frac{1}{T}\right)$$

Equation 17: Transmittance and its relation to Absorbance.

This value is usually expressed as a percentage; as the aforementioned formula shows, if for example the Absorbance is 3, the Transmittance is equal to 0,1% - only that percentage of incident light is transmitted. There is, however, a critical difference between absorbance and transmittance. Only the former is directly and linearly proportional (within certain limits, however) to the chromophore concentration. Hence, for quantitative experiments, Absorbance will be used.

Such limitations may be best explained by considering another expression of the Beer – Lambert law. To do this, imagine that a solution, contained within a cuvette. Of the total solution, let's consider an infinitely small slice *dx* of this solution. Said slice will contain a certain amount "n" of light absorbing molecules per cubic centimeter. With σ as the cross section for absorption in squared centimeters, we can define the smallest contribution *dI* of light intensity absorbed per thickness *dx* of the sample as:

$$\frac{dI}{dx} = -I\sigma n$$

with I as the incident light, and n as the number of molecules per cubic centimeter. Forcing $I = I_0$ when $x=x_0$ in the equation, and integrating, gives:

$$\ln \frac{I_o}{I} = \sigma n d$$

where d is introduced as the thickness of the sample. σ value depends strictly upon the molar extinction coefficient ε:

$$\sigma = 2{,}303 \frac{\epsilon c}{n} \; ;$$

$$n = \frac{Nc}{10^3} ;$$

$$\sigma = 3{,}82 \; x10^{-23} \epsilon$$

expressed now in cm^2.

Biological samples may deviate from the Beer Lambert law for the presence of macromolecules or other molecular actors capable of scattering light. As the concept of

"optical density" was introduced in the previous paragraph, it is worth noting that the optical density from scattered light is defined by the Rayleigh equation, $\frac{I}{\lambda^4}$

Linearity between Absorbance and chromophore concentration is theoretically true, however there are physical conditions that constraint the applicability of the Beer-Lambert law. Deviation from linearity is due to stray light; in short, with this term, a white light is identified; two sources may cause this phenomenon:

- The monochromator, which should theoretically be eliminated through good design and filters
- Light leaks around the detector or sample region, which should theoretically be eliminated by good design and masking.

Each spectrophotometer has different designs, which translate directly to different stray light characteristics, hence to different deviations to linearity, which may be more or less pronounced. In any case, to avoid such issue, it is best practice to have the intensity of the wavelength light about 10 times higher than the stray light.

Spectrophotometers, depending on their structure, may be classified as single beam, split beam, or double beam. The difference between the three is quite easy.

- A single beam spectrophotometer is the easiest setup possible. The components – light source, monochromator, sample cell, detector and amplifier – are all streamlined.

- A split beam spectrophotometer is a variant of a single beam spectrophotometer – where a single beam is split to direct it to two different cells, a sample and a reference cell. It is sometimes falsely advertised as a double beam spectrophotometer; it differs, however, from a real double beam spectrophotometer as the latter has two different light sources, one each for the sample and reference cell, each with its own light path. A split beam spectrophotometer has only one light source whose light is split (hence the name) in two different pathways, one leading to the sample, the other to the blank.

3.3 BL21(DE3) competence protocol – $CaCl_2$ –

Cells can be defined as competent when their membrane is altered to allow exogenous DNA – plasmids – within, allowing the molecule to be synthesized by the cellular apparatus, thus expressing the phenotype. Such a process needs to be conducted under sterile conditions which ensure enhanced quality downstream in the purification process.

The protocol to render BL21(DE3) cells competent starts with the preparation of Luria Bertani (LB) Broth and Agar

- Luria Bertani Broth and Agar have been employed to grow E. coli BL21(DE3) cells. Solubility of the two is: 25 g/L and 35 g/L. Once weighted, the powder was mixed with the respective amount of milliQ water, which was then autoclaved
- Autoclaving protocol: 30 minutes on "Full", 20 minutes on "3". Once out of the autoclave, the liquids are then set to cool outside the autoclave. Agar is set to cool

so that It is still liquid yet manageable, to fill up three sterile Petri dishes, 20 mL each, in sterile conditions.

Once prepared, cells can be prepared to be rendered competent by means of calcium chloride ($CaCl_2$). This technique is quite known in the scientific literature, as one of the first instances recorded was in 1979 by Dagert and Ehrlich (*E.coli* 1979). Adding this inorganic salt in a solution allows plasmidic DNA binding to lipopolysaccharides (LPS), an abundant component in bacterial cell walls. $CaCl_2$ binding to LPS neutralizes the bacterial cell wall charge, binding both the negatively charged DNA plasmid and the negatively charged LPS. The exogenous DNA is free, once the culture has been thermally shocked, to enter the cell.

Final concentration of $CaCl_2$ is 0,1M, whilst the final volume is never less than 50 mL. The entire procedure needs to be conducted in sterility; the salt solution will be later used to resuspend BL21(DE3) cell culture.

In sterile conditions, $CaCl_2$ powder was weighted on a balance and later dissolved in an appropriate volume of milliQ water, added via an appropriate graduated cylinder. Complete salt powder dissolution was achieved via magnetic stirrer.

The salt solution was then filtered via a cellulose acetate filter, 0.2 μm, and later put in a +4°C fridge to cool off. The salt solution was kept in ice every time it was not employed in the following steps of the procedure. This measure was employed to ensure no thermal shock was given to the cells beforehand.

The following step requires a 100 mL cell culture with a ΔOD/min value, at 600 nm, between 0,2 and 0,4. An aliquot of a non antibiotated overnight cell culture was spectrophotometrically evaluated. Its ΔOD/min at 600 nm was 2,27 (Jasco J-730 UV-Vis Spectrophotometer with Polystyrene cuvettes, Fig. 36, courtesy of Lorenzo Tagliazucchi).

Figure 36: Jasco V-730 UV-Vis Split Beam Spectrophotometer.

To understand the appropriate volume to be taken from said cell culture, dilutions were made in a 1 mL final volume, then the ΔOD/min at 600 nm spectrophotometrically read.

To obtain the aliquot volume, protocol limits were considered and the ΔOD value had to be lower than 0,2; this would allow the cell culture to comfortably reach the required value in a reasonable amount of time.

Following inoculation in 100 mL LB broth, its growth was followed via spectrophotometer, at fixed time intervals, until reaching the OD target.

The cell culture was centrifuged: the 100 mL were divided between four 50 mL Falcon Tubes, then centrifuged (Allegra Centrifuge, Beckmann Coulter, SX4250 rotor), 10 minutes, 4000 rpm, 4° C. Maintaining the proper temperature through this step is paramount; hence, the centrifuge was left to reach the required temperature before its start.

Once again, at the end of the centrifuge, the supernatant was discarded, and the pellet resuspended in an opportune volume of calcium chloride solution for thirty minutes, in ice.

Cells were centrifuged for a second time under the same conditions, (Allegra Centrifuge, Beckmann Coulter, SX4250 rotor), 10 minutes, 4000 rpm, 4° C. The supernatant was again discarded, and the pellet resuspended in a smaller aliquot of calcium chloride solution.

The protocol requires the cells to be kept at +4° C for a period between four and twenty hours. Cells were kept in such a condition for seventeen hours, before being aliquoted in sterile glycerol (20% of the final volume) and Eppendorf tubes, 0,5 mL, 100 microliters aliquots. Cells were then stored at -80° C.

3.4. Plasmid preparation (mini and maxiprep)

"Plasmid preparation" is a technique that allows for plasmid DNA extraction and purification from cells. As the methods evolved, with different yields and lesser security hazards, they all shared three key elements. All methods for plasmid preparation require

the growth of a bacterial cell culture, its lysis and the purification of plasmid DNA. The term "mini" or "maxi" describes the amount of cell culture used to obtain the DNA plasmid. The "miniprep" usually is a quick and clean method to obtain small amounts of plasmid – usually between 50 and 100 micrograms – It is the smallest amount obtainable from this process. The highest amount corresponds to a "Gigaprep" which starts with no less than 2,5 liters of cell culture and the yield is usually in the realm of milligrams of plasmid.

Yield itself, however, does not depends exclusively on the starting cell culture volume, but on other elements as well, such as growing conditions (temperature, humidity and so on) as much as others like the bacterial strain employed. One such element is the plasmid copy number. This element is key in ensuring that the host cell isn't encumbered with too many copies of the plasmid, nor said copies getting lost in the cell division process. Hence, plasmid DNA can be classified by the copy number yield, defined as "high copy number" or "relaxed plasmids" and "low copy number" or "stringent plasmids". These terms, however, do not refer only to the replication yield, but they also infer specific control mechanisms.

Whilst a miniprep is usually employed to ensure proper expression of the sequences, a maxiprep is usually employed to produce larger amounts of plasmid DNA to be stored and used in later occasions.

3.4.1. Cell culture

Plasmid DNA was obtained starting from a Petri dish of BL21(DE3) colonies previously transformed with the plasmid of choice. This was done with a freshly Petri dish stored at +4° C. Initiating this procedure with colonies stocked for more than 7-10 days; the fresher the colony, the higher the chances for living colonies to be found, thus higher chances of having higher yields of plasmids.

In a Pyrex® bottle, 600 mL of LB Miller broth were prepared, weighting 15 grams of powder, bringing to volume with MilliQ water. The bottle was autoclaved as per protocol, 30 minutes in "full", plus 20 minutes at 121° C. Once done, the bottle was placed in a sterilized hood to cool off. Once the temperature of the broth reached a viable temperature to be handled, 100 mg/mL of an Ampicillin stock was added, to a final concentration of 100 ug/ul (600 µL in 600 mL of broth).

Sterile conditions were achieved by cleaning the hood with ethanol and lighting up a Bunsen beaker inside, allowing for a sterility area to be formed around it. In such conditions, 5 mL of LB broth were aliquoted in a 15 mL Falcon tube. A single, isolated colony was also taken with an inoculating loop handle from the Petri dish, then inoculated inside the Falcon containing the LB broth aliquot. Taking a single isolated colony allows one to grow cells containing the same chromosomic make-up.

Figure 37: Control LB Broth in a 15 mL Falcon tube.

Together with a control Falcon (Fig.37, same LB broth from the same Pyrex bottle, minus the cell culture) the cell culture containing Falcon was put inside an incubator, 37° C, 150 rpm, around 3 hours, until opalescence is clearly visible. A small aliquot, 20 µL, was then inoculated in the 600 mL bottle, and left inside the incubator overnight, same conditions as previously reported.

Figure 38: Allegra X-22R Centrifuge, Beckman Coulter.

3.4.2. Cell harvest and lysis

The following day, the culture was transferred in Falcon Tubes, 50 mL, to be centrifuged (Allegra X-22R Centrifuge, Beckman Coulter; SX4250 rotor, 4000 x g, T 25° C, 30 minutes). The supernatant broth was eliminated; the remaining cell pellet was added with 10 mL "Resuspension Buffer (EQ1)" - 50mM TRIS-HCl pH 8, 10mM Ethylenediaminetetraacetic acid (EDTA), aq.+ RNase, with a sterile serological pipette. EDTA is an aminopolycarboxylic acid helps in inactivating DNAses, by

taking away bivalent ions such as calcium, magnesium and iron, (Ca^{2+}, Fe^{3+}, and Mg^{2+}), keeping them in solution whilst noticeably diminishing their reactivity. Buffer was gently added to the pellet, until complete resuspension was achieved.

Following this step, the cell suspension in the two Falcon tubes was treated with 10 mL of "Lysis Buffer"- 0.2 M NaOH, 1% v/v SDS. As the name suggests, this buffer is responsible for the cell lysis; while sodium dodecyl-sulphate loosen up the bacterial cell wall and membrane, sodium hydroxide precipitates proteins and double strand DNA (dsDNA) acting as a chaotropic agent. Using NaOH to the tune of 0,1 M allows for less single strand DNA (ssDNA) to be had. It is crucial that this step happens in an alkaline environment (pH between 12 and 12,5) as it presents an ideal environment for dsDNA, ssDNA and proteins to be denaturated. Under such conditions however, plasmid DNA does not, remaining in solution. As per use, the buffer was added gently to the cell suspension, until homogeneity was reached, then it was left at room temperature for 5 minutes to rest.

A "Precipitation Buffer" – 3.1M CH_3COOK pH 5.5 – was then added to the suspension. The acetate buffer allows for denaturated molecules to precipitate, whilst keeping plasmids in solution. As per use in the previous passages, the Falcon tubes containing the suspension were gently shaken and not vortexed. This was necessary as the adding of acetate to the solution causes the larger chromosomal DNA to precipitate, whilst keeping the smaller DNA plasmids in solution.

3.4.3. Plasmid DNA purification

Two silica gel columns of the kit were equilibrated with 30 mL of "Equilibration Buffer" – 0.1M CH_3COONa pH 5, 0.6M NaCl, 0.15% v/v Triton® X-100 – Silanol groups on the column, by means of sodium acetate which acts as a chaotropic salt. In such an instance, sodium from sodium acetate acts as a chaotropic agent, disrupting the hydrogen bond matrix of water molecules, disassociating them from silanol groups. Sodium thus acts as an ionic bridge between the negatively charged hydroxy groups from the silica columns, and the phosphate group of the DNA, also negatively charged.

The solution containing the plasmid DNA was transferred to the previously prepared columns, within its guard cylinder. The cylinder protects the silica column from entering in contact with the suspension, preventing the obstruction of the elution flux, which is filtered by gravity. Ten milliliters of Wash Buffer - 0.1M CH_3COONa pH 5, 0.8M NaCl – were used to wash the precipitate, directly into the guard cylinder of the column.

Fifty milliliters of Wash Buffer were then used directly into the silica column. These were added directly at the top of the silica gel and was eluted by gravity. Proteins are eluted in this phase, while plasmid DNA is still within the silica gel, as it created a matrix of hydrogen bonds and electrostatic interactions with the chaotropic sodium and silica column particles.

Plasmid DNA was eluted adding fifteen milliliters of Elution Buffer – 0.1M Tris HCl pH 8.5, 1.25M NaCl – in two sterile Falcon tubes. Elution is made possible as the alkaline nature of the buffer allows the silanol groups to detach the plasmid DNA through deprotonation.

Plasmid DNA was cleaned from the salts employed during the process by means of alcoholic precipitation. Through this method, isopropanol is used as an antisolvent of DNA, precipitating the plasmid molecules whilst maintaining everything else in solution. The soluble fraction can be then removed, keeping the precipitate and dissolving it in an opportune medium. In the case being, 10,5 milliliters of isopropanol were added to each Falcon tube, promoting the mixing of the two phases. The alcoholic solution was freeze centrifuged (Allegra Centrifuge, Beckmann Coulter, SX4250 rotor), 90 minutes, 4000 rpm, 4°C.

Five milliliters of 70% ethanol v/v were prepared from 95% ethanol, added to the Falcon tubes, then centrifuged again. Remaining ethanol traces were evaporated under hood, in a sterile environment.

Lastly, the obtained plasmid was resuspended in 350 microliters of TE Buffer – 10mM Tris HCl pH 7.5, 1mM EDTA – each Falcon tube. The plasmid was aliquoted in sterile Eppendorf centrifuge tubes, 50 microliters, and were stored at -20°C.

3.5. Expression protocol

The expression protocol allows for an endogenous molecule to be expressed inside an appropriate vector. This is usually represented by chemically competent cells, which act as the workhorse, or production site, of the molecule. Cells are made competent first, then via thermal shock their membrane is opened just enough for plasmids to be included. The

plasmid usually contains antibiotic resistance gene(s), the gene for the target molecule, and usually moieties which help during the purification process.

3.5.1. Cell culture scale-up process, and induction of expression

Main objective is to obtain pure human TS protein. This is achieved by transforming BL21(DE3) E. coli cells with pQE-80L plasmid carrying either the wild type (hTSwt) insert or one of its mutants. After a short incubation to allow the beta lactamase to be expressed by transformed cells, these are selected in a Petri dish filled with Amp+ Agar.

LB Agar (solubility: 35 g/L) and Broth (25 g/L) was prepared in the volume of 60 milliliters and 50 milliliters, respectively. Taking this information into account, 2,1 and 1,5 grams of dried powder were weighted in a sterile environment. MilliQ water was used to dissolve both powders in an opportune vessel, Pyrex glass bottles. Both have been closed with sterile gauze, sealed with autoclave tape. In the meantime, an aliquot of BL21(DE3) cells and one of DNA plasmid were taken to thaw, respectively from -80°C and -20°C. Both Eppendorf centrifuge tubes were put in ice to avoid thermal shock.

Bottles were autoclaved at "Full" for 30 minutes, then at 121°C for 20 minutes. After ensuring both cells and DNA plasmid were thawed, in a sterile environment under the biological hood, 100 microliters of BL21(DE3) E.coli cells were taken and put in a 15 mL Falcon tube; immediately after 8 microliters of pQE-80L plasmid were added in the same Falcon tube.

From there, the falcon was left for thirty minutes in ice, in order to start the thermal shock. Calcium chloride, as previously explained, allows exogenous DNA plasmids to enter bacterial cells. Cells were then subjected to a heat pulse, +42°C for 45 seconds, followed by 5 minutes again in ice. In the end 600 microliters of sterile LB broth were added to the cell culture. Cells were left in incubation at +37°C for 90 minutes, 150 rpm. A sterile Falcon tube containing sterile LB broth is left in incubation in the same conditions, to verify the absence of contaminations in the broth; this can be visualized as the broth should be clear at the end of incubation.

The transformation process is by nature, one that does not necessarily involve all cells. It is understandable how, at this point in the process, transformed cells need to be divided from non-transformed ones. One such method is the usage of an antibiotic. Plasmids commonly contain a resistance gene for one such antibiotic; hence only the cells who have been transformed will be able to express the resistance gene, surviving the following step. This ensures that the cells used from this point forward, effectively contain the DNA plasmid coding for the intended protein. Albeit far from being the only selection method, antibiotic resistance can be surely considered one of the easiest to be employed in the expression process. As the LB agar cooled off, Ampicillin was prepared and added – 1:1000 ratio. Three sterile Petri dishes were filled with 20 milliliters of Amp+ LB Agar and left to cool off and solidify in a sterile environment. Once solid, 100 microliters of the small-scale cell culture were fed to only two Petri dishes in sterility, evenly distributing the aliquot with a sterile L-shaped cell spreader. The third one, once again, would have acted as the

contamination control. The lid was then closed, and all dishes were kept in incubation at 37°C, overnight.

The following day, under sterile conditions, an aliquot of LB broth was added with Ampicillin, in a 1:1000 ratio. 5 milliliters of the antibiotated broth were put in sterile 15 milliliters Falcon tubes, to prepare the scale – up of the cell culture. Each tube was inoculated with three singled out colonies from each Petri dish, with a sterile molded plastic inoculation loop. The Falcon tubes were then left in incubation for 4 hours, at 37°C, 150 rpm. In the meantime, preparations were arranged for the following cell culture scale-up step.

In a convenient vessel (cell culture flasks, 2,5 L maximum volume), 25 grams of LB Broth powder (solubility: 25 g/L) were weighted in a sterile environment; then, one liter of milliQ water was added inside the flask. These were later closed with sterile gauze and fixed with autoclave tape. LB Broth was then sterilized in autoclave, following the previously reported protocol (30 minutes at "Full" setting, 20 minutes at 121°C). To promote broth cooling, flasks containing the broth were later put in ice. Subsequently, in a sterile environment, Ampicillin was added to the broth, 1:1000 ratio, and the broth mixed to ensure proper antibiotic dilution. Each flask was then inoculated, in a sterile environment, with 100 microliters of cell culture from the previously prepared 5 milliliters. Flasks were later left in incubation, overnight, at 37°C, 150 rpm.

3.5.2. Induction of expression

The expression process is based upon the presence of a "trigger" signal that allows users to control the exact moment in which the gene contained in the exogenous plasmid needs to be expressed. This is done for multiple reasons, the most relevant ones being

- avoiding encumbering the replication machine of the host cells with too many copies of the plasmid and related protein,
- avoid cytotoxicity which may be due to overexpression of the target protein.
- condition expression control to ensure that the molecule is expressed in a soluble fashion, avoiding its precipitation in the insoluble fraction

With this spirit, it is highly recommended to strictly control the expression of the exogenous molecule. This not only ensures an optimal environment for the molecules to be expressed, but also the survival of the cell culture itself. It is not uncommon therefore, that each molecule expressed in a vector may have different expression conditions, which do not necessarily apply to other molecules.

As the expression of the hTS molecules depended on the internalization of its plasmid DNA, it is actually easier to "encode" the "trigger" inside the same vector. As previously described, the pQE-80L plasmid vector contains one such "trigger", the LacUV5 promoter. This promoter is actually a mutated "lac" class promoter which is often used to drive the expression of a protein within the plasmid. LacUV5 is almost identical to its "wild type" counterpart, containing only two mutations (two adenines instead of a guanine and a

thymine) in the -10hexamer region. Its promoter sequence closely resembles the consensus sequence recognized by specificity factors known as “sigma factors”. These are bacterial transcription initiation factors which allow specific binding of RNA polymerases to gene promoters, much like TFIIB does in eukaryotic cells. This similarity directly translates as higher efficiency in recruiting RNA polymerases, hence to higher chances for the target gene to be transcribed, then translated.

Another important feature of the LacUV5 promoter lies in the independence from “external” activator proteins or regulative molecules, exception made for -10 and -35 promoter sequences, unlike its wild-type counterpart. LacUV5 can however, be repressed by LacI repressor, which is also present within the plasmid itself; on the other hand, it can be induced by lactose-like molecules.

One such molecule is the Isopropyl β-d-1-thiogalactopyranoside or IPTG for short. This molecule is a molecular biology reagent which mimics allolactose, a metabolite that is capable of triggering the transcription process inducing the lac operon. IPTG acts much likely to allolactose, binding the tetrameric repressor LacI via an allosteric mechanism. Unlike the allolactose however, the presence of a sulfur atom is the base for a covalent bond that cannot be hydrolyzed by the cell’s beta galactosidase, thus preventing its degradation. Its uptake does depend on its concentration (Hansen 1997), with lactose permease being paramount at lower (0,1 mM) IPTG concentration. At higher

concentrations however, (over 1mM) which are more common in protein induction, other mechanisms may be in place.

As previously reported, conditions in which the induction process is done are paramount and specific for each protein. Regarding hTSwt and its mutants, the expression was induced at 37°C, 4 hours, with the cell culture OD comprehended between 0,6 and 0,8.

The optical density value (or OD) is an indicator again of the number of cells contained in a fixed volume. Such value can be directly linked to the stage in which the cell culture is. Ideally, an optical density value, at 600 nm between 0,6 and 0,8 corresponds to the exponential growth phase of the cell culture. Optical density was read through spectrophotometry, which will be briefly discussed in a later segment of this thesis.

One milliliter of LB antibiotated broth was added in two PTFE cuvettes; these were put inside the Jasco J-750 spectrophotometer (Jasco). After registering the baseline and zeroing in the instrument, one milliliter of the cell culture was taken from the flask and the OD at 600 nm read. As the cell culture came from an overnight incubation, the OD value was well over the 0,6-0,8 range required for the induction.

Hence, as previously reported, dilutions were made to ensure that the cell culture was well below the 0,6 OD at 600 nm – the lower limit to induce the expression – targeting the final OD at around 0,35-0,4. This would allow the cell culture to comfortably reach target OD in a sensible amount of time, whilst being able to control at fixed timed intervals its growth.

Induction of the expression was always carried out between this range; after adding one milliliter of IPTG to the cell culture, at a final ratio 1;1000, the flasks were left in incubation for 4 hours, 37°C.

3.5.3. Cell pellet harvesting, and enzyme purification

The induction process stops with the cell pellet harvesting. Cells are centrifuged to separate the broth from the cells, which forms a growing cell pellet at the bottom of the vessels used for centrifugation. The whole process is conducted at a low temperature to ensure that the cell culture's metabolic processes are kept to a minimum. This is due to the fact that the centrifugation process deprives cells of nutrients; such deprivation may lead to cell death, thus to loss of protein.

The first, paramount step would have been to take note of the weight of the emptied bottles and caps. This was done to ensure that the volumes centrifuged inside each bottle was most likely the same. The ramification of misalignments in the volumes inside the bottle could, at best, stop the centrifuge for rotating unbalanced; at worst it could seriously damage the centrifuge. Hence, only small differences in volumes are generally tolerated (less than 5 milliliters on a volume of about 250)

Such a consideration calls for some preparation beforehand. The centrifuge (Allegra Centrifuge, Beckman Coulter; SX4250 rotor, 4000 x g, T +4°C, 30 minutes) was prepared in such a way that it would reach the required temperature before inserting the bottles. The centrifuge bottles, which would contain the broth, were kept in ice for the same reason.

After equilibrating the temperature of both centrifuge and bottles, an opportune volume of cell culture was inserted in each of the latter. The bottles were closed and placed inside the rotor housings. Centrifuge was then started, after checking briefly that it would not stop due to imbalance. After each centrifuge, the supernatant broth was discarded, while the pellet kept inside the centrifuge bottles. The process was repeated until no more cell culture was available. Keeping note of the initial bottles weight was paramount to determine the final pellet weight. This was used as the pellet was resuspended in an opportune buffer, which was also used for the purification process. The buffer depended on the experiments to be done with the purified protein. Phosphate presence, for instance, does not represent an issue for inhibition experiments, hence the buffer containedNaH2PO4 20mM, NaCl 30 mM, pH 7,5. On the other hand, in structural studies, phosphate presence constituted a bias, hence the buffer contained Tris-Base 30mM, NaCl 150mM, pH 8. In both cases, the cell pellet was resuspended using 2 milliliters of buffer for each gram of cell pellet. Once resuspended, the solution was moved to 50 mL Falcon tubes; then, the solution was centrifuged again (Allegra Centrifuge, Beckman Coulter; SX4250 rotor, 4000 x g, T 4°C, 30 minutes). The supernatant, once again, was discarded, and the pellet weighted and labeled; it was either stored at -80°C or used immediately to start the purification process.

3.5.4. Ultrasonication and crude extract filtration

Ultrasonication is the method that applies ultrasounds to a solution, in order to agitate particles, present within the sample. This may be achieved in two different manners, using

a so called “ultrasonic bath” or a “probe”. The cavitation and slicing forces, generated by ultrahigh sound frequencies (over 20 KHz up to 50 KHz) can disrupt the cell membrane, causing their lysis, thus allowing for its contents to be released in the extracellular environment.

In other words, the electrical forces generated by the sonicator’s power source are transmitted into the liquid as high frequency sounds, which means that the electrical energy is now converted into a mechanical one. The mechanical energy from the probe is released into the solution, where such forces create small bubbles that implode – cavitation process – causing ultimately rupture of the cell membrane, its lysis, and the release of intracellular molecules into the extracellular environment.

This technique however does not come without its own share of issues. Directing energy to a solution, just like to any other body, solid or liquid, causes also a rise in temperature. This means that the sample can heat up after being subjected to sonication. Another important issue that needs to be taken into account is the presence of cleaving enzymes which may act upon the target molecule.

This technique has allowed the extraction of the soluble fraction of the cell culture into what is commonly known as “crude extract. This would be separated from the insoluble fraction at a later point via centrifugation; for this reason, the centrifuge, its rotor, and the centrifugation tubes employed in the following step were preemptively equilibrated.

For these reasons, some work beforehand was required before sonicating the samples:

- proteases and lysosome enzymes were blocked by using "Complete" tablet. One tablet was dissolved in 2 milliliters of milliQ water with the help of a Vortex. Two milliliters of the "Complete" solution serve 50 mL of resuspended cell pellet.
- heating issue was resolved by sonicating for short periods of time, in bursts, equaling sonicating and resting periods. Sonication was always carried out maintaining the Falcon tube with the resuspended cell pellet in ice

After preparing the Complete solution, the cell pellet was taken from the -80°C fridge and was left thawing for one hour sitting on ice. As soon as the pellet ended thawing, it was resuspended in Buffer 1, 2 milliliters for each gram of cell pellet. Right after, depending on the final volume, the appropriate amount of "Complete" protease inhibitor solution was added. The cell pellet was then resuspended until no solid mass was visible in the liquid. The procedure was carried out avoiding the formation of bubbles on the surface, as they may hinder sonication efficacy.

Sonication was carried out with a Branson probe sonicator, at 70% power, with seven sonication cycles. Each cycle is composed of ten seconds of sonication, alternated to 10 seconds of ice resting. As previously stated, the sonication process was carried out by taking the probe to the Falcon tube, maintaining the latter in ice.

After completion of the sonication process, the cell lysate was centrifuged (Allegra X-22R Benchtop Centrifuge, Beckman Coulter; F0850 rotor, 12000rpm, T +4°C, 30 minutes).The crude extract was carefully separated from the insoluble fraction, by means of a sterile

serological pipette. After each manipulation step, and more in general, each time the crude extract or its derivation was not manipulated, it was stored in ice.

The crude extract corresponds to the soluble fraction of the cell lysate. Multiple molecules can be found within this solution. Separating the target molecule could prove hard to be done. Through the years, the purification process got instead easier and easier. The most work has been done on the gene vector, allowing for both proper expression of the molecule and increasingly generous insert dimensions that allowed for bigger molecules to be expressed. If engineering of the vector proved fundamental for such reasons, engineering of the insert proved as much important as that. This was done for multiple reasons: first and foremost, include moieties which would help the purification process to happen faster and with increasingly higher grades of purity.

3.5.5. FPLC purification

With this spirit, all inserts regarding this thesis, contain His-tags which allow for an easier purification step. His-tag, 6xHis-tag, or Polyhistidine tag are terms that refer to a histidine-based moiety first developed by Roche during the '70. The main idea behind the His-tag was to introduce amino acidic residues, at the end of the protein sequence, which would form bonds with some divalent metallic ions. This would have been exploited by using said ions in a resin with the aim of easing up the purification process. One such amino acidic residue was histidine. This, under specific pH conditions (around 8) would chelate the metal ion (nickel, cobalt or similar), detaching from the resin only in such conditions where salts

(imidazole for instance) were used. Imidazole has a higher binding affinity for metal ions than histidine, de facto detaching the tagged protein from the resin. In a later passage, the salt would have been separated from the protein (desalting process) hence allowing to recover the tagged protein with a high purity yield. This process was firstly described by Porath in 1989 and was called Immobilized Metal Affinity Chromatography or IMAC for short.

In other words, IMAC purification allows for protein separation exploiting the interaction between solubilized proteins and ions of transition metals bound to a solid support (usually agarose or sepharose). The histidines are mainly concerned in this regard, as their ability to bound 2:1 metal ion is at the base of the success of this technique.

Another rather relevant advantage of the His-tag + IMAC technique regards the fact that the tag structure does not usually interfere with the protein tridimensional structure, nor its function. In such a case however, advancements in the His-tag technology allow to cleave it without any other major issues.

Before introducing the protocol, a small paragraph will be dedicated to the buffer choice for the purification process. Buffers, as it is common knowledge, are solutions capable of resisting pH changes any time small acid or basic components are added to it. This is very important, as most molecules exert their activity in specific pH conditions, and this is most definitely true for enzymes, as stated in the introduction chapter "Overview of enzymes and their catalytic activity". Hence, ensuring pH stability is paramount to the success of all

experiments regarding enzymatic activity and structure. An important feature of buffers is the presence of salts, whose ions are the key element for such an activity. One of the most common buffers for protein purification, however, contains Sodium Phosphate. This molecule tends to disassociate freeing up in solution phosphate ions (Pi), also previously stated in the introduction, is one such molecule that can exert an effect over the active – inactive equilibrium of hTS.

Given the different aims of the thesis, it was deemed necessary to purify the enzymes in two different buffer conditions based on the experiments done, Structural studies based upon ITC and spectrophotometry techniques were considered as one where phosphate ions may very well be considered a bias in the experimental setup. Within this spirit came the idea to purify the enzyme in a phosphate-free buffer (no Pi) which contains 30 mM TRIZMA-base and 150 mM NaCl, pH 8. On the other hand, experiments carried out on inhibitors of hTSwt and its derivatives, may tolerate relatively small concentrations of phosphate ions in the solvent. Hence the buffer of choice was 20 mM NaH_2PO_4, 150 mM NaCl, pH 7,5.

Two more buffers have been prepared for the purification process. As already extensively explained, the FPLC technique coupled with the His-tag/IMAC purification process exploits salts to ensure elution of the tagged protein. It comes to no surprise that two more buffers have been used in the process, which only differ from the first one for having constant concentrations of imidazole, 20 mM and 1M respectively. These two additional buffers

commonly defined in the procedure as “Buffer 2” and “Buffer 3” respectively carry a specific role. As the first buffer is the one in which, in the end, the protein will be eluted at the end of the desalting process, it is important that the main components for this buffer do create an environment in which the protein does not precipitate. Buffer 2 and 3 on the other hand have a different function. The former detaches most proteins which naturally contain histidines, hence can still – weakly – bind the ions. The latter, on the other hand, is responsible for the elution of the target protein.

Independent from the experiment, buffer preparation followed always the same procedure. After weighting the powders on a balance, an opportune milliQ volume was used to completely dissolve the salts. pH was then measured via a Crison pHmeter and adjusted accordingly. Before any measurement, the pHmeter was always calibrated with its own solutions at pH 4 and 7. After adjusting the pH, the buffer was then brought to volume in a graduated cylinder. Following this operation, any and all prepared buffers have been filtered (0,45 micrometers acetate cellulose filters) and

The purification process was carried out with the AKTA Prime FPLC system. This can be considered a Fast Protein Liquid Chromatography system or FPLC. It differs from HPLC as the latter, at its core, is an analytical technique which is used mainly for either qualitative analysis or quantification of samples in a liquid solution. FPLC on the other hand uses most of the same elements of HPLC (pumps, detectors, valves and whatnot), adding also pH and conductivity monitors. FPLC can be considered a preparative technique; the core idea is to

separate protein mixtures whilst recovering the fractions of interest. Other main differences can be found in different median flow rates – around 10 milliliters per minute in HPLC, whereas in FPLC it can get to 10 times this value – and back pressures – over 5000 psi in HPLC, whilst FPLC stops at around 600 to 700 at max.

Figure 39: AKTA Prime System

Regarding the hTSwt enzyme and its mutants, the adopted protocol is the following. After centrifuging the cell lysate, as previously described, the crude extract was separated from the insoluble fraction via a sterile pipette and pipettor. The process was done in sterility, whilst maintaining every vessel that came in contact with the crude extract in ice at all times apart when manipulated. Within the same condition was carried the following step.

The crude extract was loaded in sterile a 10 milliliters syringe, then filtered and sieved via sterile 0,8 micrometers and 0,45 micrometers cellulose acetate filters. The process was

carried out in a hood, within a sterilized ambient; the filtered extract was put in sterile 50 mL Falcon tubes and let in ice until required again.

In parallel with the centrifugation process, the AKTA prime system was prepared. The AKTA prime (in picture, courtesy of Lorenzo Tagliazucchi) is a FPLC based instrument, as previously described, and it was used for all protein purifications. The system works with cartridge columns of different nature: the ones used in this process are 5 milliliters HisTrap Excel and HiTrap Desalting columns from GE Healthcare.

Figure 40: HisTrap Excel columns for FPLC purification.

- HisTrap Excel columns (Fig.40, courtesy of Lorenzo Tagliazucchi) are IMAC columns packed with "Nickel Sepharose excel". The resin is made of 6% highly crosslinked spherical agarose, with an average particle size of about 90 micrometers. The resin is stable on a wide range of pH (2 to 12). Columns are made of polypropylene, which grant for little to no interaction with the biological sample. Pressure limit within the column is about 0,5 MPa (Mega Pascal) or 5 bar.

Figure 41: HiTrap Desalting columns for FPLC purification.

- HiTrap Desalting columns (Fig.41, courtesy of Lorenzo Tagliazucchi) are size exclusion columns packed with Sephadex G-25 Superfine resin. The resin is made of crosslinked dextran beads, whose size is about 15 to 70 micrometers, and is stable on a wide range of pH, 2 to 13. Columns are made of polypropylene, which grant for little to no interaction with the biological sample. Pressure limit within the column is about 0,3 MPa or 3 bar.

Each enzyme (wildtype and its mutants) had its own couple of HisTrap Excel and HiTrap Desalting columns. This was done to avoid cross – contamination between purified proteins. As previously explained, the protocol followed for the expression and purification process is identical for all purified proteins. Hence, the following description can be extended to all and any purified enzyme in the context of this thesis.

Once the system was physically connected to a personal computer, it was turned on. After the initial background checks of the instrument, the system was set up so that the results could be followed live via the PrimeView companion software. The software was set-up so

that only the "Condition" and UV signals were visible on the monitor. As the name states, the UV signal refers to the UV detector signal, whilst the Condition one refers to the ionic concentration of salts in the solution passing through the detection chamber.

The system was then cleaned with milliQ water until the UV and Condition values became close to zero. Flow was set to 10 mL per minute. The HisTrap Excel 5 milliliters column was then connected to the AKTA system, washed – 3 to 5 column volumes or CV – with milliQ water and conditioned with the same volume of Buffer 1. Both washing and conditioning of the column was deemed satisfactory at any time in which UV and Conditioning signals were stable, and their graphs represented as parallel lines. Flow rate was set to 2 to 3 mL/min. The FPLC system was then autozeroed, the fraction collection tubes set in the accessory automatic fraction collector, and 10 mL fraction were collected from this point on.

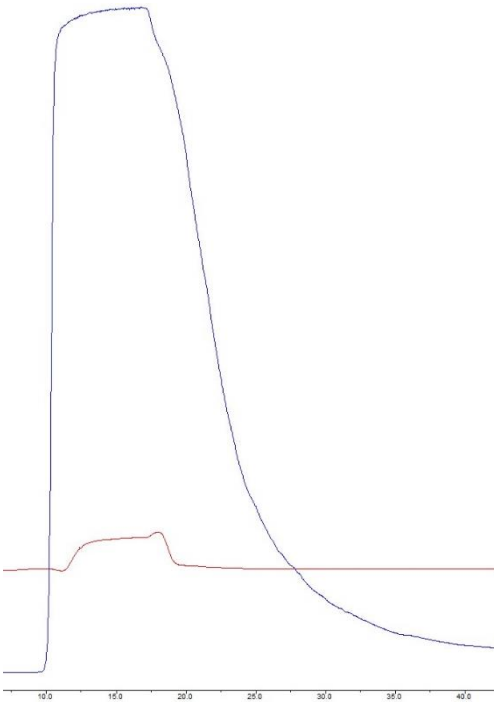

Figure 42: Depiction of Flow-Through 1 peak in FPLC

The Falcon tube containing the crude extract was put in ice and in here was loaded inside the FPLC system. The loading was carried out at a flow rate of 3 mL/min; as soon as it was completely loaded, the column was washed with 3 CV of Buffer 1. Washing with this buffer allowed for a first peak to be shown on the UV signal (Fig.42). This peak represented the fraction of proteins which did not bind or weakly

bound to the resin and the ions. This can be deduced as the peak intensity is in its thousands of milliAU (Arbitrary Units), and it usually cover more than one 10 milliliter fraction.

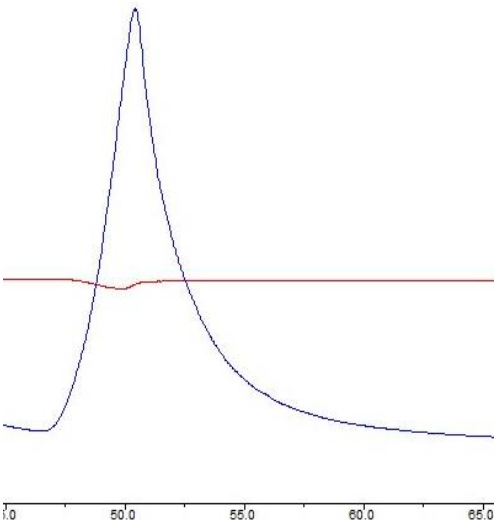

Figure 43: Depiction of Flow-Through 2 Peak in FPLC.

Immediately after, the column was washed with the same CV of Buffer 2. To ensure the same conditions of purification, a Falcon tube was put in ice beforehand, and then it was filed with the opportune Buffer 2 volume. During the whole process, the Falcon tube stayed in ice. The peak correspondent to this elution (on the left, Fig. 43) can be associated to the nonspecific proteins that may contain small amounts of histidines; these are still able to bind the HisTrap Excel resin, but not as strongly as the His-tagged protein. Compared to the Buffer 1 elution peak, this one is not as intense; this can be seen as it is usually very low in intensity and can be very well contained in a single 10 milliliter fraction.

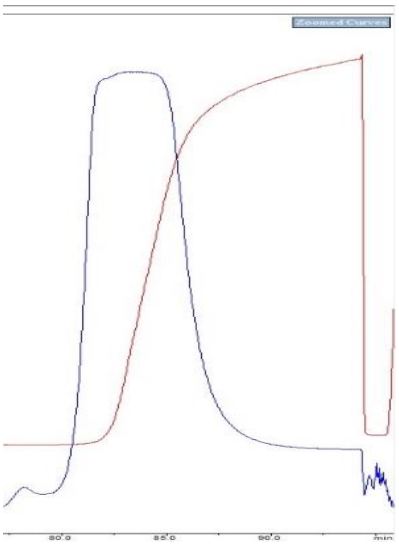

Figure 44: Depiction of Flow-Through 3 in FPLC.

Terminated the elution with Buffer 2, the FPLC system was halted, the flux reduced to 1 mL per minute, the fraction size was reduced to a volume of 1 milliliter per fraction. Another Falcon tube was put in ice beforehand and was then filled with the appropriate amount of Buffer 3. The Falcon tube was kept in ice at all times. hTSwt (chromatographic peak in Fig.44) usually eluates about 17 minutes from the moment the FPLC system run is resumed. This third peak's intensity is usually comparable to the first peak, although the peak itself is contained in more than one milliliter fraction.

Each fraction contains the eluted tagged protein and some imidazole salt. These were separated by means of the size exclusion column HiTrap Desalting. The preparation of this column followed exactly the same principles of the previous one. The column was washed first with an opportune milliQ water volume, then it was conditioned with 3 CV of Buffer 1.

The elution process was conducted at a low flow rate – 1 mL/min – and recollection volume set to 1 mL. Fractions from the precedent elution were directly loaded in the column with a sterile 1 mL syringe. This allowed the target protein and the imidazole salts to be separated.

Fractions containing the protein were isolated and kept in ice, as they were subjected to enzymatic characterization.

3.6. Enzymatic characterization

The characterization process has been done each time a molecule was purified. This process

- determines the concentration of the purified protein by means of a spectrophotometric assay
- ensures that the purified protein is working as intended, by measuring the Michaelis – Menten constants for its substrates, K_m and the K_{cat} or turnover number
- is informative of the purity grade of the purified protein by means of SDS-PAGE (Sodium Dodecyl Sulphate – Polyacrylamide Gel Electrophoresis), and the molecular weight of the purified protein

3.6.1. Protein concentration evaluation

The first step in the process was to evaluate the concentration of the purified protein. The main idea behind this step is quite simple. As the desalting process outputs aliquots which contain different portions of the protein peak, it is important to define the concentration of each for two important reasons;

- the first reason being that the following experiments have been done on specific enzymatic concentrations. It is understandable how, in a purification process, efforts are made towards having the purified protein peak in a single fraction. More often than not, however, the passage from theory to practice is not as smooth as it sounds. There will be occasions in which a single peak is divided between two or

more fractions; hence each fraction will have its own concentration of purified protein. Knowing the concentration of protein in each eluted fraction allows for a better stock process, one that, for example, allows two different concentration pools to be had. This ensures that not only the right stock is employed for the right experiments, it also cuts on wasting protein in experiments where lower concentrations or volumes are required.

- the second reason, as important, is avoiding precipitation due to high concentrations. This is key in the purification process: some proteins may show such behavior in high concentrations; a common feature of this phenomenon is one where the same fraction has two different concentrations, depending on how deep the aliquot was taken. It is usual in this case to have lower concentrations on the surface of the fraction, increasing as the aliquot is taken from deeper spots of the fraction. It comes without saying that this phenomenon needs to be avoided at all costs, hence the creation of two different concentration pools also alleviates this issue at hand.

As stated, this process was conducted through a spectrophotometric assay, with two different spectrophotometers, the split beam Jasco J-730 UV-Vis Spectrophotometer and the double beam Varian Cary 100 UV-Vis Spectrophotometer. In both cases, Suprasil quartz cuvettes, 1 cm optical reduced path were employed.

The spectrophotometry assay itself is quite linear. After having turned on the spectrophotometer, the software was opened to start the absorption spectrum program. After filling up two Suprasil quartz with Buffer 1, the instrument was zeroed in and the baseline acquired. The cuvette in the sample compartment was changed with an opportune dilution of the purified enzyme and the absorption spectrum registered in a range between 600 and 250 nm.

The concentration of each sample was then determined by reversing the Beer Lambert law

$$A = \epsilon l c; \qquad c = \frac{A}{\epsilon l}$$

Equation 18: Classic Beer - Lambert Law formula.

by taking into account that

- the molar extinction coefficient of the enzyme, at 280 nm is equal to 87780 L cm-1 mol-1
- the optical path of the cuvette is 1 centimeter
- the absorbance value is given by the instrument in AU (arbitrary units)

Once the concentration of the dilution was known, the concentration of the original fraction was obtained by simply taking into account the dilution factor. Final volume was 800 microliters, for both cuvettes.

3.6.2. K_{cat} determination

As previously described in the introduction, the K_{cat} value or turnover number is defined as the number of substrate molecules converted in product by an enzyme in one second. To evaluate this, a kinetic reaction test was prepared. This was achieved by reaching the so called "steady-state": it means that the speed at which the complex enzyme-substrate forms needs to be equal to the rate of disassociation.

It is critical that the concentration of substrate in this experiment is not a limiting factor, as the substrate-product conversion rate has to be independent of this element. For this reason, dUMP and mTHF concentration need to be well over in excess of the enzyme concentration. This means that the enzymatic assay needs to be conducted in a substrate saturating condition.

As per use for enzymes that do behave following the Michaelis – Menten law, a substrate concentration equaling at least 10 times its Km can be considered adequate to reach the enzymatic Vmax. As previously stated, in this condition, the interconversion velocity is independent of the substrate concentration.

Before any experiment conducted, the concentration of the enzymatic aliquot thawed was confirmed via a quick spectrophotometric reading, following the previously described protocol. The main idea of the experiment is to read the absorption at 340 nm in samples containing increasing concentrations of enzyme. As the reading happens in a borderline

area of the UV-Vis spectrum, there's no need for Suprasil quartz cuvettes to be used. In this case PTFE (Polytetrafluoroethylene)cuvettes have been employed.

To carry on this experiment, the Jasco J-730 split beam UV-Vis spectrophotometer was used. To have a proper reading the instrument was setup for a multireading assay; after turning on the instrument, the software was set-up for the experiment. As the instrument itself allows for 6 samples and one blank to be read at the same time, 6 different enzymatic concentrations were used in a single experiment.

Each cuvette contained the following reagents:

- dUMP and mTHF at a final concentration of 10 times their respective Km
- TES (2-[[1,3-dihydroxy-2-(hydroxymethyl) propan-2-yl] amino] ethanesulfonic acid): a zwitterionic buffer, constituting half of the final volume
- Increasing enzymatic concentrations
- milliQ water to reach the final volume

The final volume was 800 µL for all prepared cuvettes (samples and blank)

Sample cuvettes were prepared by adding the TES buffer first, then the enzyme, and the mTHF, bringing up to volume with the milliQ water. Before adding dUMP, the blank was acquired for all the sample cuvettes. As quickly as possible the dUMP was then added in all cuvettes and acquisition process start. The results were then plotted in an Excel file, and through the formula in Eq.19

$$V_{max} = K_{cat}[E]$$

Equation 19: Vmax to Kcat correlation.

the K_{cat} was identified through the slope of the V_{max} vs enzyme concentration graph.

3.6.3. dUMP – mTHF K_m determination

This is yet another spectrophotometric assay; in this case the enzymatic concentration is fixed, whilst the concentration of either substrate or co-factor was changed. In this case, the plotted graph is ΔOD/min vs either [mTHF] or [dUMP] concentration. The resulting hyperbola branch is characterized by a plateau phase at the end; the value corresponding to that is the V_{max}. It is, however, quite difficult to calculate the value in this way. Hence the K_m parameter is employed. The Km is specific for each enzyme-substrate couple, and it is mathematically defined as the substrate concentration corresponding to half of the V_{max}.

The experiment was run on the same J-730 split beam UV-Vis Spectrophotometer. As before,

- the enzyme concentration was checked before running the experiment
- 6 cuvettes were prepared with fixed concentrations of enzyme and growing concentrations of either substrate (dUMP) or co-factor (mTHF) depending which K_m was measured.
- the concentration of the non-limiting substrate is still 10 times the K_m value

- TES composed half of the cuvette's final volume, milliQ water was used to bring the solution up to volume.
- The final reagent added to start the reaction was dUMP for the mTHF K_m, and vice versa mTHF for the dUMP K_m.

The instrument allowed for the tangent to the hyperbole to be measured and its slope was given; this parameter was to be considered the V_{max}. The concentration corresponding to the half of the V_{max} was the K_m.

3.6.4. SDS-PAGE molecular weight evaluation

SDS-PAGE (Sodium Dodecyl Sulphate PolyAcrylamide Gel Electrophoresis is a widely used technique that allows for the evaluation of molecules based on their electrophoretic mobility.

As proteins are heated over 65°C, they progressively tend to lose their tridimensional structure, getting linearized. At 95°C all proteins may be considered linearized.

Figure 45: Mini-PROTEAN® TGX™ 4-20% Precast Gel

This is achieved by means of two different elements that act together: on one end, SDS is an anionic detergent whose role is to denature proteins, imparting a negative charge to them. This has a rather critical

impact in the run, as the only discriminant in the run is the protein size and length. SDS can grant this as its binding to side chains gives proteins an even negative charge per mass unit distribution, which helps in the denaturing process together with boiling the samples at 95°C.SDS is one of the components of Laemmli buffer, together with TRIS (to ensure that proteins are in a buffered environment), Glycerol (to avoid them floating away once loaded in the gel), a thiol agent like DTT or beta-mercaeptoethanol (to avoid oxidation and reduce disulphide bonds between amino acids that contain Sulphur ions in their side chain), and a colorant molecule like the bromophenol blue. The running gel used was the Mini-PROTEAN®TGX™ 4-20% Precast Gel (Fig.45, courtesy of Lorenzo Tagliazucchi).

The electrophoresis cell was the Mini-PROTEAN 3™ and the system was powered by the Power Pac Basic Power Supply, all from Bio-Rad. The running buffer is a TRIS-Glycine-SDS Buffer 10x Concentrate, 0.2 µm, pH 8.3 filtered from Sigma, which allows the electricity from the power source to run smoothly in each gel portion.

Along with SDS, Glycine has an important role in this technique. In short, strongly depending on the environmental conditions, this molecule can either be positively charge, neutral or negatively charged. Glycine has two different pK, at 2.3 and 9.6. Once the power is turned on, this molecule moves from a mildly basic environment (around 8.3) to a mildly acidic one (6,8). In the latter, Glycine is mostly found in its zwitterionic form (as in, there's a simultaneous presence of a negative and a positive charge). This stops Glycine from moving further in what is usually called the "stacking gel" portion. Cl^- ions found in the

stacking gel portion (TRIS-HCl 6.8), on the other hand, tend to move much quicker. In between the two there are the samples.

What happens in other words, is that there's a front formation, one where Cl^- ions are very quick to move, Glycine on the other hand is rather slow. When the molecules exit the stacking gel portion to enter the running gel one, things change quite a bit. The environment here is mostly basic (8.8) which means that many Glycine molecules can now be found in a negative state. Thus, said molecules will move much faster than the Cl^- ions and the proteins; the Glycine front now surpasses the proteins and gets upfront. The latter are hence found now in a narrow portion of the interface between the stacking and the running gel. The latter has an increasing concentration of acrylamide capable of opposing the movement of bigger molecules, hence the separation process can begin. At this point, the role of the "stacking gel" portion is evident; it allows all samples to get to the initial part of the "running gel" portion, so that the run may start with all the samples at the same time and place.

The applied voltage, which is directly proportional to proteins running speed in the gel, is different between the stacking and running gel. It is usually slower in the former and faster in the latter (100 V, 15 mins/ 200 V, 45 mins). Increasing the voltage means increasing the temperature at which the run is executed. Hence for this reason, the run has been standardized to the aforementioned parameters.

The samples were heated to 95°C for 7 minutes, centrifuged at 12000 x rpm for 30 seconds then added to the gel. Thus, the running buffer was added to the chamber. The run was conducted according to protocol. At the end of the run, the gel was extracted from the running buffer and the plastic plates and spacers. The gel was put in a small tray where it was then colored with a Coomassie Brilliant Blue solution, and destained multiple times until bands were clearly visible. The bands were confronted with an internal standard: a molecular weight marker that ran together with the samples.

3.7. Outline of fluorescence and basic principles of FRET

Another important element to study ligand-protein interactions is given from the study of ligands labelled with fluorophores. This evolution came from labelling ligands with molecules that were capable of emitting radiations. As they cost significantly more and posed severe health and safety hazards, a new labelling approach was required, hence invented. The main idea is to use fluorescent molecules which are mostly able to emit due to the presence of pi-systems, characterized by delocalized electrons. Of course, one such caveat of this technique is the steric encumbrance given by the fluorescent molecule, which in some cases may lead to poorer performances to the protein. It is, however, an interesting point of view to visualize different elements of the binding process through spectrofluorometry.

Luminescence is the general term intended for the emission of photons from an electronically excited species. Whenever luminescence regards a light absorption phenomenon, it is defined as photoluminescence. This term comprehends two more phenomena, phosphorescence and fluorescence.

- Phosphorescence is an emission of radiation of radiative emission from electronic states with a diverse multiplicity of spin, implying a change of the spin number. This is enabled by intersystem crossing due to spin – orbit coupling. The result is longer lifetimes 10^{-3}-10^{+2} s.
- Fluorescence is a spontaneous emission of radiation among electronic states from the same multiplicity of spin, due to a singlet transition, with one state being a fundamental one. Fluorophores are molecules capable of emitting fluorescence, presenting pi systems with delocalized electrons. A lifetime estimate of said excited states is in the order of 10^{-12}-10^{-8} s.

Before absorbing the electromagnetic radiation, molecules who will be excited find themselves into an electronic state with the lowest energy, defined as S_0. This state should be seen as a group of vibrational substates, separated from each other for a matter of some Kcal per mol^{-1}. The electromagnetic radiation contains energy, hence, by absorbing it, some of these molecules are promoted to an excited electronic state. Not all photons were created equal though, hence the energy contained from the photon and absorbed

by the molecule, promotes the latter to a singlet state with lower (S_1) or higher energy state (S_2, S_3 and so on…).

The excited molecule can dissipate the excess energy to return to its fundamental state (S_0) through radiative (photoluminescence) and non-radiative pathways. Another element to be considered is the chance that an excited molecule is still subjected to vibrations, rotations and collisions with other molecules, whose lifetimes are way lower than the average lifetime of the excited state. An example of these is the dissipation of excitation energy and its transformation in vibrational, rotational and translational energy, hence into thermal energy.

In other words, multiple pathways exist for an excited state to be deactivated. Fluorescence is just one of them. Other noteworthy elements in this sense are:

- Vibrational relaxing: the first phenomenon observed that is basically the transfer of the difference of energy between the excited state and that of the level zero corresponding to states S_x o T_x. This energy can be transferred to other molecules or to the solvent.
- Internal conversion: molecular processes through which a molecule goes to a lower energy state without radiative emission. Such a nonradiative transition happens between energy states of the same spin multiplicity $S_m \rightarrow S_n$ o $T_m \rightarrow T_n$ ($\Delta S=0$, hence there's no change in the spin multiplicity).

- Intersystem crossing: another nonradiative process in which the spin of an excited electron is inverted, bringing to a change of the multiplicity of the molecule. This element is particularly efficient in competing with fluorescence. Chances of transition are higher if there's an overlap between the two vibrational states.
- Quenching: deactivation of an excited state from another molecule able of absorbing energy from the excited molecule.

Two elements can be considered the main fluorescence properties: the excited state lifetime and the fluorescence quantic yield. The former is defined as the characteristic time of first order of decay from the excited state S_1 to the fundamental state S_0, whose formula is given as:

$$\tau^{-1} = \sum_i k_i :$$

k_i is the first order kinetic constant for the i^{th} decay process of S_i

Equation 20: Excited state lifetime

The fluorescence quantic yield is defined as the ratio between photons emitted and photons absorbed, representing the portion of excited molecules who decay due to fluorescence. Such a value is proportional to the intensity of the emitted fluorescence.

$$\varphi_f = \frac{I_f}{I_{ass}} = k_f \tau$$

Equation 21: Fluorescence quantic yield.

Lifetimes and yields strongly depend from environmental factors such as pH and temperature, but also from the ability to form hydrogen bonds.

3.7.1. Fluorescence quenching

Quenching is a term that refers to the deactivation of an excited fluorophore from a molecule capable of subtracting its energy. The energy transfer between the excited molecule (donor) to another chemically different one (acceptor) is called "heterotransfer". On the other hand, "homotransfer" refers to such an occasion where donor and acceptor are the same molecule.

Non-radiative quenching is defined whenever the acceptor molecule does not absorb donor's fluorescence. Two different occasions may be the cause: either collisional or static non radiative quenching.

- The former can happen anytime donor and acceptor come into contact with each other, after a phenomenon of diffusion brought them one versus the other. In such an occasion, quenching is a bimolecular process, whose speed depends not only on both donor and acceptor concentrations, but also from a kinetic constant, k_q.
- The latter happens anytime molecules – or portion of molecules – which are to be found at a critical distance.

The latter phenomenon is called excitation energy transfer (EET), a monomolecular event whose kinetic constant (k_{EET}) directly competes with other ones about deactivation of the donor's S_1 status. When such a transfer is coupled with a decrease in the donor emission and a contemporary increase in the acceptor emission, this quenching phenomenon is called FRET (Förster Resonance Energy Transfer).

FRET, which will be largely discussed in the next subchapter, has two critical requirements to happen:

- An energy-based condition: overlap of the donor's emission spectrum and the acceptor absorption one.
- A spatial condition: the distance between the two portions (donor and acceptor) or molecules needs to be less than 100 Å.

3.7.2. FRET – Förster Resonance Energy Transfer

The FRET process takes place anytime the emission spectrum of a fluorophore, defined as "donor", overlaps with the absorption spectrum of another molecule defined as "acceptor". Whilst it is common that the donor is a fluorophore, there's no such limitation for the acceptor, in order for this phenomenon to happen. FRET is not about the emission of light by the donor being absorbed by the acceptor molecule, as this is a function of the concentration of the latter species, as well as from other elements which will not be discussed in this context. It is important to stress that donor and acceptor are coupled in a dipole-dipole interaction. The energy transferred from one molecule to the other depends

on the distance between the two molecules (r) and the spectral overlap between the former's emission spectrum and the latter's absorption one. This is usually described as Förster distance (R_0), the distance at which the energy transfer efficiency is at 50%, which is equal to – Eq.22 –:

$$R_0 = 9.78x10^3[\kappa^2\eta^{-4}\phi\, J(\lambda)]^{1/6} \qquad (\text{in Å})$$

Equation 22: Förster distance.

- κ^2 describes the transition dipoles of the donor and acceptor molecules in this order. This value is 0 whenever the two molecules are perpendicular to each other and 1 whenever they are parallel to each other.
- η is the refraction index of the medium between donor and acceptor;
- ϕ the quantum rate of the donor in the absence of the acceptor probe
- $J(\lambda)$ defines the overlap between the emission spectra of the donor and the absorption spectra of the acceptor.

The energy transfer rate is – Eq.23 –

$$k_\tau(r) = \frac{1}{\tau_d}\left(\frac{R_0}{r}\right)^6 ; k\tau_r \text{ is the rate of energy transfer}$$

Equation 23: Energy transfer rate.

$\tau_d$is the donor decay-time when the acceptor molecule is absent.

If one wished to define the energy transfer of a single donor-acceptor couple, at a fixed distance:

$$E = \frac{R_0^6}{R_0^6 + r^6}$$

Equation 24: Energy transfer of 1 donor-acceptor couple, at a fixed distance.

It is clear how the transfer in this condition only depends from distance. As Förster distances for macromolecules are typically in the realm of some tens of angstroms (about 30 to 60), it doesn't surprise how this phenomenon has been exploited to obtain indirect measurements of distances between molecules of interest, or within the same molecule. Given the distance dependence on the energy transfer, it does not surprise how the latter may vary depending on how close the donor and acceptor molecules are due to their interacting and eventual bonding.

The FRET phenomenon can be explained in a few steps:

- First comes the absorption of a quantum of energy from a donor fluorophore which causes electrons to move from their fundamental state (S_0) to a singlet excited one (S_n)
- Decay time from excitement state is around a dozen of seconds. This may happen either via vibrational relaxation or internal conversion. Either way, there's a switch down to a lower vibrational state (S_1).

- From here, the electrons return in their fundamental state (S_0) in about 10 seconds. This may happen due to either fluorescence emission or non-radiative processes.
- If an acceptor molecule is present, the energy transfer happens. This molecule becomes excited and can then decay its energy as fluorescence.

As this phenomenon depends on dipole-dipole interactions, the maximum efficiency of transfer happens whenever these two molecules are parallel to each other.

3.8. Enzymatic conjugation with fluorescent probes

As previously reported, FRET techniques can be used as "molecular rulers" to understand the distance between two molecules, a "donor" and an "acceptor". Within this spirit, a FRET experiment was employed to test the efficacy of some hTS inhibitors whose activity disassociate the dimeric structure. In the role of the "donor" molecule, Fluoresceine-5-maleimide was used; as "acceptor" Tethrametylrodamine-5-maleimide.

These probes tend to bind cysteine residues; in each hTS monomer, 5 residues are present (C43, C180, C195, C199, C210). Taking into account the dimeric form, however, only two residues are available: C43 and C195. The protocol allowed to mask the latter using methotrexate; a competitive inhibitor of mTHF and dUMP, and an enzymatic substrate.

Two possible scenarios develop from this point: either the enzyme binds two identical probes (F2-M2 or T2-M2) or two different probes (F-M2-T or T-M2-F). Clearly, the FRET signal can be had only in such occasion where the enzyme has two different probes linked, one to each monomer. Statistically, the protocol defines at a 25% chance to have both of

the monomers of an enzymatic subunit bound to the same probe. Said percentage is 50% on the other hand, if the enzyme subunits are bound to one probe each.

A requirement of this protocol is to have a high concentration enzyme aliquot. This is due not only to the relatively low yield of the process, but also to the fact that the usable fraction of functionalized protein is usually low in concentration. As it will be described further, this is not a great issue by itself, as the enzymatic concentrations for FRET are usually low (a few hundreds of nanomolars)

The procedure requires the following materials:

- hTS highest possible concentration
- Methotrexate (MTX) 5 mM
- dUMP 9 mM
- Fluorescein maleimide in DMSO
- Tetramethylrhodamine maleimide in DMSO
- Buffer 1 (in this case, both buffers could have been used as the objective is not to gain structural evidence about the enzyme)
- Dithiothreitol (DTT) 0,5M

The first step of this procedure was to evaluate the concentration of the thawed enzyme and probes aliquot via the aforementioned spectrophotometrical assay. This was done as the following passages need an exact protein to reagent ratio. This is especially true for concentrated fractions, of mutants for instance, in which the purification yield is about a

tenth of the wild type counterpart. In the event that the concentration of a single fraction was deemed too low, multiple low concentration fractions were concentrated in a single high concentration one through VivaSpin centrifugation.

dUMP and MTX in a 50:1enzyme mix, in molar ratio were added to the hTS aliquot. A mix of the two probes, in a 2,5:1 ratio with the enzyme was prepared. An aliquot of this mix was taken to be checked via spectrophotometry, ensuring the proper molar ratio between the two. After 10 minutes from the addition of the dUMP/MTT solution, the probe mix was added. After 30 minutes, 10 microliters of DTT 0,5 M were added to the mix, inactivating all unbound probes, binding them through its thiol group. After four minutes, the mix was purified via FPLC / SEC Hi-Trap Desalting column, through the same protocol described in the previous chapter of protein purification. The chromatogram shows 3 peaks: only the first pertains to the conjugated protein. The other two peaks correspond to the elution of dUMP and MTT and the DTT-bound probes, respectively. Fractions corresponding to the conjugated enzyme were later spectrophotometrically quantified in terms of F-M2-T ratio which ideally should correspond to a 1:2:1 ratio.

3.8.1. FRET efficiency in hTS from fluorescence emission data[38]

The efficiency of FRET (φET), i.e., the fraction of excited F molecules in heterodisubstituted hTS (F-M2-T), which decay by transferring their excitation energy to their T counterparts, can be obtained by measuring the ratio of the areas of the emission spectra of F (a_F) and T

(a_T) corrected for the spectrofluorometer spectral sensitivity curve. It is simple to see that, for a mixture of F-M2-F (F2), F-M2-T (FT), and T-M2-T (T2), this ratio can be expressed in terms of the absorption rates, I_a, and of the fluorescence quantum yields (Φ) of the two probes bound to hTS (Φ = 0.6 and 0.3 (±20%) for F and T in F2 and T2 respectively, measured relative to free fluorescein dianion in 10^{-4}M NaOH (Φ = 0.95) as Eq.25:

$$\frac{a_F}{a_T} = \frac{I_a(\lambda_{ex})_{F2}\phi_F + I_a(\lambda_{ex})_{FT}(1-\varphi_{ET})\phi_F}{I_a(\lambda_{ex})_{FT}\varphi_{ET}\phi_T}$$

Equation 25; Ratio of the areas of F and T probes to determine FRET efficiency.

Given the very low absorbance at the excitation wavelengths (λ_{ex}), the rates of absorption can be approximated as $I_{aX}=I_{inc}A_X$, with I_{inc} being the incident number of einsteins per liter per second, which cancels out in the ratio, and A_X the absorbance of the F probe due to species X (F2, FT) at λ_{ex} If, as suggested by the provided UV-vis and mass spectrometric evidence, the sample composition is the statistic alone, i.e., 25% of F2 and 50% of FT, then AF2 and AFT are equal and cancel out too yielding the simplified relation in Eq.26

$$\frac{a_F}{a_T} = \frac{(\phi_F + (1-\varphi_{ET})\phi_F)}{\varphi_{ET}\phi_T}$$

Equation 26: Reduced form of Equation 25.

by which φ_{ET} is easily derived. In the above expression, we have neglected the contributions coming from direct excitation of T, both in FT and in T2, and F-to-T radiative

ET. These contributions have been estimated at λ_{ex}= 450 nm from spectra measured on an equimolar F2 and T2 mixture to be about 10% of the total a_T at full energy transfer. Values of a_T must therefore be corrected accordingly. Because of the mentioned assumptions and corrections, we estimate a confidence range of about ±25% for the values of φ_{ET} thus obtained.

3.8.2. Estimation of the maximum F/T distancein F-M_2-T[38]

The efficiency of nonradiative energy transfer can be expressed in terms of the corresponding rate constant, k_{ET}, as (Eq.27)

$$\varphi_{ET} = k_{ET}\left(k_{ET} + \tau_0^{-1}\right)^{-1}$$

Equation 27: FRET efficiency from the rate of nonradiative transfer.

with τ_0 is the donor lifetime in the absence of the acceptor, 4.4 ns for F. According to Förster's theory, k_{ET}= $\tau_0^{-1}(R_0/r)^6$with r the D-A distance and R_0 the critical Förster's radius, ca. 55 Å for the F/T pair. Given a φET larger than about 0.9, the lower limit for k_{ET} and upper limit for r given in the text are easily estimated.

3.8.3. Determination of dimer–monomer equilibrium constant from the dependence of φET on total protein concentration[38]

The equilibrium constant for the dissociation of the dimer to the monomer K = $[M]^2/[M_2]$is easily expressed in terms of φET. In fact, as φET is essentially 100% in the FT dimer and 0 for the monomers deriving from its dissociation, $F\text{-}M_{FT}$ or $M\text{-}T_{FT}$, the ratio of the residual FT dimer concentration to the sum of the concentrations of associated and dissociated FT.

$$\varphi ET = \frac{[F\text{-}M_2\text{-}T]}{([F\text{-}M_2\text{-}T] + [F\text{-}M_{FT})}$$

Equation 28: FRET efficiency as disassociation constant of the functionalized dimer.

Under the reasonable assumption that the attachment of the two probes does not affect the protein dimer–monomer equilibrium, the above ratio also represents the fraction of total associated protein dimers (FT+F2+T2)

$$\varphi ET = \frac{M_2}{[M_2] + \frac{[M]}{2}}$$

where the denominator is the total protein concentration expressed as moles of dimer L^{-1} C_T. Then,

$$[M_2] = C_T \varphi_{ET}; [M] = 2C_T(1\text{-}\varphi_{ET})$$

and, after replacing in the expression for K and rearranging, we obtain

$$\varphi_{ET} = 1 - \frac{1}{2}\left(\frac{\varphi_{ET}}{C_T}\right)^{\frac{1}{2}} K^{\frac{1}{2}}$$

So, plotting φET vs. $(\varphi ET / C_T)^{1/2}$ we should obtain a linear behavior with a slope $-K^{1/2}/2$. The error associated with K somehow derives from a combination of that provided by the linear data fitting procedure and the confidence range of φET. Because each plot refers to values of φET measured for the same conjugated protein at different total concentrations, we believe that such values may be over or underestimated by roughly the same percentage and, given the φET /$\varphi ET^{1/2}$ plot, the error on φET should under propagate into the plot slope and, thus, K.

Figure 46: Tecan GENios

3.8.4. Testing hTS dissociative inhibitors.

As reported in the previous chapters, dissociative inhibitors have been tested as a part of this thesis work. This was possible through conjugation of probes to either the wild type or the mutants of TS. All molecules tested came in powder;

1 mg was taken and dissolved in an opportune DMSO volume, in order to obtain a stock 10 mM solution of each. FRET analysis was obtained through a multiplate reader, the TECAN GENios Pro in Fig. 46, courtesy of Lorenzo Tagliazucchi.

Samples were loaded in a 96 well plate: in each, 300 nM of conjugated enzyme, and a 10, 20 or 40 micromolar concentration of the inhibitor, in duplicate. Six wells were used as control: 2 with hTS, 2 with hTS and 2 microliters of DMSO, 2 with hTS and a known inhibitor. Samples were then loaded into the plate with a multichannel pipette.

The instrument uses a protocol with an excitation wavelength (λ) of 435nm, whilst reading the probe emission at 535nm (Fluorescein maleimide) and 590nm (Fluorescein maleimide + tetramethylrhodamine maleimide).

For all compounds, absorption and emission spectra have been obtained. This was done to investigate absorption or emission in the FRET region and their water solubility – data not shown -

Some interesting molecules have been also detailed at an increased number of concentrations, directly with the Fluoromax 3 Spectrofluorometer – data not shown -.

3.9. Fluorescence anisotropy

Fluorescence anisotropy is based upon photoselective excitation of fluorophores by polarized light. This technique is capable of giving information either on size, shape or

rigidity of molecules. It has been largely employed in different contexts, from protein-protein association studies, to immunoassays.

Delving into the physical foundation of this technique, fluorophores are more prone to absorb photons characterized by electric vectors parallel to the transition moment of the fluorophores, as already mentioned before. This moment is characterized by a defined orientation on the molecular axis. In a process called photoselection, only those fluorophores characterized by an absorption transition dipole parallel to the electric vector of excitation are effectively excited. As only a partial of the population of fluorophores is excited, the consequent polarized fluorescent emission will be partial as well; one can see that as the emission itself occurs with the light polarized on a fixed axis, dependent on the fluorophore structure. Hence, the relative angle of the electric vector and the one from the transition dipole moment can determine the maximum intensity of measured anisotropy. Fluorescence anisotropy (r) and its polarization (P) are thus defined by Eq.29:

$$r = \frac{I_{\parallel} - I_{\perp}}{\left(I_{\parallel} - 2I_{\perp}\right)}$$

$$P = \frac{I_{\parallel} - I_{\perp}}{I_{\parallel} + I_{\perp}}$$

Equation 29: Fluorescence anisotropy (top) and polarization (bottom).

with $I_{\parallel}$ and $I_{\perp}$ respectively as the fluorescence intensities of the vertical and horizontal polarized emission, as the sample is excited with vertically polarized light.

Fluorescence anisotropy and polarization do define the same phenomenon; thus their values can be interchanged using P = 3r / 2+r; likewise r = 2P / 3 – P.

Albeit containing the same information, whenever polarization and anisotropy can be used, it is preferable to use the latter, as dividing for $I_{\parallel}$-2$I_{\perp}$results in simplified equations. Anisotropy spectra are expressed as anisotropy vs excitation wavelength graphs. This is due to the fact that anisotropy itself is independent of the emission wavelength.

Another noteworthy element in this context is the fluorescent anisotropy decay. This is because while the measurement itself is simple, the interpretation depends on an assumed form of decay. For example, following a pulsed excitation, the anisotropy decay r(t) of a sphere is given by (Eq.30)

$$r(t) = r_0 e^{-\frac{t}{\theta}}$$

Equation 30: Fluorescence anisotropy decay.

r_0 is the anisotropy at t = 0, θ the rotational correlation of the sphere. Anisotropy decays may be multiexponential in cases where multiple factors come at play. These, for example are to be expected in such a case where the molecule is not spherical, hence, correlation times in anisotropy decay are dictated by the rotation rates along all molecular axes. The evaluation of these sometimes lead to an estimate of the molecule's shape.

Without delving too much into details, there are two different ways in which fluorescence anisotropy is measured. These two methods are the "L-format method" and the "T-format method". The main difference between the two is that the former uses only one emission channel, as most fluorometers happen to have only one channel, whilst the latter observes the two components – parallel and perpendicular – of fluorescence anisotropy through separate channels, at the same time. There is no particular advantage in using one or the other method; L – method requires 4 measurements to happen (I_{vv}, I_{vh}, I_{hv} and I_{hh}), T – method still requires 4 measurements, but they are expressed through a ratio.

3.9.1. Time resolved fluorescence

Fluorescence measurements can be divided following different characteristics. Among one of the most critical, time is one such element that can be used to different aims.

Generally speaking, fluorescence measurements can be divided in two categories in this regard: steady state and time resolved measurements. Without delving too much into details, the former measurements are most common, with constant illumination and observation. Emission spectra recording is, in one regard, such a measurement.

On the other hand, time resolved measurements are a little more complex. These are employed whenever, for instance, intensity or anisotropy decays need to be measured. The main characteristic of such a reading is that the sample is excited with pulses of light whose widths are shorter than the phenomenon analyzed. Following the excitement, readings are obtained through high-speed detection systems, capable of measuring nanoseconds.

The two measurements can actually be considered correlated in a sense. A steady-state measurement is the average of the time resolved phenomena, by the intensity decay of the sample.

Given the formulas for intensity (Eq.31) and anisotropy decays (Eq.30)

$$I(t)=I_0 e^{-\frac{t}{\tau}}$$

Equation 31: Intensity (left) and anisotropy decay (right).

with I_0 and r_0 being the respective measurements for t=0, steady state anisotropy r can be calculated as (Eq.32)

$$r=\frac{\int_0^\infty r(t)I(t)dt}{\int_0^\infty I(t)dt}$$

Equation 32: Steady state anisotropy.

Substituting I(t) and r(t) in the previous formula gives out Perrin's equation, Eq.33

$$r=\frac{r_0}{1+(\tau+\theta)}$$

Equation 33: Perrin's equation.

τ is an important element, called measured lifetime. Dividing this for the quantum yield Q gives the natural lifetime τ_n

Within this context, TCSPC – Time Correlated Single Photon Counting – is one such manner to execute these measurements. This technique is based on the detection of single photons, measuring their arrival times with respect to a known reference signal – the light source for instance –.

TCSPC advantage is that it is a statistical method as well, one that, however, requires an important of photons to be analyzed, hence a high repetitive light source. This kind of precision is driven by a mechanism that is usually referred as a "fast, two inputs stopwatch".

What it means is that the signal source is started and stopped by a single pulse. The time between these two is measured any time a photon begins the sequence. Fluorescence intensity is then taken and reported in a "counts vs channels" histogram, representing respectively fluorescence intensity vs time.

As this phenomenon happens multiple times in a row, a phenomenon called "pulse pile-up" may happen. This one phenomenon occurs whenever multiple photons are detected per "light" flash. As is, it's fundamental that each light flash corresponds to a single detected photon, or else these may affect the statistics, meaning erroneous results may be achieved. This is avoided by keeping the photon rate low in comparison to the rate of the excited lamp.

Steady state and time resolved fluorescence readings have been employed in this project with the aim to gain as much fluorometry data as possible on both the active and inactive conformers of hTS, with the idea of identifying, if possible, elements that could represent the "fingerprint" of the two conformers. Data was acquired via two different spectrofluorometers, the Horiba Jobin-Yvon Fluoromax 3 and 4, in Fig.47.

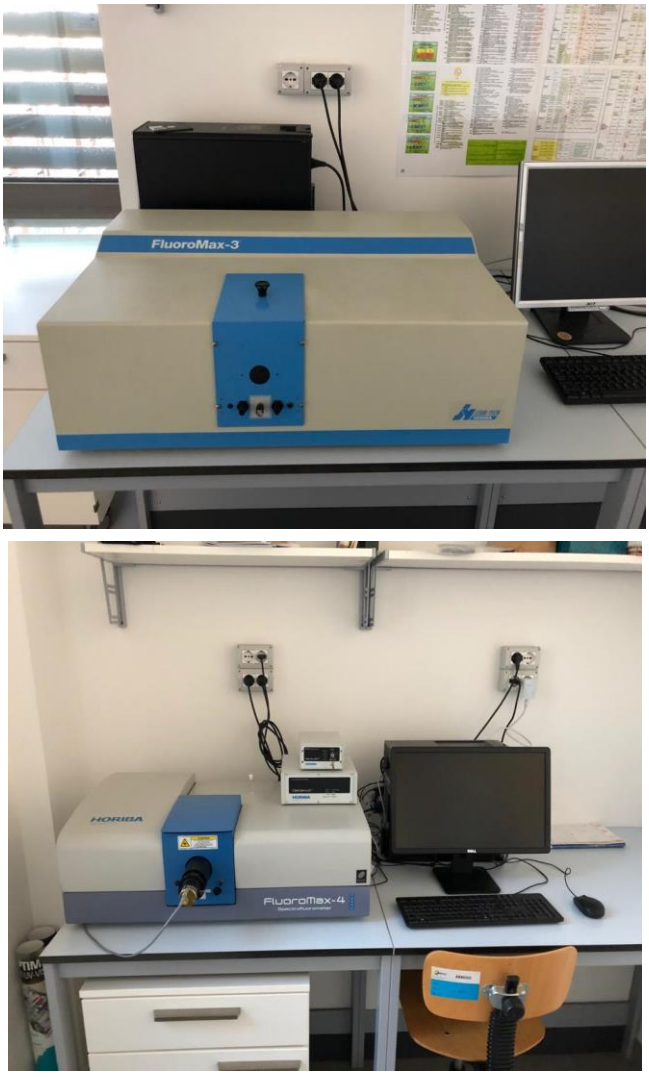

Figure 47: Horiba Jobin Yvon Fluoromax 3 - on Top - and 4 - bottom.

3.10. Isothermal titration calorimetry

Isothermal titration calorimetry (ITC) is a part of Thermal Analysis techniques, where specific properties of a sample are measured and expressed as a time function, whilst subjected to a temperature-controlled program and environment. Given the conditions, said parameters will also be expressed as a function of temperature. In calorimetry, the most regarded property measured is heat. Within this context, titration calorimetry (TC) can be considered a manner of obtaining thermodynamic data about molecules interacting within a solution. Without going too much into the specifics, TC can be used to either determine:

- the concentration of molecules in solution and their stoichiometry
- variations in enthalpy between interacting molecules in solution
- determination of both equilibrium constants and enthalpy variations.

Isothermal Titration Calorimetry, hence, is a technique that allows this to be done whilst keeping the temperature constant. Titration also imply that this process can be followed in two different ways: either as a continuous addition of titrant, usually at a constant rate, or as increments. In adding the titrant with the former method, however, corrections need to be applied as the time in which the calorimeter responds can be quite long. These are however balanced with two key advantages: continuous titration methods are less time consuming and usually give more points out for the titration curve vs incremental titration

methods. For this reason, the experiments conducted in this thesis regard incremental additions of titrant.

The ITC instrument used in this thesis is the MicroCal VP-ITC. As most ITC instruments, it is equipped with two different cells, referred as "Sample" and "Reference" cells. These cells are shaped as coins: both are enclosed within an adiabatic portion, an outer shield defined as "Jacket". This grants little to no heat exchange with the external environment and the measurement of up to micro-nanocalories of heat. Cells can be accessed only from the top portion of the instrument, whose volume is fixed at 1.44 mL.

As a consequence of the titration process, changes in temperature are to be expected. For this reason, a temperature sensor is sandwiched between the two cells. Constant readings allow the sensor to register any temperature variation in the sample cell by confronting this with the temperature in the reference cell. Said variations are then converted in power units and displayed to the user as a differential vs time graph. Hence, for each titrated volume, the instrument is capable of outputting a signal as a function of time, which is usually referred as the "feedback" power needed to maintain the temperature. Exothermic reactions can be described with a decrease of DP power: as the heat from the interaction goes into the environment, the machine is alarmed by the sensor to not feed more heat to the cell system. On the other hand, with endothermic reactions, the system is alarmed to heat a little bit more the resistive portion of the instrument in order to increase the cell temperature and maintaining the target temperature.

As DP is expressed in power units, the time integration of this value contains thermal energy, ΔH. As the binding occurs between the titrant and the titrated molecules, and in reason of the quantity of binds occurred, heat is either released or absorbed by the solution. This is true until no more binding can be had; the signal is then mostly assigned to the heat dilution due to the titrating process having reached and surpassed the saturation point.

Through the VP-ITC system the user is capable of setting up the experimental conditions - temperature, number of injections, injection volumes. Origin Software is then used to analyze the ITC data through fitting models to calculate stoichiometry, binding constant(s), enthalpy and entropy.

To complete this setup, the titrating apparatus is constituted of a syringe capable – if needed – to stir the solution in the sample cell during the titration process.

In this case, two experiments have been conducted.

- Titration of the hTSwt enzyme in a phosphate – free buffer with dUMP following an addition of 180 mM of phosphate.

  The main idea behind the experiment was to have the hTSwt in an environment where the inactive conformer was mostly present vs the inactive one. This was achieved by taking into account a high concentration of effectors that may be able to switch the active-inactive equilibrium towards the inactive conformer. The chosen effector was, in this case, phosphate ions. By titrating the solution with dUMP, the

progression in the thermogram, after subtracting the dilution heat, should at least reflect both the binding process of hTSwt and dUMP, as well as the interconversion from the inactive conformer to the active one.

- Hence, the second experiment was the titration of the precedent solution with dUMP, in absence of the protein.

  This was done to obtain the most information possible upon the heat dilution of dUMP.

It is important at this point to spend a couple of words on the heat dilution. This is the heat associated to the interaction of a concentrated solution of titrant with another one which contains a lesser concentration of the same titrant molecule. It is mostly defined in terms of enthalpy (enthalpy of dilution), one of the thermodynamic properties of a system. In other words, the enthalpy of dilution is defined as a variation associated to the dilution process, of a solution component, at a constant pressure.

Heat dilution needs to be subtracted from the total signal to obtain a clear picture of the heat components pertaining exclusively to protein-ligand interactions.

A 4 mL solution was made from a Pi free Buffer 1, added with 180 mM of sodium phosphate monobasic from a 1 M solution stock. Both solutions were filtered with a 0.45 micrometers acetate cellulose sterile filter. The solution was then degassed via ThermoVac, a sample degasser for the MicroCal VP-ITC instrument. In the end, the protein was added

to the degassed solution. This was done to avoid unnecessary stress to the protein, caused by the degassing process. The final concentration of hTSwt was 20 μM.

A 1.21 mM, 4 mL dUMP solution stock was prepared and degassed in the same fashion. Once the system was prepped up and ready, the dUMP was loaded in the titrating syringe, and the syringe was purged and refilled twice to ensure proper syringe loading and no bubbles were present at the time of loading. 1.44 mL of hTSwt solution was added in both sample and reference cell with a Hamilton gas free syringe. The system was equilibrated to 25°C, the titration syringe was placed with its needle in the sample cell, and the run was started. The run consisted in 125 injections of 2 microliters of dUMP, with a 240 seconds time interval between two consecutive injections. Each injection of consisted of 1.4 μM, to a final dUMP concentration of about 180 μM.

3.11. PHX and MTX tests

As already discussed in the Introduction, pharmacological treatments aimed at tumor cells are sporting side effects and pharmacoresistance, which greatly decreases the chances that these can successfully be employed. In this sense, chemotherapeutic agents have been long employed, with the side effect, however, that little to no difference is made between physiological and malign/benign tumor cells. Within this context, targeted therapies aim at approaching this issue in a different manner, synthesizing molecules that directly interact with critical targets. In this concept, Phototrexate®(PHX) was synthesized in Prof. Dr. Pau Gorostiza group. The aim of this molecule is to demonstrate that molecules may be

designed in such a way where they activate only when they reach the target tissue. A light-controlled molecule, PHX was designed as a derivative of another largely used antitumoral, Methotrexate (MTX). As a light-activated molecule can be activated with a certain spatio-temporal precision, thanks to the presence of already clinically approved light sources, aiming at enhancing the efficacy of treatments by reducing side effects and reducing the required concentration of a molecule to obtain a visible effect.

Within this context, the aim was to develop a protocol to study the behavior of PHX and MTX in different bladder cancer cell lines. A base protocol has been provided with HeLa cells, derived by previous studies conducted in the laboratory.

5 cell lines were thawed, but only 4 were actively tested, as one line, MGH-U3 was unable to growth to a number of cells sufficient to be tested.

The remaining four cells lines were: RT112, 5637, 97-1 and J82. Initial experiments have been carried out with two different cell lines (data not reported), one from the ECACC (European Collection of Authenticated Cell Cultures).

3.11.1. Cells and cell culture protocol

Tested cell lines derive from humans, both sexes: 97-1, (male, 28 y.o.), J82 (male, 58 y.o.) 5637 (male, 68 y.o.) and RT112 (female, no age data). Tested cell lines were derived from Prof. Jesus Paramio lab.

Cells were originally conserved in liquid nitrogen, in a 10% DMSO for culture, 90% Fetal Bovine Serum, in a NUNClone freeze vial. All cells shared the same protocol, from the beginning to the end.

In a sterile hood, cleaned with a 70% EtOH solution, cell medium was prepared: 50 mL DMEM (Dulbecco's Modified Eagle Medium) + Phenol Red + Glutamine. 10% FBS (Fetal Bovine Serum), 1% Streptomycin/Penicillin, and 1% Pyruvate were added. All reagents were thawed first at 37°C in a heated bath, until completely thawed. In some cases, it has been beneficial for the cell growth to do the following

- Store the cell culture media in a flask (Polystyrene Canted Corning Flasks, 25 cm^3) then store it for at least half an hour inside the incubator (5% CO_2, 37°C).
- Retake 30 to 50% of the used cell media, aliquot it 1:2 with fresh one, to be used in new cell passages.

After having prepared the media, cells were thawed and resuspended with an adequate volume of cell culture media, properly pipetted to ensure complete detachment between the cells, and then centrifuged for 20 minutes at about 1500 rpm at room temperature. This step allowed the supernatant, containing DMSO to be diluted and mostly removed from the cells via vacuum, under a sterilized hood, with a sterile glass pipette, Cells were then resuspended in an opportune amount of cell media and placed in a Polystyrene Canted Corning Flasks, 25 cm^3, overnight, in incubation, 37°C, 5% CO_2. The next day, the medium was removed, and the cells washed with an opportune volume (about 5 mL) of

PBS 1x. After having thoroughly washed the cells to remove any excess DMSO cells may have accumulated, cells were left in incubation until they reached confluence.

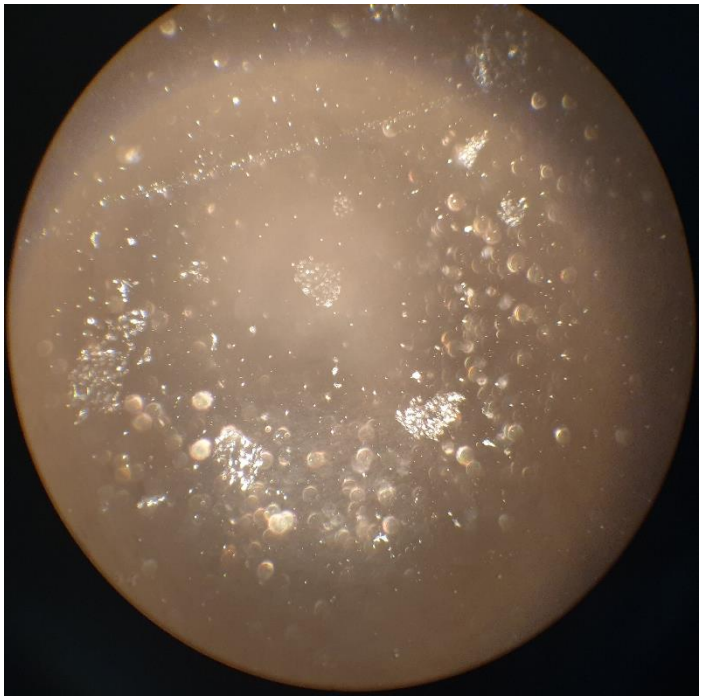

Figure 48: J82 cell line image in Confocal Microscopy.

Confocal microscopy was employed to ensure proper cell confluence (picture on the left) When cells reached about 80% flask confluence, their media was removed, and any excess washed away with a PBS 1 x wash. 500 microliters of Accutase or Trypsin were used to detach cells from the flask. To enhance the speed of detachment, cells were left in incubation for a couple of minutes, to ensure proper detachment of all cells. After being detached, cells were counted and about 500 thousand cells were taken and placed in two new flasks, each with a total cell medium volume of 5 mL.

Cells were allowed at least one full passage before being employed in experiments. This was done mostly to allow them to recover properly from the thawing process, avoiding that results obtained by treating the cells would be hindered by this bias. 5637 cells proven quite difficult to grow, as it was found out that they grow better when confluent.

This was found out after letting them grow in a 6-well plate, (an example picture on the right) which allowed for their slow recovery until a proper number of cells was obtained to switch back to a flask, as it can be seen on Fig. 49.

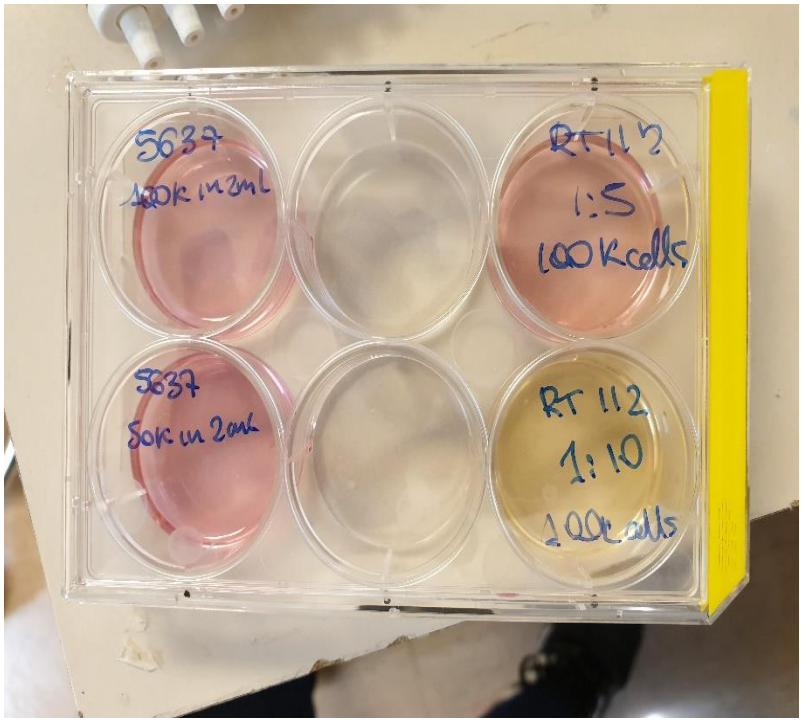

Figure 49: Six well plate employed for cell growing.

3.11.2. MTX and PHX experiments

In short, experiments were conducted on all cell lines. It was deemed necessary to find the optimal conditions, as stated in the Results chapter of this thesis. This meant, for each cell line, to look at the number of starting cells, as the concentrations were already established: from 100 micromolar to 1 nanomolar.

Three different conditions were tested: MTX, PHX cis and trans.

MTX was solubilized from powder. A master solution, 1 mM was prepared and from there, all dilutions were prepared directly in cell medium. Each dilution contained 100 micromolars of NaOH, which acted as a vector, and so did the controls.

PHX cis and trans were obtained from a powder, diluted in a 1 mM master solution and from there:

- PHX cis was obtained via photoisomerization, by taking a transilluminator and a LED plaque capable of emitting UVA light. The system (transilluminator + LED plaque and the PHX solution in an opportune quartz vessel) was then isolated from the rest of the room, to prevent any issues with the use of UVA light. Protection glasses were used at all times when working with UVA lights. Dilutions were then prepared directly in cell medium and added following protocol to the cells.
- PHX trans was obtained by the same 1 mM solution, by heating the master solution to 65°C, then diluting it directly in the cell medium and added to cells following protocol.

As this process aimed at obtaining a working protocol for each cell line, cells were tested at different numbers per well and time of treatment.

All trials, however, shared some common elements here described: the rest has been delved into the Results chapter in this thesis. All tests were conducted in a 96 well plate Nunclon® Delta Surface. The survivability assay used in this case, for all cell lines was MTS. Before treatment, cells were allowed an overnight period to let them stabilize inside the well. Each concentration was tested in quadruplicates.

MTS is a colorimetric assay, for the quantification of viable cells. The assay used is called CellTiter 96 ® AQueous One Solution Cell Proliferation Assay.

The NAD(P)H-dependent dehydrogenase enzymes in metabolically active cells cause the reduction of MTS tetrazolium compound and generate the colored formazan product that is soluble in cell culture media. Versus MTT: less cell manipulation as formazan crystals are already soluble.

After the first day, the medium was discarded, then the cells were treated according to protocol. After 48h or 72h – as explained in the Results section of this thesis – medium was discarded, and cells were treated with MTS diluted in PBS (Fig.50) and left in incubation for one hour. An example can be seen in the image below (Fig. 50).

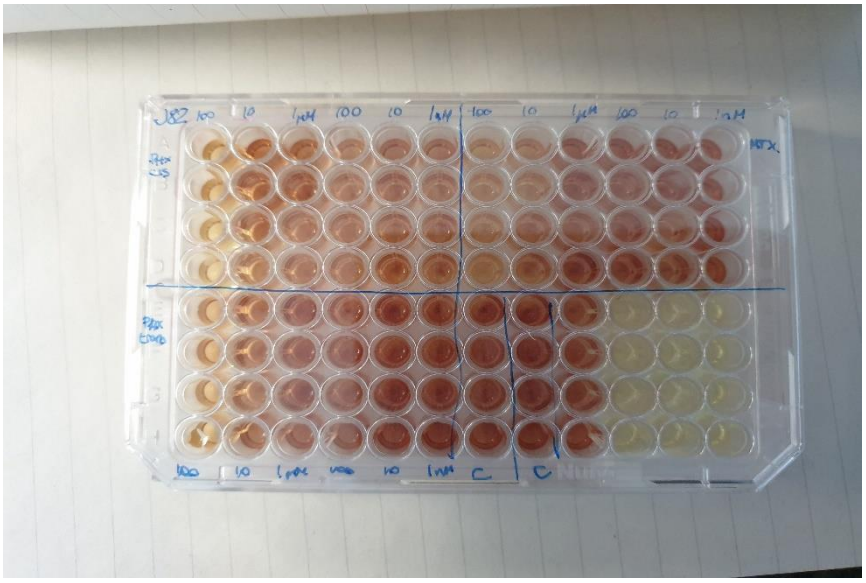

Figure 50: J82 cell line 96 well plate treated with MTS and left to incubate for one hour, 37, 5% CO_2.

Following this, cell plates were read with a Thermo Scientific MultiSkan FC, at 450 nm.

Obtained results were taken from the instrument via an USB drive and in Excel was obtained the relative % of proliferation / control, vs concentration of the molecule.

For each cell line at least 2 experiments were performed, whose data has been reported as a percentage of survival vs concentration graph, with error bars representing the standard deviation, in the Results section of this thesis.

Page intentionally left blank

Bibliography

1. Navalgund, L. G., Rossana, C., Muench, A. J. & Johnson, L. F. Cell cycle regulation of thymidylate synthetase gene expression in cultured mouse fibroblasts. *J. Biol. Chem.* **255**, 7386–7390 (1980).

2. Jenh, C. - H, Rao, L. G. & Johnson, L. F. Regulation of thymidylate synthase enzyme synthesis in 5 - fluorodeoxyuridine - resistant mouse fibroblasts during the transition from the resting to growing state. *J. Cell. Physiol.* **122**, 149–154 (1985).

3. Jenh, C. H., Geyer, P. K. & Johnson, L. F. Control of thymidylate synthase mRNA content and gene transcription in an overproducing mouse cell line. *Mol. Cell. Biol.* **5**, 2527–2532 (1985).

4. Ayusawa, D. *et al.* Cell-cycle-directed regulation of thymidylate synthase messenger RNA in human diploid fibroblasts stimulated to proliferate. *J. Mol. Biol.* **190**, 559–567 (1986).

5. Mathews, C. K., van Holde, K. E. & Ahern, K. G. *Biochimica*. (Casa Editrice Ambrosiana, 2004).

6. Voet, D., Voet, J. G. & Pratt, C. W. *Fondamenti di Biochimica*. (Zanichelli, 2001).

7. Salo-Ahen, O. M. H. & Wade, R. C. The active-inactive transition of human thymidylate synthase: Targeted molecular dynamics simulations. *Proteins Struct. Funct. Bioinforma.* **79**, 2886–2899 (2011).

8. Gibson, L. M., Lovelace, L. L. & Lebioda, L. The R163K mutant of human thymidylate

synthase is stabilized in an active conformation: Structural asymmetry and reactivity of cysteine 195. *Biochemistry* **47**, 4636–4643 (2008).

9. Costi, P. M. *et al.* Phthalein derivatives as a new tool for selectivity in thymidylate synthase inhibition. *J. Med. Chem.* **42**, 2112–2124 (1999).

10. Tondi, D. *et al.* Structure-based discovery and in-parallel optimization of novel competitive inhibitors of thymidylate synthase. *Chem. Biol.* **6**, 319–331 (1999).

11. Berger, S. H., Berger, F. G. & Lebioda, L. Effects of ligand binding and conformational switching on intracellular stability of human thymidylate synthase. *Biochim. Biophys. Acta - Proteins Proteomics* **1696**, 15–22 (2004).

12. Phan, J. *et al.* Structure of Human Thymidylate Synthase Suggests Advantages of Chemotherapy with Noncompetitive Inhibitors. *J. Biol. Chem.* **276**, 14170–14177 (2001).

13. Chu, E. & Allegra, C. J. The role of thymidylate synthase as an RNA binding protein. *BioEssays* **18**, 191–198 (1996).

14. Costi, M. *et al.* Thymidylate Synthase Structure, Function and Implication in Drug Discovery. *Curr. Med. Chem.* **12**, 2241–2258 (2005).

15. Du, X. *et al.* Insights into protein–ligand interactions: Mechanisms, models, and methods. *Int. J. Mol. Sci.* **17**, 1–34 (2016).

16. Rang, H. P. The receptor concept: Pharmacology's big idea. *Br. J. Pharmacol.* **147**, 9–

16 (2006).

17. Fuxreiter, M. & Tompa, P. Fuzzy Complexes: A More Stochastic View of Protein Function. in *Fuzziness: Structural Disorder in Protein Complexes* (eds. Fuxreiter, M. & Tompa, P.) 1–14 (Springer US, 2012). doi:10.1007/978-1-4614-0659-4_1.

18. Hughes, J. P., Rees, S. S., Kalindjian, S. B. & Philpott, K. L. Principles of early drug discovery. *Br. J. Pharmacol.* **162**, 1239–1249 (2011).

19. Spencer, H. T., Villafranca, J. E. & I, J. R. A. Bf. 575–578 (1993).

20. Myers, C. E. The pharmacology of the fluoropyrimidines. *Pharmacol. Rev.* **33**, 1 LP – 15 (1981).

21. Maybaum, J., Ullman, B., Mandel, H. G., Day, J. L. & Sadee, W. Regulation of RNA- and DMA-directed Actions of 5-Fluoropyrimidines Mouse T-Lymphoma (S-49) Cells1. 4209–4215 (1980).

22. Wilkinson, D. S., Tlsty, T. D. & Jane Hanas, R. The Inhibition of Ribosomal RNA Synthesis and Maturation in Novikoff Hepatoma Cells by 5-Fluorouridine. *Cancer Res.* **35**, 3014–3020 (1975).

23. Jackman, A. L. *et al.* Mechanisms of acquired resistance to the quinazoline thymidylate synthase inhibitor ZD1694 (Tomudex) in one mouse and three human cell lines. *Br. J. Cancer* **71**, 914–924 (1995).

24. Sikora, E., Jackman, A. L., Newell, D. R. & Calvert, A. H. Formation and retention and

biological activity of N10-propargyl-5, 8-dideazafolic acid (CB3717) polyglutamates in L1210 cells in vitro. *Biochem. Pharmacol.* **37**, 4047–4054 (1988).

25. Rhee, M. S., Wang, Y., Nair, M. G. & Galivan, J. Acquisition of Resistance to Antifolates Caused by Enhanced γ-Glutamyl Hydrolase Activity. *Cancer Res.* **53**, 2227 LP – 2230 (1993).

26. Touroutoglou, N. & Pazdur, R. Thymidylate synthase inhibitors. *Clin. Cancer Res.* **2**, 227 LP – 243 (1996).

27. Forsthoefel, A. M., Peña, M. M. O., Xing, Y. Y., Rafique, Z. & Berger, F. G. Structural Determinants for the Intracellular Degradation of Human Thymidylate Synthase. *Biochemistry* **43**, 1972–1979 (2004).

28. Li, B. *et al.* Competitive Binding Between Id1 and E2F1 to Cdc20 Regulates E2F1 Degradation and Thymidylate Synthase Expression to Promote Esophageal Cancer Chemoresistance. *Clin. Cancer Res.* **22**, 1243 LP – 1255 (2016).

29. Skwarczynska, M. Skwarczynska2015. (2015).

30. Sheng, C., Dong, G., Miao, Z., Zhang, W. & Wang, W. State-of-the-art strategies for targeting protein-protein interactions by small-molecule inhibitors. *Chem. Soc. Rev.* **44**, 8238–8259 (2015).

31. Salo-Ahen, O. M. H. *et al.* Hotspots in an obligate homodimeric anticancer target. Structural and functional effects of interfacial mutations in human thymidylate

synthase. *J. Med. Chem.* **58**, 3572–3581 (2015).

32. Cardinale, D. *et al.* Protein-protein interface-binding peptides inhibit the cancer therapy target human thymidylate synthase. *Proc. Natl. Acad. Sci. U. S. A.* **108**, (2011).

33. Valkov, E., Sharpe, T., Marsh, M., Greive, S. & Hyvönen, M. Targeting Protein–Protein Interactions and Fragment-Based Drug Discovery BT - Fragment-Based Drug Discovery and X-Ray Crystallography. in (eds. Davies, T. G. & Hyvönen, M.) 145–179 (Springer Berlin Heidelberg, 2012). doi:10.1007/128_2011_265.

34. Matera, C. *et al.* Photoswitchable Antimetabolite for Targeted Photoactivated Chemotherapy. *J. Am. Chem. Soc.* **140**, 15764–15773 (2018).

35. Avci, P. *et al.* Low-level laser (light) therapy (LLLT) in skin: Stimulating, healing, restoring. *Semin. Cutan. Med. Surg.* **32**, 41–52 (2013).

36. Gibson, L. M., Celeste, L. R., Lovelace, L. L. & Lebioda, L. Structures of human thymidylate synthase R163K with dUMP, FdUMP and glutathione show asymmetric ligand binding. *Acta Crystallogr. Sect. D Biol. Crystallogr.* **67**, 60–66 (2011).

37. Luo, B. B. *et al.* Human thymidylate synthase with loop 181-197 stabilized in an inactive conformation: Ligand interactions, phosphorylation, and inhibition profiles. *Protein Sci.* **20**, 87–94 (2011).

38. Genovese, F. *et al.* Dimer-monomer equilibrium of human thymidylate synthase monitored by fluorescence resonance energy transfer. *Protein Sci.* **19**, 1023–1030

(2010).

J.R.Lakowicz, Principles of fluorescence spectroscopy, Springer, New York, 2006